QUANTIFYING THE EFFECTS OF ALTERED-GRAVITY AND SPACEFLIGHT COUNTERMEASURES ON ACUTE CARDIOVASCULAR AND OCULAR HEMODYNAMICS

A Dissertation

by

RICHARD STUART WHITTLE

Submitted to the Graduate and Professional School of
Texas A&M University
in partial fulfillment of the requirements for the degree of

DOCTOR OF PHILOSOPHY

Chair of Committee,	Ana Diaz Artiles
Committee Members,	Bonnie J. Dunbar
	Christopher R. Woodman
	David C. Zawieja
Special Appointment,	Jay C. Buckey Jr.
Head of Department,	Ivett A. Leyva

August 2023

Major Subject: Aerospace Engineering

ABSTRACT

The cardiovascular system is strongly dependent on the gravitational environment. Gravitational changes cause mechanical fluid shifts and, in turn, autonomic effectors influence systemic circulation and cardiac control. For future long-duration spaceflight, these gravitational effects could be related to decreased cardiovascular performance, the pathoetiology of spaceflight associated neuro-ocular syndrome (SANS), and increased venous thromboembolism (VTE) risk. The development of novel countermeasure protocols using, for example, lower body negative pressure (LBNP) or short-radius centrifugation (SRC) requires a full understanding of the detailed cardiovascular response to gravity and to different levels of countermeasure intervention.

In this research effort, we use a complementary experimental and modeling approach to generate acute dose-response curves for systemic, autonomic, and cephalad parameters of the cardiovascular system in graded tilt (as an analog for altered-gravity), graded LBNP, and graded SRC. In the experimental approach, 24 subjects (12 male and 12 female) experienced 1) a graded tilt profile in the range of 45° head-up tilt to 45° head-down tilt in 15° increments; and 2) a graded LBNP profile from 0 mmHg to –50 mmHg in 10 mmHg increments. Using two different statistical techniques (mixed-effects modeling and Bayesian hierarchical multivariate modeling) we generate dose-response curves for the cardiovascular and ocular response. In the computational approach, we further develop an existing lumped-parameter model of the cardiovascular system to incorporate cephalad hemodynamics and the effects of body tissue weight. In addition, we also further develop a complementary lumped-parameter model of the eye. We simulate the same tilt and LBNP profiles, along with a graded SRC profile and a gravitational field change using simulated 50^{th} percentile male and female subjects.

The quantification of cardiovascular hemodynamics as a function of changes in the gravitational vector or the presence of countermeasure interventions presented here provides a terrestrial model to reference spaceflight-induced changes, contributes to the assessment of the pathogenesis of SANS and spaceflight VTE events, and informs the development of countermeasures.

DEDICATION

To Leo, Max, and Ava: may you grow up in a world where you can follow your dreams and reach for the stars.

Elara Sophie Mia Whittle (9/4/2020 – 12/27/2020)

Daddy loves you to the Moon and back and the ends of the universe.

ACKNOWLEDGMENTS

First and foremost, I want to thank my advisor, Dr. Ana Diaz Artiles, for her tireless support over the last few years. Ana, you have been the best advisor and friend I could have asked for on this journey. It has been an honor and a privilege to be your first Ph.D. student! The culture that you have grown and developed in the Bioastronautics and Human Performance lab is inspiring and you have been an incredible role model as a scientist and helped me grow and develop as both a researcher and teacher. I feel so confident taking the reins and moving on to setting up and running my own lab in large part because I have such a great point of reference. I am sad to be leaving you and the lab, but at the same time excited for the future and looking forward to many years of collaborations! Thanks also for instilling me with your love of statistics – it has gone from being my most hated school subject to my favorite, no going back now!

I would also like to thank the other members of my doctoral committee: Dr. Bonnie Dunbar, Dr. Christopher Woodman, and Dr. David Zawieja. Thank you for your support throughout this research effect, for your helpful and insightful comments that have guided the direction of this project. Dr. Woodman, your class on exercise physiology was key in giving me the knowledge to succeed, and your teaching style is something I have tried to replicate in my own teaching. Additionally, I would like to add special thanks to Dr. Jay Buckey, a special appointment to my committee from the Dartmouth Geisel School of Medicine, for taking the time to read and comment on my dissertation. Thank you also for sharing your wisdom on modeling, hydrostatic gradients, tissue forces, and SANS many times over the past couple of years. Your insights were invaluable in the direction of this research, and I look forward to many future discussions.

BHP lab, you're the best! To the grad students: Nathan Keller, Logan Kluis, Poonam Josan, Hrudayavani Vellore, Yasmin Zaman, Renee (and Kevin) Abbott, and Alexis Gangeme. Thanks for being the best lab mates ever. I have loved working with y'all (we live in Texas, I need to get it in somewhere) over the past few years. I'm excited to watch you finish your time here at Texas A&M and move on to the next exciting adventure. I look forward to working with as many of you

as possible in the future with our shared passion for human spaceflight, though in the meantime I will have to find new friends to terraform Mars with! Matteo Fois, I know you were only with us for a short time as a visiting student and are back in Italy now, but in the time that you spent here you helped me so much with data collection. You will always be a part of the BHP team and I look forward to catching up in the future. Eric Hall, it has been a pleasure to work with you on ocular perfusion pressure and everything else over the last few years. I have no doubt you will be an excellent physician and I look forward to following your progress through EnMed. Finally, to the other undergrads: Fèlix Real Fraxedas, Safiyya Patanam, Lindsay de la Zerda (Stapleton), Callie Wynn, Braeden Stewart, and Víctor Sainz Ubide. Thank you for all the help you have given me with data collection over the past few years, sometimes at crazy early hours in the morning.

I would also like to thank Dr. Vikram Kinra and the other members of the graduate teaching fellowship program. I was privileged to have the opportunity to teach two courses during my time at Texas A&M thanks to the GTF program. My confidence in teaching and presenting has grown immensely as a result and I have enjoyed our lunchtime discussions sharing our experiences. You have all been a great sounding board for teaching and research advice, and your feedback on seminars and research presentations has been invaluable.

Gail Rowe, Kelsie Allen (Thompson), Kelly Ganske, Julie Allen, Brandi Bolin, Andrea Loggins, Rodney Inmon, John Petitt, Lance Isenhour, Lois Rockwell, Jen Swartz, Jason Howard, Jo-z Cisneros, and the rest of the AERO staff: thanks for all the incredible work you do behind the scenes to support the running of the department and allow us to conduct our research. None of this work would be possible without you. Sorry for all the times I messed up the paperwork!

Within the wider University community, I would like to acknowledge the staff and volunteers in the Aggie Honor System Office and the Veteran Resource and Support Center. Thanks for all your support and advice over the last few, I have enjoyed and appreciated the time I spent working with the AHSO and the chance to meet and interact with students and faculty from across the University. I would also like to thank my anonymous subjects for their participation in the experimental portion of this research. Thanks for letting me tilt you and put you in a pressure chamber, sometimes at 6

a.m. without even allowing you caffeine beforehand to wake up.

I would like to thank my family back in the UK: Mum and Dad, Harry and Meg, Nan, and Carole and Jim. You have always loved, supported, and encouraged me in whatever I chose to do. Despite the miles, you have constantly been there for H and I through the highest and lowest moments of our lives. Thank you!

Lastly and most importantly, I would like to thank my wife, H, for her constant unconditional love and support. You have given up so much to allow me to follow my dream, moving halfway around the world and putting your career on hold to provide the best environment to raise our family (you are also the best editor)! Thank you; I love you and I couldn't have achieved any of this without you. Finally, to our kids: Leo, Max, Elara, and Ava. I love you unconditionally to the Moon and back and the ends of the universe. Being your daddy is the best job in the world; I am so proud of the people you are becoming and I'm excited to watch how you continue to grow and learn. This dissertation is dedicated to you, and I hope one day that I can share it with you!

CONTRIBUTORS AND FUNDING SOURCES

Contributors

This work was supported by a dissertation committee consisting of Professors Ana Diaz Artiles (chair of committee) and Bonnie J. Dunbar of the Department of Aerospace Engineering, Professor Christopher R. Woodman of the Department of Kinesiology and Sport Management, Professor David C. Zawieja of the Department of Medical Physiology, and Professor Jay C. Buckey Jr., a special appointment, of the Dartmouth Geisel School of Medicine.

Half of the experimental data ($n = 7$ of 13) for the study on intraocular pressure (IOP) and ocular perfusion pressure (OPP) described in Section 4.6 were provided by Professor Lonnie G. Petersen, then at the University of California, San Diego, now at the Massachusetts Institute of Technology. Some of the work in Section 4.6 has been modified, with permission, from a publication written in conjunction with Dr. Petersen[1]. All other work conducted for the dissertation was completed by Richard S. Whittle independently.

Funding Sources

Graduate study was supported by the National Aeronautics and Space Administration (NASA) Human Research Program grant 80NSSC20K1521, a Graduate Teaching Fellowship from the College of Engineering, and multiple Aerospace Graduate Excellence Fellowships from the Department of Aerospace Engineering at Texas A&M University.

NOMENCLATURE

A_{CCA}	Cross-Sectional Area of Common Carotid Artery
A_{IJV}	Cross-Sectional Area of Internal Jugular Vein
ABR	Arterial Baroreflex
aCORM	Abbreviated Carbon Monoxide (CO) Rebreathing Method
AGSM	Anti-G Straining Maneuver
ASEE	American Society for Engineering Education
ASGSR	American Society for Gravitational and Space Research
AsMA	Aerospace Medical Association
BARG	Bayesian Analysis Reporting Guidelines
BF	Bayes Factor
BF_{10}	Bayes Factor in favor of H_1 over H_0
BMI	Body Mass Index
`brms`	Bayesian Regression Models using 'Stan' *(R Package)*
BRS	Baroreflex Sensitivity
CBF	Cerebral Blood Flow
CCA	Common Carotid Artery
CDF	Cumulative Density Function
CI	Cardiac Index
CI	Confidence Interval
CIF	Cumulative Influence Factor
CO	Cardiac Output
CoM	Center of Mass

COV	Coefficient of Variation
CPP	Cerebral Perfusion Pressure
CPR	Cardiopulmonary Reflex
CrI	Credible Interval
CV	Cardiovascular
CVP	Central Venous Pressure
DAG	Directed Acyclic Graph
DAP	Digital Astronaut Project
DBP	Diastolic Blood Pressure
DCS	Decompression Sickness
`DHARMa`	Residual Diagnostics for Hierarchical (Multi-Level/Mixed) Regression Models *(R Package)*
DPTI	Diastolic Pressure-Time Index
DPTI/SPTI	Diastolic Pressure-Time Index to Systolic Pressure-Time Index Ratio *(cf. MO)*
DRM	Design Reference Mission
ECG	Electrocardiogram
EDF	Effective Degrees of Freedom
EDV	End Diastolic Velocity
EMM	Estimated Marginal Mean
`emmeans`	Estimated Marginal Means *(R Package)*
EPC	Endothelial Progenitor Cell
EVA	Extravehicular Activity
EVP	Episcleral Venous Pressure
g-LOC	G-force Induced Loss of Consciousness
GAMM	Generalized Additive Mixed Model
GLMM	Generalized Linear Mixed Model

`glmmTMB`	Generalized Linear Mixed Models using Template Model Builder *(R Package)*
HDI	Highest Density Interval
HDT	Head-Down Tilt
HDTBR	Head-Down Tilt Bed Rest
HF	Spectral Power Density in the High Frequency (0.15–0.4 Hz) Band
HFNorm	Normalized HF
HMC	Hamilton Monte Carlo
HR	Heart Rate
HRV	Heart Rate Variability
HRVTi	Heart Rate Variability Triangular Index
HUT	Head-Up Tilt
IBI	Intrabeat Interval
IBMP	*(Russian)* Institute of Biomedical Problems
ICA	Internal Carotid Artery
ICP	Intracranial Pressure
IIH	Idiopathic Intracranial Hypertension
IJV	Internal Jugular Vein
IJVF	Internal Jugular Vein Blood Velocity Waveform Flow Pattern
IJVP	Internal Jugular Vein Pressure
IML-1	International Microgravity Laboratory *(Mission)*
IOP	Intraocular Pressure
ISGP	International Society of Gravitational Physiology
ISS	International Space Station
JVP	Jugular Venous Pressure
LBNP	Lower Body Negative Pressure

LF	Spectral Power Density in the Low Frequency (0.04–0.15 Hz) Band
LF/HF	Ratio of Low Frequency to High Frequency Spectral Power Density
LFNorm	Normalized LF
LHS	Latin Hypercube Sampling
LKJ	Lewandowski-Kurowicka-Joe *(Distribution)*
`lme4`	Linear Mixed-Effects Models using 'Eigen' and S4 *(R Package)*
`lmerTest`	Tests in Linear Mixed Effects Models *(R Package)*
LMM	Linear Mixed Model
LVEDP	Left Ventricular End Diastolic Pressure
MAP	Mean Arterial Pressure
MAP_{eye}	Mean Arterial Pressure at Eye Level
MCMC	Markov Chain Monte Carlo
MCP	Mid-Coronal Plane
`mgcv`	Mixed GAM Computation Vehicle with Automatic Smoothness Estimation *(R Package)*
MIT	Massachusetts Institute of Technology
MO	Myocardial Oxygen Supply:Demand Index *(cf. DPTI/SPTI)*
MSNA	Muscle Sympathetic Nerve Activity
NASA	National Aeronautics and Space Administration
NE	Norepinephrine
NHST	Null Hypothesis Significance Testing
`nlme`	Linear and Nonlinear Mixed Effects Models *(R Package)*
NN	*(Interval)* Normalized RR Interval with Unreliable Data Excluded
NPY	Neuropeptide Y

NUTS	No-U-Turn Sampler
ONSD	Optic Nerve Sheath Diameter
OPP	Ocular Perfusion Pressure
pd	Probability of Direction
PP	Pulse Pressure
PRCC	Partial Rank Correlation Coefficient
PRU	Peripheral Resistance Units *(mmHg.s/ml)*
PSL-LBNP	Presyncopal Symptom Limited Lower Body Negative Pressure
PSV	Peak Systolic Velocity
RAAS	Renin-Angiotensin-Aldosterone System
REML	Restricted Maximum Likelihood
RI	Resistive Index
RMSDD	Root Mean Square of Direct Differences of NN Interval
ROPE	Region of Practical Equivalence
RPD	Reticular Pseudodrusen
RPP	Rate Pressure Product
RR	*(Interval)* Time Elapsed Between Two Successive R-waves of the QRS Signal on the Electrocardiogram
SANS	Spaceflight-Associated Neuro-Ocular Syndrome
SARS-CoV-2	Severe Acute Respiratory Syndrome Coronavirus 2
SBP	Systolic Blood Pressure
SD	Standard Deviation
SDNN	Standard Deviation of NN Intervals
SE	Standard Error
SI	Stroke Index
SPTI	Systolic Pressure-Time Index

SRC	Short Radius Centrifugation
SV	Stroke Volume
SVR	Systemic Vascular Resistance *(cf. TPR)*
TAMU	Texas A&M University
TBV	Total Blood Volume
TFESCNASPE	Task Force of the European Society of Cardiology and the North American Society of Pacing and Electrophysiology
TLPG	Translaminar Pressure Gradient
TPR	Total Peripheral Resistance
TS	Transverse Sinus
UCSD	University of California, San Diego
USSR	United Socialist Soviet Republic
VA	Vertebral Artery
VIIP	Visual Impairment Intracranial Pressure *(cf. SANS)*
VLF	Spectral Power Density in the Very Low Frequency (0.0033–0.04 Hz) Band
VO2	Oxygen Consumption
VTE	Venous Thromboembolism Events

TABLE OF CONTENTS

Page

LIST OF FIGURES

FIGURE Page

LIST OF TABLES

TABLE Page

1. INTRODUCTION

The spaceflight environment, and altered gravity in general, affects all the physiological systems in the body. In particular, the cardiovascular system experiences deconditioning through a variety of mechanisms including cardiac atrophy and vascular remodeling[2,3]. Conflicting evidence exists with regard to changing baroreflex function in space, although the major structure appears to remain intact[4,5]. Whilst many of these effects take place over a time period of weeks and months, in the short term there is an immediate cephalad fluid shift, causing systemic and autonomic changes[6,7]. These changes, combined with cardiac deconditioning, can present medical and operational issues on return to a gravitational environment after a period in reduced gravity, including increased risk of orthostatic intolerance. Additionally, the cephalad fluid shift may be etiologically associated with an observed set of ocular pathologies collectively termed spaceflight associated neuro-ocular syndrome (SANS)[8]. Finally, there have recently been concerns that altered flow patterns in the jugular veins could lead to an increased occurrence of venous thromboembolism events (VTE)[9–13]. Thus, an enhanced understanding of the quantitative changes that occur in the cardiovascular system in altered gravity environments can aid in predicting and managing operational risk of human spaceflight. These quantitative data can also be used to compare the efficacy of countermeasures, which may help to reduce cardiac deconditioning, or manifestations of SANS or VTE.

This dissertation quantifies acute cardiovascular changes in multiple orthostatic regimes. First, altered-gravity through a graded tilt paradigm, i.e., changing the gravitational vector resolved along the craniocaudal axis. Second, through graded lower body negative pressure (LBNP), a promising countermeasure for reducing cephalad fluid shift in microgravity. For these two regimes, cardiovascular dose-response curves are generated using a combined experimental and computational modeling approach. Finally, a pure modeling approach is used to explore the acute cardiovascular response to short radius centrifugation (SRC), as well as the influence of body tissue weight on cardiovascular hemodynamics.

Section 2 outlines the background related to cardiovascular deconditioning during spaceflight. It also covers some proposed countermeasures (including LBNP and SRC), along with a discussion on sex differences in cardiovascular physiology and the use of computational models to simulate physiological systems. Section 3 clarifies the specific research aims.

Section 4 presents in detail the first experiment: the generation of gravitational dose-response curves for cardiovascular parameters related to the systemic circulation, autonomic system, and head and neck in graded head-up and head-down tilt in male subjects. This section also considers sex differences in the cardiovascular response to tilt, along with a pilot study to measure gravitational effects on intraocular pressure (IOP) and ocular perfusion pressure (OPP). Section 5 presents the second experiment: the generation of gravitational dose-response curves for cardiovascular parameters related to the systemic circulation, autonomic system, and head and neck in graded LBNP. In this experiment both males and females were considered together, although the sex differences were still examined. The methodology to generate the dose-response curves was also altered, from a frequentist to a Bayesian approach. This method allowed us to further consider the multivariate relationship between all of the parameters examined. Section 6 presents the modeling element of the research. In this section, the additions to an existing computational model are detailed, along with the results of a sensitivity analysis and simulations of a range of orthostatic conditions (tilt, LBNP, and SRC). Finally, conclusions, contributions, and ideas for further research are presented in Section 7.

2. BACKGROUND AND LITERATURE REVIEW

2.1 Gravitational physiology

The human body has evolved through thousands of millennia to be uniquely suited to a terrestrial, 1g, environment. Despite this, the body contains an array of control systems to regulate physiological systems in response to a changing gravitational vector. The simple act of lying down or standing up causes a 90° shift in the experienced gravitational vector, to which physiological systems must respond to in order to maintain homeostasis. However, it in only in the last 60 or so years, the age of human spaceflight, that humans have been subjected to prolonged shifts in the gravitational environment for days, weeks, or months at a time. To date, with the exception of nearly 25 man-days[i] on the lunar surface in the Apollo program, all of the time humans have spend in space has been in microgravity (the majority in Low Earth Orbit). In the next few years, future plans will take humans back to the Moon for longer periods in a 1/6g environment. Longer-term, human missions to Mars will require extended time at 3/8g (30-90 days for an opposition-class mission, with up to 500 days for a conjunction-class mission), with long periods in microgravity either side during transit[15]. Further, the advances of technology have enabled humans to be subjected to acute periods of gravitational stress far beyond those designed by evolutionary mechanisms. In spaceflight, launch and re-entry profiles can create acute gravitational loads as high as 7g in the G_x direction[16]. Outside of the space-domain, acute hypergravity conditions are experienced in many scenarios where operator function is critical, including in high-performance aviation (for example the F-16 Fighting Falcon, the world's most numerous fixed-wing military jet, is capable of sustaining 9g G_z loads[17]).

Broadly, the human body can be split into 11 physiological systems: the cardiovascular, nervous, digestive, renal, endocrine, reproductive, immune, respiratory, integumentary, muscular, and skeletal systems[18]. To a greater or lesser extent, gravity (or the combination of microgravity with

[i] 24 days, 22 hours, 56 minutes[14]

other characteristics of the spaceflight environment including radiation) influences all of these systems during spaceflight. Although not critical to life preservation on a timescale of minutes or hours, even systems such as the digestive tract experience changes in space (including disorganized secretory function, fluctuated intestinal microecology, and altered metabolic capacity[19]). The increased risk of renal stone formation in space has also been known for some time[20]. Due to its life critical functionality, as well as effect on operational performance, the cardiovascular system is one of the most important systems affected by the spaceflight environment[7]. This is true on both acute and longer duration timescales.

2.2 Cardiovascular degradation in space

The cardiovascular system exhibits a deconditioning effect due to the spaceflight environment. In the short-term, on entering microgravity there is an removal of all hydrostatic gradients and tissue weight forces leading to redistribution of fluid in the body[5,7] (see Figure 2.1), which, in turn, leads to altered systemic function and variation in baroreceptor activity[4]. This is counteracted by a loss in circulatory plasma volume of 10-17%, due to movement of fluid from intravascular to extravascular space and endocrine-related effects[21]. Intracranial pressure (ICP) does not appear to be pathologically elevated[22], however a sustained increase in intraocular pressure (IOP) has been noted with respect to a standing position on Earth[23,24]. In both ICP and IOP, diurnal variation with postural changes, which occur naturally on Earth, do not take place in microgravity[1]. On a longer-term scale, the lack of gravitational stress can cause atrophy of cardiac muscles[25], altered vascular and microvascular compliance[6,26], and there exists conflicting evidence of impaired autonomic response[27–30].

On Earth, the heart is maintained by the work required to return venous blood to the heart in order to maintain arterial pressure. Further, when standing, the heart must act against the gravitational vector in order to pump blood to the brain. In microgravity, there is no significant gravity, therefore less contractility is required to send blood to the head or provide adequate venous return. As a result, the heart can shrink by as much as 8-10% in just 10 days[32]. After spaceflight, a decrease in stroke volume combined with an increase in sympathetic nervous activity has been

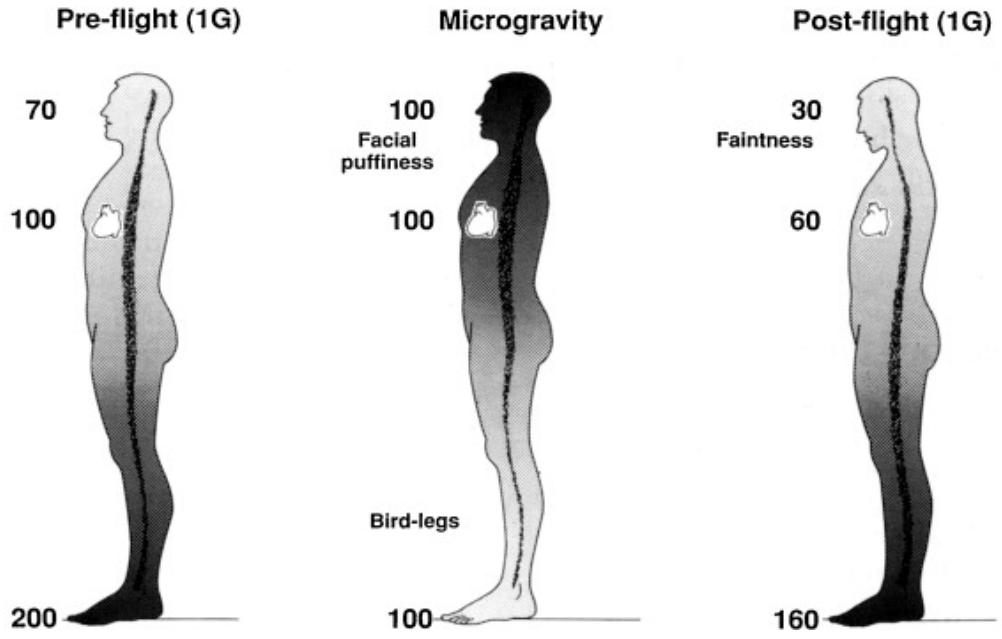

Figure 2.1: Diagrammatic representation of the hemodynamic fluid shift that occurs in microgravity. Pre-flight, the majority of blood is pooled in the lower venous system. In microgravity, the removal of hydrostatic pressure gradients leads to a cephalad fluid shift; over time, this shift promotes a reduction in circulating blood volume. Post-flight, the return of hydrostatic pressure gradients in combination with reduced blood volume and cardiovascular deconditioning can lead to orthostatic intolerance. Image reproduced from Watenpaugh and Hargens[31].

observed, combined with increased vascular resistance and reduced vasoconstriction. In particular, orthostatic hypotension is observed in 64% of astronauts after even short duration space flights[33]. The NASA Human Research Roadmap characterizes the risk due to cardiac deconditioning in the form of a directed acyclic graph (DAG)[34]. The cardiovascular risk DAG connects the causes of cardiovascular degradation with potential adverse mission and crew outcomes, and links to other risks in the Human Research Roadmap. Further, cardiovascular changes are also associated with one other Human Research Roadmap risk and one concern. These are the risk of spaceflight-associated neuro-ocular syndrome (SANS) and the concern of venous thromboembolism (VTE). Both of these risks/concerns have their own DAGs. All three are described below.

2.2.1 Risk of Cardiovascular Adaptations Contributing to Adverse Mission Performance and Health Outcomes

The cardiovascular risk DAG is presented in Figure 2.2. In this DAG, yellow nodes represent spaceflight hazards, blue nodes represent contributing factors, blue nodes containing a black vertical line represent mission level outcomes, light grey nodes represent links to other human systems risks, and dark grey nodes represent exogenous contributing factors. Green edges represent causal links and black edges represent causal links from exogenous nodes. The cardiovascular risk DAG incorporates three former risks into a single risk to the cardiovascular system itself[34].

There are two principal impacts of the cardiovascular adaptive response. First, from a medical perspective, a weakening of the cardiac system may lead to increased risk of cardiovascular disease[2] or the manifestation of previously asymptomatic pathologies[35]. The impaired cardiac function may also lead to reduced aerobic fitness and impaired organ perfusion, impacting operations where a high level of physical exertion is required (for example extravehicular activity)[36]. The medical illness node in the DAG captures a range of medical conditions including dysrhythmias, myocardial infarction, and vascular conditions, which may influence crew performance and long term health outcomes. The second impact occurs during a gravitational transition, either a return to Earth gravity or to a reduced planetary gravity. Cardiac deconditioning in space leads to an increased risk of orthostatic intolerance due to changes in organ perfusion, particularly in the brain. Whilst in standard nominal returns from the International Space Station (ISS), a well-trained medical ground-crew can limit the risk, this could be hazardous to crew health in an emergency landing situation or a number of off-nominal situations where a high level of crew physical activity is required immediately on landing. Importantly, with plans for the return of long-duration exploratory spaceflight to the Moon and Mars, at the destination surface, there will not be a ground-crew on standby to offset the risks of astronaut incapacitation. Further, in particular for Mars missions, the transit duration is longer, and mass and volume constraints may not permit the same level of countermeasures on board the transit vehicle in order to limit the scale of the degradation[37,38].

Finally, whilst government-selected astronauts are subject to exacting physical and health re-

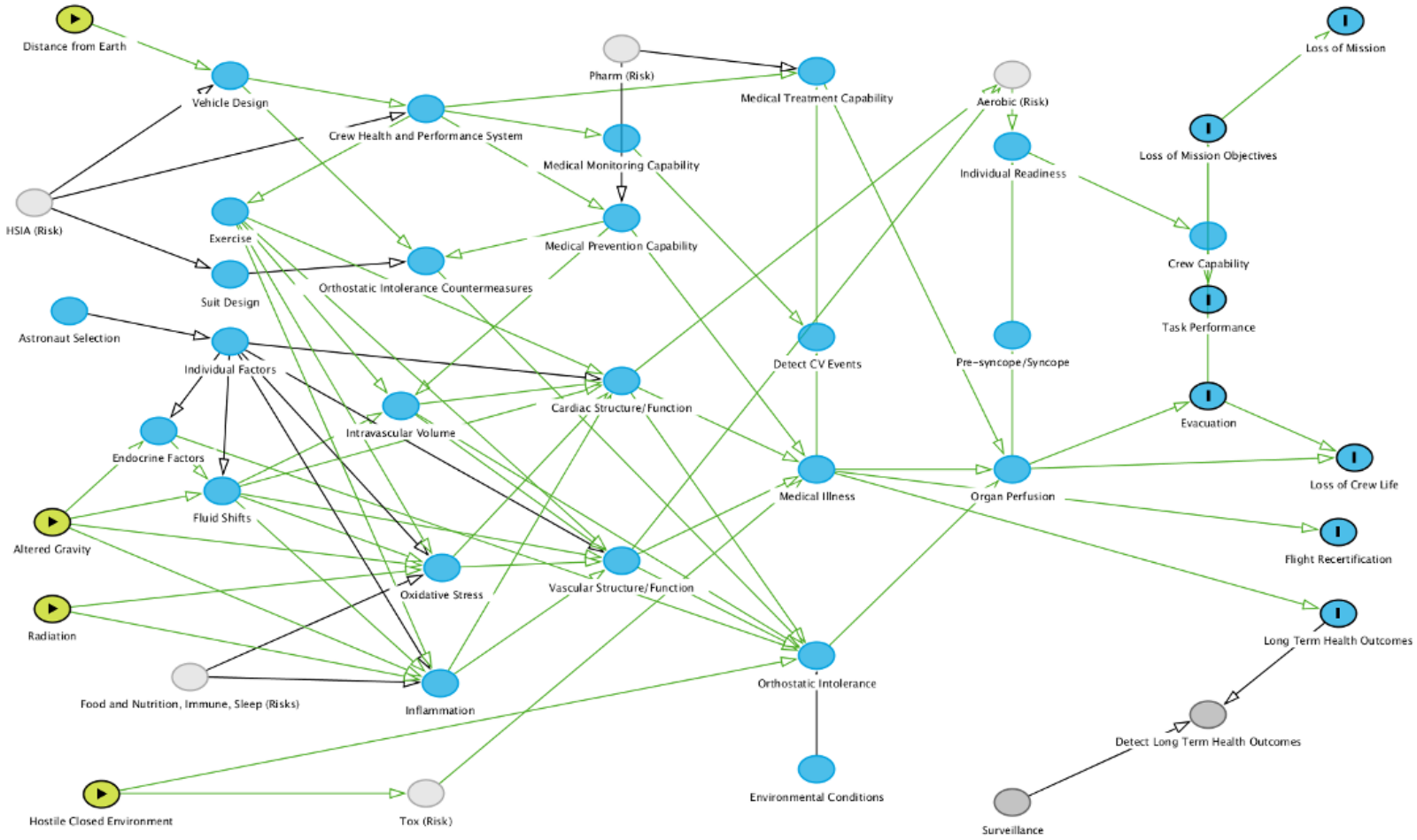

Figure 2.2: Directed acyclic graph (DAG) visualizing the risk of cardiovascular adaptations contributing to adverse mission performance and health outcomes. See text for descriptions of the symbology. Image reproduced from Antonsen *et al.*, 2022, NASA/TP-20220015709[34].

quirements to reduce the risk of medical emergencies, we are now beginning to see a large scale increase in the number of commercial astronauts on either suborbital or orbital flights. Although there are medical standards in place for commercial crew[39,40], they are not the same standards as government astronauts[41]. Further, the demographic for commercial crew is dependent on who can afford the trip, thus exposing a generally older and much broader spectrum of the population to the spaceflight environment. These crew will all have unique medical histories, and there is the potential for travelers with previously undetected (or even known) cardiac conditions or comorbidities to be subjected to the physiological stresses and orthostatic challenges of spaceflight, including the major gravity transitions on launch and landing. Beyond short suborbital hops, with plans for commercialization of orbit (space hotels etc.), the problem becomes even more pronounced, particularly if commercial crew members do not follow the same exercise protocols.

In summary, cardiovascular degradation has the potential to present a significant impact on crew health and operations during long duration and/or commercial space missions. Future space missions will require a careful analysis and risk management of cardiovascular degradation due to changing crew demographics and mission profiles.

2.2.2 Risk of Spaceflight Associated Neuro-ocular Syndrome (SANS)

The SANS risk DAG is presented in Figure 2.3. Symbology is identical as Figure 2.2, however in addition, dashed lines represent hypothetical causal links.

SANS is a collection of ocular pathologies that can occur in spaceflight. Initially identified in 2011 and termed visual impairment intracranial pressure (VIIP), the symptoms were recognized in seven US astronauts after ISS stays. These symptoms included disc edema, globe flattening, choroidal folds, and decreased near vision (a hyperopic shift)[42]. Diagnoses was based on papilledema Frisén grades with five classes. Subsequent investigation revealed that Russian cosmonauts had experienced similar symptoms. Mader *et al.* also examined 300 post-flight questionnaires and discovered that 29% of short duration astronauts and 60% of long duration astronauts had experienced some form of visual change. Additional ocular manifestations including cotton wool spots, and nerve fiber layer thickening have also been reported, although these no longer

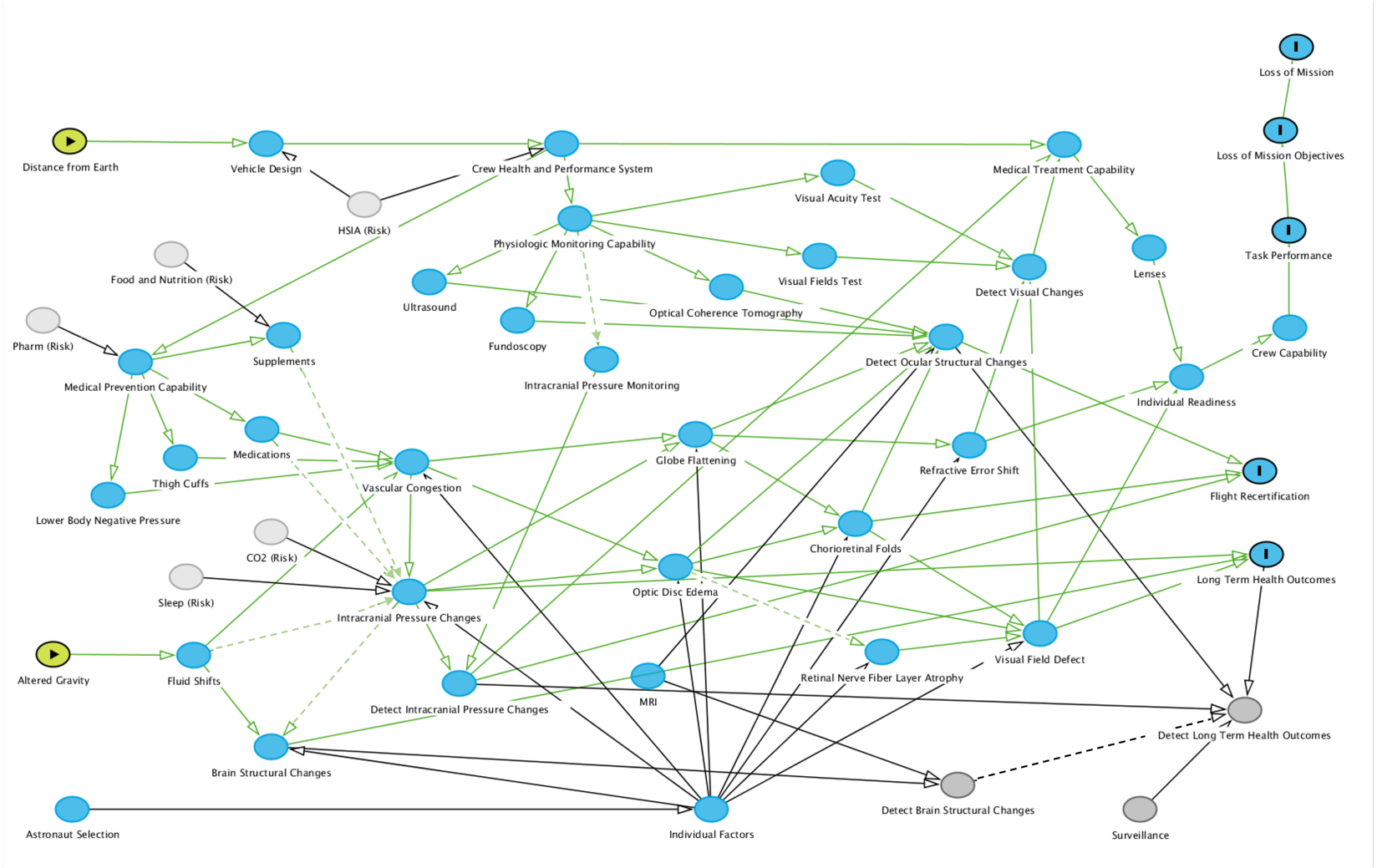

Figure 2.3: Directed acyclic graph (DAG) visualizing the risk of spaceflight-associated neuro-ocular syndrome (SANS). See text for descriptions of the symbology. Image reproduced from Antonsen *et al.*, 2022, NASA/TP-20220015709[34].

fall under current clinical guidelines for SANS[43]. Critically, in some cases, the symptoms did not resolve on return to Earth[44,45].

Early hypotheses posited that VIIP was related to increased ICP due to the cephalad fluid shift in microgravity. The similarity to terrestrial idiopathic intracranial hypertension (IIH) was noted, although some classic symptoms of IIH were not present, including chronic headaches, diplopia, transient visual obscurations, and pulse-synchronous tinnitus[46]. Due to uncertainty as to the role of ICP, the name was changed to SANS. Current diagnosis is still based on papilledema and officially stands at 16% of crewmembers based on the NASA evidence report of ISS Expeditions 1-48[47,48]. However, 38-51% of crewmembers developed one or more of the findings associated with SANS[47], questioning the need for a better diagnostic methodology.

NASA currently classes SANS as one of the "Red Risks" for the Human Research Program, requiring mitigation for deep space journey/habitation and planetary design reference missions (DRM)[47]. Overtime, multiple competing (or complementary) hypotheses have emerged as to the pathogenesis of SANS. These include: ICP; IOP and the pressure differential across the lamina cribrosa[49]; body weight[50]; ocular perfusion pressure (OPP)[1]; genetic factors such as the presence of certain biomarkers[51] and/or the One-Carbon metabolism[52,53]; spaceflight exposures such as elevated atmospheric carbon dioxide[54,55] or radiation[56,57]; diet, sodium and exercise factors[58]; and structural brain changes[59]. Many of these hypotheses are captured in Figure 2.3.

Two previously unconsidered contributing factors were considered in this research. First is the role of ocular perfusion pressure (OPP). Changes in OPP due to changes in gravity, in combination with the other hypotheses presented, is one of the most recent arguments as an important factor in the development of SANS[1]. In this research, we demonstrated that OPP has a dependency on the gravitational environment. Of note, OPP (defined as the difference between mean arterial pressure at eye level and IOP, $OPP = MAP_{eye} - IOP$) is elevated in head-down tilt compared to the baseline value in a supine posture, since IOP is more gravitationally dependent than MAP_{eye}. Further, case studies of terrestrial elevated OPP (for example due to traumatically induced ocular hypotony) exhibit identical symptoms to SANS, including papilledema and globe flattening[60] (Figure 2.4).

Second, we consider the role of body weight and external tissue pressures as a contributing factor in the development of SANS. Buckey *et al.* demonstrated the relationship between body weight and IOP changes in microgravity[61], suggesting that preflight body weight and anthropometric factors may predict microgravity-induced ocular changes. Buckey further hypothesizes that the removal of hydrostatic gradients reduces transmural pressure at the rear of the eye leading to the ocular remodeling observed in SANS, and that this reduction in transmural pressure is greater in subjects with a higher preflight body weight[50].

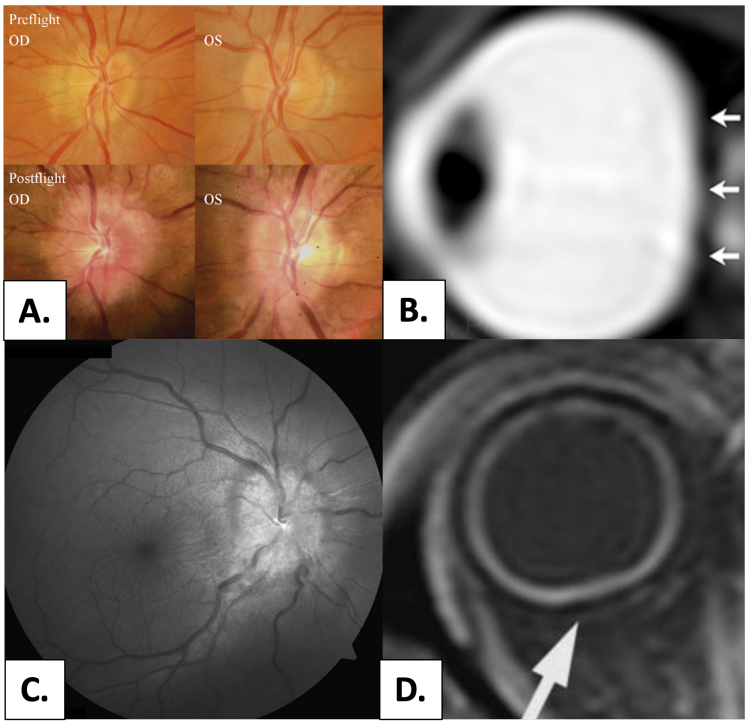

Figure 2.4: Papilledema (**A** and **C**) and globe flattening (**B** and **D**) in case reports of SANS (**A** and **B**)[42] and traumatically induced ocular hypotony (**C** and **D**)[60]. Image modified from Mader *et al.*[42] and de Guimarães *et al.*[60].

In order to further investigate the hypothesis that OPP may be linked to the development of SANS, as well as to investigate the potential efficacy of countermeasures, it is necessary to quantify the response of both IOP and cephalad hemodynamics in altered gravity environments. Whilst we

are unable to remove tissue weight in terrestrial studies, we consider this through computational modeling.

2.2.3 Concern of Venous Thromboembolism

The final concern due to cardiovascular changes in spaceflight is the recently identified concern of venous thromboembolism events (VTE). The associated DAG is presented in Figure 2.5.

More recently, studies have reported alterations in jugular venous return, including flow stasis and, in some cases, flow reversal[12,62]. The spaceflight environment also increases hypercoagulability and endothelial dysfunction in the vascular system[11,63]. In particular, hematologic index alterations such as changing hematocrit in response to hypoxia and atmospheric conditions can lead to blood viscosity changes, which affect coagulability. Further, oxidative stress and/or psychological stress can induce endothelial damage through inflammation[34]. In combination with flow stasis, these factors increase the thrombotic risk of spaceflight via Virchow's Triad[10]. Significantly, at least one case study has reported the clinical manifestation of venous thrombosis occurring in an astronaut onboard the International Space Station (ISS)[9]. Flow stasis and venous thrombosis in the upper body presents a previously unidentified and potentially serious medical risk to both professional and recreational astronauts[13]. Increased thrombogenicity could lead to embolic events on return to a gravitational environment if preformed thrombi are dislodged during reentry and landing[10]. With the growth of commercial spaceflight, recreational astronauts are likely to be particularly at risk due to the possibly reduced medical standards and the possibility for participants with multiple pre-existing comorbitidies and/or undiagnosed asymptomatic cardiovascular pathologies to travel to space[64–66].

2.3 Current Countermeasures

Multiple countermeasures are currently in use on the International Space Station in order to maintain astronauts' cardiovascular health. These countermeasures are generally specifically focused on either the cardiovascular system alone, or the cardiovascular and musculoskeletal systems together, rather than functioning as truly system-integrated countermeasures.

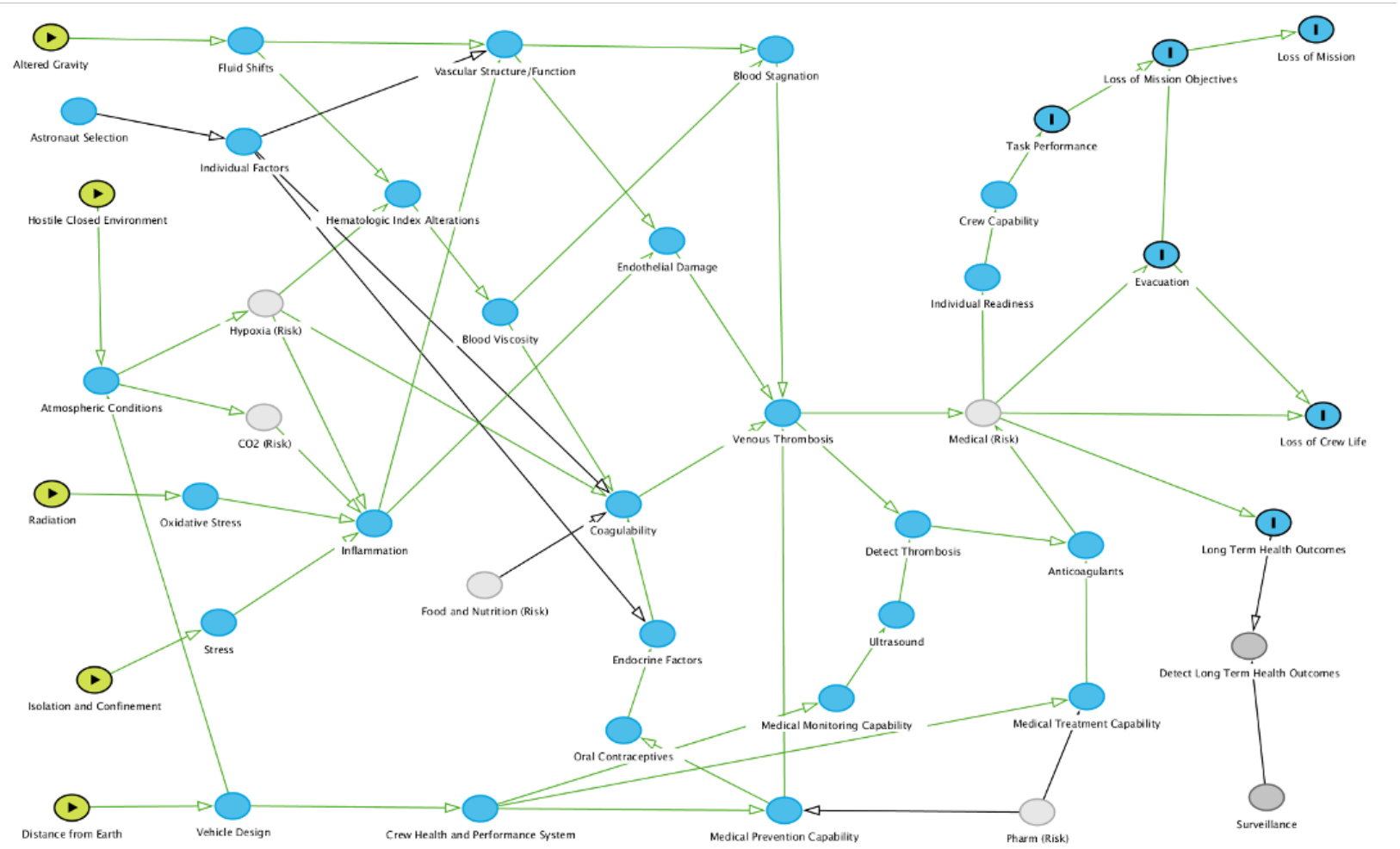

Figure 2.5: Directed acyclic graph (DAG) visualizing the concern of venous thromboembolism (VTE). See text for descriptions of the symbology. Image reproduced from Antonsen *et al.*, 2022, NASA/TP-20220015709[34].

The primary countermeasure is exercise. Current protocols dictate that astronauts exercise for around 2.5 hours each day[38,67]. The exercise protocols comprise of a mixed set of aerobic, anaerobic, and resistive exercises using three devices, shown in Figure 2.6: the advanced resistive exercise device (ARED – a system to simulate the free weight exercises, including squats, deadlifts, and calf raises using vacuum tubes and flywheel cables), the Treadmill with Vibration Isolation Stabilization System (TVIS - multiple versions have been flown including the Combined Operational Load-Bearing External Resistance Treadmill – COLBERT), and the Cycle Ergometer with Vibration Isolation Stabilization System (CEVIS)[68].

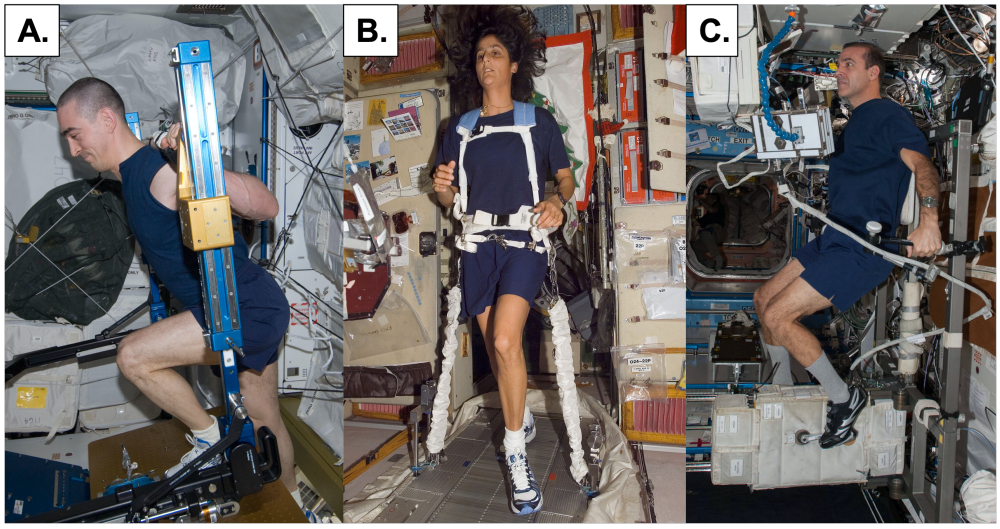

Figure 2.6: Exercises devices currently in use on the International Space Station (ISS). **(A)** Advanced resistive exercise device (ARED); **(B)** Treadmill with Vibration Isolation Stabilization System (TVIS); **(C)** Cycle Ergometer with Vibration Isolation Stabilization System (CEVIS). All images credit: NASA.

Other countermeasures are generally pharmacological[35]. Existing and proposed mechanisms to counter hypovolemia include fludrocortisone[69,70] and salt loading[71]. Pharmacological solutions to preserve vasoconstriction include midodrine and vasopressin[69,70]. Fluid loading has been used by the US space program to prepare astronauts for re-entry, decreasing the risk of orthostatic hypotension[72]. However, physical activity remains the primary countermeasure with the least side

effects, aside from the time penalty.

2.4 Proposed Countermeasures

Two of the most promising countermeasures proposed to prevent or decrease cardiovascular deconditioning in space are Lower Body Negative Pressure (LBNP) and Short Radius Centrifugation (SRC).

2.4.1 Lower Body Negative Pressure

LBNP is the application of a pressure below atmosphere to a subject's lower half. Military fighter pilots often employ positive pressure g-suits, which combat g-force induced loss of consciousness (g-LOC) by applying external pressure to the abdomen and legs, restricting blood pooling in the lower body during high-g maneuvers. In contrast, LBNP works in the opposite fashion, by using negative pressure to draw blood from the head, counteracting the cephalad fluid shift induced by reduced gravity. The pressure gradient created by LBNP forces the heart to exert additional work to return venous blood from the lower body, thereby reducing cardiovascular deconditioning. The reduced venous pressure at the heart leads to central hypovolemia, causing baroreflex activation to increase neurohumoral-mediated heart rate and vasoconstriction[73].

The first paper on the effects of LBNP was published in 1965[74]. Gilbert and Stevens claimed that -60 mmHg LBNP had a similar cardiac response to 90° of tilt without decreasing cerebral blood pressure, thus preserving baroreceptor response[75]. Pre- and post-flight use of LBNP during the Apollo program with –50 mmHg in a ramp protocol over 15 minutes was common for testing of orthostatic intolerance[76]. The first in-flight use of LBNP occurred during the Skylab program in 1973-74 (Figure 2.7). In this protocol, implemented every 2-3 days, calf volume increases were induced by LBNP[77], and the cardiovascular response in microgravity was demonstrated to predict the degree of post-flight orthostatic intolerance[78]. Simultaneously, the United Socialist Soviet Republic (USSR) first used in-flight LBNP with the Veter device on Salyut-1 in 1971[79]. The Chibis LBNP suit was subsequently developed by the Soviet Institute of Biomedical Problems (IBMP) and used on Salyut flights, Mir, and ISS[79]. Most recently, the Chibis-M suit was developed in 2012

for use on the ISS[80] (Figure 2.8). The Chibis protocol developed by IBMP is short, consisting of 2 min at –25 mmHg followed by 3 min at –35 mmHg[81]. This contrasts with the longer soak protocols (–30 mmHg for 4 hours) used the day before landing on some shuttle flights[80]. Chibis is used both to evaluate other countermeasures (i.e., exercise, pharmocologicals), and towards the end of missions as a countermeasure in itself for post-flight orthostatic intolerance[80].

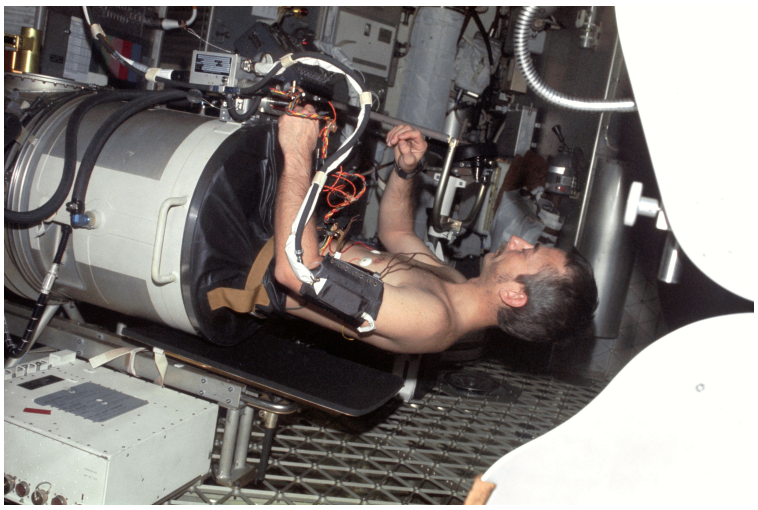

Figure 2.7: Astronaut Owen Garriott in a lower body negative pressure (LBNP) chamber on Skylab 3 (1973). Image credit: NASA.

In the spaceflight environment, some of the functions that an LBNP device could perform include: the reduction of the cephalad fluid shift[82]; when combined with exercise, the simultaneous stress of the cardiovascular and musculoskeletal system[83]; the reduction of the susceptibility to orthostatic intolerance prior to returning to a gravitational environment[84–86]; or the decrease of cerebrospinal fluid pressure on the optic nerve sheath[87]. Terrestrial studies have shown a decrease in intracranial pressure[88].

There are also many terrestrial uses for LBNP. Goswami *et al.*[73] detail many use cases, including assessment of autonomic function, screening pilots, or analyzing heat stress, shock, and central volume expansion. Military medicine makes regular use of LBNP to simulate hemorrhage[89,90]. Further, from a practical perspective, the capability of LBNP to reduce intracranial pressure has

Figure 2.8: Chibis-M lower body negative pressure (LBNP) device. Image credit: NASA.

obvious applications in cranial trauma[88,91].

There is a renewed interest in LBNP both as a volume efficient countermeasure against cardiovascular deconditioning, but also to study the etiology of, and as as a potential countermeasure against, SANS (see discussion below)[92]. However, the application of LBNP as a countermeasure for SANS is not certain. If LBNP lowers intraocular pressure more than intracranial pressure, it may even exacerbate the issue by increasing the translaminar pressure gradient[93,94]. Further, LBNP has the potential to lower IJV flow, which may alter the recently identified risk of thrombosis[9,12,92,95]. Thus, in order to fully develop effective protocols, it is necessary to have a complete and quantitative understanding of the physiological fluid shift response of LBNP. Thus, by measuring the cardiovascular response to a graded LBNP protocol, we are able to map the dynamic fluid changes and compare them between different levels of altered gravity. This dose-response can provide insight into which levels of LBNP are effective at reproducing desired hemodynamic effects.

2.4.2 Artificial Gravity

Artificial gravity encompasses any means of generating a gravitational field in space. Artificial gravity in spacecraft has been a staple of science fiction for many years, although many proposed solutions lie outside the realm of science. Artificial gravity is a multisystem countermeasure; by reproducing Earth-like (i.e., 1g) or partial gravity conditions in a spacecraft, the physiological systems still need to exert the same or similar effort to Earth conditions. Thus, they do not experience the same level of deconditioning[96]. There are two principal forms of space-based artificial gravity: linear and centrifugal. Both rely on the relativistic principle of the equivalence of gravitational and inertial mass. Linear artificial gravity can be generated by constantly accelerating a spacecraft at a given rate along a trajectory[97]. The propellant mass required to achieve the level of thrust required for such a trajectory means that such a countermeasure is currently challenging. By contrast, artificial gravity generated by centrifugation uses a rotational motion to generate a centrifugal force, which is experienced as gravity by a rotating subject. Centrifugation could be on a large scale (e.g., a spinning habitat module on a spacecraft, or even an entire rotating spacecraft) or on a smaller scale[98].

The history of artificial gravity dates back to Konstatin Tsiolkovsky in 1883 and has been a staple of early space habitat concepts[98]. Hugely popularized by Clarke and Kubrick in the novel and film '2001: A Space Odyssey' (both 1968)[99,100] (Figure 2.9), rotational artificial gravity viewed as practically a necessity by both futurists and engineers such as O'Neill, Korolev, Noordung, and von Braun[98]. The first serious technical proposals were conducted by NASA and the American Society for Engineering Education (ASEE) in 1975 and presented in 'Space Settlements: A Design Study' by Johnson and Holbrow (1977)[101]. However, despite continued scientific interest, budgetary constraints have principally limited actual in-flight artificial gravity experience to animal experiments[98]. In this context, there have been a number of studies on fish, rodents, and turtles as well as smaller microorganisms and organic matter. In particular, studies on rodents have repeatedly demonstrated that artificial gravity can act as a countermeasure against cardiovascular and musculoskeletal deconditioning[102–104], although some studies have noted adverse effects on

visual, vestibular, and motor coordination[98].

Figure 2.9: Artificial gravity in science fiction: Astronaut Dave Bowman runs around the spinning habitat of Discovery One in Clarke and Kubrick's 2001: A Space Odyssey (1968). Image credit: Metro-Goldwyn-Mayer[100].

Human subjects experiments have been limited to a few anecdotal episodes of self-generated artificial gravity (astronauts running around the inside of Skylab), along with incidental results from neurovestibular studies. Of note, STS-42 included the Spacelab International Microgravity Laboratory (IML-1) mission, in which four subjects were rotated and experienced 0.22g $-G_z$ at the head and 0.36g $+G_z$ at the feet. In this case, the 0.22g stimulus was insufficient to provide a vertical reference in any test subject[105]. Later, in 1998, four subjects were tested at 0.5g and 1g for seven minute protocols and described a perception of gravity. It is currently unknown how the 'perception' of artificial gravity is related to its utility as a countermeasure. Interestingly, the four tested crewmembers exhibited an increased tolerance to orthostatic stress on landing, whilst the remaining three crewmembers all experienced orthostatic intolerance[98]. The significance of this finding is inconclusive without further testing. In past years there have been multiple plans to place a human-rated short radius centrifuge on the ISS. However, none have come to fruition due to various constraints including finance[106–108]. Multiple planned commercial space habitats may include designs for artificial gravity, once again bringing the concept closer to reality.

There is a complicated set of trade-offs related to the generation of artificial gravity by short radius centrifugation. In particular, the level of experienced gravity is produced through a combination of spin speed and radius according to Equation 2.1:

$$a_{centrifugal} = r\omega^2 \tag{2.1}$$

where r is the radius in meters, and ω is the angular speed in rad/s. The difference in radius between the subject's head and feet generates a gravity gradient given by Equation 2.2:

$$\frac{a_{head}}{a_{feet}} = \frac{r-h}{r} \tag{2.2}$$

where h is the subject's height. The second consideration is Coriolis acceleration. Any change in posture (either a large change such as standing up or sitting down, or a small change such as moving the head) induces a Coriolis acceleration of magnitude:

$$a_{coriolis} = 2\omega\dot{r} \tag{2.3}$$

where $\dot{r}$ is the rate of change of the magnitude of the position vector, in a perpendicular direction to the centrifugal acceleration. Since the Coriolis acceleration is independent of the radius, the only way to reduce it is to minimize the angular speed, requiring a larger radius to maintain the same gravitational field.

The physics of artificial gravity present a number of human factors considerations that must be considered. First and most important is the gravity level. Physiologically, what is the level of generated gravity required in order to act as a) an effective countermeasure to mitigate spaceflight deconditioning (cardiovascular and other systems)? Further, depending on how the artificial gravity is to be used operationally (i.e., what tasks must the subjects perform whilst experiencing artificial gravity), b) what level is useful or necessary from a utility standpoint? Based on Earth studies, Russian scientists have recommended that a minimum of 0.5g is required for a perception of well-being and normal performance over extended timescales[109], whilst astronauts may not be

able to perceive levels under 0.22g while in space[110]. Second, what level of coriolis acceleration is tolerable? Previous studies recommended that Coriolis acceleration be no higher than 25% of the artificial gravity level[111], however more recent studies have indicated that this is conservative and adaptation is possible[112–116]. Parabolic flight studies have indicated that motion sickness or disorientation due to Coriolis forces may be related to the total gravity, such that if less than 1g is generated, a higher proportion of Coriolis acceleration may be tolerable[117,118]. Finally, what is the influence of gravity gradient on both subject comfort and physiological response? Here, the limited number of studies with short radius centrifugation have precluded a systemic study of changing gravity gradient, although recent studies on short radius centrifuges at MIT[119,120] and :Envihab[121] have indicated that both physiological benefit and minimal subject discomfort are obtainable in the presence of a large gravity gradient.

Previous research on short radius centrifugation has focused on protocols both at rest[121] and in combination with exercise[119,120]. However, similar to LBNP, there has not been a systematic study quantifying the complete physiological response of the cardiovascular system to graded levels of generated gravity. In order to fully develop concepts both for countermeasure protocols and even structural designs of space-based centrifuges, it is necessary to have a deeper understanding of the physiological response to different levels of SRC-generated gravity and a quantitative framework to compare the cardiovascular effects of SRC to both constant gravity and other potential countermeasures such as LBNP.

2.5 Terrestrial Altered Gravity

In order to quantify the cardiovascular response to LBNP and SRC compared to changing the gravitational field, it is necessary to have a baseline that is possible to reproduce on Earth. Tilt studies are an important analog for the understanding of cardiovascular changes in altered gravity conditions. By changing the angle of tilt, we adjust the effective gravitational stress in the rostrocaudal G_z direction. Tilt studies are commonly used to mimic the cardiovascular and musculoskeletal effects of spaceflight on Earth. In particular, six degrees of head-down tilt (HDT) has been used as an analog for microgravity conditions in multiple studies; including studies of the

acute effects of tilt[1,122–127], and long duration HDT bed rest[128–134]. Since, on Earth, gravity always acts in a vertical direction, when placed on a tilt table, the magnitude of the gravitational vector resolved in the subject's rostrocaudal axis can be calculated as:

$$g_{Tilt} = g_{Earth} sin\,(\theta) \tag{2.4}$$

where g_{Tilt} is the equivalent gravity in the rostrocaudal axis, g_{Earth} is 9.81 m/s^2, and θ is the tilt angle from the horizontal. Thus, for example, a tilt of 9.5° approximately represents Lunar gravity, while a tilt of 22.3° represents Martian gravity[126].

Whilst there are many examples of tilt studies in literature, most have focused on one or few physiological parameters, and considered limited tilt angles in either head-up tilt (HUT) or HDT. These include studies related to systemic[135–139], cerebral[123], ocular hemodynamics[124], and autonomic function[140]. Studies that cover both HUT and HDT (for example[139]) are generally limited to one or two tilt angles in each condition.

Gravity always remains present during tilt studies, therefore, by reversing posture between prone and supine we are able to effectively flip the gravitational vector. Through isolating changes purely due to this reversal of the gravitational vector, we may be able to gain some insight into the importance of tissue weight and/or the effects of thoracic pressure on gravitational hemodynamics[61,141]. A limited number of studies have considered differences between supine and prone postures during tilt[1,142], and such changes have been demonstrated to influence regional hemodynamics[143–145].

Tilt studies also have important application outside of human spaceflight. Multiple surgeries including lower abdominal surgery, central venous catheter placement, and minimally invasive glaucoma surgery are often performed in the Trendelenburg position (i.e., 15-30° HDT) to facilitate access to pelvic organs and/or improve surgeon positioning (Figure 2.10). However, there is controversy over the efficacy of this positioning and its potential adverse complications[146–148]. Similarly, the use of a Wilson frame (or equivalent) in back surgery places the patient in a prone position where the head is hydrostatically lower than the heart[149,150]. A greater understanding of the

hemodynamic and operative response to such conditions may improve perioperative management and clinical decision making[151].

Figure 2.10: Trendelenburg position used during lower abdominal surgery, central venous catheter placement, gynecological surgeries, and minimally invasive glaucoma surgery. Image credit: Steris Healthcare[152].

Understanding the quantitative physiological response to altered gravity through a tilt paradigm is important in itself, but can also be directly beneficial to the development of countermeasures. As discussed, there are currently open questions as to the levels of countermeasures (e.g., LBNP or SRC) that should be used in spaceflight protocols. Deeper knowledge of the equivalence between these altered gravity environments (i.e, what level of LBNP or SRC is functionally equivalent to a given tilt angle induced altered-gravity) can provide informative knowledge for the development of protocols[153,154]. Thus, in the context of this study, tilt acts as the baseline from which to compare and contrast the efficacy of the two previously described countermeasures.

2.6 Sex Differences

To date, the majority (88.5%) of astronauts, both US and international, have been male[ii]. Future space flight missions will see an increase in the number of female crew members. In the last NASA astronaut selection, 40% of the selected astronaut candidates were female. It is well established in literature that males and females exhibit differing physiological responses to both cardiovascular stress and aging[155–159]. Furthermore, it is equally established that there is a significant effect of sex on population means for a variety of cardiovascular parameters. These differences can either be based purely on allometry and relative body size (e.g., total blood volume, vascular length), but also related to vascular compliance and musculature. To cite two examples, Maffessanti *et al.*[160] found that sex was highly significant in studies of right ventricular parameters, while Monahan and Ray[161] also noted sex differences in venous compliance. These differences may influence cardiovascular adaptations to microgravity. Platts *et al.* highlight a number of identified research priorities that should be considered related to sex and cardiovascular adaptation to spaceflight. These include sex-specific mechanisms of autonomic regulation (including the effect of estrogen and other hormone levels), allometric differences (e.g., center of gravity), and sex-specific effects on vascular aging mechanisms as a predictor of cardiovascular risk and mortality[162].

Tilt studies have had mixed conclusions on the effect of sex in cardiovascular response. Females are more susceptible than males to orthostatic intolerance[162]. Some studies (e.g., Arzeno *et al.*[163]) noted differences in baroreflexive control of blood pressure between males and females. On the other hand, Patel *et al.*[164] found no significant effect of gender on autonomic indices in a protocol involving HUT, HDT, and lower body negative pressure.

With respect to SANS, there may also be a sex difference in the the pathophysiology. Contrary to previous reports[47], SANS has now been diagnosed in both male and female crewmembers[48]. To date, the majority of clinical diagnoses have occurred in males due to the larger sample size[165]. As far as the relationship between IOP and the pathoetiology of SANS, there also is conflicting evidence on the role of the menstrual cycle in IOP variation. Adhikari *et al.*[166] found significant

[ii] 65 females had flown in space out of 566 people total as of June 2020.

influence of menstrual phase on measurement of IOP, whilst in a previous study, Qureshi *et al.*[167] found the variation to be statistically insignificant. The hypothesis of body weight as a causal factor for SANS would potentially also skew the distribution of cases towards male astronauts[50].

In summary, the effect of sex-differences in cardiovascular response to altered gravity is an important consideration. When examining the quantitative dose-response of any given cardiovascular parameters, sex should be considered as an effect to determine whether or not there is a significant difference between the male and female response.

2.7 Computational Modeling

Computational modeling of physiological systems can provide further insight into their behaviour where experimentation is prohibitive, either due to cost or technological constraints. Even where a protocol can be performed, modeling can quickly provide insight into detail where measurement is difficult. For example certain regional blood flows. As Heldt succinctly summarizes: "the physiological interpretation of limited experimental data can benefit substantially from the concomitant use of a reasonably complete mathematical model"[168]. NASA uses a large multi-system model in the form of the digital astronaut project (DAP), which has replicated the cardiovascular results found by a number of studies[36,169,170]. Since Guyton's early models[171,172], a variety of modeling techniques have been used to investigate various aspects of the cardiovascular system. These techniques cover a range of functions, including investigating the effects of exercise[120,153], microgravity[169], head-up tilt[173–175], lower body negative pressure[173,176,177], centrifugation[154], deconditioning[178], and postural changes[1,179–181]. Thus, modeling techniques allow us to expand beyond the limits imposed by human experimentation and therefore, to make predictions on the risk of orthostatic intolerance, the efficacy of countermeasures, and the variation in responses elicited by different individuals.

In general, models are designed to perform a specific function, and caution should be taken extrapolating performance to scenarios outside of the designed range. Furthermore, the principle of "garbage in, garbage out" applies particularly with the selection of model parameters. This creates a challenging scenario as 10 different literature sources could give 10 relatively different ranges

for a particular physical parameter, and sometimes they must be estimated based on animal studies. The danger here can be mitigated with a sensitivity analysis to determine the most important parameters.

The cardiovascular system in altered gravity environments has previously been modeled by Heldt[168,173] as a 21-compartment lumped-parameter hemodynamic transport model incorporating detailed cardiac function, systemic circulation, pulmonary circulation, and two control systems (the arterial baroreflex and cardiopulmonary reflex). Whilst several other cardiovascular models had been previously designed to look at the effects of gravity (for example Melchior *et al.*, Croston *et al.*, and Peterson *et al.*[182–184]), Heldt built on much of their work to develop a comprehensive systemic model. He followed this with a detailed parameter estimation to develop a model that has been validated in a number of scenarios. Heldt's model was later extended first by Zamanian[185] to include the effects of centrifugation, and then by Diaz-Artiles[120,153,154] to incorporate the effects of exercise. This baseline model is introduced in Section 6.

3. DISSERTATION AIMS

3.1 Research Gaps

Review of literature highlights the following research gaps that will be addressed:

- Previous studies have demonstrated cardiovascular changes in both head-up and head-down tilt, however there is no literature quantifying these changes in a systematic manner in the form of dose-response curves.
- Similarly, whilst the effect of countermeasures such as LBNP and SRC have been considered, there is little comprehensive comparison of their effects on the cardiovascular system to the changes that take place in altered gravity (either through microgravity or through tilt).
- There have been few studies quantifying the differences between males and females in cardiovascular response to altered gravity environments, or more generally, individual variations in the systemic response to countermeasures.
- A number of systemic models of the cardiovascular system exist, although few include the effects of the cardiovascular control system (the arterial baroreflex and the cardiopulmonary reflex). Similarly, there are models of the cephalad hemodynamic system at multiple scales. However, there is no model that incorporates both a complete systemic hemodynamic model (including cardiovascular control) along with detail on cephalad hemodynamics and pressure changes.

3.2 Dissertation Aims

This dissertation addresses these research gaps through a combined experimental and computational modeling approach. The three aims of the dissertation are:

1. To empirically investigate the acute cardiovascular response to graded head-up and head-down tilt. In particular, the specific objectives are:

1.1 To generate dose-response curves for cardiovascular parameters, including the systemic circulation, the autonomic response, and head and neck hemodynamics over the range 45° head-up tilt (HUT) to 45° head-down tilt (HDT).

- *Hypothesis 1.1: Systemic hemodynamics will follow an approximately linear response to HUT and HDT in the range observed. The response of the autonomic system and head/neck will be non-linear.*

1.2 To quantify the differences between the supine (face-up) and prone (face-down) response to graded tilt as an analog to consider the influence of body weight on cardiovascular hemodynamics.

- *Hypothesis 1.2: Altered body positioning will influence cardiovascular response. In particular, the additional pressures due to body weight on the thoracic cavity in the prone position will impair baroreflex function and venous return.*

1.3 To quantify the difference between the male and female response to graded tilt.

- *Hypothesis 1.3: Anthropometric considerations will be the principal driving force between differences between males and females in cardiovascular response.*

2. To empirically investigate the acute cardiovascular response to graded lower body negative pressure (LBNP). In particular, the specific objectives are:

2.1 To generate dose-response curves for cardiovascular parameters, including the systemic circulation, the autonomic response, and head and neck hemodynamics over the range 0 mmHg to –50 mmHg of LBNP.

- *Hypothesis 2.1: Systemic hemodynamics will follow an approximately linear response to graded LBNP. The response of the autonomic system and head/neck will be non-linear..*

2.2 To quantify the multivariate relationship between systemic, autonomic, and head/neck cardiovascular parameters in graded LBNP.

- *Hypothesis 2.2: Cardiovascular variables should not be considered in isolation. In particular, a network structure exists between the parameters and latent subject characteristics (for example body weight) such that there is a relationship connecting all of the variables.*

2.3 To quantify the difference between the male and female response to graded LBNP.

- *Hypothesis 2.3: Anthropometric considerations will be the principal driving force between differences between males and females in cardiovascular response.*

3. To develop a cardiovascular model to capture the effects of tilt, LBNP, short-radius centrifugation (SRC), and microgravity on cardiovascular hemodynamics. In particular, the specific objectives are:

   3.1 To expand an existing cardiovascular model to incorporate detailed modeling of blood flow through the head and eyes.

   3.2 To incorporate the effects of tissue weight into a cardiovascular model in order to determine the influence of its removal in microgravity on cardiovascular hemodynamics.

   3.3 To validate the cardiovascular model with dose-response curves generated from experimental measurements of subjects in tilt and LBNP.

   3.4 To investigate the effects of SRC and microgravity on representative subjects.

Aims 1, 2, and 3 will be addressed in Sections 4, 5, and 6, respectively.

4. EXPERIMENT 1: TILT*

4.1 Motivation

The human cardiovascular system is strongly dependent on the gravitational environment. Changes in the gravitational vector influence the systemic circulation through mechanical and autonomic effects. Mechanically, any alteration in gravity causes redistribution of fluid volumes and dynamic pressures due to changing hydrostatic pressure gradients. For example, in weightless conditions, the total loss of hydrostatic gradients induces a cephalad fluid shift and a redistribution of fluid from intravascular to extravascular spaces. Amongst other acute effects, this fluid shift promotes venous return increasing stroke volume via the Frank-Starling mechanism and a change in compliance[188]. Other changes include a fall in interstitial fluid pressure[7], reduced systemic vascular resistance[6], decreased heart rate[189], slightly decreased systolic and diastolic blood pressures[6,190], and decreased central venous pressure[3]. Simultaneously, these acute dynamic pressure and volume changes influence autonomic receptors, including arterial baroreceptors in the carotid sinus and aortic arch, and cardiopulmonary receptors in the atrio-caval junctions, atrial and ventricular walls, and pulmonary vasculature[4]. On an acute timescale, autonomic response due to stimulation of the arterial baroreflex and cardiopulmonary reflex receptors leads to changes

*Part of this chapter is reprinted with permission from the following publications:

- Petersen LG, Whittle RS, Lee JH, Sieker J, Carlson J, Finke C, Shelton CM, Petersen JCG, Diaz-Artiles A. Gravitational effects on intraocular pressure and ocular perfusion pressure. *J Appl Physiol*. 2022;132:24–35.[1] Copyright 2022 by the American Physiological Society.
- Whittle RS, Keller N, Hall EA, Vellore HS, Stapleton LM, Findlay KH, Dunbar BJ, Diaz-Artiles A. Gravitational dose response curves for acute cardiovascular hemodynamics in a tilt paradigm. *J Am Heart Assoc*. 2022;11:e024175.[186] Copyright 2022 by The Authors.
- Whittle RS, Diaz-Artiles A. Gravitational effects on jugular and carotid characteristics in graded head-up and head-down tilt. *J Appl Physiol*. 2023;134:217–229.[187] Copyright 2023 by the American Physiological Society.

in sympathetic and vagal activity, further altering the homeostatic set points of the hemodynamic system. Chronically, longer durations in a reduced gravity environment can lead to overall cardiovascular deconditioning, atrophy of cardiac muscles, reduction in circulating fluid volume, and impaired autonomic response[191]. Together, these changes induce an elevated risk of syncope when subjected to orthostatic stress on return to a gravitational environment[192].

More recently, studies have reported alterations in jugular flow, including flow stasis and, in some cases, flow reversal[12,62]. The spaceflight environment also increases hypercoagulability and endothelial dysfunction in the vascular system[11,63]. In combination with flow stasis, these factors increase the thrombotic risk of spaceflight[10]. Significantly, at least one case study has reported the clinical manifestation of venous thrombosis occurring in an astronaut onboard the International Space Station (ISS)[9]. Flow stasis and venous thrombosis in the upper body presents a previously unidentified and potentially serious medical risk to both professional and recreational astronauts[13]. Increased thrombogenicity could lead to embolic events on return to a gravitational environment if preformed thrombi are dislodged during reentry and landing[10]. With the growth of commercial spaceflight, recreational astronauts are likely to be particularly at risk due to the possibly reduced medical standards and the possibility for participants with multiple pre-existing comorbidities and/or undiagnosed asymptomatic cardiovascular pathologies to travel to space[41,64–66]. Upcoming long duration exploration missions to the Moon and Mars will require significant time periods of weeks, months, or even years in altered gravity conditions. Thus, there is a need to develop novel countermeasures to counteract cardiovascular degradation or venous flow alterations, ensuring astronauts are healthy and fully operationally capable on return to a gravitational environment.

Tilt studies are an important analog for the understanding of cardiovascular changes in altered gravity conditions. By changing the angle of tilt, we adjust the effective gravitational stress in the rostrocaudal G_z direction. Six degrees head-down tilt (HDT) has been used as an analog for the cardiovascular and musculoskeletal effects of microgravity in multiple studies; including studies of the acute effects of tilt[1,122–127], and long duration HDT bed rest[128–134]. To date, most studies of

head-up tilt (HUT) or HDT have focused on one or few physiological parameters, and considered limited tilt angles. These include studies related to systemic [135–139], cerebral [123,193], ocular hemodynamics [124], and autonomic function [140,193]. Studies that cover both HUT and HDT (for example Lieshout *et al.* [139]) are generally limited to one or two tilt angles in each tilt condition. A limited number of studies have also considered differences between supine and prone postures during tilt [1,142]. Further insight into postural differences (i.e., supine versus prone posture) may lead to a deeper understanding of the importance of tissue weight on gravitational hemodynamics by isolating changes purely due to the reversal of the gravitational vector in the G_x axis [61]. Such changes have been demonstrated to influence regional hemodynamics [143–145]. Finally, limited studies have measured jugular characteristics in altered gravity environments [12,194,195]. However, at present there exist no predictive models for the expected jugular hemodynamic response to any given dose of gravity (including partial gravities). Thus, it is important to quantify jugular hemodynamics as a function of changes in the gravitational vector in order to inform the assessment of the pathogenesis of both spaceflight venous thromboembolism events and SANS.

There exists some controversy over how representative 6° HDT is as a spaceflight analog, due to differences in the physiological response compared to microgravity [128,196,197]. One example is the response of central venous pressure, which is observed to increase in HDT, yet decrease in microgravity [3,198]. Quantifying hemodynamics in a tilt paradigm is also informative for surgical applications on Earth, where HDT is used in a clinical setting. For example, Trendelenburg positioning is used to increase surgical access for a number of surgeries including abdominal and gynecological procedures [146–148]. Internal jugular vein cannulation is frequently used, both in routine surgery and Trendelenburg positioning, for hemodynamic monitoring and central venous access [199,200]. During venous cannulation, the size of the vein is important to minimize complications [201], and differences between the relative sizes of right and left side veins have previously been reported [202–204].

Cerebral venous drainage via the internal jugular veins is critical for regulation of intracranial pressure (ICP). In the upright position the jugular vein collapses, acting as a starling resistor to protect the cerebral and central venous systems from severe negative pressure due to their anatom-

ical position above the hydrostatic indifference point[12]. On Earth, diurnal variation and postural changes act as part of the regulatory system for ICP. Previous terrestrial head-down tilt bed rest and spaceflight studies[12,205] have suggested that the acute increase in IJVP compared to the 1g standing position due to weightlessness, and the removal of daily variation patterns caused by postural changes in a gravitational field, are related to the increase in ICP and transmural central venous pressure (with respect to the upright position) found during microgravity exposure[22,206]. These changes in cerebral pressures are likely part of the etiology of SANS[1]. Further, the engorgement of the jugular veins could suggest an increase in passive blood pooling in the upper body venous system[207]. Blood pooling, as an indicator of flow alterations, is related, via Virchow's Triad, to increased thromboembolic risk[208]. Our study aims to fully characterize the evolution of the carotid and jugular vessels pressure and area when systematically exposed to increasing HDT angles. We aim to generate terrestrial models that serve as a reference for spaceflight and that can be used to compare the magnitude of microgravity (or partial gravity) response. Our work also expands on previous work by Marshall-Goebel *et al.*[12] by capturing variation on both the left and right sides of the vascular system as well as in both supine and prone positions. We also consider a greater range of tilt angles.

Understanding the physiological response to altered gravity through a tilt paradigm can also be directly beneficial to the development of countermeasures[120,209]. For example, artificial gravity is one posited countermeasure for combating cardiovascular deconditioning. Whilst artificial gravity generated through short radius centrifugation creates a gravity gradient (as opposed to a constant gravity field), quantifying the baseline response to gravity through tilt can provide insight into what level of centrifugation should be targeted to provide a given physiological response[119,153,154,210].

The aim of this study is to construct dose-response curves to quantify the behavior of the cardiovascular system across a large range of HUT and HDT. These curves will encompass a wide range of hemodynamic and autonomic measures, as well as carotid and jugular venous characteristics, providing a holistic picture of cardiovascular circulation and control. While there have been many studies using tilt in specific angles (for example 6° HDT as a microgravity analog), it is

not currently possible to estimate the physiological response to any particular gravitational "dose". Thus, in this study we measure the acute response to altered gravity across a wide range of tilt angles (45° HUT to 45° HDT, supine and prone). Further, we use the experimental data to build hemodynamic, autonomic, and jugular/carotid gravitational dose-response curves, thus indicating the predicted response in a representative non-pathological population. We hypothesize that many of the relationships between tilt angle and a given systemic cardiovascular or autonomic parameter can be explained by linear models, but that the dose-response of the carotid/jugular will be non-linear. Together, these results lead to a greater understanding of the gravitational influence on the cardiovascular system, aiding in the future development of spaceflight countermeasures, as well as clinical applications. By placing subjects in both supine (face-up) and prone (face-down) positions, we can reverse the direction of the gravitational vector, gaining additional insight into the role of extravascular pressures on hemodynamic response.

4.2 Methods

4.2.1 Subjects and Study Approval

Twelve healthy, recreationally active male subjects between 23 and 33 years old were recruited from the Texas A&M University System to participate in the study. From the initial pool of volunteers, the age range of selected subjects was limited as much as possible to avoid confounding factors related to changes in the cardiovascular system with age. Sample size and the number of tilt angles required was determined based on a power curve analysis of pilot data. Subject characteristics (mean ± SD), including blood pressure at screening, are shown in Table 4.1. Prior to participating in the study, subjects completed a questionnaire designed to identify any exclusion criteria, including current use of any cardiac, blood pressure, muscle relaxant, anticoagulant, or stimulant medications, thyroid disease, chronic cardiovascular pathologies, extreme obesity, and history of hypertension. One subject was unable to complete one single condition (45° HDT, supine position) due to discomfort; however, he was returned to a head-up tilt position and experienced no lasting symptoms. The remainder of his data are included in the results. All other subjects

completed the full protocol and experienced no adverse effects. Each subject received written and verbal explanations of the study protocols and gave written informed consent to participate in the experiment. All procedures performed in the study were in accordance with the 1964 Helsinki Declaration and its later amendments. The study protocol was approved by the Texas A&M Human Research Protection Program with Institutional Review Board number IRB2020-0724F.

Table 4.1: Characteristics of the 12 recreationally active male subjects who participated in the study. Characteristics were recorded during baseline session prior to testing sessions. Data are reported as mean ± SD where appropriate. Race categories: W, White; B, Black or African American; A, Asian. Abbreviations: BMI, body mass index; SBP, systolic blood pressure; DBP, diastolic blood pressure.

Characteristic	**Value**
n	12
Race	W (8), B (1), A (3)
Age (years)	26.8 ± 2.9
Height (cm)	179.0 ± 8.3
Weight (kg)	84.7 ± 18.7
BMI (kg/m^2)	26.3 ± 4.9
SBP (mmHg)	129.5 ± 14.5
DBP (mmHg)	82.3 ± 6.5

4.2.2 Experimental Design and Testing Protocol

We implemented a counterbalanced, within-subjects, experimental design such that every subject experienced every tilt condition and posture. Subjects were tilted from 45° HUT to 45° HDT in two separate postures: supine (face-up) and prone (face-down). The procedure was identical for each posture. Experimental sessions took place on three separate days within a two-week period. In the first session, subjects gave informed consent and baseline measurements were collected in a seated posture. In the additional two experimental sessions, subjects were tested once in supine position and once in prone position (order counterbalanced). To control for potential circadian effects, all sessions were scheduled in the morning at approximately the same time. In addition,

subjects were asked to refrain from drinking caffeine and exercising prior to each test session.

In a single experimental session (supine or prone), subjects were placed on a tilt table (World Triathlon Corporation, Tampa Bay, FL) initially at 45° HUT. In the prone position, subjects rested with their forehead on a thin cushion in order a) to support the weight of the head and prevent excessive stress on neck musculature, b) to keep the cervical spine in an anatomically similar position to when supine, and c) to facilitate normal ventilation, with the mouth and nose slightly displaced from the tilt table. Continuous measurements of blood pressure and electrocardiography were recorded throughout the test. Subjects initially remained at rest for a period of six-minutes to allow any hemodynamic transients to settle. After the rest period, an inert gas rebreathing device was used to collect discrete measurements of cardiac parameters. Following this, a number of further measurements were collected from the subjects, including ocular tonometry, ultrasonography, and non-invasive measurement of internal jugular venous pressure. The total procedure at a single tilt angle lasted for approximately 12 minutes. Subjects were then tilted downwards 15°, and the entire process repeated, starting with the six-minute resting period. The total protocol included seven tilt angles: 45° HUT, 30° HUT, 15° HUT, 0° (horizontal), 15° HDT, 30° HDT, and 45° HDT. The procedure for the seated baseline conducted on the first experimental session was identical to the procedure for a single tilt angle.

4.2.3 Dependent Variables

Dependent variables include eight hemodynamic metrics, seven autonomic indices, and three measures related to the head/neck. The hemodynamic measurements considered were: 1) heart rate (HR, bpm); 2) stroke volume (SV, ml/beat); 3) cardiac output (CO, l/min); 4) total peripheral resistance (TPR, mmHg.s/ml); 5) systolic blood pressure (SBP, mmHg); 6) diastolic blood pressure (DBP, mmHg); 7) rate pressure product (RPP, mmHg/min), used as a metric for myocardial stress and energy consumption[211]; and 8) oxygen consumption (VO2, l/min).

Autonomic analysis was performed from measurements of heart rate variability (HRV) and baroreflex sensitivity. HRV analysis can be performed over short duration timescales, often of the order of five minutes, although shorter analyses have been used successfully to analyze autonomic

changes in parabolic flight over a single parabola[212]. In particular, two key classes of HRV indices exist[213]: time-domain measures and frequency-domain measures. Time-domain measures are metrics related to the variation in the intrabeat interval (IBI) between normal sinus beats (the NN interval). Frequency-domain metrics consider the distribution of IBI variation in the power spectral density of various frequency bands. Three time-domain and three frequency-domain indices were considered. The three time-domain indices were: 1) the standard deviation of the NN intervals (SDNN); 2) the root mean square of direct differences of the NN interval (RMSDD); and 3) heart rate variability triangular index (HRVTi). As a time-dependent measure of autonomic function, baroreflex sensitivity (BRS) was also included in this set of metrics. SDNN and HRVTi represent estimates of total heart rate variability incorporating sympathetic and parasympathetic activity[213]. RMSDD represents short term variability and thus, is closely correlated with vagal-mediated cardiac control[214]. Finally, baroreflex efferents translate into HRV via the cardiac sinoatrial node, providing blood pressure buffering and cardioprotection[215]. Thus, BRS represents a metric of total autonomic control over the cardiovascular system via the arterial baroreflex, with implications in the regulation of systemic fluid pressures[216,217]. The three frequency-domain indices were: 1) spectral power density in the low frequency (0.04–0.15 Hz) band (LF); 2) spectral power density in the high frequency (0.15–0.4 Hz) band (HF); and 3) the ratio between low frequency and high frequency power spectral densities (LF/HF). Following the recommendations of the Task Force of the European Society of Cardiology and the North American Society of Pacing Electrophysiology (TFESCNASPE)[213], LF and HF are shown in both absolute units (ms^2) and normalized units (LFNorm and HFNorm), which represent relative contributions of each power component in proportion to the total power minus the very low frequency (VLF, 0.0033–0.04 Hz) component. LF is used as a marker of sympathetic activity (particularly when expressed in normalized units), HF is closely correlated with vagal activity, while LF/HF represents sympathovagal balance[213].

Finally. the following metrics were collected related to cephalad blood circulation: 1) Common Carotid Artery Cross Sectional Area (A_{CCA}, mm^2, right and left side); 2) Internal Jugular Vein Cross Sectional Area (A_{IJV}, mm^2, right and left side); and 3) Internal Jugular Vein Pressure (IJVP,

mmHg, right and left side). Areas A_{CCA} and A_{IJV} were obtained using ultrasound (US) imagery (VScan Extend, GE Healthcare, Chicago, IL). Pressure measurements were collected using a non-invasive peripheral venous pressure measuring device (VeinPress, VeinPress GmbH, Münsingen, Switzerland) attached to the probe head of the ultrasound.

4.2.4 Instrumentation and Data Collection

Hemodynamic measurements were collected using two instruments, an Innocor inert gas rebreathing device (Cosmed: The Metabolic Company, Rome, Italy) and a Finapres NOVA (Finapres Medical Systems B.V., Enschede, the Netherlands). Full calibration was performed on devices daily, and ambient data calibrations were also performed prior to each subject test (mean ± SD: temperature 20.5 ± 2.0°C, relative humidity 53.9 ± 11.0%, pressure 767.2 ± 4.8 mmHg). Innocor rebreathes were performed at every tilt angle. The inert gas rebreathing method was used to obtain noninvasive measures of pulmonary blood flow by analyzing the changing concentrations of a soluble gas (nitrous oxide, 5%) and an insoluble gas (sulfur hexafluoride, 1%) in an oxygen-enriched air mixture over 5-6 breaths. The mixture is rebreathed using a bag for approximately 30 seconds. During the rebreathe, subjects inspired and expired at a rate of 20 breaths per minute, following this rhythm with a metronome (respiration at all other times was at a normal relaxed respiration rate). After each rebreathe, the gas concentration traces were visually inspected by a trained operator to ensure correct function of the device. The Innocor device was used to measure HR, SV, CO, and VO2. Further details on the inert gas rebreathing methodology can be found in Whittle *et al.* [126].

Finapres data (finger arterial pulse contour waveform and 5-lead electrocardiogram) were collected continuously throughout the protocol. Pressure was corrected to heart level with a hydrostatic height sensor placed laterally on the mid-coronal plane at the fifth intercostal space. At each tilt angle, the Finapres pressure waveform was calibrated with a discrete blood pressure measurement using a brachial sphygmomanometer. Finapres data were used to measure SBP, DBP, and RPP. Further, total peripheral resistance (TPR) was calculated by equation 4.1:

$$TPR = \frac{MAP}{CO} \tag{4.1}$$

using the mean arterial pressure (MAP) from the Finapres, and the CO from the Innocor. Autonomic indices were derived from the Finapres ECG trace and beat-to-beat RR interval. Calculations were performed automatically by the Finapres software. Three of the four time-domain measures (SDNN, RMSDD, and HRVTi), and all of the frequency-domain measures, were continuously calculated using a 300 s sliding window. The BRS measure used a 10 s sliding window to compute baroreflex sensitivity as the transfer gain of the cross-spectra between beat-to-beat systolic blood pressure and RR interval, resampled to 1 Hz[218]. After visual inspection of the traces, measurements from the Finapres (hemodynamic and autonomic) were averaged using a 95% trimmed mean during the entire sixth minute at each tilt angle to give a single value for each subject-condition. This ensured that there was no temporal overlap with the forced respiration rate imposed during the Innocor measurements, which could have influenced HRV.

Measurements of A_{CCA} were obtained from two four-second, 15 Hz US videos recorded in each experimental condition (i.e., angle-position-side combination), capturing a transverse view of the CCA. Measurements were collected approximately 30 mm inferior to the CCA bifurcation point (around the C3 vertebral level). These two video files were separated into 120 individual images (60 images per video). The images were processed using cell segmentation techniques: images were thresholded[219] and subsequently segmented using a watershed algorithm[220]. Each image was manually inspected and segmentation failures were discarded. The CCA was identified in each of the successfully segmented images based on pixel count. Finally, the A_{CCA} for each angle-position-side combination was calculated as the 20% trimmed mean of all the CCAs previously identified. The 20% mean includes the central 80% density mass in the calculation, ignoring the highest and lowest 10% of the data, respectively. Figure 4.1A shows a flow diagram of the A_{CCA} calculation algorithm.

In each experimental condition, ultrasound images of the IJV were collected using a transverse view at the same level as the CCA (i.e., C3 vertebra). All images were collected at end-expiration.

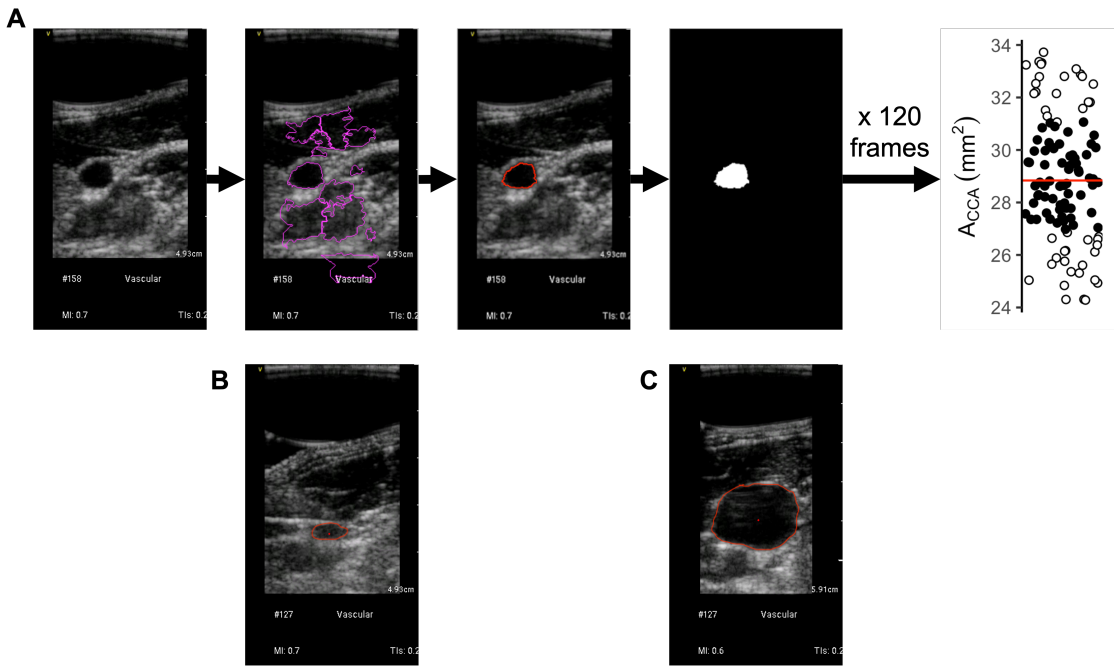

Figure 4.1: Methodology used to capture CCA and IJV cross sectional area. **(A)** Flow diagram for the common carotid artery (CCA) area, A_{CCA}, calculation algorithm. Individual frames of two, four-second, 15 Hz videos (60 frames per video, a total of 120 frames) are filtered and segmented to identify the CCA area based on pixel count. This process is repeated for all 120 available frames. Lastly, the A_{CCA} at each experimental condition (i.e., angle-position-side combination) is calculated as the 20% trimmed mean of all the CCAs previously identified. **(B-C)** Internal jugular vein (IJV) area, A_{IJV}, shown for the same subject in two conditions: **(B)** 45° head-up tilt (HUT) and **(C)** 45° head-down tilt.

Due to its irregular shape and varying size, A_{IJV} could not be obtained using the previously described segmentation methods that were used to calculate A_{CCA}. Instead, two trained operators, acting independently, manually identified and circumscribed the IJV on each image to calculate A_{IJV} based on pixel count. If the two measured areas from the different operators differed by less than 10%, the final A_{IJV} in that condition was calculated as the average of the two independently measured areas. However, if the measured area differed by more than 10%, a third operator repeated the circumscription and the final A_{IJV} in that condition was calculated as the average of the three independently measured areas (Figure 4.1B-C).

Internal jugular vein pressure, IJVP, was obtained by manually compressing the IJV with the VeinPress manometer attached to the head of the US. The VeinPress device was zeroed prior to

each measurement. Pressure was recorded at the point at which the walls of the IJV vessel were just about to touch each other. When this occurred, the pressure reading was allowed to stabilize for two seconds to counter any inertial effects. Two IJVP measurements were collected at each angle-position-side combination, and the final IJVP in that condition was calculated as the average of the two measurements.

4.2.5 Statistical Analysis

4.2.5.1 Systemic/Autonomic Measurements

Data from the hemodynamic measurements were distributed approximately normally at each tilt angle and position (supine or prone) combination, assessed using Shapiro-Wilk tests. Two-factorial linear mixed-effects models (LMMs) were used to assess the effects of angle and position on the hemodynamic measurements within subjects. Subjects were included as random factors with *Angle* and *Position* (supine or prone) as fixed factors. LMMs were fit using restricted maximum likelihood. Diagnostic plots for all models were examined visually to confirm normality of residuals, and homoscedasticity was assessed using Levine's test. Data related to the autonomic response were severely right-skewed, with multiple violations of normality. Since all autonomic indices used are bounded by $\in [0, \infty]$, and following a methodology used in multiple studies[221–224], data were fit to generalized linear mixed-effects models (GLMMs) with a gamma distribution and a log link (i.e., expected value of the dependent variable μ is given by $\log(\mu) = \eta$, where η is the linear predictor) using the same fixed (i.e., *Angle* and *Position*) and random (i.e., subjects) factors as the LMMs. GLMMs were fit to maximum likelihood estimated via adaptive Gauss-Hermite quadrature[225]. Diagnostic plots of all GLMMs were examined visually, and fit assessed using tests for dispersion, outliers, and distribution (Kolmogorov-Smirnof). LFNorm and HFNorm did not present the same heteroscedasticity so were fit with LMMs as per the hemodynamic parameters. Significant effects of *Angle*, *Position*, or their interaction were followed by post-hoc contrasts between the LMM/GLMM estimated marginal means (EMMs) and the seated baseline condition, which was used as the control condition. Significance was adjusted using Dunnett's many-to-one

comparison test ($\alpha = 0.05$)[226]. When only the factor *Angle* was significant, contrasts were performed disregarding the factor *Position* (i.e., supine and prone values were pooled). Further, when the factor *Position* was significant, a post-hoc contrast between supine and prone was performed excluding the seated baseline. If this contrast was significant, then further contrasts were performed between supine and prone at each tilt angle on the EMMs using Benjamini and Hochberg's correction for false discovery rates ($\alpha = 0.05$)[227].

Gravitational dose-response curves between 45° HUT and 45° HDT were constructed for each dependent variable by refitting the models (LMM and GLMM) without the seated baseline, using tilt angle as a quantitative continuous variable. Model fit was assessed as above. The following linear predictor (equation 4.2) was used to generate dose-response curves for each dependent variable measured:

$$\eta_{ij} = \beta_0 + \beta_1 \sin(Angle) + \beta_2 (Position_j) + \beta_3 (\sin(Angle) \times Position_j) + \gamma_i + \varepsilon_{ij} \quad (4.2)$$

where, for each dependent variable, the linear predictor η_{ij} for subject i ($i = 1:12$) in *Position* j ($j = 1:2$, supine and prone) is described by the tilt *Angle* (from +45°, HUT, to –45°, HDT), the fixed effects β (where β_0 represents the intercept), the random intercept γ_i (associated with each subject and the within-subjects design), and the residual error ε_{ij}. Given that the gravitational vector is aligned with the global vertical plane (as opposed to the subject's G_z axis), tilt angle was transformed using a sinusoid function[228], as can be seen in equation 4.2. Dose-response curves are shown as mean and 95% confidence band. If the main effect of the factor *Position* was not significant, supine and prone data were pooled (i.e., the dose-response curve is modeled using only the factor *Angle*). If the main effect of *Angle* was not significant, tilt angle data were pooled (i.e., the dose-response curve is just modeled using the factor *Position*). None of the interaction effects were statistically significant and therefore, they were not included in the model.

4.2.5.2 Cephalad Measurements

Data from all cephalad measurements were distributed approximately normally at each tilt angle, side (left or right), and position (supine or prone) combination, assessed by Shapiro-Wilk tests. Due to the observed non-linearity between tilt angle and the cephalad variables, gravitational dose-response curves were constructed using generalized additive mixed-effects models (GAMMs). GAMMs were used to assess the effects of position (supine or prone), side (left or right), and tilt angle on measurements within subjects. *Position* (supine or prone) and *Side* (left or right) were included as parametric terms, and the sine of the tilt *Angle* was included as a smoothed term (the seated baseline was not included in GAMMs). Sine of the angle was chosen to represent the resolved craniocaudal component of gravitational vector acting in the vertical direction. The smoothed term was fit using shrinkage cubic splines, with individual splines fit to each factor (*Position* or *Side*) where those factors were significant. Subjects were included as a random intercept. GAMMs were fit using restricted maximum likelihood. Diagnostic plots for all models were examined visually to confirm normality and homoscedasticity of residuals. Since ultrasonography images were two-dimensional, the variance of measurements of A_{CCA} and A_{IJV} increased with the size of the measurement. Thus, a square-root transformation was performed on A_{CCA} and A_{IJV} before fitting the model, avoiding issues with heteroscedasticity. We elected to use $\sqrt{\text{area}}$ (as opposed to a diameter) since, whilst CCA were approximately circular in all subjects, the transverse IJV section was highly irregular and greatly varied in shape. The GAMM function used is shown in Equation 4.3:

$$y_{ijk} = \beta_0 + \beta_1 \left(Position_j\right) + \beta_2 \left(Side_k\right) + f_{jk} \left(\sin \left(Angle\right)\right) + \gamma_i + \varepsilon_{ijk} \tag{4.3}$$

where, for each dependent variable, the measurement y_{ijk} for subject i ($i = 1 : 12$) in *Position* j ($j = 1 : 2$, supine and prone, respectively) on *Side* k ($k = 1 : 2$, left and right, respectively) is described by the tilt *Angle* (from +45° HUT, to –45° HDT), the parametric coefficients β (where β_0 represents the intercept), the smoothed splines $f_{jk}\left(\cdot\right)$, the random intercept γ_i (associated with

each subject and the within-subjects design), and the residual error ε_{ijk}. GAMM are shown as mean ± 95% confidence interval and only significant effects are included.

All statistical analyses were completed using R version 4.1.0[229] with LMMs and GLMMs fit using the `lme4`[225] and `glmmTMB`[230] packages. GAMMs were fit using the `mgcv` package[231]. Diagnostics were assessed using the `lmerTest`[232] and `DHARMa`[233] packages. Adjusted means and contrasts were calculated using the `emmeans` package[234]. Significance level was set at $\alpha = 0.05$ (two-sided).

4.3 Results

4.3.1 Hemodynamic Response

Figure 4.2 shows the evolution of hemodynamic parameters (mean ± SE) as a function of tilt angle (including the seated baseline). Table 4.2 reports the results of the LMM analyses. There were no significant interaction effects between *Angle* and *Position* in any of the models. All hemodynamic parameters except for VO2 showed a significant effect of *Angle*, and all hemodynamic parameters except for SBP showed a significant effect of *Position*. A follow-up contrast between supine and prone positions (excluding the seated baseline) also showed no difference in DBP. Heart Rate decreased with increasing HDT ($p < 0.001$) and HR in the prone position was significantly higher than in the supine position at most of the tilt angles. On average, HR in prone position was 5.5 ± 2.1 bpm (95% CI: 1.6 to 9.3 bpm) higher than HR in the supine position. The SV and CO increased significantly with increasing HDT ($p < 0.001$ and $p < 0.001$, respectively). On average, SV in supine position was 8.8 ± 1.5 ml/beat (95% CI: 5.8 to 11.8 ml/beat; $p < 0.001$) higher than SV in the prone position, with significant differences in a pairwise comparison between supine and prone at 15° HUT, 0°, 15° HDT, 30° HDT, and 45° HDT. Differences between CO in supine and prone position were found marginally significant ($p = 0.048$), with CO in supine position being 0.2 ± 0.1 l/min (95% CI: 0.0 to 0.4 l/min; $p = 0.048$) higher than CO in the prone position. However, no significant differences were found in an adjusted pairwise comparisons at each tilt angle. TPR decreased significantly with increasing HDT ($p < 0.001$). There was no main effect of *Posi-*

tion on SBP ($p = 0.251$). However, SBP showed a gentle (and significant) decrease with increasing HDT ($p = 0.005$). SBP decreased from 128.6 ± 3.3 mmHg (95% CI: 123.2 to 133.9 mmHg) at 45° HUT to 124.4 ± 2.7 mmHg (95% CI: 119.0 to 129.8 mmHg) at 45° HDT. SBP was only significantly different from the seated baseline at 30° HDT. DBP also decreased significantly with increasing HDT ($p < 0.001$). While there was a main effect for *Position* in DBP ($p = 0.002$), significant differences were not found between Supine and Prone ($p = 0.172$) (i.e., the main effect in *Position* is most likely driven by differences from the seated baseline). DBP was significantly different from the seated baseline at 0°, 15° HDT, 30° HDT, and 45° HDT. On average, the RPP in prone position was 480 ± 141 mmHg/min (95% CI: 200 to 759 mmHg/min; $p < 0.001$) higher than in the supine position. In addition, RPP also decreased with increasing HDT ($p < 0.001$), showing significant differences between the seated baseline and 45° HUT prone, 30° HDT (supine and prone), and 45° HDT (supine and prone). Finally, there was no main effect of *Angle* on VO2 ($p = 0.244$). However, VO2 was significantly higher in the prone position than in the supine position, with an average increase of 0.04 ± 0.01 l/min (95% CI: 0.02 to 0.06 l/min; $p < 0.001$) between the two conditions.

4.3.2 Autonomic Response

Figure 4.3 shows the evolution of time-domain autonomic indices (mean ± SE) as a function of tilt angle (including the seated baseline). Table 4.2 reports the results of the GLMM analyses. There were no statistically significant interaction effects between *Angle* and *Position* in any of the indices. All four indices showed statistically significant main effects of *Angle* (SDNN: $p < 0.001$; RMSDD: $p < 0.001$; HRVTi: $p < 0.001$; BRS: $p < 0.001$), where all parameters increased with increased angles of HDT. The statistical analysis did not reveal a significant effect of *Position* in SDNN ($p = 0.214$) or HRVTi ($p = 0.710$). Results for BRS did not reveal statistically significant differences between prone and supine position ($p = 0.066$). Thus, supine and prone results were pooled for SDNN, HRVTi, and BRS. The SDNN index increased from 36.4 ± 3.7 ms (95% CI: 30.0 to 44.8 ms) at 45° HUT to 58.0 ± 5.9 ms (95% CI: 47.4 to 70.8 ms) at 45° HDT and was significantly different from the seated baseline at 45° HUT and 30° HUT. The HRVTi index in-

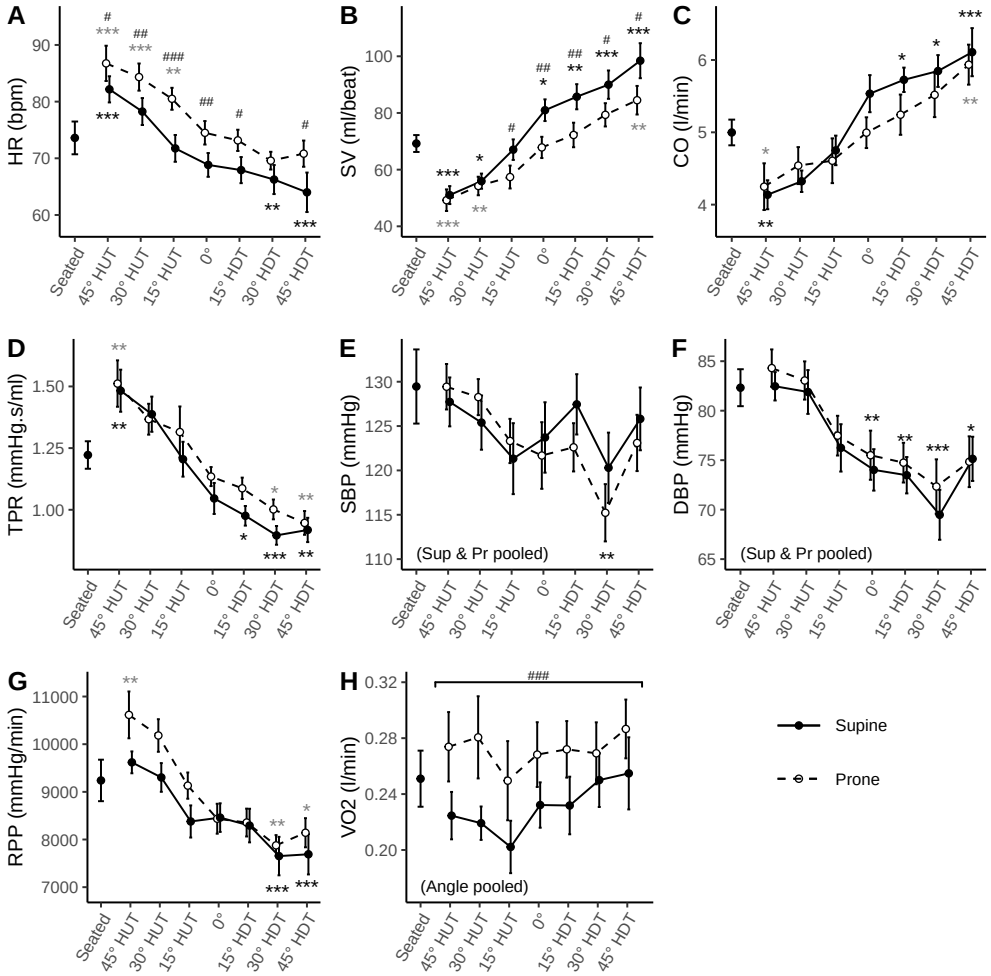

Figure 4.2: **(A-H)** Hemodynamic variables as a function of tilt angle in supine (solid line, filled circles) and prone (dashed line, unfilled circles) positions, collected on 12 male subjects. Measurements were taken at a seated baseline, 45° head-up tilt (HUT), 30° HUT, 15° HUT, 0°, 15° head-down tilt (HDT), 30° HDT, and 45° HDT. Data are presented as means ± SE at each tilt angle. Asterisks (*; black, supine; grey, prone) indicate statistically significant differences between a specific tilt condition and the seated baseline condition. When the statistical analysis indicated no significant differences between the supine and prone positions, these conditions were pooled (see Systolic Blood Pressure (SBP) and Diastolic Blood Pressure (DBP); in these cases, black asterisks represent both positions together). Pound signs (#) represent statistically significant differences between prone and supine postures at a given angle. **(A)** HR, heart rate; **(B)** SV, stroke volume; **(C)** CO, cardiac output; **(D)** TPR, total peripheral resistance; **(E)** SBP, systolic blood pressure; **(F)** DBP, diastolic blood pressure; **(G)** RPP, rate pressure product; **(H)** VO2, oxygen consumption. $^{***}p < 0.001$, $^{**}p < 0.01$, $^{*}p < 0.05$, $^{\#\#\#}p < 0.001$, $^{\#\#}p < 0.01$, $^{\#}p < 0.05$.

creased from 9.0 ± 0.8 (95% CI: 7.5 to 10.7) at 45° HUT to 12.3 ± 1.1 (95% CI: 10.3 to 14.8) at 45° HDT and was significantly different from the seated baseline at 45° HUT and 30° HUT. The

Table 4.2: Statistical results of the linear mixed model and generalized linear mixed model analysis. Fixed factors included *Angle*, *Position*, and their interaction. Subjects were included as random factors. See text for abbreviations and model details. $^{***}p < 0.001$, $^{**}p < 0.01$, $^{*}p < 0.05$.

	Significance p			
	Angle	**Position**[†]	**Angle** $\times$ **Position**	Supine vs Prone[‡]
Hemodynamic Measurements:				
HR	<0.001***	<0.001***	0.609	<0.001***
SV	<0.001***	<0.001***	0.157	<0.001***
CO	<0.001***	<0.001***	0.266	0.048*
TPR	<0.001***	<0.001***	0.834	0.024*
SBP	0.005**	0.251	0.645	—
DBP	<0.001***	0.003**	0.997	0.172
RPP	<0.001***	<0.001***	0.308	<0.001***
VO2	0.244	<0.001***	0.915	<0.001***
Time-Domain Autonomic Indices:				
SDNN	<0.001***	0.214	0.656	—
RMSDD	<0.001***	0.002**	0.789	<0.001***
HRVTi	<0.001***	0.710	0.555	—
BRS	<0.001***	<0.001***	0.386	0.066
Frequency-Domain Autonomic Indices:				
LF	<0.001***	0.106	0.776	—
HF	<0.001***	0.250	0.515	—
LFNorm	<0.001***	0.745	0.615	—
HFNorm	<0.001***	0.746	0.615	—
LF/HF	<0.001***	0.300	0.084	—

Notes:
[†]Main effect of *Position* includes seated baseline.
[‡]Post-hoc contrast to determine whether there is a true difference between supine and prone positions (i.e., does not include seated baseline).

BRS index increased from 6.6 ± 0.7 ms/mmHg (95% CI: 5.3 to 8.3 ms/mmHg) at 45° HUT to 17.1 ± 2.0 ms/mmHg (95% CI: 13.6 to 21.5 ms/mmHg) at 45° HDT and was significantly different from the seated baseline at 45° HUT, 30° HDT, and 45° HDT. Finally, RMSDD was, on average, 1.16 ± 0.05 (95% CI: 1.06 to 1.25; $p < 0.001$) times (statistically significantly) higher in supine than in prone (ratio and tests on log scale for GLMMs), although adjusted pairwise comparisons did not show significant differences at any tilt angle. The RMSDD index increased in supine posi-

tion from 17.6 ± 2.7 ms (95% CI: 13.0 to 23.8 ms) at 45° HUT to 40.5 ± 6.4 ms (95% CI: 29.7 to 55.0 ms) at 45° HDT, and in prone position from 16.4 ± 2.6 ms (95% CI: 12.1 to 22.3 ms) at 45° HUT to 33.8 ± 5.2 ms (95% CI: 25.0 to 45.8 ms) at 45° HDT. RMSDD was significantly different from the seated baseline at 45° HUT, 30° HUT, and 15° HUT (in both supine and prone positions), and at 0° (only in prone position).

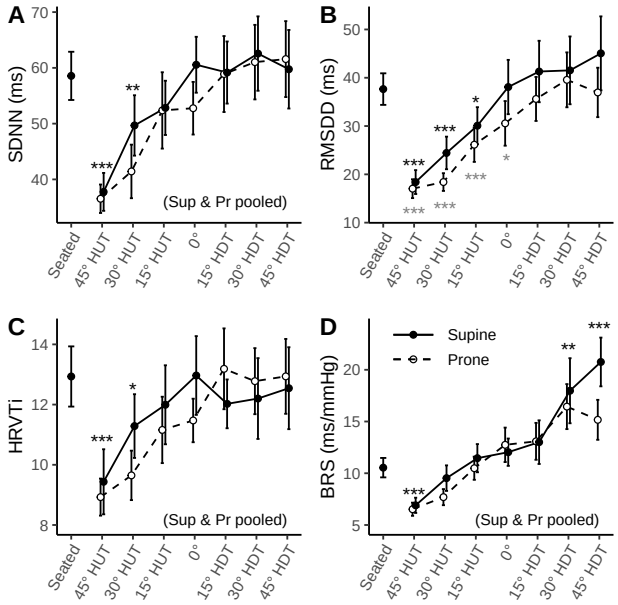

Figure 4.3: **(A-D)** Time-domain autonomic indices as a function of tilt angle in supine (solid line, filled circles) and prone (dashed line, unfilled circles) positions, collected on 12 male subjects. Measurements were taken at a seated baseline, 45° head-up tilt (HUT), 30° HUT, 15° HUT, 0°, 15° head-down tilt (HDT), 30° HDT, and 45° HDT. Data are presented as means ± SE at each tilt angle. Asterisks (*; black, supine; grey, prone) indicate statistically significant differences between a specific tilt condition and the seated baseline condition. When the statistical analysis indicated no significant differences between the supine and prone positions, these conditions were pooled (where noted, black asterisks represent both positions together). **(A)** SDNN, standard deviation of NN intervals (normalized RR intervals); **(B)** RMSDD, root mean square of direct differences of NN intervals; **(C)** HRVTi, heart rate variability triangular index; **(D)** BRS, baroreceptor sensitivity. ***$p < 0.001$, **$p < 0.01$, *$p < 0.05$.

Figure 4.4 shows the evolution of the frequency-domain autonomic indices (mean ± SE) as a function of tilt angle (including the seated baseline). Table 4.2 reports the results of the LMM

and GLMM analyses. There were no statistically significant interaction effects between *Angle* and *Position* or statistically significant main effect of *Position* in any of the indices. Thus, supine and prone results were pooled for all frequency-domain variables considered. All indices showed statistically significant main effects of *Angle* (LF: $p < 0.001$; LFNorm: $p < 0.001$; HF: $p < 0.001$; HFNorm: $p < 0.001$; LF/HF: $p < 0.001$). LF increased from 516 ± 77 ms^2 (95% CI: 385 to 691 ms^2) at 45° HUT to 888 ± 134 ms^2 (95% CI: 661 to 1192 ms^2) at 45° HDT, with statistically significant differences from the seated baseline at 45° HUT and 30° HUT. Similarly, HF increased from 98 ± 24 ms^2 (95% CI: 60 to 160 ms^2) at 45° HUT to 407 ± 102 ms^2 (95% CI: 249 to 665 ms^2) at 45° HDT, with statistically significant differences from the seated baseline at 45° HUT, 30° HUT, 15° HUT, and 0°. However, when expressed in normalized units, LFNorm (i.e, the proportion of total power minus VLF power) decreased from 83.8 ± 2.9% (95% CI: 78.0 to 89.6%) at 45° HUT to 68.2 ± 2.9% (95% CI: 62.3 to 74.0%) at 45° HDT. Accordingly, HFNorm increased from 16.2 ± 2.9% (95% CI: 10.4 to 22.0%) at 45° HUT to 31.8 ± 2.9% (95% CI: 26.0 to 37.7%) at 45° HDT. LFNorm and HFNorm differed from the seated baseline at 45° HUT and 30° HUT. Thus, LF/HF decreased from 5.7 ± 0.9 (95% CI: 4.2 to 7.8) at 45° HUT to 2.5 ± 0.4 (95% CI: 1.8 to 3.4) at 45° HDT, differing from the seated baseline at 45° HUT.

4.3.3 Dose-Response Curves for Systemic and Autonomic Response

Figures 4.5 and 4.6 show the estimated dose-response curves for all of the hemodynamic and autonomic parameters considered within the range of 45° HUT to 45° HDT. Curves are shown as mean and 95% confidence interval. Since there was no difference between supine and prone for SBP, DBP, SDNN, HRVTi, BRS, LF, LFNorm, HF, HFNorm, and LF/HF, supine and prone position results were pooled and these dose-response curves are combined into a single estimate. The dose-response curves corresponding to VO2 are modeled as constant functions for supine and prone positions since the statistical analysis did not show a significant effect of *Angle*. Model details are presented in Table 4.3.

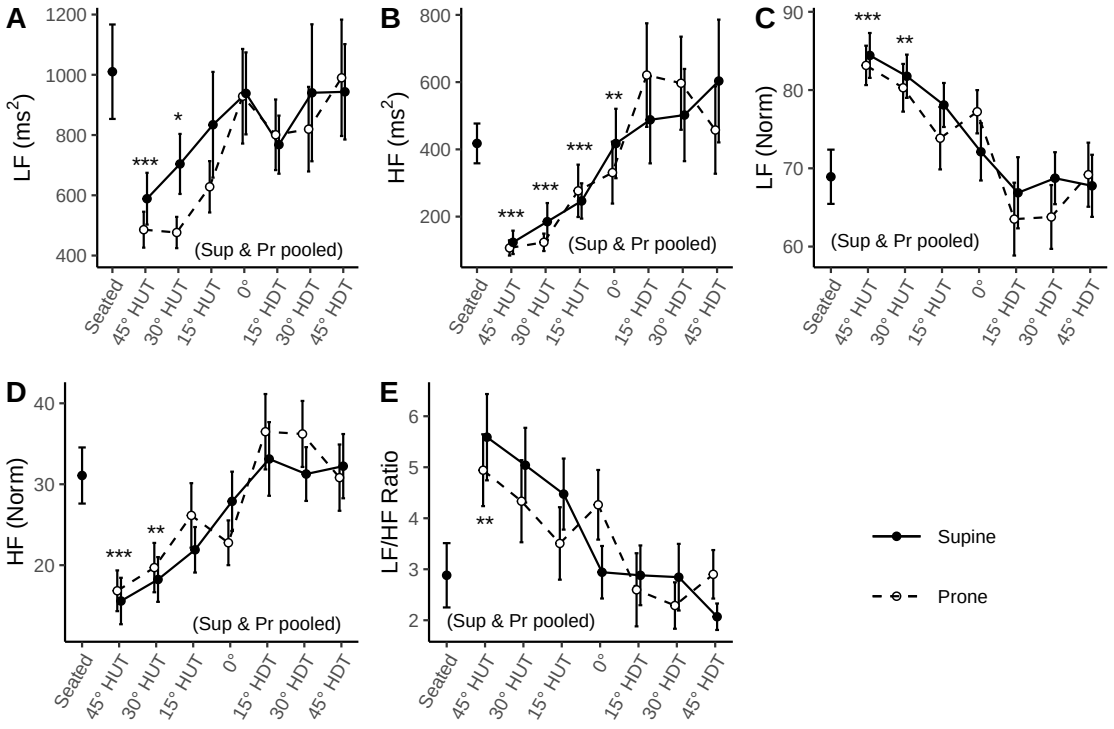

Figure 4.4: **(A-E)** Frequency-domain autonomic indices as a function of tilt angle in supine (solid line, filled circles) and prone (dashed line, unfilled circles) positions, collected on 12 male subjects. Measurements were taken at a seated baseline, 45° head-up tilt (HUT), 30° HUT, 15° HUT, 0°, 15° head-down tilt (HDT), 30° HDT, and 45° HDT. Data are presented as means ± SE at each tilt angle. Asterisks (*; black, supine; grey, prone) indicate statistically significant differences between a specific tilt condition and the seated baseline condition. When the statistical analysis indicated no significant differences between the supine and prone positions, these conditions were pooled (where noted, black asterisks represent both positions together). **(A)** LF, power density in the low frequency range (0.04 — 0.15 Hz); **(B)** HF, power density in the high frequency range (0.15 — 0.4 Hz); **(C)** LFNorm, LF (normalized units); **(D)** HFNorm, HF (normalized units); **(E)** LF/HF Ratio, ratio of low to high power densities. ***$p < 0.001$, **$p < 0.01$, *$p < 0.05$.

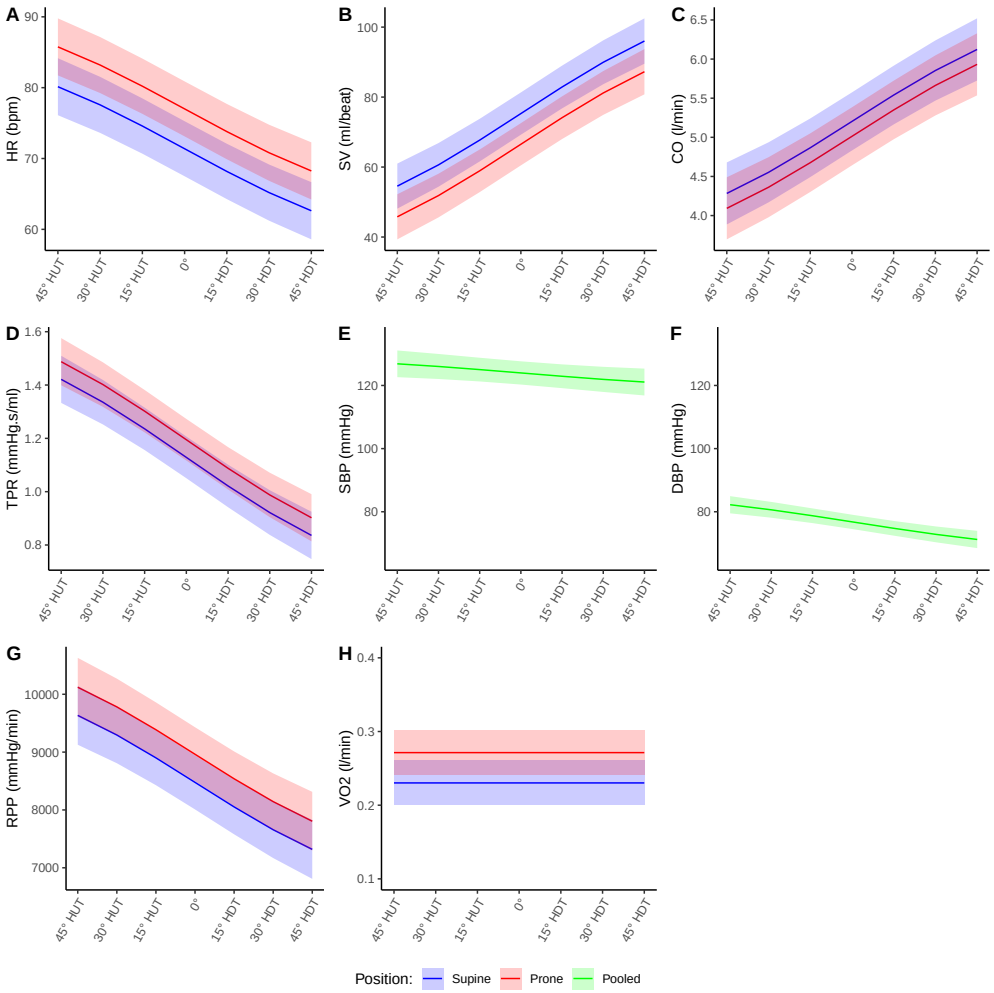

Figure 4.5: **(A-H)** Estimated gravitational dose-response curves for hemodynamic parameters in the range 45° head-up tilt (HUT) to 45° head-down tilt (HDT). Curves were fit via linear mixed-effects models as described in the main text. Curves are presented as means ± 95% confidence interval. Blue, supine; red, prone; green, supine and prone pooled. **(A)** HR, heart rate; **(B)** SV, stroke volume; **(C)** CO, cardiac output; **(D)** TPR, total peripheral resistance; **(E)** SBP, systolic blood pressure; **(F)** DBP, diastolic blood pressure; **(G)** RPP, rate pressure product; **(H)** VO2, oxygen consumption.

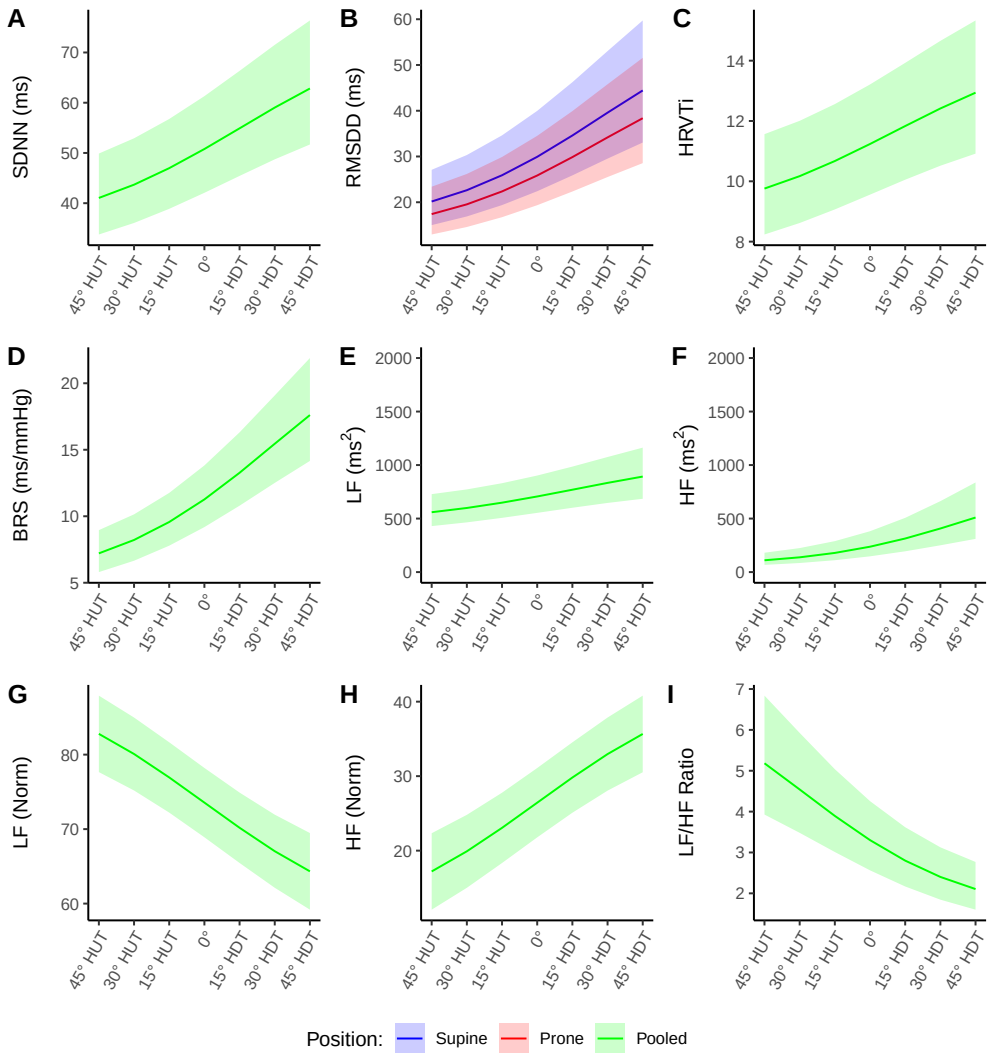

Figure 4.6: **(A-I)** Estimated gravitational dose-response curves for autonomic parameters in the range 45° head-up tilt (HUT) to 45° head-down tilt (HDT). Curves were fit via linear mixed-effects models (LFNorm, and HFNorm) and generalized linear mixed-effects models (remaining parameters) as described in the main text. Curves are presented as means ± 95% confidence interval. Blue, supine; red, prone; green, supine and prone pooled. **(A)** SDNN, standard deviation of NN intervals (normalized RR intervals); **(B)** RMSDD, root mean square of direct differences of NN intervals; **(C)** HRVTi, heart rate variability triangular index; **(D)** BRS, baroreceptor sensitivity; **(E)** LF, power density in the low frequency range (0.04–0.15 Hz); **(F)** HF, power density in the high frequency range (0.15–0.4 Hz); **(G)** LFNorm, LF (normalized units); **(H)** HFNorm, HF (normalized units); **(I)** LF/HF Ratio, ratio of low to high power densities.

Table 4.3: Estimated model coefficients for the gravitational dose-response curves displayed in Figures 4.5 and 4.6 generated by linear mixed models (LMMs) and generalized linear mixed models (GLMMs). Estimated coefficients are presented as mean ± SE. Only significant terms were included in the models.

	Model[†]	Link[‡]	Units	Estimated Coefficients[§]			Std Dev of Random Effect[††]
				β_0 Intercept	β_1 $\sin(\text{Angle})$[‖]	β_2 Position[¶]	
Hemodynamic Measurements:							
HR	LMM	$\mu = \eta$	bpm	71.4 ± 2.0	12.4 ± 1.1	5.6 ± 0.7	6.6
SV	LMM	$\mu = \eta$	ml	75.3 ± 3.1	–29.3 ± 1.6	–8.8 ± 1.6	9.9
CO	LMM	$\mu = \eta$	l/min	5.20 ± 0.19	–1.30 ± 0.10	–0.19 ± 0.10	0.61
TPR	LMM	$\mu = \eta$	mmHg.s/ml	1.13 ± 0.04	0.41 ± 0.03	0.07 ± 0.03	0.12
SBP	LMM	$\mu = \eta$	mmHg	124.0 ± 1.9	4.1 ± 1.5	—	6.0
DBP	LMM	$\mu = \eta$	mmHg	76.7 ± 1.2	7.8 ± 1.1	—	3.6
RPP	LMM	$\mu = \eta$	mmHg/min	8477 ± 239	1638 ± 145	486 ± 140	752
VO2	LMM	$\mu = \eta$	l/min	0.23 ± 0.02	—	0.04 ± 0.01	0.05
Time-Domain Autonomic Indices:							
SDNN	GLMM	$\ln(\mu) = \eta$	ms	3.928 ± 0.096	–0.300 ± 0.037	—	0.148
RMSDD	GLMM	$\ln(\mu) = \eta$	ms	3.399 ± 0.148	–0.559 ± 0.044	–0.147 ± 0.041	0.213
HRVTi	GLMM	$\ln(\mu) = \eta$	—	2.419 ± 0.083	–0.199 ± 0.037	—	0.131
BRS	GLMM	$\ln(\mu) = \eta$	ms/mmHg	2.422 ± 0.104	–0.631 ± 0.054	—	0.184
Frequency-Domain Autonomic Indices:							
LF	GLMM	$\ln(\mu) = \eta$	ms^2	6.564 ± 0.125	–0.326 ± 0.074	—	0.238
HF	GLMM	$\ln(\mu) = \eta$	ms^2	5.470 ± 0.243	–1.080 ± 0.100	—	0.490
LFNorm	LMM	$\mu = \eta$	—	73.6 ± 2.4	13.1 ± 1.6	—	7.8
HFNorm	LMM	$\mu = \eta$	—	26.4 ± 2.4	–13.1 ± 1.6	—	7.8
LF/HF	GLMM	$\ln(\mu) = \eta$	—	1.198 ± 0.129	0.634 ± 0.078	—	0.268

Notes:

[†]All models use a linear predictor of the form: $\eta_{ij} = \beta_0 + \beta_1 \sin(Angle) + \beta_2 (Position_j) + \gamma_i + \varepsilon_{ij}$ for subjects i ($i = 1:12$) and position j ($j = 0:1$). All GLMMs have a Gamma distribution.

[‡]Link function between the linear predictor, η, and the expectation of the dependent variable, μ.

[§]For GLMMs, coefficients β are given on the scale of the linear predictor for subject i, $\eta_i = \boldsymbol{X}\beta + \gamma_i$. The coefficient β_3 corresponding to the interaction effect $\sin(Angle) \times Position$ was never significant so was not included in the models or table.

[‖]Sine of tilt angle from –0.707 ($\sin(-45°)$) to 0.707 ($\sin(45°)$), positive angles represent head-up tilt, negative angles represent head-down tilt.

[¶]$Position_j$: supine $= 0$, prone $= 1$.

[††]Standard deviation, σ, of random intercept, γ, for subject i. $\gamma_i \sim N\left(0, \sigma^2\right)$. Units for σ are the same as the estimated coefficients.

4.3.4 Carotid and Jugular Response

Figure 4.7A shows the A_{CCA} as a function of tilt angle (including the seated baseline). Table 4.4 reports the results of the GAMM analysis. There was no significant effect of *Position* ($p = 0.341$), *Side* ($p = 0.849$), or $\sin(Angle)$ ($p = 0.262$). In the supine posture, A_{CCA} increased from 34.3 ± 1.9 mm^2 in 45° HUT to 46.0 ± 3.1 mm^2 in 45° HDT (averaged left and right sides). However, this change was not statistically significant when all factors were considered. In the prone posture, there was no noticeable trend of A_{CCA}: 36.9 ± 1.6 mm^2 in 45° HUT and 34.0 ± 3.5 mm^2 in 45° HDT (averaged left and right sides). The lack of significance of any factors was captured by the dose-response curve constructed via GAMM in Figure 4.7B, which appears as a horizontal line. Due to the observable fluctuations in measured A_{CCA}, a gravitational dose-response curve constructed in this fashion was only able to explain 22.6% of the observed deviance.

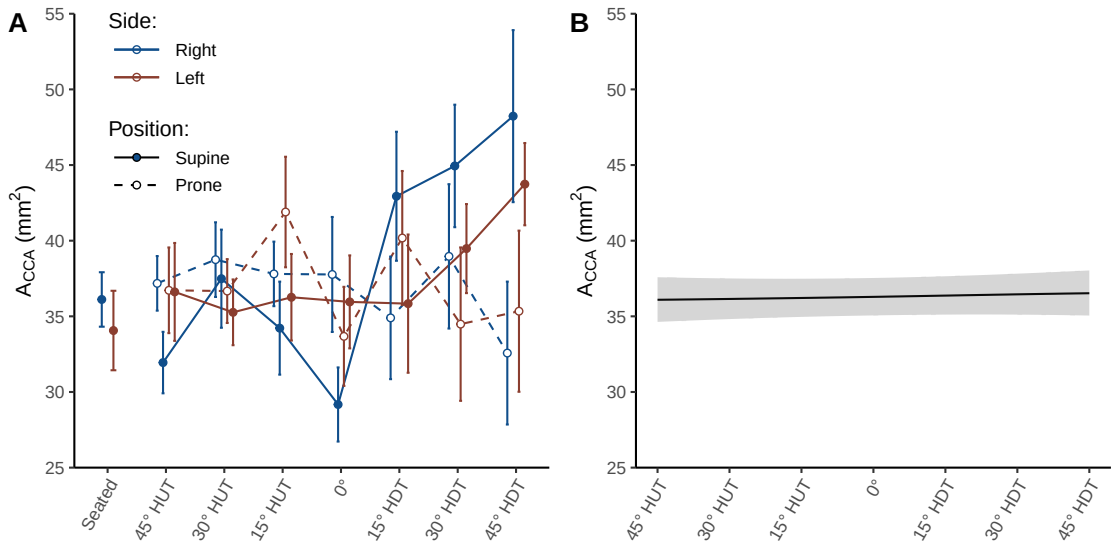

Figure 4.7: Common carotid artery cross sectional area response to tilt, collected on 12 male subjects. **(A)** Right (blue) and left (red) common carotid artery cross sectional area, A_{CCA}, as a function of tilt angle in supine (solid line, filled circles) and prone (dashed line, unfilled circles) positions, collected on 12 male subjects. Measurements were taken at a seated baseline, 45° head-up tilt (HUT), 30° HUT, 15° HUT, 0°, 15° head-down tilt (HDT), 30° HDT, and 45° HDT. Data are presented as means ± SE at each tilt angle. **(B)** Gravitational dose-response curve (mean and 95% confidence interval) fitted from experimental data using generalized additive mixed-effects models (see text for methodology).

Table 4.4: Details of generalized additive mixed models (GAMM) analyses for three dependent variables: common carotid artery cross-sectional area ($\sqrt{A_{CCA}}$), internal jugular vein cross-sectional area ($\sqrt{A_{IJV}}$), and internal jugular vein pressure (IJVP). Significance of parametric and smoothed terms, effective degrees of freedom of smoothers, size of subject random effect, and model goodness of fit (deviance explained). See text for abbreviations and model details.

	Parametric Terms				**Smooth Terms**[§]				**Subject**	**Deviance**
	Position[†]		**Side**[‡]		$\sin($**Angle**$)$[‖]				**Std Dev**[††]	**Explained**[‡‡]
	t	p	t	p	Curve	EDF[¶]	F	p	σ	%
$\sqrt{\mathbf{A_{CCA}}}$[§§] (mm)	–0.954	0.341	–0.190	0.849	—	0.23	0.048	0.262	0.49	22.6
$\sqrt{\mathbf{A_{IJV}}}$[§§] (mm)	0.439	0.663	–3.923	<0.001	Right	4.18	84.874	<0.001	1.10	78.0
					Left	3.41	58.191	<0.001		
IJVP (mmHg)	3.521	<0.001	–0.287	0.775	Supine	3.43	67.334	<0.001	5.92	76.2
					Prone	3.34	72.441	<0.001		

Notes:
[†]*Position*: Supine or Prone; t reports effect size of prone compared to supine.
[‡]*Side*: Right or Left; t reports effect size of left compared to right.
[§]Shrinkage-penalized cubic regression splines fit to each *Position* and *Side* combination. Plots of the smoothers are included as Figure 4.10.
[‖]Sine of the tilt *Angle* in radians, positive values indicate head-up tilt (HUT); F reports effect size.
[¶]Effective degrees of freedom.
[††]Random effect $\gamma \sim \mathcal{N}\left(0, \sigma^2\right)$.
[‡‡]Goodness of fit, equivalent to the unadjusted R^2.
[§§]See main text. Measurements of CCA and IJV size were homoscedastic in diameter, thus a square-root transformation was used on the cross-sectional area response.

Figure 4.8A shows the A_{IJV} as a function of tilt angle (including the seated baseline). Table 4.4 reports the results of the GAMM analysis. There was no significant effect of *Position* ($p = 0.663$). However, the factor *Side* was statistically significant ($p < 0.001$) as well as the smoothed term $\sin(Angle)$ for both the left and right sides ($p < 0.001$ for both sides). The IJV markedly expanded from 45° HUT (right side: 18.6 ± 2.6 mm^2, left side: 15.1 ± 2.2 mm^2, average of supine and prone positions) to 45° HDT (right side: 196 ± 15.8 mm^2, left side: 161 ± 14.1 mm^2, average of supine and prone positions). On both sides, the expansion was non-linear. Given the significant differences found between the right and left side, we constructed two gravitational dose-response curves, shown in Figure 4.8B, one for each side. Together, they fit the experimental dataset well, explaining 78.0% of the observed variation in the data.

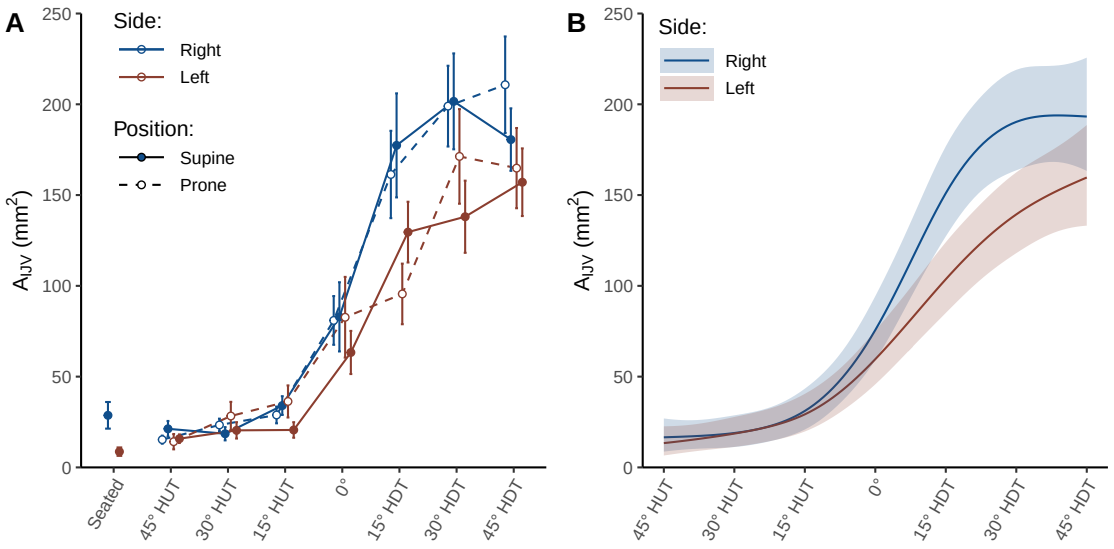

Figure 4.8: Internal jugular vein cross sectional area response to tilt, collected on 12 male subjects. **(A)** Right (blue) and left (red) internal jugular vein cross sectional area, A_{IJV}, as a function of tilt angle in supine (solid line, filled circles) and prone (dashed line, unfilled circles) positions, collected on 12 male subjects. Measurements were taken at a seated baseline, 45° head-up tilt (HUT), 30° HUT, 15° HUT, 0°, 15° head-down tilt (HDT), 30° HDT, and 45° HDT. Data are presented as means ± SE at each tilt angle. **(B)** Gravitational dose-response curves (mean and 95% confidence interval) fitted from experimental data using generalized additive mixed-effects models (see text for methodology); separate curves created for right and left sides.

Figure 4.9A shows the IJVP as a function of tilt angle (including the seated baseline). Table 4.4 reports the results of the GAMM analysis. There was no significant effect of *Side* ($p = 0.775$). However, the factor *Position* was statistically significant ($p < 0.001$) as well as the smoothed term $\sin(Angle)$ for both the supine and prone postures ($p < 0.001$ for both postures). IJVP increased from 45° HUT (supine: 10.4 ± 2.0 mmHg, prone: 11.6 ± 2.0 mmHg, average of left and right sides) to 45° HDT (supine: 56.0 ± 2.1 mmHg, prone: 59.4 ± 2.2 mmHg, average of left and right sides). On average, IJVP was 4.3 ± 1.2 mmHg higher in the prone posture than in the supine posture. Similarly to A_{IJV}, the increase in pressure was non-linear. Given the significant differences found between the supine and prone postures, we constructed two gravitational dose-response curves, shown in Figure 4.9B, one for each posture. Together, they explain 76.2% of the observed variation in the data.

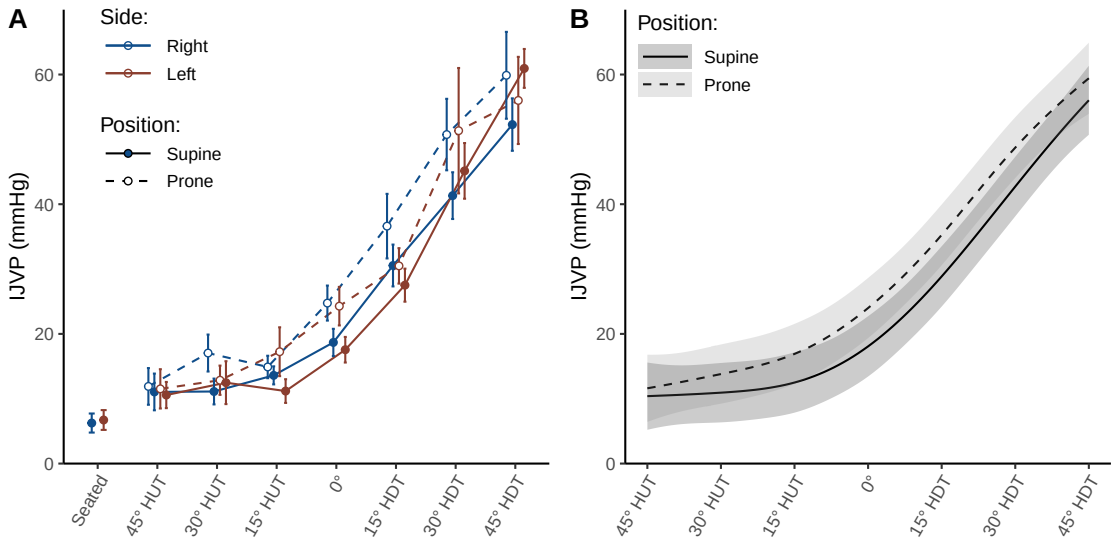

Figure 4.9: Internal jugular vein pressure response to tilt, collected on 12 male subjects. **(A)** Right (blue) and left (red) internal jugular vein pressure, IJVP, as a function of tilt angle in supine (solid line, filled circles) and prone (dashed line, unfilled circles) positions, collected on 12 male subjects. Measurements were taken at a seated baseline, 45° head-up tilt (HUT), 30° HUT, 15° HUT, 0°, 15° head-down tilt (HDT), 30° HDT, and 45° HDT. Data are presented as means ± SE at each tilt angle. **(B)** Gravitational dose-response curves (mean and 95% confidence interval) fitted from experimental data using generalized additive mixed-effects models (see text for methodology); separate curves created for supine and prone positions.

The fitted smoothed terms used to construct the GAMMs in Figures 4.7B, 4.8B, and 4.9B are presented in Figure 4.10.

4.4 Discussion

This study investigated the acute gravitational dependence of cardiovascular hemodynamics and autonomic control in a tilt paradigm. To our knowledge, this study represents the most comprehensive analysis of hemodynamic and autonomic responses over the widest range of tilt angles to date, whilst also considering supine and prone differences. Our main findings related to the systemic and autonomic response show that: (1) almost all hemodynamic parameters and autonomic indices present a strong gravitational dependence; (2) the effect of body position (supine or prone) is important for HR, SV, CO, TPR, and VO2, but not for blood pressure or autonomic regulation; and (3) in the range between 45° HUT and 45° HDT, linear models can effectively describe the relationship between tilt angle and hemodynamic/autonomic response. Related to the cephalad response, we find that: (1) A_{CCA} is not gravitationally dependent. In addition, there is no significant differences between the left and right sides; (2) In contrast, IJV characteristics show a high gravitational dependency, exhibiting a marked non-linear behavior; (3) A_{IJV} is larger on the right side and expands more than on the left side; and (4) IJVP is higher in the prone position than in the supine position.

4.4.1 Systemic/Autonomic Response

Some studies have previously considered the hemodynamic[137,138], autonomic[235], or endocrine[228] response to acute graded HUT. Other studies have considered the hemodynamic[135,136] or autonomic[136,236] response to graded HDT. However, studies that investigated both HUT and HDT are scarce: Lieshout *et al.*[139] considered hemodynamic response in nine subjects at 20° HUT, horizontal 0°, and 20° HDT (all supine). Further, we could find no studies that considered supine and prone hemodynamic differences in HUT or HDT. Additionally, only the Laszlo *et al.*[228] study on autonomic response to graded HUT attempts to fit dose-response curves to the experimental data. Thus, the present study gives unique insight into the complete gravitational and postural cardio-

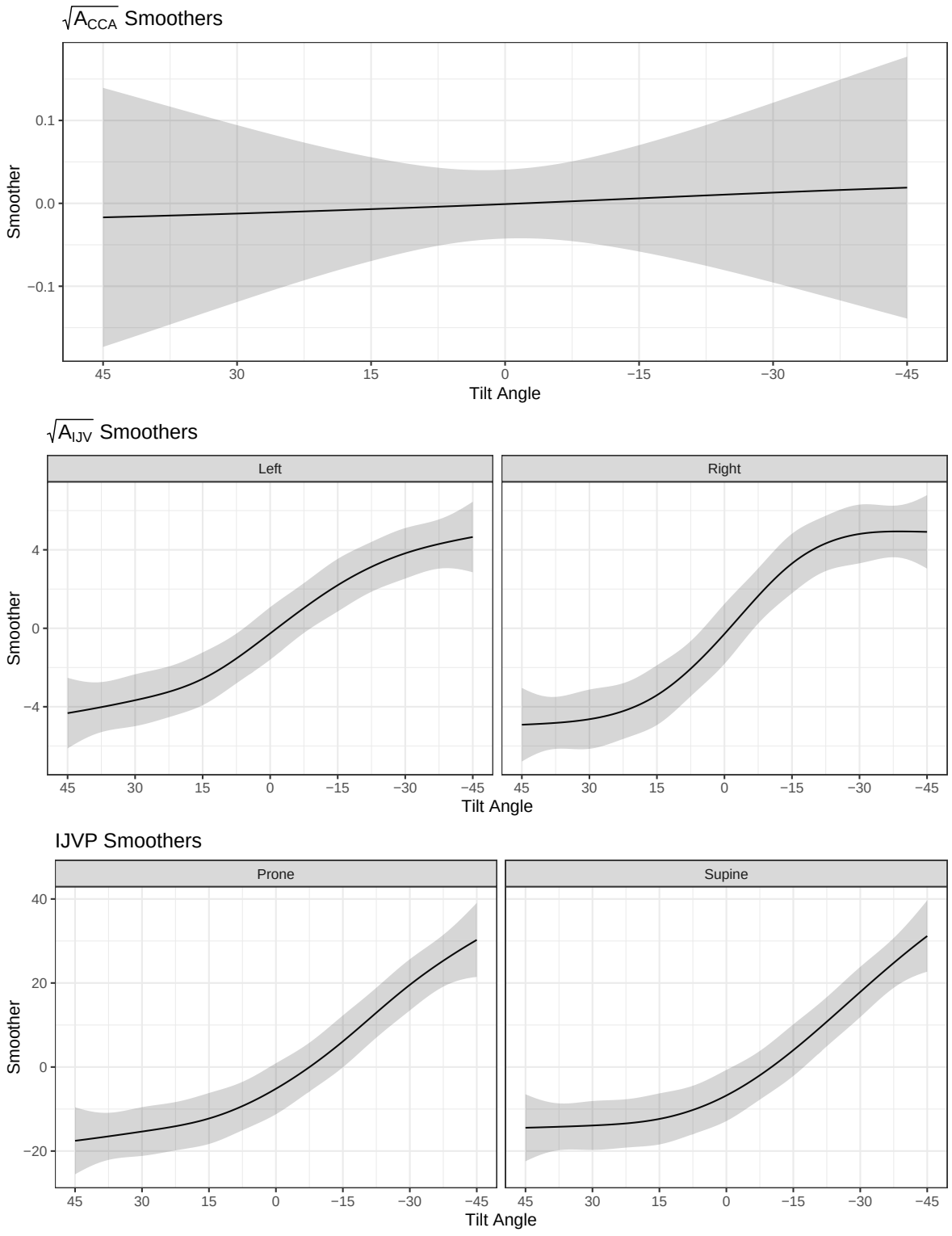

Figure 4.10: Fitted smoothed terms for generalized additive mixed-effects models (GAMMs).

vascular response over both HUT and HDT, in supine and prone positions, with applications in spaceflight and terrestrial surgery.

Multiple studies have shown either a decrease in CO with increased angles of HUT from the supine posture, or an increase in CO with increased angles of HDT[122,137,193,198]. With respect to the horizontal supine 0° posture, our 21.9% (95% CI: 12.8 to 31.0%) decrease in CO to 30° HUT matches closely the 19% decrease found by Tuckman *et al.*[237]. They did not measure CO at 15°, but our decrease of 14.2% (95% CI: 5.1 to 23.3%) at 15° HUT is between their reported changes at 10° HUT (5% decrease) and 20° HUT (17% decrease). Similarly, Bundgaard-Nielsen *et al.*[238] found a decrease in CO by 0.7 l/min (95% CI: 0.2 to 1.2 l/min) from 0° supine to 45° HUT, which is within our 95% confidence limits of a 1.4 l/min (95% CI: 0.6 to 2.2 l/min) decrease, although they did not find an increase in CO during any angles of HDT (15°, 45°, 70°, or 90° HDT). Stroke volume is principally controlled by the Frank-Starling mechanism: during HUT, a reduction in central blood volume and reduced venous return due to pooling in the abdominal and lower extremity vasculature leads to decreased cardiac filling and left ventricular end diastolic pressure (LVEDP), reduced myocyte stretch, and hence, reduced contraction force and lower stroke volume. Conversely, we expect the opposite behavior in graded HDT: the cephalad fluid shift leads to increased central blood volume, increased LVEDP and thus, increased SV[239]. The reduction in HR with HDT (and increase with HUT), along with the reduction in TPR, are primarily driven by autonomic activity[18,240]. In HDT, increased pressure on the arterial baroreflex stimulates vagal activity while simultaneously withdrawing sympathetic nervous stimulation, promoting a bradycardic response together with vasorelaxation[239]. The converse is true in HUT: HR and TPR increase with HUT driven by vagal withdrawal and sympathetic stimulation, which promote tachycardia and vasoconstriction. This explanation is supported by our findings on HRV. However, the fact that CO still increases in HDT indicates that the increase in SV is proportionally greater than the reduction in HR.

Our results also indicate a reduction of SBP with increasing HDT, but this is only a small change. Between 45° HUT and 45° HDT, SBP decreases by 4.2 ± 2.7 mmHg (95% CI: -3.1 to

11.5 mmHg), which is equivalent to 3.3% of the seated baseline SBP. On the other hand, DBP presents a larger decrease over the same interval: between 45° HUT and 45° HDT, DBP decreases by 8.6 ± 1.9 mmHg (95% CI: 3.5 to 13.7 mmHg) or 10.4% of the seated baseline value. In the absence of syncope (which we did not observe in any of our subjects), this is to be expected since maintenance of arterial pressure is the primary function of cardiovascular control[239]. In effect, the rest of the hemodynamic and autonomic changes we observe in tilt are effected in order to maintain arterial pressure. Our results fall between Mukai *et al.*[241], who observed no changes in either SBP or DBP in graded HUT; and Zaidi *et al.*[137], who found an increase of 11.9% and 20.3% in SBP and DBP respectively from horizontal supine to 45° HUT. The data also align with Mosqueda-Garcia *et al.*[242] who found little change in SBP, a small increase in DBP, and an increase of around 14 bpm in HR when subjects were tilted from 0° supine to 45° HUT compared to our increase of 13.3± 1.9 bpm (95% CI: 7.6 to 19.1 bpm) under the same conditions. While SBP is essentially controlled in tilt, we hypothesize that the apparent reduction in DBP with HDT is an artifact of bradycardia combined with vasorelaxation in the terminal resistance arterioles, increasing both the diastolic time interval and the rate of pressure drop during diastole[243]. Since blood pressure is largely maintained, bradycardia in HDT also leads to a reduction in RPP, indicating a reduction in myocardial oxygen consumption with HDT. Although, on appearance, this may provide evidence for an reduced risk of cardiovascular events during reduced gravity conditions[244], long-term cardiovascular deconditioning likely outweighs any acute benefits[178].

VO2 was the only hemodynamic parameter that did not show a strong response to tilt. Studies on cardiopulmonary response to graded tilt are scarce. Diaz-Artiles *et al.*[125] found no difference in VO2 consumption at rest across a range of tilt angles from 90° HUT to 6° HDT. Further, our results are concordant with Prisk and his colleagues, who noted no significant change to VO2 between standing and supine on Earth, or in microgravity, in a study of eight subjects on SLS-1 and SLS-2[245]. Based on these findings, we preliminarily conclude that VO2, and more broadly pulmonary function, is more dependent on the gravitational vector in the G_x direction (which also supports our experimental results indicating VO2 differences between prone and supine positions)

than in the G_z direction, most likely as a result of the weight of the thoracic cavity[141].

HRV indices provide additional insight into autonomic responses to changes in gravitational loads. Our results indicate that, in general, HRV increases with increasing angles of HDT (shown by the increase in HRVTi, Figure 4.3C). The increase in SDNN (Figure 4.3A) points to a combined increase in sympathetic and vagal activity[213]. Results indicate, based on changes in RMSDD (Figure 4.3B) and HF (Figure 4.4B and D), that vagal activity increases with HDT. Conversely, whilst the total power spectral density in the LF band increases with HDT (Figure 4.4A), we noticed that, in normalized units (Figure 4.4C), LF power decreases with increasing HDT. TFESCNASPE[213] recommends using LF in absolute units as an index of total sympathovagal activity, whereas LF Norm is more indicative as marker for sympathetic activity only. Taking all the indices together, results indicate an increase in vagal activity and sympathetic withdrawal with HDT. Once again, comparison with previous literature is precluded by the limited number of studies considering HRV in graded tilt. Our results are congruent with Sharma *et al.*[246], who considered 10° and 70° HUT, finding an increase in sympathetic activity (increased LF Norm and LF/HF ratio) and vagal withdrawal (decreased HF Norm and RMSDD) combined with an overall decrease in autonomic activity (decreased SDNN), compared with the 0° supine position. Similarly, Malhotra *et al.*[247] found a decrease in sympathetic activity in 30° HDT (decrease in LF Norm) compared to the 0° supine position, whilst both Mosqueda-Garcia *et al.*[242] and Saito *et al.*[248] found an increase in sympathetic activity in HUT. We also noted an increase in BRS (Figure 4.3D) from 6.6 ± 0.8 ms/mmHg (95% CI: 5.3 to 8.3 ms/mmHg) at 45° HUT to 17.1 ± 2.0 ms/mmHg (95% CI: 13.6 to 21.5 ms/mmHg) at 45° HDT. This is congruent with Schroeder *et al.*[193] who noted that HUT suppressed baroreflex sensitivity. Our values in seated position (baseline) and horizontal 0° closely match those given in a review by Rovere *et al.*[217]. Although our study did not differentiate between the relative sensitivity of the two divisions of the autonomic system, O'Leary *et al.*[249] suggest that during HUT, the sympathetic arm is the dominant mediating cardiovascular control.

Differences in supine vs. prone positioning on cardiac function also match what has been previously reported in literature. Dharmavaram *et al.*[149] compared HR, SV, and CO between 0° supine

and a variety of prone positioning systems designed for spinal surgery. Although they do not use a control group (i.e., simple 0° prone position with no positioning device), their data using the Jackson spinal table and the longitudinal bolster are the most insightful (horizontal position, body anatomically straight). They reported a non-significant decrease of 0.5 ± 0.6 l/min in cardiac output from supine to prone on the Jackson table, which closely matches our 0.54 ± 0.25 l/min (95% CI: –0.15 to 1.23 l/min; $p = 0.202$) decrease from supine to prone at 0°. Further, they reported a decrease of 7.2 ± 4.7 ml/beat in stroke volume on the Jackson table, and 14.8 ± 6.6 ml/beat using the longitudinal bolster. These values are in close agreement with our 13.1 ± 4.0 ml/beat (95% CI: 2.2 to 24.1 ml/beat; $p = 0.005$) decrease from supine to prone at 0°. It must be noted that Dharmavaram *et al.*[149] also found a decrease in heart rate of 6 ± 3 bpm from supine to prone (Jackson table) compared with the increase that we found at 0° (5.7 ± 1.9 bpm; 95% CI: 0.5 to 10.9 bpm; $p = 0.008$). We hypothesize that this decrease could potentially be due to differences in their methodology: patients were in an anaesthetized state, with supine measurements performed first and prone measurements performed some time later. Fentanyl, vecuronium, and thiopental used by Dharmavaram *et al.*[149] in the anaesthetization process have varying temporal effects on heart rate and autonomic function[250–252]. Further studies found no change in blood pressure between prone and supine positions, but increased TPR and reduced SV and CO in the prone position compared to the supine position[253–256]. Studies by Sudheer *et al.*[255], Schaefer *et al.*[256], Yap *et al.*[257], and Pump *et al.*[254] also found increased HR in the prone position. These data are all in agreement with our findings. Taken together, the hemodynamic differences between prone and supine are likely explained by compression of the thorax and inferior vena cava, reducing venous return[256,258]. This is combined with attenuated pulsation of the arteries while in prone position, further inhibiting baroreflex function, leading to increased sympathetic nervous system activity and hence, an increase in HR and vascular resistance[254]. Blood pressure is maintained between prone and supine postures via the concomitant reflexive peripheral vasoconstriction[258]. We further suggest that the increase in VO2 found in the prone position may be a result of this thorax compression. Studies have shown that limited thorax compression can increase ventilatory efficiency by reducing expi-

ratory cost[259], and the additional pressure on the musculature of the thorax may lead to a dyspnea sensation in subjects, reflexively inducing hyperventilation and thus, increasing VO2[260]. Pump *et al.*[254] further suggested that these findings identify a limitation of the 6° HDT microgravity analog in that cardiac function is regulated by the gravitational vector in the G_x direction as well as the G_z direction. Our results also support this conclusion. Further, we found RMSDD to be significantly higher in the supine position. Viewing RMSDD as an index of vagal activity, this supports the hypothesis of vagal withdrawal due to baroreflex inhibition when prone, leading to a higher HR compared to the supine position.

Our study only considers angles from 45° HUT to 45° HDT; over this interval the tilt angle and its respective sine differ by less than 10%. Therefore, we construct dose-response curves using the sine of the tilt angle rather than the angle itself in order to capture the underlying mechanisms as accurately as possible. This follows the methodology of multiple other studies including Critchley *et al.*[261] (MAP, HR, and SV), Khurana *et al.*[262] (HR, SBP, and DBP), and Smith *et al.*[263] (SV, CO, and TPR). In line with these studies, if we were to expand our range of measurement from 90° HUT to 90° HDT, we would hypothesize to see the linear trend continue in the sine of the angle between ±1. Thus, this would set maximal and minimal responses when angle is plotted on a linear scale. These dose-response curves form a comprehensive baseline for the range of hemodynamic parameters and autonomic indices across a range of tilt angles representing a change in the direction of the gravitational vector. Thus, in the context of human spaceflight, they can be used as a reference to assess and compare the efficacy and impact of various countermeasures (for example lower body negative pressure, or short radius centrifugation) designed to alter hemodynamic performance to prevent the deconditioning effects of altered gravity on the cardiovascular system.

Tilt studies also have important application outside of human spaceflight. Multiple surgeries including lower abdominal surgery, central venous catheter placement, and minimally invasive glaucoma surgery are often performed in the Trendelenburg position (i.e., 15° to 30° HDT) to facilitate access to pelvic organs and/or improve surgeon positioning. However, there is controversy over the efficacy of this positioning and its potential adverse complications[146–148]. Similarly, the

use of a Wilson frame (or equivalent) in back surgery places the patient in a prone position where the head is hydrostatically lower than the heart[149,150]. A greater understanding of the hemodynamic and operative response to such conditions may improve perioperative management and clinical decision making[151]. Finally, the recent COVID-19 pandemic has brought to public attention the practice of proning SARS-CoV-2 patients to improve respiratory function[264]. These dose-response curves provide a reference from non-pathological subjects that can be used for clinical management purposes to assess expected hemodynamic and autonomic variation. This has applications in surgical cases such as Trendelenburg positioning or surgeries using spinal frames, along with tests of orthostatic response[151].

4.4.2 Carotid/Jugular Response

In the 0° supine posture, we measure A_{CCA} as 34.1 ± 1.6 mm^2 (average of supine and prone, left and right sides); equivalent to a vascular diameter of 6.6 ± 0.5 mm. These results are congruent with reference values found in the literature, including Scheel *et al.*[265] (6.0 ± 0.7 mm) and Krejza *et al.*[266] (6.5 ± 1.0 mm). Further, existing studies have found no significant difference between the left and right CCA geometries[267]. Multiple studies have considered measurements of carotid arteries during tilt interventions, often in the context of investigating cerebral blood flow[268–270]. Many of these studies measure the geometry of the internal carotid arteries (ICA) and/or the vertebral arteries (VA). It is likely that the same trends found in ICA during tilt would be followed by CCA due to the similar characteristics of the two sections of the vessel[271]. During an acute HUT maneuver (from supine to 70° HUT), Van Campen *et al.* noted no change in the diameter of the VA or right ICA, and only a minor decrease in the diameter of the left ICA from 4.63 ± 0.46 mm to 4.49 ± 0.50 mm ($p < 0.05$)[268]. These results are similar to data from Sato *et al.*, who reported a slight decrease in ICA diameter (4.9 ± 0.1 mm to 4.7 ± 0.1 cm; $p < 0.05$) between 0° and 60° HUT, along with no significant change in VA diameter[270]. Our measurements do not include HUT conditions over 45° HUT; however, we do not find any significant difference between A_{CCA} at 45° HUT and at a seated baseline. In contrast, Hannerz *et al.* noted a slight significant increase in CCA diameter of 0.3 mm shortly after entering 15° HDT from 0° supine in subjects with chronic

tension-type headaches, although the authors also noted that this increase was reversed 30 minutes after a placebo injection[272]. We can hypothesize that any transient change in CCA geometry due to a sudden fluid shift is likely to be very short-lived, on the order of minutes. Even a long period in mild altered-gravity does not appear to alter the size of the CCA. For example, Palombo *et al.* noted no change in CCA geometry or stiffness after five weeks of head-down tilt bed rest (HDTBR)[269]. Similarly, Ogoh *et al.* found no significant change in CCA compliance after 57 days of HDTBR[273].

In contrast to CCA results, our findings show that the A_{IJV} is highly dependent on tilt, and that there is a difference between the geometries of the left and right IJV. Lorchirachooonkul *et al.* measured a larger IJV diameter on the right side compared to the left side (right: 13.4 ± 4.5 mm, left: 11.0 ± 4.4 mm; $p < 0.05$) in a moderate Trendelenburg position (15° HDT)[202]. Our results are consistent with Lobato *et al.*, who also noted the larger size of the right IJV with respect to the left IJV[203]. Further, Lobato and his colleagues compared the increase in size of the left and right IJV between the 0° supine and the 10° HDT Trendelenburg positions, noting an approximately 20 mm^2 increase in the left IJV compared to a 35 mm^2 increase in the right IJV. The differences in size between the left and right IJV are likely explained by a combination of anatomy[274] and embryologic origins[275,276]. Variation in the expansion of the left and right IJVs shown in Figure 4.8B suggests that there could be a difference in compliance between the two IJVs. A paucity of data exists on left IJV compliance. However, further analysis of data from Tarnoki *et al.* would suggest values for specific compliance (i.e., compliance per unit length) of 3.9 ± 0.2 ml/mmHg/mm for the right IJV and 2.5 ± 0.2 ml/mmHg/mm for the left IJV in a study of 169 subjects[277].

Anatomically, blood drains into the IJVs from the cranial sinuses via the left and right transverse sinuses (TS)[278]. Saiki *et al.* demonstrated different drainage patterns between individuals. They noted that in 73.6% of 91 subjects, the superior sagittal sinus drained principally (either perfectly or imperfectly – 100% or the vast majority) into the right TS (and hence, the right IJV), whilst in 72.6% of subjects, the smaller straight sinus drained equivalently into both the left and right TS or favored the left TS[274]. Thus, in the majority of people, the blood flow through the right IJV originates principally from the larger sagittal sinus and the blood flow through the left

IJV originates from the smaller straight sinus. In addition, Saiki hypothesized that the difference in jugular vein size is related to embryonic development, specifically the anastomosis of the left and right anterior cardinal veins leading to the disappearance of the left superior vena cava. This leads to a lower vascular resistance in the right side path, leading to a shift of superior sagittal sinus drainage towards the right TS. We hypothesize that increased venous compliance in the right IJV is also related to this early development, with the increased blood flow in the right IJV leading to increased compliance as a result of previously identified mechanotransduction pathways during embryonic development[279].

Conversely, we found no significant differences between the left and right IJVP. The venous system splits at the confluence of sinuses before rejoining at the superior vena cava[18]. Across the anatomical distance where the left and right sides are separated, the largest pressure drop occurs between the distal sigmoid and jugular bulb[280] such that, by the section where we took our measurements, distal to the jugular bulb, IJVP on both sides is only slightly elevated above central venous pressure[281,282]. Thus, we do not expect pressures on either side to be much elevated above CVP, and hence we do not expect to find a difference between the left and right side at the measured point. However, we note a significant difference in IJVP between the prone and supine positions. Specifically, in the prone position, IJVP was, on average, 4.3 ± 1.2 mmHg higher than in the supine position. To our knowledge, this is the first study comparing the effect of posture (supine vs. prone) on IJVP. Moreover, our results are congruent with broader hemodynamic measures collected during the same study[186]. We previously hypothesized that thorax compression in the prone position leads to a decreased stroke volume and cardiac output, along with increased total peripheral resistance. We further hypothesize here that this thorax compression elevates intrathoracic pressure[283] and hence, central venous pressure in the prone position[284]. This is reflected in our measurements as an increase in IJVP. This is supported by studies demonstrating elevated central venous pressure during a Valsalva maneuver[285,286].

4.4.2.1 Comparison with Spaceflight Studies

A preliminary assessment of the gravitational dose-response curves can be made by comparing our results with a variety of studies that have measured A_{IJV} and IJVP in altered-gravity conditions. Figure 4.11 presents experimental data from studies by Marshall-Goebel *et al.*[12], Lee *et al.*[194], and David *et al.*[195], superimposed on our A_{IJV} and IJVP gravitational dose-response curves. Marshall-Goebel *et al.* conducted a cohort study with 11 astronauts to investigate the left IJV on Earth (in seated, supine, and 15° HDT positions) and during long duration spaceflight, with data collected in-flight on day 50 (FD50) and day 150 (FD150). Lee *et al.* conducted a parabolic flight study where investigators collected experimental data from the right IJV (right A_{IJV} in 9 subjects, right IJVP in 6 subjects) in different gravitational conditions: 1g seated, 0.75g, 0.50g, 0.25g, and microgravity. David *et al.* conducted a study in a single Russian astronaut in which the right A_{IJV} was measured pre-flight across a range of tilt angles. Partial gravity data collected during parabolic flight (Lee *et al.*[194]) are depicted in figure 4.11 as the equivalent tilt position obtained by projecting the gravitational vector along the craniocaudal axis for tilt (e.g., 0.50g is placed at 30° HUT since $\arcsin(30^\circ) = 0.5$). Data obtained in microgravity conditions (Lee *et al.*[194] and Marshall-Goebel *et al.*[12]) are superimposed at 6° HDT, since this is the most commonly used analog for microgravity[1,125,126,287].

Data for A_{IJV} demonstrates good agreement with the dose-response curves for both parabolic flight and tilt data. Data for IJVP in the same conditions is more difficult to interpret due to the low number of points and reduced number of subjects. Data from Marshall-Goebel *et al.* indicate that, although A_{IJV} in-flight is elevated with respect to the seated position, it is actually reduced with respect to the supine position. This decrease seems to be exacerbated with more prolonged time in microgravity. IJVP is elevated from the (pre-flight) supine position after 50 days in microgravity, then reduced when remeasured after 150 days in microgravity. Based on a 6° HDT model for microgravity, we would expect A_{IJV} and IJVP to be elevated compared to 0° supine. There are multiple potential reasons for this difference. First, the dose-response curves generated represent an acute rather than chronic response. Entry to microgravity conditions precipitates a number of

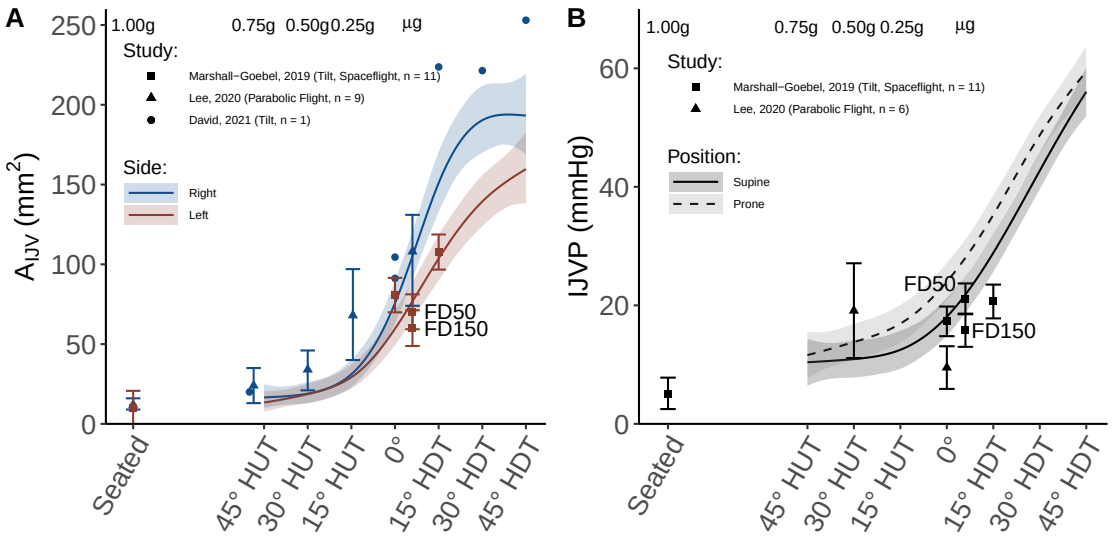

Figure 4.11: **(A-B)** Comparison of the internal jugular vein area (A_{IJV}) and the internal jugular vein pressure (IJVP) gravitational dose-response curves with spaceflight-related studies that include relevant data during tilt (Marshall-Goebel, 2019[12]; David, 2021[195]), parabolic flight (Lee, 2020[194]), and in-flight (Marshall-Goebel, 2019[12]). Data collected in a weightless condition are placed at 6° head-down tilt (HDT), data at partial gravity from parabolic flight are placed at a tilt angle representative of the equivalent gravitational vector resolved along the craniocaudal axis. **(A)** A_{IJV}; **(B)** IJVP.

chronic changes in the hemodynamic system[6]. Principal among these changes is the reduction in circulating blood volume due to the fluid shift from intravascular to extravascular spaces as well as neurally-mediated reduction by the Renin-Angiotensin-Aldosterone (RAAS) endocrine system[288]. This reduction in blood volume, which occurs over the first few hours in space, lowers fluid pressures throughout the systemic circulation, leading to decreased distension after a prolonged period[12,21]. Second, measurement of the IJVP using the non-invasive VeinPress device is dependent on the tissue surrounding the vein. Measurements of IJVP using the VeinPress are likely slightly elevated compared to the true venous pressure, due to compression of the tissue surrounding the IJV. Changes in fluid compartmentalization[289–291], including fluid shift to extravascular spaces as well as potential changes in the neck tissue due to chronic muscular deconditioning over long duration spaceflight, may result in both a reduced venous pressure, as well as an underestimation of that measurement[292]. Third, there are fundamental differences in the vascular response to tilt

compared to true microgravity. One key difference refers to the central venous pressure (CVP) response. On Earth, in a tilt paradigm, central venous pressure has been demonstrated to increase in HDT[147,293] with respect to the supine position. However, data from spaceflight indicates that CVP actually decreases in microgravity (with respect to the same supine reference position). Buckey *et al.* hypothesize that the reason for this disparity is driven by the removal of external pressures on the vascular system when exposed to true microgravity, due to the absence of tissue weight[50]. Computational models of systemic circulation accounting for this removal of tissue weight support this hypothesis, demonstrating the anticipated reduction, rather than rise, in CVP[95]. Given that IJVP is only minimally elevated above CVP, we further hypothesize that this decrease in CVP in microgravity also leads to a decreased IJVP and A_{IJV} with respect to the anticipated response from the dose-response curves generated in 1g conditions using a tilt paradigm. These differences suggest that, in cases where fluid shift and hemodynamic pressures in the head and neck are important, for example when considering the pathoetiology of SANS or venous thromboembolic events, the standard 6° HDT model of microgravity may require re-evaluation.

Overall, our results are congruent with studies supporting an increase in both jugular vein engorgement and jugular venous pressure in space compared to the seated or standing position[12,205–207,294]. These data serve as a reference terrestrial model that can be used to compare the magnitude of A_{CCA}, A_{IJV}, and IJVP changes occurring on entry to microgravity (and in the future, partial gravity) conditions. In addition, these dose-response models can be an invaluable resource to support the development of spaceflight countermeasures focused on counteracting the headward fluid shift and the associated hydrostatic changes (e.g., artificial gravity[119,154]). Such countermeasures could be used to reduce incidence of SANS and decrease venous thromboembolic risk[295].

4.4.3 Limitations

We acknowledge several limitations of our study. First, our study population consisted of only male subjects, which limits variability in our results. However, Arzeno *et al.*[163] noted gender differences in baroreflexive control of blood pressure. On the other hand, Patel *et al.*[164] found no significant effect of gender on autonomic indices in a protocol involving HUT, HDT, and lower

body negative pressure. Studies by Scheel *et al.* and Krejza *et al.* have demonstrated that the CCA is significantly smaller in women than in men[265,266]. Similarly, Choudhry *et al.* found that men presented a larger CCA at the bifurcation point than women[267]. In order to reduce variability in the dose-response curves, it was determined that males and females should be considered separately. This is supported by recent work by Patterson *et al.* suggesting significant differences in the attenuation of the jugular vein in response to orthostatic stress between men and women[295]. Patterson *et al.* conclude that data should be interpreted in a sex-dependent manner. We will consider differences between male and female subjects in Section 4.7 below.

Second, our study only measured acute responses. Much literature has reported on the long term effects of altered gravity environments, and our investigation did not consider those hemodynamic changes with a longer time-course, for example cardiovascular degradation[178,189], reduction in total blood volume due to endocrine response, or long term autonomic changes[4,140,296]. From the discussion of Figure 4.11 it was determined that chronic effects play a role in jugular vein hemodynamics, particularly in spaceflight studies. Consideration should be given to the chronic trends in the terrestrial dose-response curves (for example through head-down tilt bed rest[55] or computational models[178]), in order to determine whether they follow the same pattern of deconditioning/adaptation observed in flight studies[12]. However, we believe that understanding and mapping the physiological mechanisms behind the acute response to altered gravity still provides insight into the expected response to countermeasures. Further, there are also situations in spaceflight where optimal operational performance is critical immediately after a gravity transition (for example immediately after entering orbit or landing), when the acute response is dominant. In order to minimize the transient effects of large fluid shifts, we elected to progress, as opposed to randomize, the tilt angle in our methodology. It is established that there exists some amount of hysteresis in the venous vascular system. However, there are conflicting data as to whether this leads to significant creep[297,298]. Whilst our data undoubtedly contain some component of vascular creep, we do not believe it to be significant in the context of the magnitude of the area and pressure changes shown.

Third, the entire study was conducted using noninvasive methods. Future work should consider the addition of more invasive measurements to improve accuracy and provide additional dose-response relationships. In particular, a direct measurement of cardiac output would provide the most accurate dose-response relationship as there are observable differences between the results of different methodologies[126,299]. Further, for the autonomic measures, samples of blood plasma catecholamines and other neurohormones along with intracellular magnesium levels[300,301] could provide further insights into cardiovascular control. Finally, invasive measurement of central venous pressure would provide informative data on cardiac loading conditions and thoracic blood volume[302,303]. The VeinPress device used in the study was chosen for its heritage of use in previous spaceflight and parabolic flight investigations[12,194,292], thus, facilitating direct comparison between studies. It is acknowledged that invasive measures, such as venous catheterization, may provide more accurate measurements of IJVP. However, non-invasive measurements using ultrasonography are well-established in a clinical environment[304–306].

Fourth, in this study we attempted to capture the mean response of the common carotid artery, as opposed to pulsatility. The data analysis workflow involved measuring and averaging A_{CCA} at 15 Hz across a number of heartbeats in a four-second window. Thus, the data represent an arithmetic mean (similar to mean arterial pressure) used to determine whether there are larger systemic changes outside of the pulsatility. Future work should investigate the role of pulsatility of the carotid artery at different degrees of headward fluid shift. Ideally, this would be supplemented with flow measurements (i.e., peak systolic and end diastolic flow) to capture a more complete hemodynamic response.

Finally, related to the IJV, pressure and area measurements are only two parts of the very complex picture of vascular hemodynamics. Whilst the pressure and area data are useful and informative on their own, future studies should also include flow measurements to provide a more complete understanding of jugular venous flow. In particular, an assessment of the characteristics of jugular vein flow as performed by Marshall-Goebel *et al.* may prove insightful. However, it is noted that they did not find any flow stagnation in a terrestrial setting in seated, supine, or 15° HDT

positions[12]. In Section 5 we add flow measurements to our consideration of LBNP hemodynamics.

4.5 Summary of Experiment 1

We implemented a tilt paradigm to investigate the acute changes in multiple hemodynamic parameters and autonomic indices across a range of 45° HUT to 45° HDT in both supine and prone positions. Our data revealed a strong gravitational dependence of almost all metrics considered, explained by cephalad fluid shift in HDT combined with alterations of baroreflex function. Based on the experimental data collected, we constructed gravitational dose-response curves for all variables across the tilt ranges considered. Further, we confirmed statistically significant differences between supine and prone positions in heart rate, stroke volume, cardiac output, total peripheral resistance, oxygen consumption, and internal jugular vein pressure but not in blood pressure. This difference is likely due to thorax compression inhibiting baroreflex function whilst prone, leading to an increase in sympathetic activity and raised central venous pressure. Results show that the right IJV distends more than the left IJV. Pressure is not statistically different between the left and right internal jugular veins. Comparison of the jugular vein dose-response curves with external studies reveals good agreement in tilt. However, differences between tilt and true microgravity are also revealed, likely as a result of reduced compressive forces on the venous system in weightless conditions due to a combination of a reduction of intrathoracic pressure and the removal of tissue weight. These findings lead to a greater understanding of acute cardiovascular hemodynamics in altered gravity, while the gravitational dose-response curves provide a unique and comprehensive baseline to support spaceflight countermeasure development, as well as other Earth applications, such as terrestrial surgery in prone or HDT positions.

4.6 Addendum 1: Intraocular Pressure and Ocular Perfusion Pressure

Due to the importance of intraocular pressure and its relationship to SANS, we studied the gravitational effect of IOP over a wider range than the ±45° covered in the main tilt experiment. This experiment used a separate subject pool to the original experiment. Thus, we have elected to report on the IOP results as an addendum separate to the main experiment. In this study, we

further considered the gravitational effects on ocular perfusion pressure and the implications for the pathoetiology of SANS.

4.6.1 Motivation

Any change in posture induces gravitational fluid shifts and accompanying changes in regional pressures[307–309]. Because of the elongated shape of the human body and eccentric placement of eyes and brain, these organs are exposed to particularly large pressure changes every time we stand up and lie down[310,311]. Human physiology is well adapted to these common gravitational pressure changes and compensatory systemic and intrinsic mechanisms, including cerebral autoregulation, that work efficiently to maintain appropriate blood perfusion. Removal of gravitational stress, such as during spaceflight, is associated with a chronic headward fluid shift and loss of diurnal pressure variability, which likely results in a mild, but persistent elevation in cephalad pressures compared to a standing or seated position on Earth[22,312,313]. This might be related to a series of ocular changes occurring during spaceflight. More than half of astronauts on long-term missions develop structural and functional changes at the back of the eye, including disc edema, widening and possible kinking of the optic nerve, choroidal folds, globe flattening, loss of visual acuity, and small retinal infarctions (cotton wool spots), collectively referred to as Spaceflight Associated Neuro-ocular Syndrome (SANS)[47,57]. The exact etiology of SANS remains unknown, primarily because we do not fully understand the gravitational influence on ocular health and thus, we are unable to predict the consequences of removing, or more generally altering, the gravitational stress.

Normal ocular and visual function depend on appropriate arterial perfusion of the eye, which is characterized as ocular perfusion pressure (OPP) and calculated as mean arterial pressure (MAP) at eye level (MAP_{eye}) minus intraocular pressure (IOP), Equation 4.4:

$$OPP = MAP_{eye} - IOP \tag{4.4}$$

IOP is determined by the production and absorption rate of aqueous humor plus episcleral venous pressure as defined by the Goldmann equation (4.5):

$$IOP = \frac{(F - U)}{C} + P \tag{4.5}$$

where F is aqueous flow rate through the anterior chamber, U is the outflow rate through the uveoscleral drainage pathway, C is the trabecular outflow facility, and P is episcleral venous pressure[24]. Postural changes in IOP, on a short timeline, are primarily driven by episcleral venous pressure and as such, linked to the systemic circulation[314]. However, because the eye overall constitutes a smaller hydrostatic system than the systemic circulation, changes in the gravitational vector have a comparatively smaller impact on IOP than MAP_{eye}[22,24,142,238,315–318]. Due to the anterior position of the eye, not only upright versus lying down (G_y) but also prone versus supine posture (G_x) affect ocular pressure and hemodynamics (including the ophthalmic arteries, the central retinal arteries, and the posterior ciliary arteries) by inducing a short hydrostatic column from the base of the rostral globe to the mid-caudal plane. The resultant hydrostatic pressure gradient influence IOP and, hence, OPP. Previous studies have shown IOP to be elevated in the prone position compared to the supine position[142,319].

Changes in OPP are associated with pathologies of the eye. For example, reduced OPP due to reduced MAP_{eye} and/or elevated IOP is a well-known risk factor for the prevalence, incidence, and progression of glaucoma[320–322]. Similarly, choroidal thinning in early progression of patients with reticular pseudodrusen (RPD) has also been associated with reduced OPP[323]. In particular, the optic disc excavation seen in glaucomatous eyes is opposite to the edema found in many cases of SANS. We hypothesize that increases in OPP due to the mismatch between autoregulation of MAP_{eye} and IOP in altered-gravity conditions leads to swelling of the hyperemic choroid and thus, it is an important marker for understanding the etiology and progression of SANS.

Here, we investigate how changes in the full range (360°) of the gravitational vector from upright standing to full inversion through supine and prone postures affect IOP, MAP_{eye}, and thus OPP. We hypothesize that head-down tilt postures increase MAP_{eye} to a greater extent than IOP, thereby increasing OPP. We also hypothesize that any degree of head-down tilt in prone postures increases IOP to a greater extent than in supine posture, and thus are associated with a lower OPP.

Finally, we hypothesize that these changes can be predicted and explained by passive hydrostatic changes.

4.6.2 Methods

4.6.2.1 Subjects and Study Approval

Thirteen healthy male volunteers (mean ± SD: age 22.1 ± 1.1 years; height 180.91 ± 7.74 cm; weight 76.8 ± 12.22 kg) were enrolled in this study after providing oral and written consent. None took any medication (prescription or over the counter) at the time of the study, and all were instructed to avoid strenuous exercise and caffeine 12-hours prior to the trial. The subjects self-reported no history of chronic cardiovascular or ocular conditions (e.g., glaucoma) and no ocular surgery (including keratomileusis/keratectomy) within the previous 12 months. The protocol was approved by the Institutional Review Board at both the University of California San Diego (UCSD) and Texas A&M University (TAMU) and in accordance with the declaration of Helsinki. The study was conducted in two separate locations; UCSD ($n = 7$) and TAMU ($n = 6$).

4.6.2.2 Procedure

Subjects were placed on an inversion tilt table fitted with ankle clamps to keep the subject from sliding at steeper angles of tilt. After an initial rest period subjects were, in a randomized order, exposed to varying tilt angles. Figure 4.12 shows a visual representation of the angle convention used. For the supine posture, these angles were 90° (fully upright), 45°, 30°, 15°, 0° (supine horizontal), 345°, 330°, 315°, 300°, 285°, and 270° (fully head-down). For the prone posture, angles were 90° (fully upright), 135°, 150°, 165°, 180° (prone horizontal), 195°, 210°, 225°, 240°, 255°, and 270° (fully head-down). Thus, the full 360° range of tilt angles were measured for each subject (Figure 4.12). Each tilt angle was maintained for five minutes before recording cardiovascular variables and IOP of both left and right eye, subjects rested in a fully head-up (90°) posture for 5 minutes between each experimental tilt angle.

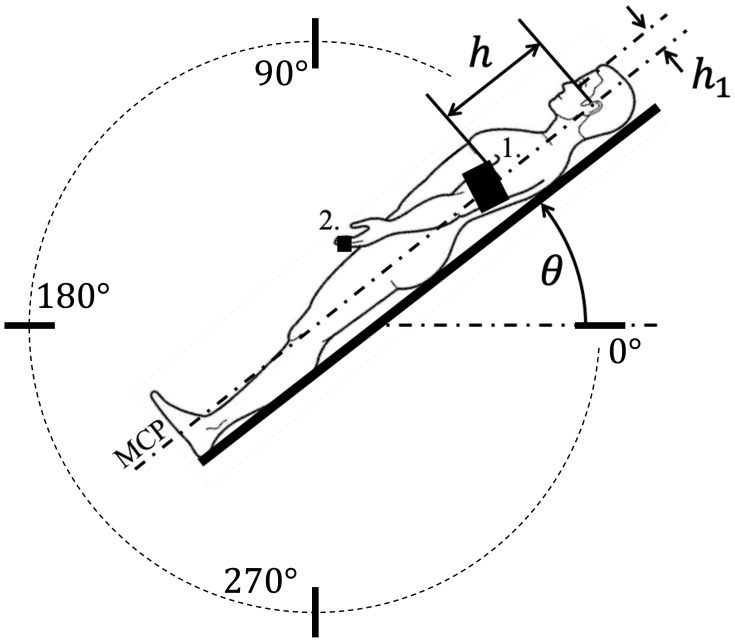

Figure 4.12: Experimental setup. Subject is tilted through the full 360° range of tilt angles. MAP was measured using either 1) a brachial cuff ($n = 6$) or 2) a finger cuff ($n = 7$) then corrected to eye level (MAP_{eye}). Supine position is the angles 270° (full inversion) through 0° (horizontal supine) to 90° (upright), prone position is 90° (upright) through 180° (horizontal prone) to 270° (full inversion). θ, angle of tilt; h, distance from heart to eye level along mid-coronal plane; h_1, perpendicular distance from mid-coronal plane to the globe of the eye; MCP, mid-coronal plane.

4.6.2.3 Equipment and Materials

Left and right IOP (26 eyes total) were measured non-invasively using a rebound technology (iCare Pro Handheld Tonometer, iCare, Vantaa, Finland). The version of tonometer used, the IC200, was specifically designed to allow accurate measurement with positional freedom across, providing accurate measurements at all tilt angles considered. To account for heart rate and respiratory fluctuation, each IOP measurement from each eye, in each posture, was repeated five times and presented as average.

Blood pressure and heart rate were recorded either continuously by the volume-clamp method (N=7) using a cuff around the third finger (Nexfin, Netherlands) and corrected to eye level (MAP_{eye}) by fixing the Nexfin height sensor at the lateral canthus; or during steady state by oscillometric method ($n = 6$) using a brachial cuff on the right arm at heart level (Omron, USA) and mathe-

matically corrected to eye level (MAP_{eye}) by accounting for a) the hydrostatic pressure difference between heart and eye-level (h in Figure 4.12) the perpendicular distance from mid-coronal plane of the body to anterior placement of the globe of the eye (h_1 in Figure 4.12). These distances, h and h_1, were measured for each subject before the study.

4.6.2.4 Statistical Analyses

Data and statistical analyses were performed in R version 4.1.0 (R foundation for statistical computing, Vienna, Austria). Linear mixed models (LMM) were constructed with tilt angle (on a 360° scale as described in Figure 4.12), eye (left or right), and study location (UCSD or TAMU) as fixed effects, and subject as the random effect. Separate models were constructed for the three dependent variables: IOP, MAP_{eye} (no eye factor), and OPP. Significant effects of tilt angle were followed with two sets of contrasts. Differences from 0° supine were examined using Dunnett's multiple comparison procedure[226]. Pairwise comparisons between prone and supine were conducted at each tilt angle with Benjamini and Hochberg's false discovery rate correction applied[227]. LMMs were fit with the `nlme` package using restricted maximum likelihood (REML) and variance was allowed to vary across tilt angles to compensate for increased heterogeneity at more severe head-down tilts. Data are given as means and standard errors (SE). The level of statistical significance was set to $\alpha = 0.05$.

4.6.3 Results

There was no significant difference in the effect of study location on the measurement of IOP values ($p = 0.695$). Thus, location was removed as a factor and both locations were combined for subsequent analysis. Further, there was no significance for eye (left or right) on the measurement of IOP ($p = 0.193$); hence, it was also removed as a factor. Mean IOP in 0° supine posture was 19.2 ± 0.6 mmHg. A statistically significant decrease of –3.3 ± 0.6 mmHg ($p < 0.001$) was measured when tilting to 90° (fully upright, Figure 4.13 and Table 4.5). There were no other significant changes in a head upwards position. A statistically significant increase of 20.7 ± 1.7 mmHg ($p < 0.001$) was measured during supine head-down tilt to 270° (fully inverted). In supine pos-

ture, there was a statistically significant increase in IOP from 0° supine when tilting downwards at all angles: 345° ($p = 0.043$), 330° ($p < 0.001$), 315° ($p < 0.001$), 300° ($p < 0.001$), 285° ($p < 0.001$), and 270° ($p < 0.001$). In prone posture, there was a statistically significant increase in IOP compared to 0° supine at prone horizontal position (180°, $p < 0.001$), and all HDT angles: 195° ($p < 0.001$), 210° ($p < 0.001$), 225° ($p < 0.001$), 240° ($p < 0.001$), 255° ($p < 0.001$), and 270° ($p < 0.001$). Figure 4.13 shows the IOP mean ± SE across all tilt angles.

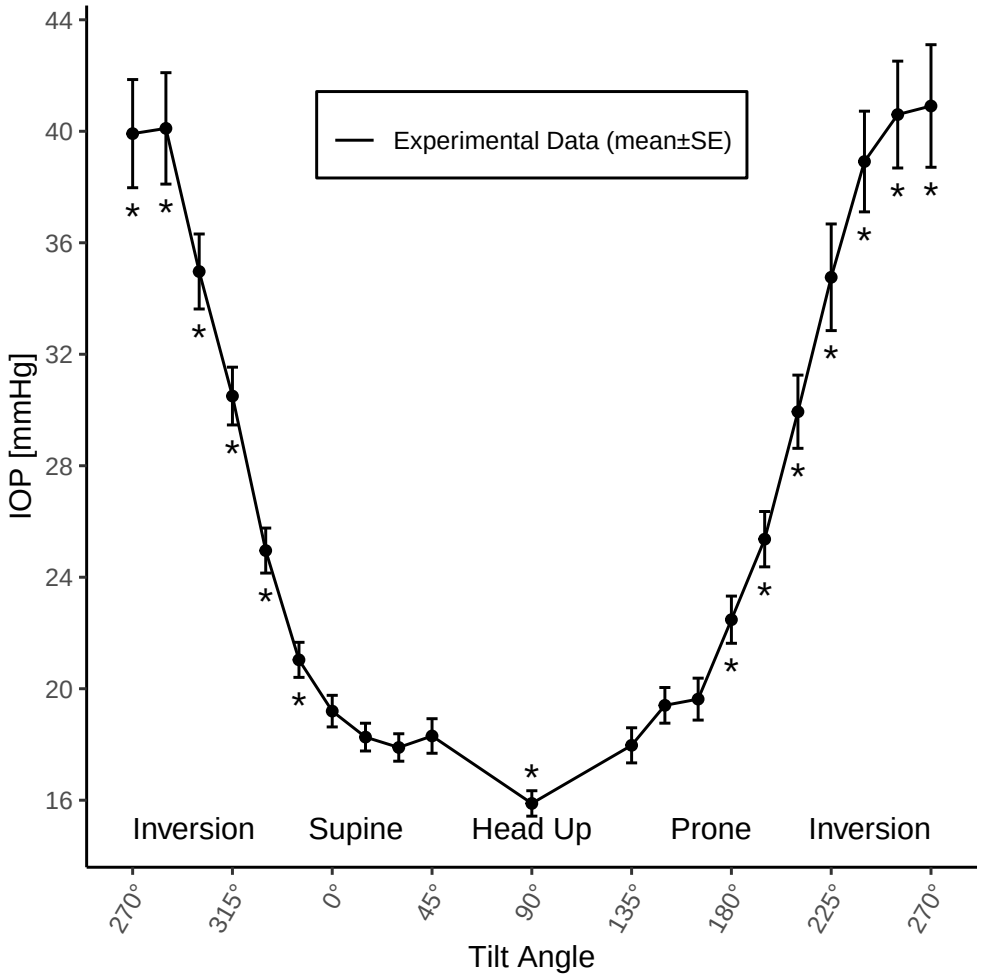

Figure 4.13: Intraocular Pressure (mean ± SE) as a function of tilt angle across all subjects ($n = 13$). *$p < 0.05$ compared with 0º supine horizontal position.

There was no significant difference in the effect of study location on the measurement of

MAP_{eye} values ($p = 0.358$). Thus, location was removed as a factor and both locations were combined for subsequent analysis. MAP_{eye} followed a trend similar to IOP, and decreased significantly from supine posture at 0° (81.3 ± 1.7 mmHg) to 90° (fully upright; 60.8 ± 3.2 mmHg, $p < 0.001$, Figure 4.14 and Table 4.5), while increasing during head-down tilt postures to 119.8 ± 4.5 mmHg ($p < 0.001$) at 270° (fully inverted). Significant differences from supine 0° were found at all tilt angles apart from 345° ($p = 0.051$, 15° HDT supine), 15° ($p = 0.074$, 15° HUT supine), and 165° ($p = 0.999$, 15° HUT prone). Figure 4.14 shows the MAP_{eye} mean ± SE across all tilt angles.

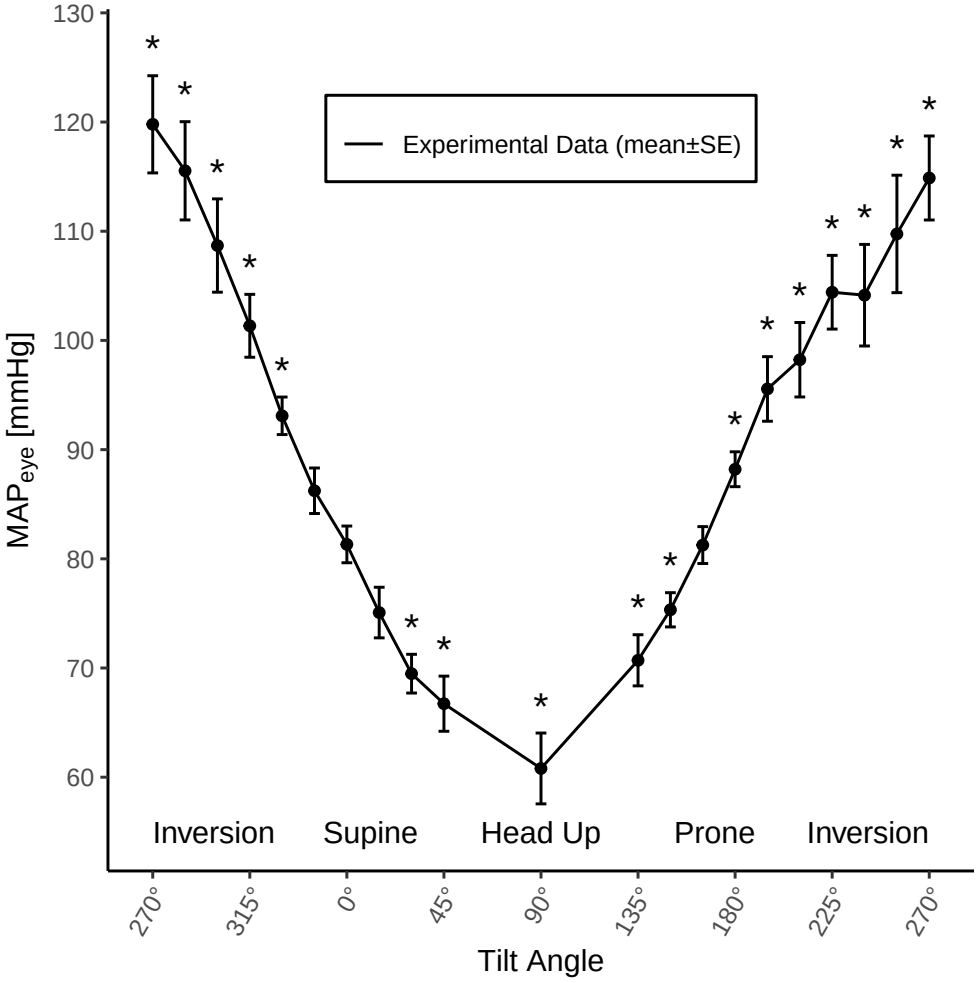

Figure 4.14: Mean arterial blood pressure (mean±SE) at the level of the eye as a function of tilt angle across all subjects ($n = 13$). *$p < 0.05$ compared with 0º supine horizontal position.

There was no significant difference in the effect of study location on the measurement of OPP values ($p = 0.384$). Thus, location was removed as a factor and both locations were combined for subsequent analysis. Further, there was no statistically significant difference for eye (left or right) on the measurement of OPP ($p = 0.418$); hence, it was also removed as a factor. OPP decreased significantly from 0° supine (62.1 ± 1.4 mmHg) to 90° upright (45.6 ± 2.2 mmHg; $p < 0.001$, Figure 4.15), while supine fully inverted head-down tilt significantly increased OPP to 79.4 ± 3.7 mmHg ($p < 0.001$). In supine posture, OPP was significantly different from 0° supine at all tilt angles except for 345° ($p = 0.148$, 15° HDT supine). In prone posture, OPP was significantly different from 0° supine at 135° ($p < 0.001$), 150° ($p < 0.001$), 195° ($p = 0.002$), 225° ($p = 0.010$), and 270° ($p < 0.001$). Figure 4.15 shows OPP (mean ± SE) across all tilt angles.

Table 4.5 shows a summary of all the changes from 0° supine with SE and p values for IOP, MAP_{eye}, and OPP.

4.6.3.1 Prone vs Supine

IOP in prone posture was significantly higher at all angles of tilt between 60° HDT and 30º HUT compared to the supine posture (Figure 4.16 and Table 4.5). These angles correspond to the maximum influence of the hydrostatic column caused by the offset of the eye from the mid-caudal plane, which varies with the cosine of the tilt angle (Equation (4)). In particular, in the horizontal position, IOP was 3.5±0.8 mmHg (p<0.001) higher in prone posture compared to supine posture. OPP in prone posture was also significantly higher compared to the supine posture at 15º HDT (p=0.045), 15º HUT (p=0.044), and 30º HUT (p=0.044). Conversely, OPP was non-significantly higher in supine than in prone at severe HDT angles (90º, p=0.198; 75º, p=0.225; and 60º, p=0.051). Figure 4.16 and Table 4.6 show the change in IOP between supine and prone across all tilt angles. Table 4.6 also shows the OPP differences between prone and supine postures.

4.6.4 Discussion

This study confirms that IOP and MAP_{eye} are both gravity dependent variables. In addition, the study further contributes to the understanding of gravitational changes on OPP. A statistically

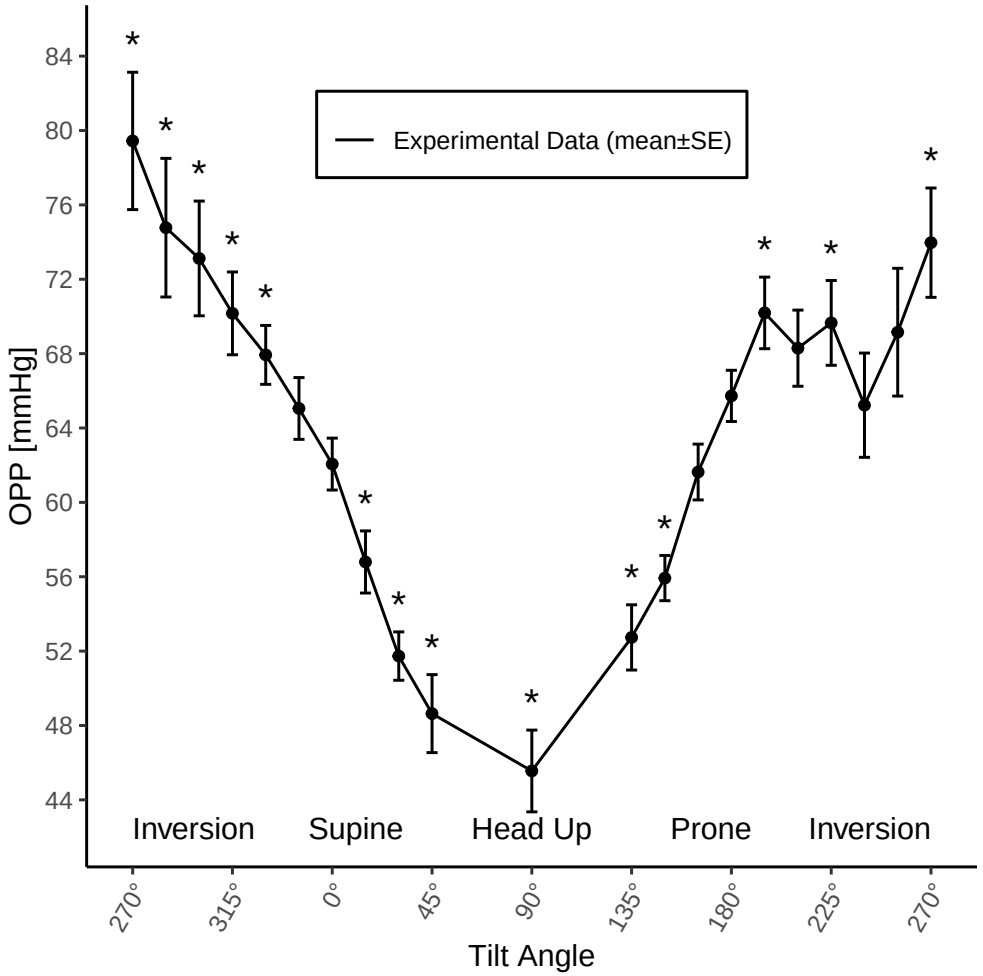

Figure 4.15: Ocular perfusion pressure (mean ±SE) as a function of tilt angle across all subjects ($n = 13$). *$p < 0.05$ compared with 0º supine horizontal position.

significant increase in IOP was measured in both eyes when subjects were tilted from 0° to 90° head-down, while a small decrease in IOP was measured in both eyes when subjects were tilted from 0° to 90° upright that was only significant at 90°. This occurred in both supine (face up) and prone (face down) postures. No significant differences were found between the left and right IOP at any tilt angle. MAP_{eye} significantly decreased from 0° supine to 90° upright while MAP_{eye} significantly increased when subjects were tilted from 0° to 90° head-down in both supine and prone postures.

These results are consistent with data from multiple studies across a smaller range of tilt angles.

Table 4.5: Change from 0° supine for intraocular pressure (IOP), mean arterial pressure at eye level (MAP_{eye}), and ocular perfusion pressure (OPP). Significance is adjusted using Dunnett's multiple comparison procedure for 20 tests. $*p < 0.05$.

Angle		IOP (mmHg)			$\mathbf{MAP_{eye}}$ (mmHg)			OPP (mmHg)		
		Change from 0°	**SE**	p	**Change from 0°**	**SE**	p	**Change from 0°**	**SE**	p
Supine	270°	20.7	1.7	<0.001*	38.5	4.1	<0.001*	17.4	3.2	<0.001*
	285°	20.9	1.7	<0.001*	34.2	4.1	<0.001*	12.7	3.3	0.002*
	300°	15.8	1.2	<0.001*	27.4	3.8	<0.001*	11.1	2.6	<0.001*
	315°	11.3	0.9	<0.001*	20.0	2.6	<0.001*	8.1	1.8	<0.001*
	330°	5.8	0.8	<0.001*	11.8	1.7	<0.001*	5.9	1.5	0.001*
	345°	1.8	0.6	0.043*	4.9	1.7	0.051	3.0	1.2	0.148
	0°	—	—	—	—	—	—	—	—	—
	15°	–0.9	0.6	0.636	–6.2	2.2	0.074	–5.3	1.5	0.010*
	30°	–1.3	0.6	0.295	–11.8	2.1	<0.001*	–10.3	1.5	<0.001*
	45°	–0.9	0.7	0.889	–14.6	2.6	<0.001*	–13.4	2.1	<0.001*
Upright	90°	–3.3	0.6	<0.001*	–20.5	3.4	<0.001*	–16.5	2.5	<0.001*
Prone	135°	–1.0	0.6	0.679	–10.6	2.7	0.002*	–9.6	1.8	<0.001*
	150°	0.4	0.6	0.993	–6.0	1.8	0.017*	–6.4	1.3	<0.001*
	165°	0.6	0.7	0.961	–0.1	1.9	0.999	–0.7	1.5	0.999
	180°	3.5	0.8	<0.001*	6.9	1.9	0.006*	3.4	1.5	0.296
	195°	6.4	0.9	<0.001*	14.2	3.0	<0.001*	7.8	2.0	0.002*
	210°	10.9	1.2	<0.001*	16.9	3.5	<0.001*	5.9	2.1	0.082
	225°	15.8	1.7	<0.001*	23.1	3.4	<0.001*	7.3	2.1	0.010*
	240°	19.9	1.6	<0.001*	22.8	4.7	<0.001*	2.9	2.7	0.942
	255°	21.6	1.7	<0.001*	28.4	5.4	<0.001*	6.8	3.3	0.360
	270°	21.9	1.9	<0.001*	33.6	3.7	<0.001*	11.6	2.6	<0.001*

Laurie *et al.* demonstrated a significant increase in IOP from 15.0 mmHg measured in supine position to 15.7 mmHg measured at 6° HDT (0.7 mmHg increase)[317]. Similarly, Blecha *et al.* demonstrated an increase in IOP from 19.9 ± 0.4 mmHg at 0° supine to 30.7 ± 0.6 mmHg at 45° HDT after 30 minutes of exposure. This is consistent with our data, which show an increase in IOP from 19.2 ± 0.6 mmHg at 0° supine to 30.5 ± 1.0 mmHg at 45° HDT[315]. Further, Marshall-Goebel *et al.* found an increase in IOP from 15.7 ± 0.3 mmHg at 0° supine to 17.9 ± 0.4 mmHg at 12° HDT (2.1 mmHg increase), and 18.7 ± 0.4 mmHg at 18° HDT (3.0 mmHg increase)[124]. Concerning

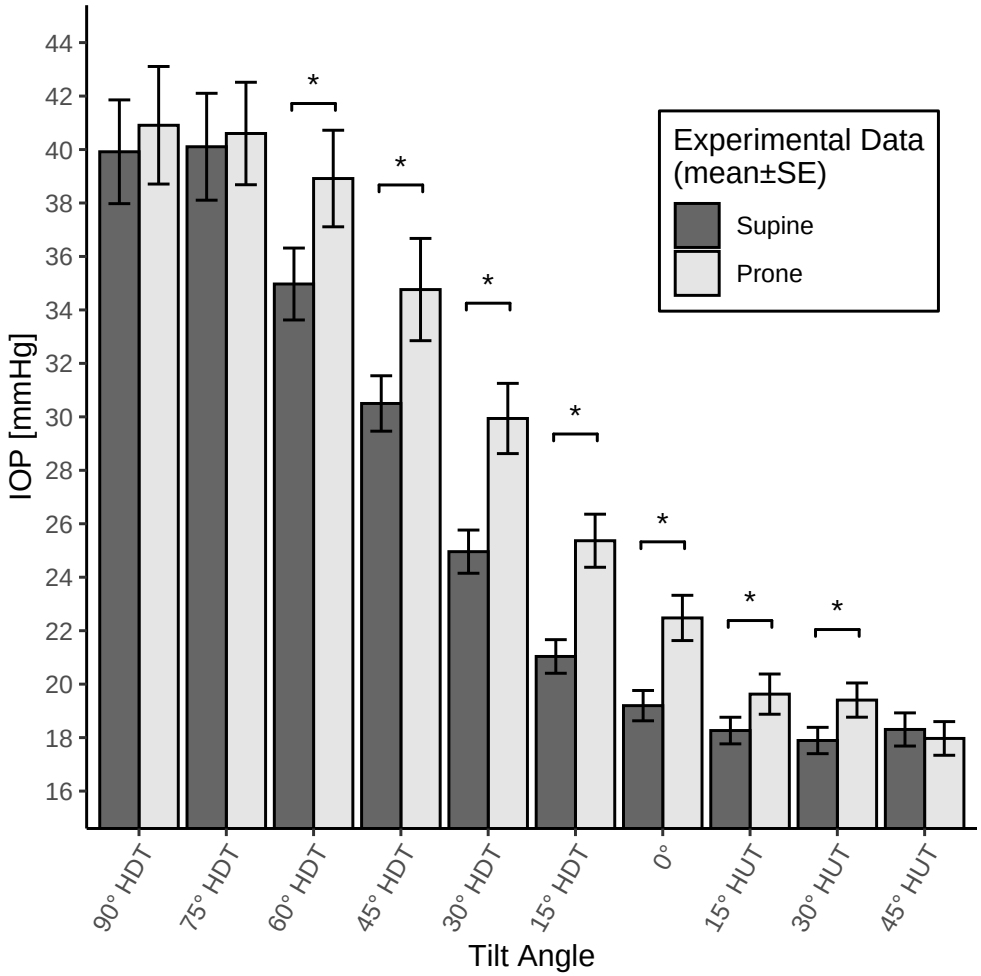

Figure 4.16: Prone and supine intraocular pressure (mean ± SE) as a function of tilt angle. Dark bars represent supine posture, light bars represent prone posture. $*p < 0.05$.

HUT, Mayalı *et al.* found a non-significant decrease in IOP from 0° supine (18.5 ± 0.6 mmHg) to 90° HUT (17.1 ± 0.5 mmHg, p=0.07)[318], which is consistent with the decrease in our data. Conversely, Chiquet *et al.* did not find a significant increase in IOP in 6° HDT compared to the supine position[316]. However, their study involved 7 days HDT bed rest and they reported a decrease in IOP after day 5. These differences in IOP results are most likely explained by the timescale differences between our studies. While we considered acute changes, Chiquet *et al.* performed their first IOP measurements after at least 24 hours of HDT bed rest, when the body's autoregulatory processes have already begun to act on systemic and cephalad hemodynamics.

Table 4.6: Increase in IOP and OPP in prone position versus supine position. Significance is adjusted using Benjamini and Hochberg's false discovery rate correction for 10 tests. *$p < 0.05$.

Angle	IOP (mmHg)			OPP (mmHg)		
	Increase in Prone vs Supine	**SE**	p	**Increase in Prone vs Supine**	**SE**	p
90° HDT	1.2	2.5	0.785	–5.8	3.9	0.198
75° HDT	0.7	2.3	0.847	–5.9	4.4	0.225
60° HDT	4.1	1.8	0.033*	–8.2	3.5	0.051
45° HDT	4.5	1.7	0.018*	–0.8	2.4	0.819
30° HDT	5.2	1.2	<0.001*	0.0	2.2	0.983
15° HDT	4.5	0.8	<0.001*	4.8	1.9	0.045*
0°	3.5	0.8	<0.010*	3.4	1.5	0.057
15° HUT	1.6	0.5	0.009*	4.5	1.7	0.044*
30° HUT	1.7	0.5	0.002*	3.9	1.5	0.044*
45° HUT	–0.1	0.7	0.852	3.8	2.5	0.198

This study also demonstrated the effect of supine vs prone postures on IOP. Our experimental data show a 3.5 ± 1.0 mmHg increase in IOP from 0° supine to 0° prone. Our results are consistent with data from Anderson *et al.*, who found a 6.6 ± 0.8 mmHg increase between 0° supine and 0° prone in 24 subjects[142]. This evidence supports the conclusion that hydrostatic forces play an important role in ocular hemodynamics, and while the hydrostatic difference between heart and eye level is clearly the dominant influence, the anterior eccentric placement of the eye is also an important factor to take into account.

Changes in OPP are an important factor to consider that may have important implications for the occurrence of SANS. We have demonstrated significant effects of posture on OPP, which significantly decreased from 0° supine to 90° upright and significantly increased from 0° supine to fully head-down. In particular, and more relevant to the spaceflight domain, Figure 4.15 demonstrates that the increase in IOP due to head-down tilt is relatively small compared to the increase in MAP_{eye}; therefore, OPP significantly increases during head-down tilt. Notably, in a head-down tilt bed rest study, subjects developing early symptoms of SANS displayed elevated cerebral perfusion pressure[55], therefore elevated OPP[324]. This also matches surgical studies where patients in steep

Trendelenburg position have demonstrated elevated cerebral perfusion pressure[325].

SANS remains a critical roadblock for long-term space exploration missions. While the exact pathophysiological mechanisms behind the neuro-ocular findings of SANS remain unknown, several possible explanations have been proposed and explored. An increase in intracranial pressure due to the cephalad fluid shift in microgravity environments has been the prevailing theorized mechanism behind SANS. However, recent data suggests that the absence of gravity in space does not pathologically increase ICP but rather prevents the typical reduction of ICP seen in the upright position when on Earth, which over time may lead to the neuro-ocular symptoms of SANS[22,326,327]. It has also been suggested that a compromise in the balance between ICP and IOP due to microgravity exposure could result in alterations in the translaminar pressure gradient (TLPG) across the lamina cribrosa, which may induce remodeling of the eye leading to SANS[328,329].

Pathologically elevated OPP can occur as a result of significantly increased MAP_{eye}[330,331], and/or decreased IOP[60]. Case reports of hypertension and ocular hypotony due to trauma display identical clinical manifestations to SANS, including optic disc edema, posterior globe flattening, cotton wool spots, and loss of visual acuity[60,330–332]. We have demonstrated that changing the gravitational vector through head-down tilt can increase both IOP and OPP simultaneously. In microgravity, the loss of the habitual hydrostatic pressure gradient is likely associated with an increase in MAP_{eye} (as well as changes in aqueous humor outflow[142]) compared to the terrestrial seated position (in addition to the removal of diurnal variation) and hence an increase in OPP in addition to the increase in IOP. The same mechanisms that generate the TLPG are also responsible for the manifested mismatch between MAP_{eye} and IOP and hence elevated OPP[333]. This elevated perfusion of the posterior parts of the eye can lead to edema formation[321,334].

Despite previous studies examining the role that ICP and IOP may have on the development of SANS, the role of OPP has yet to be explored. Maintaining proper OPP is crucial for regulating blood flow into the ocular tissue, and alterations in OPP may result in inadequate perfusion of the eye and pathologies. Changes in OPP have been implicated in the pathogenesis of several eye diseases such as open angle glaucoma, which has been associated with a decrease in OPP[335].

The significant gravitational dependency of OPP and IOP demonstrated in this study implies that the pressure and flow regulation of ocular tissues are likely affected both by changes in, or abolishment of, the gravitational vector. While changes in IOP, MAP_{eye}, and OPP in microgravity may be relatively low in comparison to more steep HDT angles, continuous microgravity exposure may result in a mild but constant state of augmented perfusion of the ocular tissue. While the exact pathophysiological mechanism is unknown, changes in OPP due to alterations in the gravitational vector may play a role in the neuro-ocular findings of SANS. Thus, we propose that a greater understanding of gravitational and weightlessness effects on OPP is crucial to fully understand the etiology of SANS.

Limited data exist examining whether the regulation of OPP and IOP can be described through passive hydrostatics or an active regulation system. The increase in IOP and subsequent decrease in OPP in the prone positions vs the supine positions demonstrated in this study supports the significance of an additional hydrostatic column. These data suggest that OPP regulation can be captured through a simple passive hydrostatic system.

The significant effects of gravity on IOP also have clinical implications on Earth. The Trendelenburg position, where patients are tilted 15-30° HDT, is often used in surgery to allow for optimal access to the pelvic organs[336]. However, extended periods of time in this HDT position have been associated with cases of postoperative blindness and cognitive dysfunction[148,337]. Previous studies have already demonstrated increases in IOP and decreases in OPP during the Trendelenburg position[315,338]. The effect of gravity on IOP and OPP demonstrated in this study further confirms these previous studies and suggests that changes in IOP and OPP may be responsible for the ocular disruptions seen in the Trendelenburg position. Prone positioning during surgery has also been associated with visual loss after spine surgery due to elevated IOP and a change in the hemodynamics affecting optic nerve perfusion[319]. Similarly, the Wilson frame, which places the patient in a prone head-down position, has also been associated as a risk factor for ischemic optic neuropathy and perioperative visual loss[339].

4.6.4.1 Limitations

The overall aim of this study was to demonstrate changes in intraocular pressure and ocular perfusion pressure as a consequence of passive hydrostatics over the full range of tilt angles (360°). While small tilt angles primarily induce passive fluid shift, larger angles of tilt inevitably impose a multitude of physiological effects and compensatory reactions[310]. As pooling of venous blood in the splanchnic circulation and legs is augmented during increasing head-up tilt angles, a larger sympathetic response and a multitude of integrated reflexes are elicited with the ultimate goal of preventing cerebral hypoperfusion. All of these effects in concert modulated the postural responses of IOP, MAP_{eye}, and OPP. Additionally, pulmonary function and $PaCO_2$ are affected by posture with significant effect on particular cerebral vasculature and thus potentially perfusion to the eye. While head-down tilt initially facilitates cardiac filling, steeper angles may be associated with impaired filling and contraction due to mechanical compression from abdominal organs and possibly overstretching of heart musculature[238]. Taken together, the intricate integrative human physiology includes a multitude of reactions and counter-reactions which ultimately all modulated our data, however, the close correlation with the model demonstrated that much of these short-term gravitational effects on ocular pressure and perfusion can be explained by passive hydrostatics, indicating that these organs are highly gravity-dependent.

4.6.5 Summary of IOP/OPP Experiment

This study demonstrates the impact of gravitational stress on OPP and underlines the potential role of OPP for maintaining ocular health relative to both gravity and weightlessness. Angles of HDT resulted in a greater increase in MAP_{eye} relative to IOP, thereby increasing OPP. This increase in OPP may be significant for visual and ocular pathology following, for example, surgical procedures performed in HDT on Earth. Moreover, mild but persistent elevation in OPP during spaceflight may contribute to the well described ocular changes associated with SANS. Additionally, we confirm the effects of a hydrostatic pressure column that increases IOP in the prone position compared to the supine position, which supports that these regional pressures, and thus

OPP, are primarily regulated by passive hydrostatics.

4.7 Addendum 2: Sex Differences

4.7.1 Motivation

In Section 4.4.3 we discussed how one of the limitations of the original study was that it only included male subjects. Future spaceflight will see a higher proportion of female crewmembers and given the aim of the Artemis program to land the first woman on the Moon it is important to consider the effect of sex when examining cardiovascular function. Further, it has already been highlighted that multiple studies have noted sex dependent differences in hemodynamic function, autonomic response, and in particular the hemodynamics of the neck[163,265–267,295]. Where the VTE concern is considered, it should also be noted that the case report of a venous thrombosis onboard ISS was detected in a female crewmember[9]. Thus, in this addendum, we extend the original study by incorporating 12 additional female subjects. We keep the methodology and protocol the same as in the original experiment, but add *Sex* as an additional factor into our dose-response models.

4.7.2 Methods

4.7.2.1 Subjects and Study Approval

In addition to the 12 male subjects, we further recruited 12 healthy, recreationally active female subjects. The same inclusion and exclusion criteria as used in Section 4.2.1 were applied, with the addition of pregnancy as an exclusion. The female subjects were selected in order to match the age range and BMI of the male subjects. Subject characteristics (mean ± SD), including blood pressure at screening, are shown in Table 4.7. The data also present a comparison with the male subjects as assessed by a two-sample t-test. One subject was unable to complete the 45° HDT condition in both the supine and prone positions due to discomfort; an additional subject was unable to complete the 45° HDT condition in the prone position. Both subjects were returned to a head-up tilt position and experienced no lasting symptoms. The remainder of their data are included in the results. All other subjects completed the full protocol and experienced no adverse effects. All procedures performed in the study were in accordance with the 1964 Helsinki Declaration

and its later amendments. The study protocol was approved by the Texas A&M Human Research Protection Program with Institutional Review Board number IRB2020-0724F.

Table 4.7: Characteristics of the 12 recreationally active female subjects who participated in the study. Characteristics are presented alongside the 12 male subjects from Table 4.1 and were recorded during baseline session prior to testing sessions. Data are reported as mean ± SD where appropriate. Race categories: W, White; B, Black or African American; A, Asian. Abbreviations: BMI, body mass index; SBP, systolic blood pressure; DBP, diastolic blood pressure. The final column, p, shows where the values are significantly different from the male subjects as assessed by a two-sample t-test: $^{***}p < 0.001$, $^{**}p < 0.01$, $^{*}p < 0.05$.

Characteristic	**Male**	**Female**	p
n	12	12	—
Race	W (8), B (1), A (3)	W (6), A (6)	—
Age (years)	26.8 ± 2.9	27.9 ± 4.4	0.479
Height (cm)	179.0 ± 8.3	159.4 ± 6.9	$<0.001^{***}$
Weight (kg)	84.7 ± 18.7	61.3 ± 15.9	0.003^{**}
BMI (kg/m^2)	26.3 ± 4.9	24.1 ± 6.4	0.344
SBP (mmHg)	129.5 ± 14.5	120.3 ± 18.7	0.192
DBP (mmHg)	82.3 ± 6.5	80.8 ± 13.1	0.722

4.7.2.2 Experimental Design and Testing Protocol

The experimental design and testing protocol was identical to the procedure described in Section 4.2.2.

4.7.2.3 Dependent Variables

The dependent variables collected were identical to those described in Section 4.2.3, including eight measures of systemic hemodynamics, four time-domain and five frequency-domain autonomic indices, and three measures related to the neck hemodynamics.

4.7.2.4 Instrumentation and Data Collection

Instrumentation and data collection were largely the same as presented in Section 4.2.4. However, we used two separate ultrasound devices. The VScan Extend was used to collect measure-

ments of IJVP in conjunction with a VeinPress device, whilst measurements of A_{CCA} and A_{IJV} were collected using a Butterfly iQ+ ultrasound (Butterfly Network Inc., Burlington, MA). The areas were collected from images taken at end diastole, with the vessels (both CCA and IJV) being manually circumscribed onto the images by a trained operator.

4.7.2.5 Statistical Analysis

In order to construct the dose-response curves whilst including the effect of *Sex*,we use a similar procedure to the one fully described in Section 4.2.5, with an additional fixed effect of *Sex*. We constructed dose-response curves using LMMs, GLMMs (gamma distribution/log link), and GAMMs for the systemic hemodynamic, autonomic, and cephalad measurements, respectively. For the LMMs and GLMMs, the linear predictor took the form:

$$\begin{aligned}\eta_{iikl} = \beta_0 &+ \beta_1 \sin\left(Angle_j\right) + \beta_2\left(Sex_k\right) + \beta_3\left(Position_l\right) + \beta_4\left(\sin\left(Angle_j\right) \times Sex_k\right) \\ &+ \beta_5\left(\sin\left(Angle_j\right) \times Position_l\right) + \beta_6\left(Sex_k \times Position_l\right) \\ &+ \beta_7\left(\sin\left(Angle_j\right) \times Sex_k \times Position_l\right) + \gamma_i + \varepsilon_{ijkl}\end{aligned} \tag{4.6}$$

where, for each dependent variable, the linear predictor η_{ijkl} for subject i ($i = 1:24$) is described by the tilt *Angle* ($j = 1:7$, from 45° HUT to 45° HDT), the *Sex* of the subject ($k = 1:2$, male or female), *Position* ($l = 1:2$, supine or prone), the fixed effects β (where β_0 represents the intercept), the random intercept γ_i (associated with each subject and the within-subjects design), and the residual error ε_{ijkl}. Dose-response curves are shown as mean and 95% confidence band. If the main effect of a factor and any interactions involving that factor were not significant, that factor was removed. Interaction effects were only included if statistically significant. For the cephalad measurements, the dose-response of the GAMM was given by Equation 4.7, where separate smoothed splines were used for each significant parametric effect including the *Side* ($m = 1:2$, right or left):

$$y_{ijklm} = \beta_0 + \beta_1 (Sex_k) + \beta_2 (Position_l) + \beta_3 (Side_m) + f_{klm} (\sin (Angle_j)) + \gamma_i + \varepsilon_{ijklm} \tag{4.7}$$

Diagnostics were assessed using the same procedure as described in Section 4.2.5. All statistical analyses were completed using R version 4.2.2[340] with LMMs and GLMMs fit using the `lme4`[225] and `glmmTMB`[230] packages. GAMMs were fit using the `mgcv` package[231]. Diagnostics were assessed using the `lmerTest`[232] and `DHARMa`[233] packages. Significance level was set at $\alpha = 0.05$ (two-sided).

4.7.3 Results

4.7.3.1 Experimental Data

Figure 4.17 shows the evolution of hemodynamic parameters (mean ± SE) as a function of tilt angle (including the seated baseline). Table 4.8 reports the results of the LMM analyses. Results for the female subjects follow the same trend as results from the male subjects. All variables, with the exception of VO2, show a linear effect of tilt angle. For SBP, as with the male subjects, a small effect of tilt angle appears present, however systolic blood pressure is largely controlled across the tilt range measured. There is a significant main effect of *Sex* for RPP ($p = 0.042$) and VO2 ($p < 0.001$). On average, males have an RPP 1020 ± 490 mmHg/min ($t_{52} = 2.082$) higher than females, and a VO2 0.143 ± 0.025 l/min ($t_{61} = 5.797$) higher than females. CO has a significant interaction effect between *Angle* and *Sex* ($p = 0.011$) but no significant main effect of *Sex* ($p = 0.363$), such that CO increases 0.11 ± 0.04 l/min/15° faster in males than in females ($t_{302} = 2.552$). Similarly, TPR has a significant interaction effect between *Sex* and *Position* ($p = 0.037$) but no significant main effect of *Sex* ($p = 0.189$), with TPR being lower in the supine position for males, but higher in the supine position for females. Contrary to the results in Section 4.3.1 and Figure 4.5, when female subjects are included, we find no effect of position on stroke volume (higher in supine by 0.12 ± 3.39 ml, $t_{298} = 0.036$, $p = 0.971$). We further find no effect of position on RPP (lower in supine by 530 ± 310 mmHg/min, $t_{302} = -1.714$, $p = 0.088$).

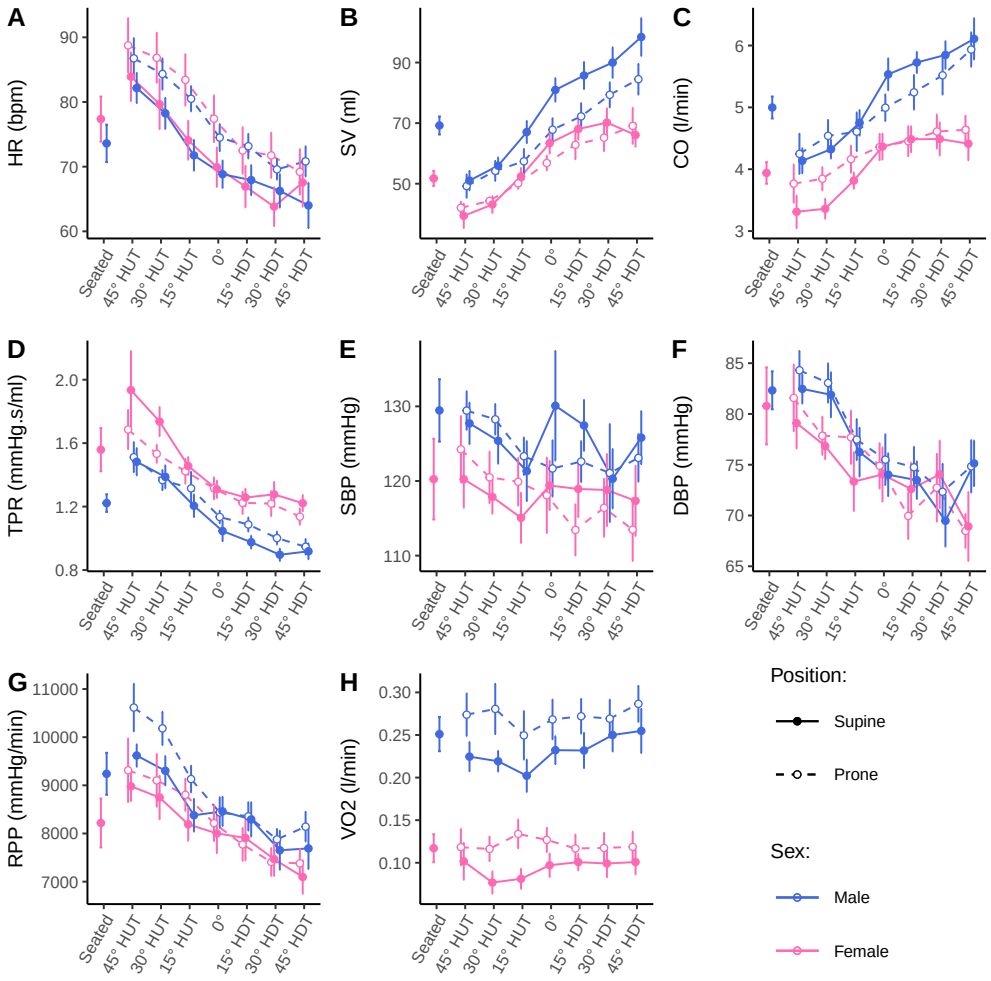

Figure 4.17: **(A-H)** Hemodynamic variables as a function of tilt angle in supine (solid line, filled circles) and prone (dashed line, unfilled circles) positions, collected on 12 male (blue) and 12 female (pink) subjects. Measurements were taken at a seated baseline, 45° head-up tilt (HUT), 30° HUT, 15° HUT, 0°, 15° head-down tilt (HDT), 30° HDT, and 45° HDT. Data are presented as means ± SE at each tilt angle. **(A)** HR, heart rate; **(B)** SV, stroke volume; **(C)** CO, cardiac output; **(D)** TPR, total peripheral resistance; **(E)** SBP, systolic blood pressure; **(F)** DBP, diastolic blood pressure; **(G)** RPP, rate pressure product; **(H)** VO2, oxygen consumption.

Table 4.8: Statistical results of the linear mixed model and generalized linear mixed model analysis incorporating sex differences. Fixed factors included *Angle*, *Sex*, *Position*, and their interactions. Subjects were included as random factors. See text for abbreviations and model details. $^{***}p < 0.001$, $^{**}p < 0.01$, $^{*}p < 0.05$.

	Significance p						
	Angle	**Sex**	**Position**	**Angle × Sex**	**Angle × Position**	**Sex × Position**	**Angle × Sex × Position**
Hemodynamic Measurements:							
HR	<0.001***	0.397	<0.001***	0.296	0.160	0.455	0.492
SV	<0.001***	0.283	0.971	0.080	0.559	0.771	0.198
CO	<0.001***	0.363	0.011*	0.011*	0.102	0.184	0.889
TPR	<0.001***	0.189	0.008**	0.685	0.086	0.037*	0.410
SBP	0.012*	0.358	0.120	0.646	0.073	0.474	0.538
DBP	<0.001***	0.469	0.186	0.837	0.228	0.601	0.406
RPP	<0.001***	0.042*	0.088	0.242	0.243	0.298	0.663
VO2	0.821	<0.001***	0.018*	0.602	0.385	0.367	0.754
Time-Domain Autonomic Indices:							
SDNN	<0.001***	0.908	0.017*	0.894	0.229	0.456	0.718
RMSDD	<0.001***	0.876	0.051	0.218	0.646	0.754	0.862
HRVTi	<0.001***	0.743	0.003**	0.408	0.042*	0.275	0.556
BRS	<0.001***	0.197	<.009**	0.115	0.346	0.090	0.296
Frequency-Domain Autonomic Indices:							
LF	0.003**	0.439	0.004**	0.783	0.564	0.404	0.737
HF	<0.001***	0.904	0.030*	0.305	0.117	0.336	0.456
LFNorm	<0.001***	0.566	0.431	0.107	0.574	0.825	0.588
HFNorm	<0.001***	0.565	0.431	0.107	0.574	0.824	0.589
LF/HF	<0.001***	0.883	0.739	0.021*	0.345	0.412	0.078

Figure 4.18 shows the evolution of time-domain autonomic indices (mean ± SE) as a function of tilt angle (including the seated baseline). Table 4.8 reports the results of the GLMM analyses. In none of the variables do we find a significant main effect of *Sex*, or any significant interactions involving *Sex*. Further, contrary to the results in Section 4.3.2 and Figure 4.6, when the female subjects are considered, we find significant main effects of *Position* for SDNN, HRVTi, and BRS, but no significant main effect of *Position* for RMSDD ($z = 1.95$, $p = 0.051$). For SDNN, the index is, on average, 1.23 times higher in the supine position than in the prone position ($z = 2.39$, $p = 0.017$). BRS is 1.39 times higher in the supine position than in the prone position ($z = 2.62$, $p = 0.009$). For HRVTi, there is both a significant main effect of *Position* ($z = 2.97$, $p = 0.003$) and a significant interaction between *Angle* and *Position* ($z = -2.04$, $p = 0.042$).

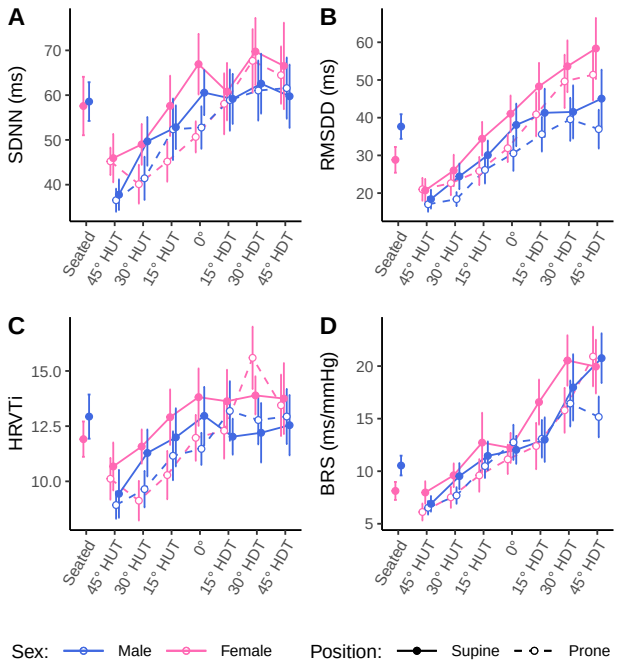

Figure 4.18: **(A-D)** Time-domain autonomic indices as a function of tilt angle in supine (solid line, filled circles) and prone (dashed line, unfilled circles) positions, collected on 12 male (blue) and 12 female (pink) subjects. Measurements were taken at a seated baseline, 45° head-up tilt (HUT), 30° HUT, 15° HUT, 0°, 15° head-down tilt (HDT), 30° HDT, and 45° HDT. Data are presented as means ± SE at each tilt angle. **(A)** SDNN, standard deviation of NN intervals (normalized RR intervals); **(B)** RMSDD, root mean square of direct differences of NN intervals; **(C)** HRVTi, heart rate variability triangular index; **(D)** BRS, baroreceptor sensitivity.

Figure 4.19 shows the evolution of the frequency-domain autonomic indices (mean ± SE) as a function of tilt angle (including the seated baseline). Table 4.8 reports the results of the LMM and GLMM analyses. With the inclusion of the female subjects, the normalized low- and high-frequency dose-response is the same as with only male subjects. However, we find a significant interaction effect between *Angle* and *Sex* in the LF/HF ratio with the decrease in LF/HF ratio being 1.10 times lower in males ($z = 0.2.306$, $p = 0.021$). Further, with the inclusion of female subjects, we now find a significant effect of *Position* on the absolute low- and high-frequency response. In the supine position, LF and HF are on average 1.70 and 1.67 times higher than in the prone position (LF: $z = 2.85$, $p = 0.004$; HF: $z = 2.166$, $p = 0.030$), respectively.

Figure 4.20 shows the evolution of A_{CCA}, A_{IJV}, and IJVP (mean ± SE) as a function of tilt angle (including the seated baseline). Table 4.8 reports the results of the GAMM analyses. With the addition of female subjects, we see no significant effect of *Sex* on any of the three neck variables ($p = 0.557$, $p = 0.465$, and $p = 0.938$ for A_{CCA}, A_{IJV}, and IJVP respectively). However, contrary to the male only results, we now find a significant effect of *Side* ($t = -2.125$, $p = 0.034$) and a small effect of tilt *Angle* ($F = 1.659$, $p = 0.002$ on the right side, $F = 0.747$, $p = 0.021$ on the left side) for A_{CCA}. For A_{IJV} in male only subjects we saw a significant effect of *Side*, with the right IJV expanding more than the left. With the addition of female subjects we now see an additional small significant effect of *Position* ($t = 2.525$, $p = 0.012$), such that A_{IJV} is slightly larger in the prone position compared to the supine position. For IJVP, the results are similar to those of male only subjects, in that we find no significant effect of *Side* ($t = -0.469$, $p = 0.640$) but do find a significant effect of *Position* ($t = 6.653$, $p < 0.001$), with IJVP being significantly higher in the prone position.

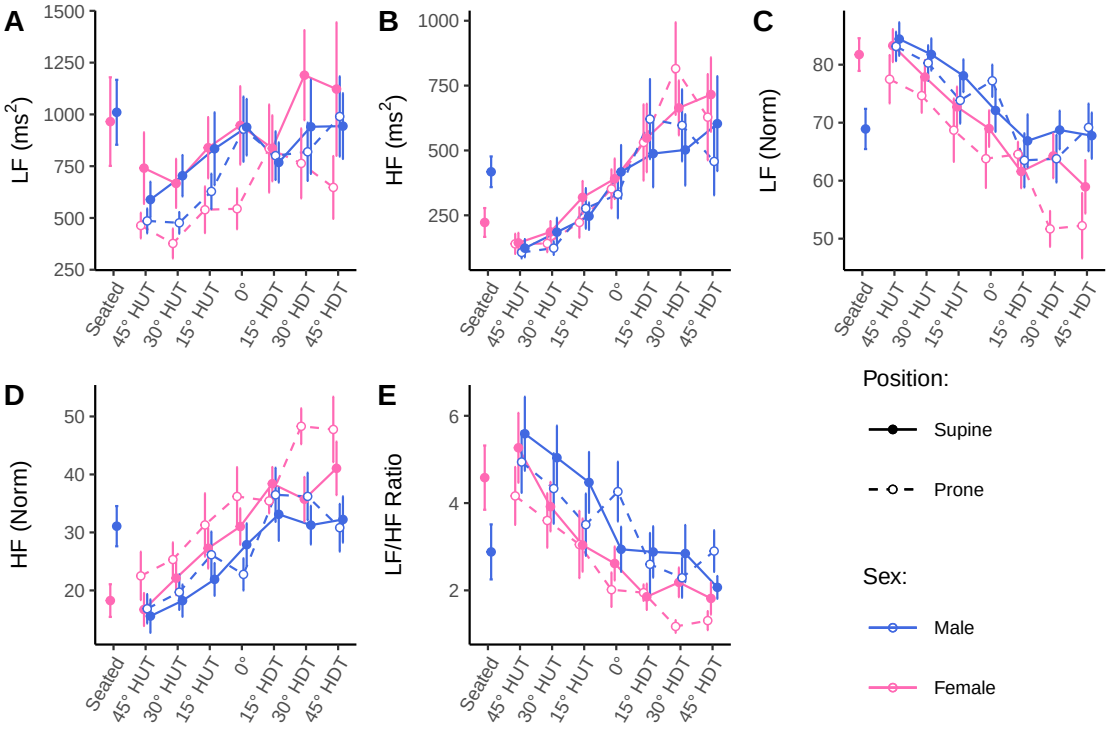

Figure 4.19: **(A-E)** Frequency-domain autonomic indices as a function of tilt angle in supine (solid line, filled circles) and prone (dashed line, unfilled circles) positions, collected on 12 male (blue) and 12 female (pink) subjects. Measurements were taken at a seated baseline, 45° head-up tilt (HUT), 30° HUT, 15° HUT, 0°, 15° head-down tilt (HDT), 30° HDT, and 45° HDT. Data are presented as means ± SE at each tilt angle. **(A)** LF, power density in the low frequency range (0.04 — 0.15 Hz); **(B)** HF, power density in the high frequency range (0.15 — 0.4 Hz); **(C)** LFNorm, LF (normalized units); **(D)** HFNorm, HF (normalized units); **(E)** LF/HF Ratio, ratio of low to high power densities.

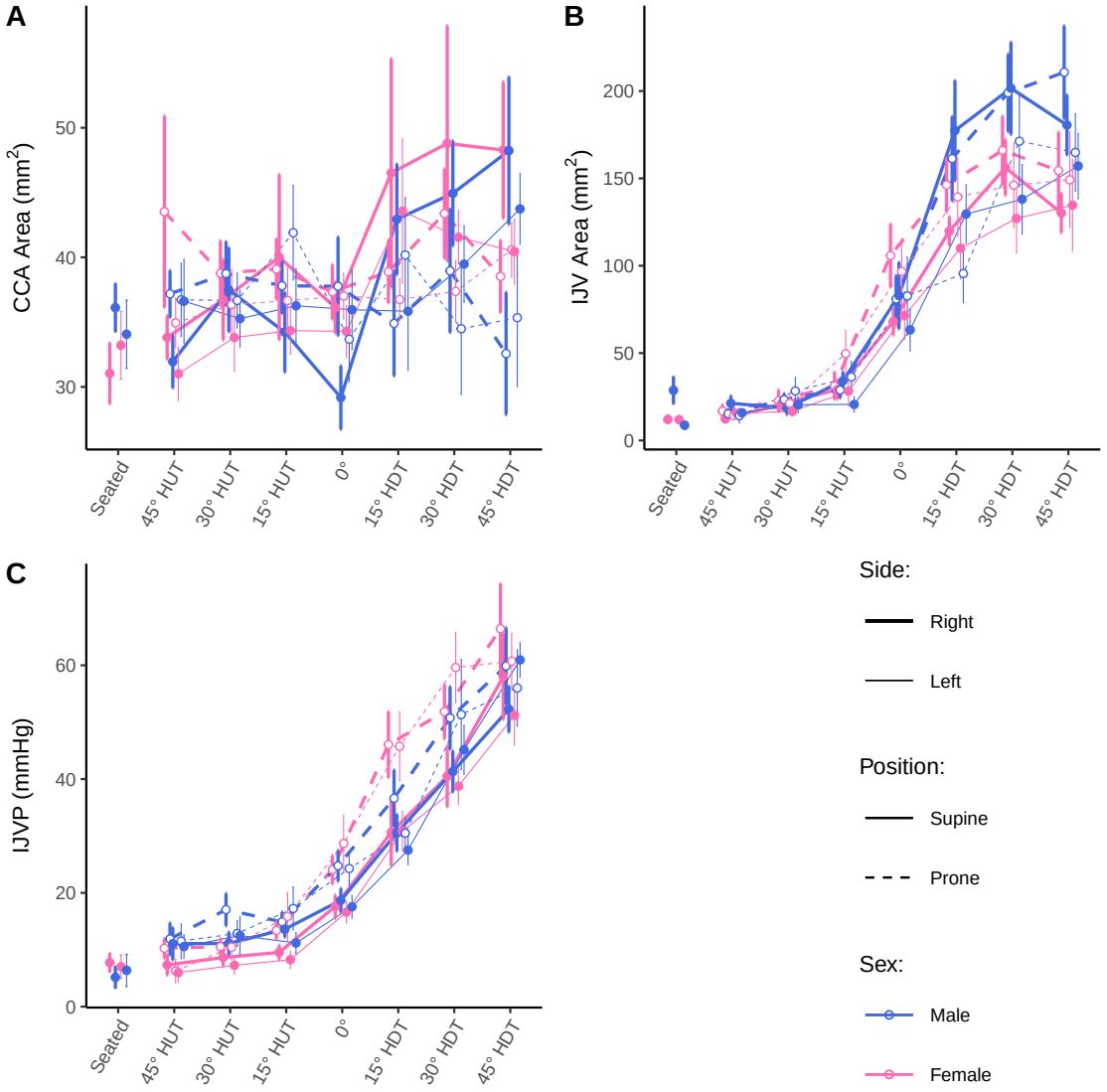

Figure 4.20: **(A-C)** A_{CCA}, A_{IJV}, and IJVP as a function of tilt angle in supine (solid line, filled circles) and prone (dashed line, unfilled circles) positions, collected on 12 male (blue) and 12 female (pink) subjects on both the right (thick line) and left (thin line) sides. Measurements were collected at a seated baseline, 45° head-up tilt (HUT), 30° HUT, 15° HUT, 0°, 15° head-down tilt (HDT), 30° HDT, and 45° HDT. Data are presented as means ± SE at each tilt angle. **(A)** A_{CCA}, common carotid artery cross-sectional area; **(B)** A_{IJV}, internal jugular vein cross-sectional area; **(C)** IJVP, internal jugular vein pressure.

Table 4.9: Details of generalized additive mixed models (GAMM) analyses for three dependent variables: common carotid artery cross-sectional area ($\sqrt{\mathbf{A_{CCA}}}$), internal jugular vein cross-sectional area ($\sqrt{\mathbf{A_{IJV}}}$), and internal jugular vein pressure (IJVP), fit to 12 male and 12 female subjects. Significance of parametric and smoothed terms, effective degrees of freedom of smoothers, size of subject random effect, and model goodness of fit (deviance explained). See text for abbreviations and model details.

	Parametric Terms						**Smooth Terms**[‖]				**Subject**	**Deviance**
	Position[†]		**Side**[‡]		**Sex**[§]		$\sin(\textbf{Angle})$[¶]				**Std Dev**[‡‡]	**Explained**[§§]
	t	p	t	p	t	p	Curve	EDF[††]	F	p	σ	%
$\sqrt{\mathbf{A_{CCA}}}$[‖‖] (mm)	–0.884	0.377	–2.125	0.034	0.587	0.557	Right	1.43	1.659	0.002	0.53	32.7
							Left	1.02	0.747	0.021		
$\sqrt{\mathbf{A_{IJV}}}$[‖‖] (mm)	2.525	0.012	–3.633	<0.001	–0.731	0.465	Supine/Right	4.21	75.865	<0.001	1.02	75.6
							Supine/Left	3.86	57.911	<0.001		
							Prone/Right	4.14	79.797	<0.001		
							Prone/Left	3.16	57.016	<0.001		
IJVP (mmHg)	6.653	<0.001	–0.469	0.640	0.078	0.938	Supine	3.69	107.743	<0.001	4.53	72.8
							Prone	3.79	133.329	<0.001		

Notes:
[†] *Position*: Supine or Prone; t reports effect size of prone compared to supine.
[‡] *Side*: Right or Left; t reports effect size of left compared to right.
[§] *Sex*: Male or Female; t reports effect size of female compared to male.
[‖] Shrinkage-penalized cubic regression splines fit to each significant *Position*, *Side*, and *Sex* combination. Plots of the smoothers are included as Figure 4.24.
[¶] Sine of the tilt *Angle* in radians, positive values indicate head-up tilt (HUT); F reports effect size.
[††] Effective degrees of freedom.
[‡‡] Random effect $\gamma \sim \mathcal{N}\left(0, \sigma^2\right)$.
[§§] Goodness of fit, equivalent to the unadjusted R^2.
[‖‖] See main text. Measurements of CCA and IJV size were homoscedastic in diameter, thus a square-root transformation was used on the cross-sectional area response.

4.7.3.2 Dose-Response Curves

Figure 4.21 shows the estimated dose-response curves for the hemodynamic parameters considered within the range of 45° HUT to 45° HDT. The parameters for the dose-response curves are captured in Table 4.10. Curves are shown as mean and 95% confidence interval. Since there was no significant difference between male and female data for HR, SV, SBP, and DBP, *Sex* data was pooled for those responses. Further, since there was no significant effect of *Position* for SV, SBP, DBP, and RPP, supine and prone estimates are also pooled for those dose-response curves. Thus, for example, the dose-response curve for HR consists of two separate curves (supine and prone), the dose-response curve for RPP also consists of two curves (male and female), whereas the dose-response curve for VO2 is four separate curves, one for each male/female and supine/prone combination. Similarly, the dose-response curves for SV, SBP, and DBP consist of a single curve for male/female and supine/prone data all together.

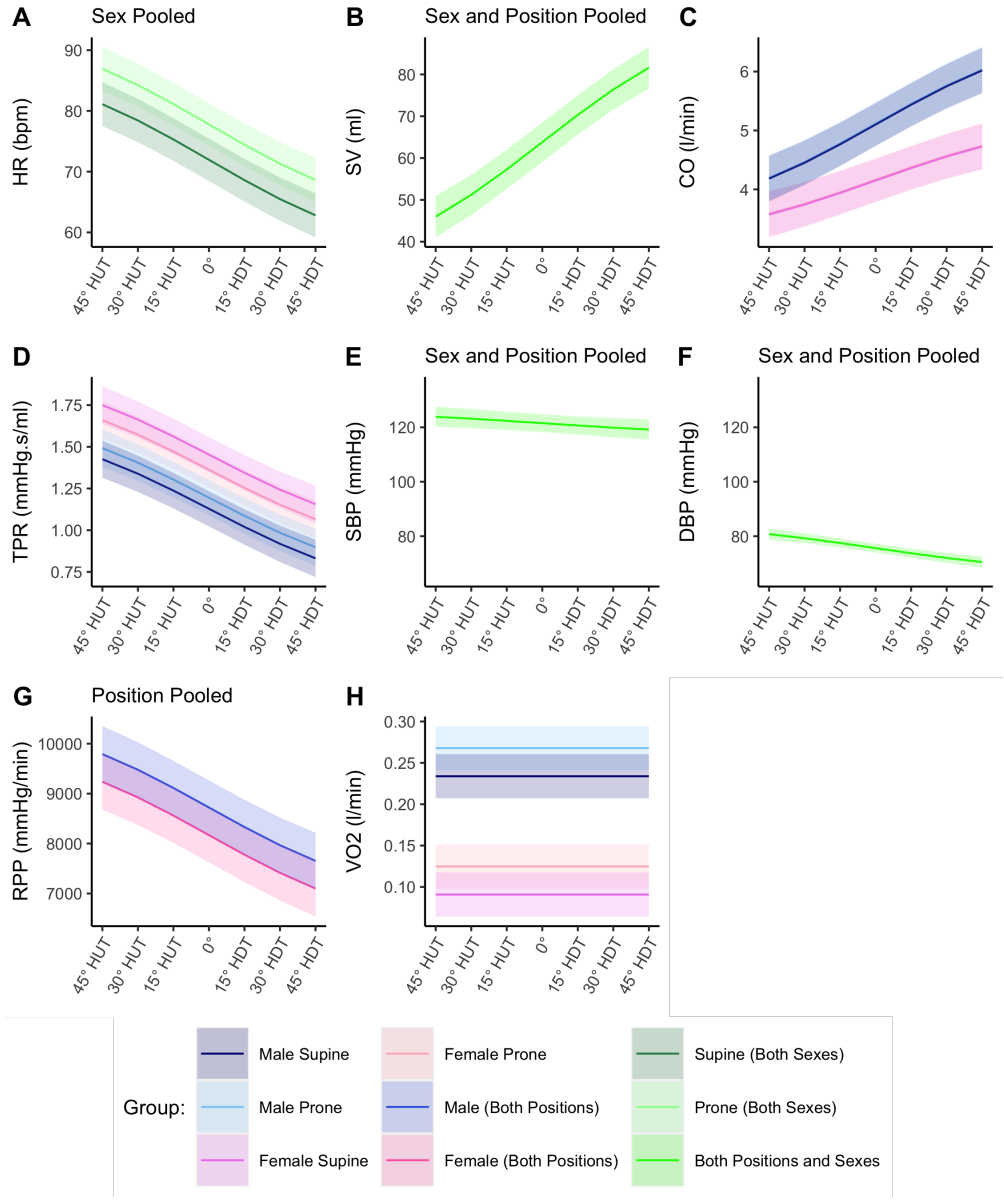

Figure 4.21: **(A-H)** Estimated gravitational dose-response curves for hemodynamic parameters in the range 45° head-up tilt (HUT) to 45° head-down tilt (HDT) incorporating sex differences. Curves were fit via linear mixed-effects models as described in the main text. Curves are presented as means ± 95% confidence interval. Dark blue, male supine; pale blue, male prone; dark pink, female supine; pale pink, female prone; blue, male (position pooled); pink, female (position pooled); dark green, supine (sex pooled); pale green, prone (sex pooled); green, position and sex pooled. **(A)** HR, heart rate; **(B)** SV, stroke volume; **(C)** CO, cardiac output; **(D)** TPR, total peripheral resistance; **(E)** SBP, systolic blood pressure; **(F)** DBP, diastolic blood pressure; **(G)** RPP, rate pressure product; **(H)** VO2, oxygen consumption.

Table 4.10: Estimated model coefficients for the gravitational dose-response curves displayed in Figures 4.21 and 4.22 generated by linear mixed models (LMMs) and generalized linear mixed models (GLMMs). Estimated coefficients are presented as mean ± SE. Only significant terms were included in the models.

	Model[†]	Link[‡]	Units	Estimated Coefficients[§]					Std Dev of Random Effect[§§]
				β_0 Intercept	β_1 sin(Angle)[‖]	β_2 Sex[¶]	β_2 Position[††]	Additional βs[‡‡]	
Hemodynamic Measurements:									
HR	LMM	$\mu = \eta$	bpm	72.0 ± 1.8	12.9 ± 0.7	—	5.8 ± 0.7	—	8.4
SV	LMM	$\mu = \eta$	ml	63.8 ± 2.4	–25.2 ± 1.2	—	—	—	11.3
CO	LMM	$\mu = \eta$	l/min	4.14 ± 0.19	–0.82 ± 0.09	0.95 ± 0.26	0.01 ± 0.06	$Angle \times Position$: –0.48 ± 0.13	0.62
TPR	LMM	$\mu = \eta$	mmHg.s/ml	1.45 ± 0.05	0.42 ± 0.03	–0.32 ± 0.08	–0.09 ± 0.04	$Position \times Sex$: 0.16 ± 0.05	0.16
SBP	LMM	$\mu = \eta$	mmHg	121.5 ± 1.6	3.3 ± 1.3	—	—	—	7.5
DBP	LMM	$\mu = \eta$	mmHg	75.6 ± 0.8	7.2 ± 0.9	—	—	—	3.5
RPP	LMM	$\mu = \eta$	mmHg/min	8170 ± 280	1510 ± 100	550 ± 390	—	—	930
VO2	LMM	$\mu = \eta$	l/min	0.091 ± 0.014	—	0.143 ± 0.019	0.034 ± 0.005	—	0.044
Time-Domain Autonomic Indices:									
SDNN	GLMM	$\ln(\mu) = \eta$	ms	4.002 ± 0.055	–0.300 ± 0.029	—	–0.087 ± 0.028	—	0.253
RMSDD	GLMM	$\ln(\mu) = \eta$	ms	3.419 ± 0.083	–0.619 ± 0.038	—	—	—	0.396
HRVTi	GLMM	$\ln(\mu) = \eta$	—	2.484 ± 0.047	–0.149 ± 0.041	—	–0.062 ± 0.027	$Angle \times Position$: –0.136 ± 0.058	0.210
BRS	GLMM	$\ln(\mu) = \eta$	ms/mmHg	2.521 ± 0.063	–0.684 ± 0.042	—	–0.154 ± 0.040	—	0.274
Frequency-Domain Autonomic Indices:									
LF	GLMM	$\ln(\mu) = \eta$	ms^2	6.665 ± 0.097	–0.338 ± 0.064	—	–0.281 ± 0.059	—	0.432
HF	GLMM	$\ln(\mu) = \eta$	ms^2	5.653 ± 0.155	–1.141 ± 0.079	—	–0.134 ± 0.073	—	0.717
LFNorm	LMM	$\mu = \eta$	—	70.5 ± 1.6	15.0 ± 1.2	—	—	—	7.3
HFNorm	LMM	$\mu = \eta$	—	29.5 ± 1.6	–15.0 ± 1.2	—	—	—	7.3
LF/HF	GLMM	$\ln(\mu) = \eta$	—	0.899 ± 0.095	0.785 ± 0.085	0.302 ± 0.134	—	$Angle \times Sex$: –0.159 ± 0.119	0.296

Notes:

[†]All models use a linear predictor of the form: $\eta_{ijk} = \beta_0 + \beta_1 \sin(Angle) + \beta_2 (Sex_j) + \beta_3 (Position_k) + \beta_4 (...) + \gamma_i + \varepsilon_{ijk}$ for subjects i ($i = 1:24$), Sex j ($j = 0:1$), and position k ($k = 0:1$). All GLMMs have a Gamma distribution.

[‡]Link function between the linear predictor, η, and the expectation of the dependent variable, μ.

[§]For GLMMs, coefficients β are given on the scale of the linear predictor for subject i, $\eta_i = \boldsymbol{X}\beta + \gamma_i$. The coefficient β_4 corresponding to any significant interaction effects is noted where appropriate.

[‖]Sine of tilt angle from –0.707 ($\sin(-45°)$) to 0.707 ($\sin(45°)$), positive angles represent head-up tilt, negative angles represent head-down tilt.

[¶]Sex_j: female = 0, male = 1.

[††]$Position_k$: supine = 0, prone = 1.

[‡‡]Additional coefficients for interaction effects as noted.

[§§]Standard deviation, σ, of random intercept, γ, for subject i. $\gamma_i \sim N(0, \sigma^2)$. Units for σ are the same as the estimated coefficients.

Figure 4.22 shows the estimated dose-response curves for the autonomic indices (both time-domain and frequency-domain) considered within the range of 45° HUT to 45° HDT. The parameters for the dose-response curves are captured in Table 4.10. Curves are shown as mean and 95% confidence interval. Since there was no significant difference between male and female data for all of the variables except LF/HF ratio, *Sex* data was pooled for those responses. Since there was no significant effect of *Position* for RMSDD, LF (Norm), HF (Norm) and LF/HF ratio, supine and prone estimates are also pooled for those dose-response curves.

Figure 4.23 shows the estimated dose-response curves for A_{CCA}, A_{IJV}, and IJVP within the range of 45° HUT to 45° HDT. The effect sizes and model parameters are presented in Table 4.9. Curves are shown as mean and 95% confidence interval. Since there was no significant difference between male and female data for any of the variables, *Sex* data was pooled in all cases. Since there was no significant effect of *Position* for A_{CCA}, supine and prone data were pooled. Finally, right and left side data were pooled for IJVP, since there was no significant effect of *Side*. As described in Section 4.2.5.2, a square-root transformation on the dependent variable was used to construct the dose-response curves for A_{CCA} and A_{IJV} since the data exhibited significant heterogeneity with regards to the area measurements as a function of tilt angle. The fitted smoothed terms used to construct the GAMMs in Figure 4.23 are presented in Figure 4.24.

4.7.4 Discussion

This study augmented our original work by adding female subjects and characterizing the effect of sex on cardiovascular hemodynamics and autonomic response. Our main findings show that: (1) most parameters measured do not exhibit a significant effect of sex, with significant differences only found in five out of 20 variables considered; (2) in the hemodynamic response, we find a significant difference in CO, TPR, RPP and VO2; (3) in the autonomic response, we only see a significant difference in LF/HF ratio, a marker of sympathovagal balance; and (4) we find no sex effect in any of the variables related to carotid or jugular hemodynamics.

Considering the hemodynamic response, we only find a significant effect of sex in four of the measured variables. In particular, we see a sex effect in CO, TPR, RPP, and VO2, and we

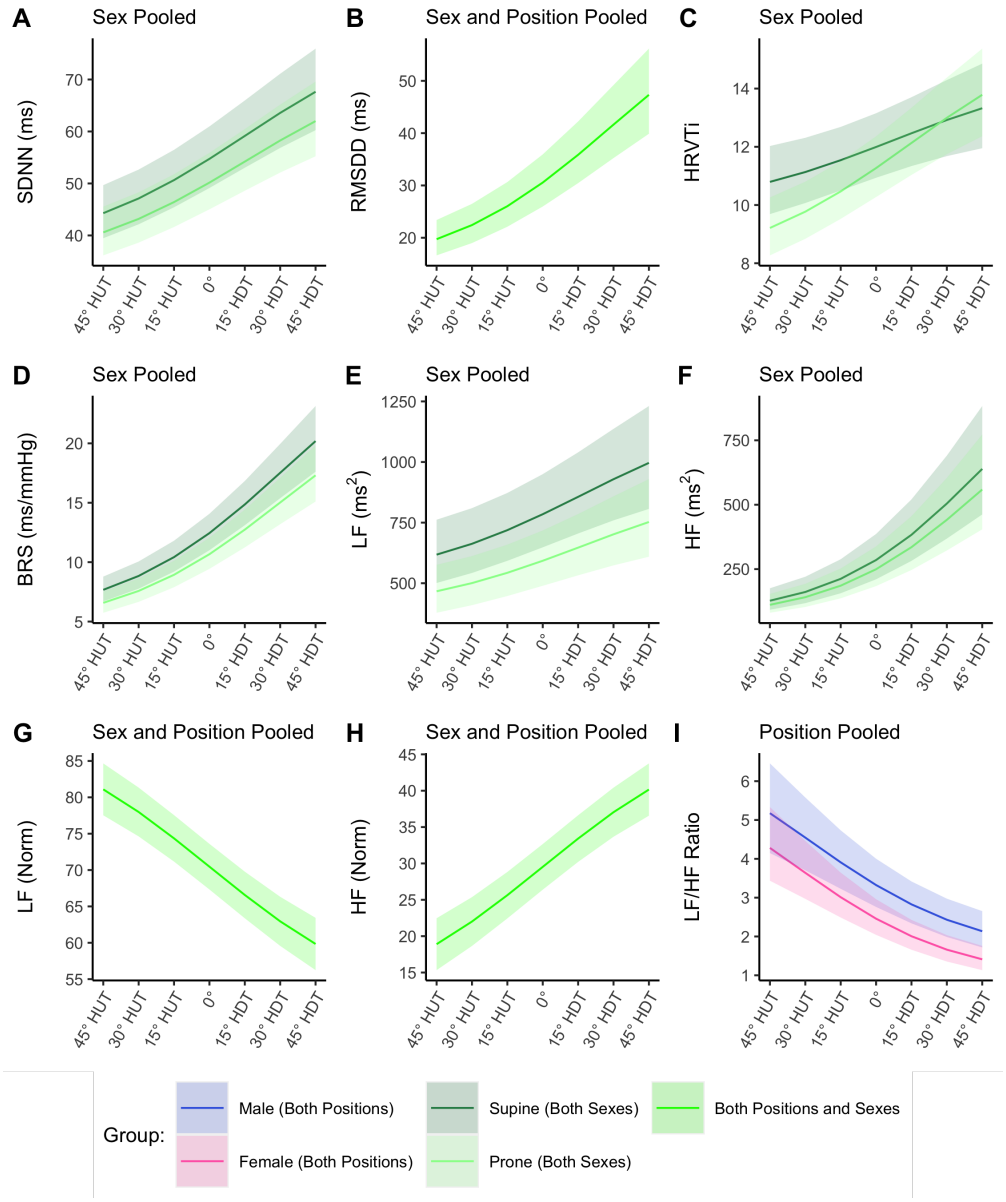

Figure 4.22: **(A-I)** Estimated gravitational dose-response curves for autonomic parameters in the range 45° head-up tilt (HUT) to 45° head-down tilt (HDT) incorporating sex differences. Curves were fit via linear mixed-effects models (LFNorm, and HFNorm) and generalized linear mixed-effects models (remaining parameters) as described in the main text. Curves are presented as means ± 95% confidence interval. Blue, male (position pooled); pink, female (position pooled); dark green, supine (sex pooled); pale green, prone (sex pooled); green, position and sex pooled. **(A)** SDNN, standard deviation of NN intervals (normalized RR intervals); **(B)** RMSDD, root mean square of direct differences of NN intervals; **(C)** HRVTi, heart rate variability triangular index; **(D)** BRS, baroreceptor sensitivity; **(E)** LF, power density in the low frequency range (0.04–0.15 Hz); **(F)** HF, power density in the high frequency range (0.15–0.4 Hz); **(G)** LFNorm, LF (normalized units); **(H)** HFNorm, HF (normalized units); **(I)** LF/HF Ratio, ratio of low to high power densities.

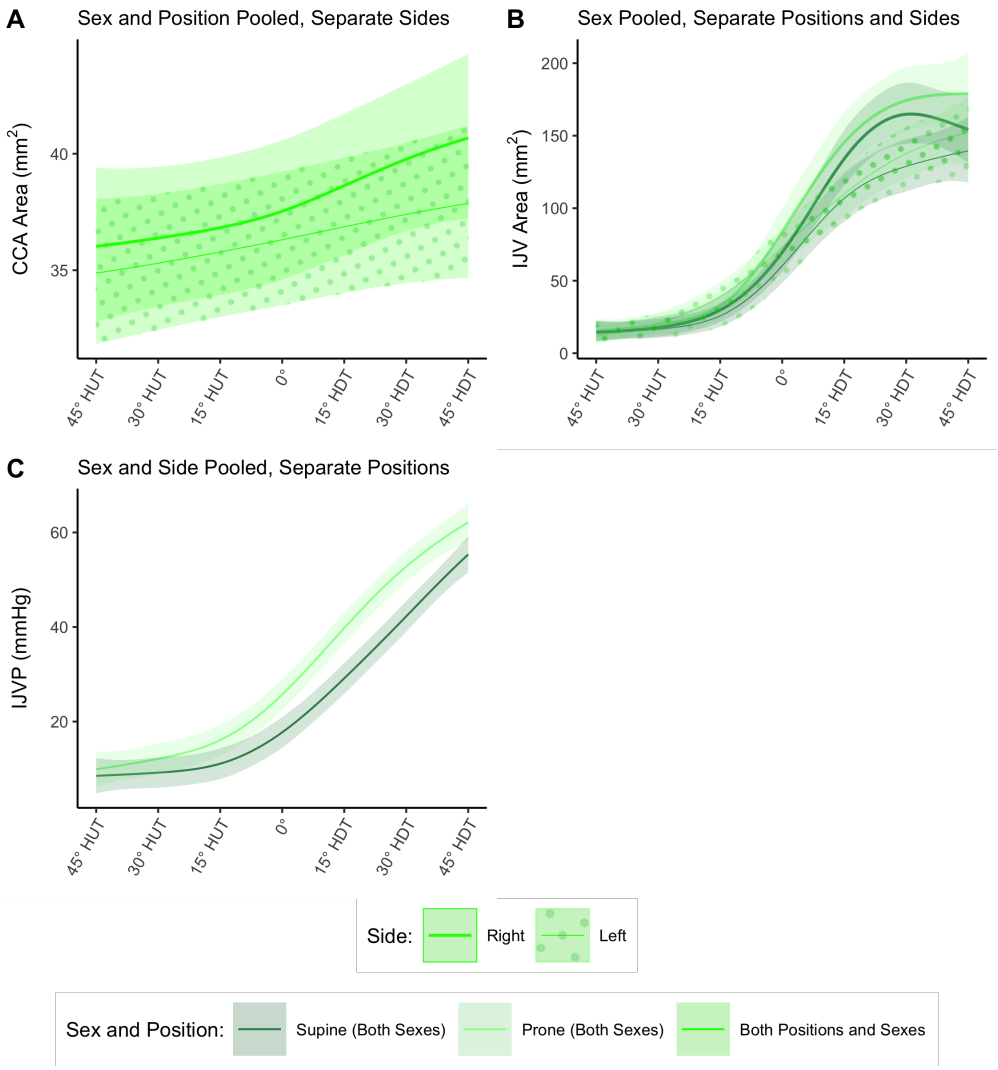

Figure 4.23: **(A-C)** Estimated gravitational dose-response curves for A_{CCA}, A_{IJV}, and IJVP in the range 45° head-up tilt (HUT) to 45° head-down tilt (HDT) incorporating sex differences. Curves were fit via generalized additive mixed-effects models as described in the main text. Curves are presented as means ± 95% confidence interval. Dark green, supine (sex pooled); pale green, prone (sex pooled); green, position and sex pooled. Thick line and no fill pattern, right side; thin line and circles fill pattern, left side. **(A)** A_{CCA}, common carotid artery cross-sectional area; **(B)** A_{IJV}, internal jugular vein cross-sectional area; **(C)** IJVP, internal jugular vein pressure.

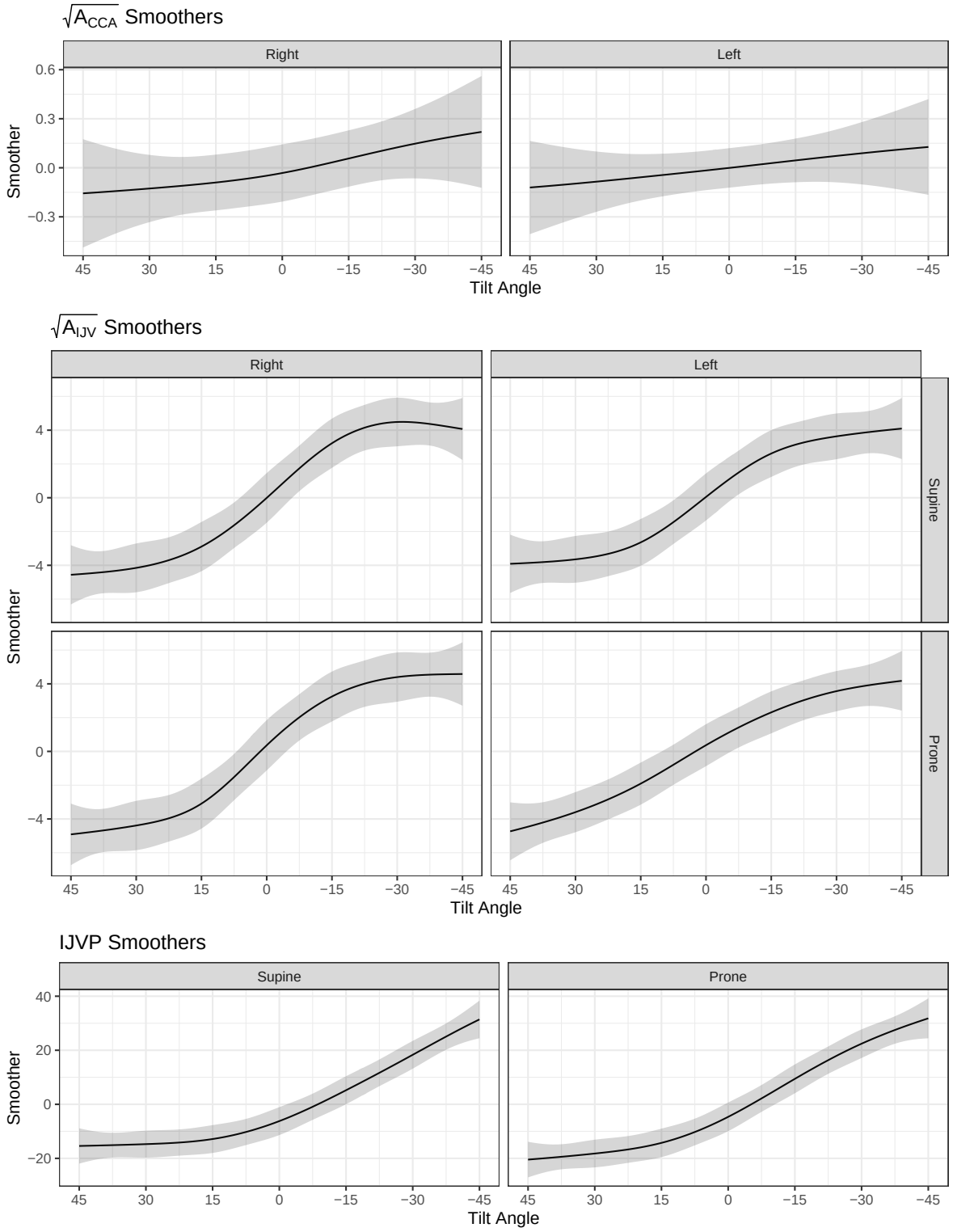

Figure 4.24: Fitted smoothed terms for generalized additive mixed-effects models (GAMMs) incorporating sex differences.

only find a significant interaction effect between sex and tilt angle in CO. Diaz-Canestro *et al.* hypothesized that sex differences in hemodynamic response to tilt can largely be explained by blood volume and oxygen carrying capacity[341]. Regarding the interaction effect, our results are congruent with Sarafian and Miles-Chan, who found an interaction effect in CO between males and females in graded tilt, with males responding more strongly to tilt[342]. This is interesting and is potentially evidence of a different autonomic response between males and females. Badrov *et al.* found no sex differences in heart rate, stroke index, or cardiac index, lending evidence to an anthropometrically driven difference. However they also noted a significantly greater TPR in hypertensive female subjects in graded HUT[343], which is matched in our study in normotensive subjects. Finally, Afrin Rimi *et al.* concluded that the cardiovascular response to tilting was less pronounced in females[344]. We observe this in the interaction effect of the CO response, but do not observe the significant interaction between sex and tilt angle for SBP that the authors noted.

We find marginal evidence of a differing autonomic response between males and females, given that we only found a significant effect of sex in the LF/HF ratio, a marker of sympathovagal balance. However, as with the male subjects, there was a large variance in the HRV metrics in female subjects, which could obscure smaller effect sizes of sex differences. Robertson *et al.* found that in upright tilt LF/HF increased more in males than in females ($p = 0.044$)[345]. They hypothesize that this is due to sympathetic modulation of HR to control blood pressure in men, versus more parasympathetic modulation in women. However, they also note a significant effect of sex on baroreflex sensitivity, which we do not observe. In a more chronic study, Schäfer Olstad *et al.* found that male runners exhibited higher markers of sympathetic activity during training and competitions, whilst females had higher markers of parasympathetic activity during training[346]. Dart *et al.* seek to explain this difference by examining the effect of hormones on autonomic control[347]. They note that oestrogen enhances parasympathetic activity whilst promoting choline uptake and acetylcholine synthesis and release[348]. Conversely, they present evidence that testosterone enhances norepinephrine (NE) and neuropeptide Y (NPY) synthesis and reduces NE clearance[349–351]. Both of these are sympathetic co-transmitters, lending support to greater sympathetic activity in

males and greater parasympathetic activity in females.

Finally, we did not find any sex dependent differences in A_{CCA}, A_{IJV}, or IJVP. This is in contrast to Patterson *et al.* who noted greater jugular venous attenuation in males than in females in HDT[295]. However, in a study measuring the influence of a neck compression collar on cerebrovascular and autonomic function, Joshi *et al.* found no sex effect in A_{CCA} or A_{IJV} in the baseline condition[352]. The authors did find a significant effect of sex when wearing the compression collar on A_{IJV} at end-inhalation and on both A_{CCA} and A_{IJV} at end-exhalation. They hypothesize that these differences are likely explained by the previously identified autonomic differences between males and females. We could find no studies examining sex differences in IJVP between males and females, however studies of central venous pressure found no significant difference between males and females[353].

4.7.4.1 Limitations

The limitations for this experiment remain broadly as described in Section 4.4.3, although we remove the limitation of only considering one sex. It should further be noted that, whilst we maintain most of the previously used protocol, we used a different ultrasound device and methodology to record A_{CCA} and A_{IJV} for male and female subjects. In particular, for male subjects we used a VScan Extend to record videos of the CCA, which were analyzed via an image processing algorithm, whereas for female subjects we collected a single image using a Butterfly iQ+ at end-diastole. The net effect of this change is that for male subjects, A_{CCA} represents the average area throughout the pulsatile waveform, whereas for female subjects A_{CCA} represents the value at end-diastole. There is a large variance in these A_{CCA} measures, both within-subjects and between-subjects, compared to any gravitational effects. In both cases, the effect size of *Angle* is small enough that even where we observe a significant effect of tilt, the dose-response curve is still largely flat with a wide confidence band. As such, we do not believe that this measurement difference invalidates any conclusions.

4.7.5 Summary of Sex Differences

We augmented our initial experiment by incorporating female subjects in order to look at the effects of sex on cardiovascular parameters in graded tilt. Our data revealed that only a few vari-

ables displayed a significant effect of *Sex*. In particular, we found a significant effect of sex in CO, TPR, RPP, VO2, and LF/HF ratio. Further, we only found a significant interaction effect between sex and tilt angle in two variables: CO and LF/HF ratio. The greater increase in CO seen in male subjects with increasing HDT is likely due to the larger blood volume in males. Overall, the data reveal that there are not large sex differences in the hemodynamic response to tilt. These findings support our original experiment and demonstrate that the gravitational dose-response curves created can be used for spaceflight countermeasure development for crewmembers of both sexes.

5. EXPERIMENT 2: LOWER BODY NEGATIVE PRESSURE

5.1 Motivation

Future long-duration exploration missions will require novel countermeasure protocols to counteract the degrading effects of the microgravity environment. In particular, three of the risks identified by the NASA Human Research Program[34] directly related to the cephalad fluid shift that occurs in astronauts are: (1) the risk of cardiovascular adaptations contributing to adverse mission performance and health outcomes[7]; (2) the risk of spaceflight associated neuro-ocular syndrome (SANS)[47,57,165]; and (3) the concern of venous thromboembolism[9–13,62,63]. Lower body negative pressure (LBNP) has a long spaceflight heritage since the Skylab Program in the 1970s[77,78], both for physiological research and as a countermeasure to prevent post-flight orthostatic intolerance. Currently, Russian cosmonauts on the International Space Station (ISS) use the Chibis-M suit, developed in 2012, as a countermeasure prior to landing[80]. The Chibis protocol developed by the Institute for Biomedical Problems of the Russian Academy of Sciences (IBMP) is short, consisting of 2 min at –25 mmHg followed by 3 min at –35 mmHg[81]. The primary effect of LBNP is to pull blood down towards the feet, reducing venous return and introducing central hypovolemia[73]. Thus, LBNP is also used terrestrially to study the effects of acute hypovolemia and hemorrhagic shock[90,354]. Although it does not restore hydrostatic gradients or affect tissue weight, this footward fluid shift could counteract the microgravity induced cephalad fluid shift and has been demonstrated to effectively reduce intraocular pressure[355], intracranial pressure (ICP)[88], and optic nerve sheath diameter[87] in multiple ground-based studies. In addition to its use as a countermeasure to prevent orthostatic intolerance, LBNP has also been posited as a potential long-term countermeasure to mitigate cardiovascular degradation, SANS, and VTE[327].

To effectively develop successful LBNP protocols, it is important to fully quantify the influence that changing the amount of pressure has on different aspects of the cardiovascular system. This is not just limited to the systemic hemodynamics, but rather a complete understanding of the hemo-

dynamic and autonomic response. Additionally, and particularly important for SANS and VTE, it is also necessary to quantify the specific effects on the ocular system and blood flow in the head and neck. Finally, there is a large amount of individual variation between crewmembers in terms of both anthropometry[188] and LBNP tolerance[356]. Thus, it is further important to characterize any relationships between cardiovascular variables and easily measurable subject characteristics such as age, height, and weight. As one example, Buckey *et al.* have previously identified an association between IOP changes in microgravity and body weight[50]. This is particularly important as the profile of spaceflight participants broadens with the rise of commercial spaceflight[41].

LBNP has been extensively studied in literature[73,80,86–88,354,356–364]. Multiple studies have previously looked at the difference between males and females, with the majority of them noting a difference in orthostatic tolerance[161,295,353,358,365–367]. For example, Patterson *et al.* highlight the importance of sex as a factor in the CV response to LBNP[295]. However, none of the studies examined have considered the same range of hemodynamic, autonomic, and head/neck measurements as will be considered in this study. Further, there are some studies that examine tilt and LBNP as two separate interventions (e.g., Patterson *et al.*[295], Greenwald *et al.*[355], Ogoh *et al.*[368]). However, we could only find a few studies where both HDT and LBNP are considered together (i.e., LBNP during HUT or HDT), and in most of these cases only a single value or small range of LBNP are examined[164,326,369]. Finally, the Bayesian workflow that we introduce in this study is unique, with no previous studies examining the network of associations between variables.

The aim of this study is to construct dose-response curves to quantify the acute response of the cardiovascular system to a range of levels of LBNP. We aim to encompass a wide range of systemic and autonomic parameters, as well as variables related to the head and neck, in order to provide a holistic picture of the response to LBNP, particularly as it relates to potential use cases as a spaceflight countermeasure. Whilst other studies have considered the acute response to LBNP across multiple cardiovascular variables, we intend to focus on the spaceflight application and also answer the question: "how much LBNP is required to compensate for the changes induced by a cephalad fluid shift?" in any given variable of interest. We further intend to quantify any sex-dependent

differences in LBNP response. Finally, in the process of analyzing our data, we developed a novel workflow for the construction of dose-response curves using Bayesian multivariate analysis. This allowed us to capture the relationships between all of the measured variables, as well as subject characteristics such as age, height, and weight. Such a methodology could be expanded beyond the cardiovascular system to encompass other organ systems. Together, these results lead to a greater understanding of LBNP as a potential spaceflight countermeasure, aiding the development of future protocols.

5.2 Methods

5.2.1 Subjects and Study Approval

Twenty-four healthy, recreationally active subjects (12 male, 12 female) between 22 and 42 years old were recruited from the Texas A&M University System to participate in the study. Of these subjects, twenty-one (10 male, 11 female) were also participants in Experiment 1 described in Section 4. Subjects were matched for age and body mass index (BMI) between the male and female groups. Sample size and the number of pressure levels required was determined based on a power curve analysis of pilot data. Subject characteristics (mean ± SD) are presented in Table 5.1. Table 5.1 also gives the Bayes Factor showing evidence for the alternative hypothesis as opposed to the null hypothesis (BF_{10}) that the effect size, d, of the difference in a characteristic between groups is negligible (where negligible is defined by a region of practical equivalence, ROPE, of ±0.1)[iii], such that:

$$H_0 : -0.1 < d < 0.1 \tag{5.1}$$

Prior to participating in the study, subjects completed a questionnaire designed to identify any exclusion criteria, including current use of any cardiac, blood pressure, muscle relaxant, anticoagulant, or stimulant medications, thyroid disease, chronic cardiovascular pathologies, extreme obesity, history of hypertension, or possible pregnancy. Testing was discontinued immediately if

[iii] Kruschke suggests ±0.1 as a default value for a standardized parameter[370], equivalent to a negligible effect size according to Cohen[371].

Table 5.1: Characteristics of the 24 recreationally active subjects (12 male, 12 female) who participated in the study. Characteristics were recorded during baseline session prior to testing sessions. Data are reported as mean ± SD where appropriate. BF_{10} presents the Bayes Factor evidence against the null hypothesis (defined in Equation 5.1) that the measurements are equivalent between the groups. Abbreviations: BMI, body mass index; HR, heart rate; MAP, mean arterial pressure.

Characteristic	**Male**	**Female**	BF_{10}
n	12	12	—
Age (years)	28.8 ± 5.4	28.1 ± 4.2	0.335
Height (cm)	178.9 ± 7.0	160.3 ± 7.8	50,800****
Weight (kg)	86.1 ± 18.9	62.9 ± 16.4	10.4**
BMI (kg/m^2)	26.8 ± 5.2	24.5 ± 6.3	0.492
HR (bpm)	73.8 ± 12.0	75.8 ± 11.5	0.341
MAP (mmHg)	106.8 ± 12.4	94.9 ± 5.4	7.81*

Notes:
*Moderate evidence against the null hypothesis.
**Strong evidence against the null hypothesis.
***Very strong evidence against the null hypothesis.
****Extreme evidence against the null hypothesis.

subjects experienced discomfort, or presented physiological markers of presyncope such as unrestrained rising heart rate, falling blood pressure, and/or perfuse perspiration. In the 0° supine position presyncope was reached in seven subjects at –40 mmHg ($n = 2$, both female) and –50 mmHg ($n = 5$, 4 female, 1 male). In the 15° HDT position, presyncope was reached in two subjects (both female) at –40 mmHg ($n = 1$) and –50 mmHg ($n = 1$). After discontinued application of LBNP, no subjects experienced lasting symptoms. The remainder of the data for these subjects up to the point of discontinuation are included in the results. All other subjects completed the full protocol and experienced no adverse effects. Each subject received written and verbal explanations of the study protocols and gave written informed consent to participate in the experiment. All procedures performed in the study were in accordance with the 1964 Helsinki Declaration and its later amendments. The study protocol was approved by the Texas A&M Human Research Protection Program with Institutional Review Board number IRB2020-0724F.

5.2.2 Experimental Design and Testing Protocol

The experimental design followed broadly a similar procedure as for the tilt experiment described in Section 4, with lower body negative pressure substituted for tilt[186]. The full experimental design is described here for completeness. The experiment was designed as a counterbalanced, within-subjects, experiment such that every subject experienced every pressure level and posture. Subjects were exposed to graded LBNP from 0 mmHg to –50 mmHg in 10 mmHg increments (in a progressive order) in two separate postures: 0° supine (face-up) and 15° head-down tilt (HDT) supine. The procedure was identical for each posture. Experimental sessions took place on two separate days within a two-week period. In each of the two experimental sessions, subjects were tested once in the 0° supine position and once in the 15° HDT position (order counterbalanced). Additionally, in the first session, baseline measurements were collected in a seated posture prior to the main testing. To control for potential circadian effects, all sessions were scheduled in the morning at approximately the same time. In addition, subjects were asked to refrain from drinking caffeine and exercising prior to each test session.

In a single experimental session (0° supine or 15° HDT), subjects were placed in a lower body negative pressure chamber (Technavance, Austin, TX) initially at 0 mmHg. Continuous measurements of blood pressure and electrocardiography were recorded throughout the test. Subjects initially remained at rest for a period of six-minutes to allow any hemodynamic transients to settle. After the rest period, an inert gas rebreathing device was used to collect discrete measurements of cardiac parameters. Following this, measurements of ocular tonometry, ultrasonography, and non-invasive measurement of internal jugular venous pressure were collected from the subjects. The total procedure at a single pressure level lasted for approximately 12 minutes. The LBNP pressure level was then increased (more negative) by 10 mmHg and the entire process repeated, starting with the six-minute resting period. The total protocol included six pressure levels: 0 mmHg, –10 mmHg, –20 mmHg, –30 mmHg, –40 mmHg, and –50 mmHg. The procedure for the seated baseline conducted on the first experimental session was identical to the procedure for a single pressure level.

5.2.3 Dependent Variables

Dependent variables include 11 hemodynamic metrics, seven autonomic indices, and eight measures related to the head/neck/eyes. The hemodynamic measurements considered were: 1) heart rate (HR, bpm); 2) stroke volume (SV, ml); 3) cardiac output (CO, l/min); 4) oxygen consumption (VO2, l/min); 5) systolic blood pressure (SBP, mmHg); 6) diastolic blood pressure (DBP, mmHg); 7) rate pressure product (RPP, mmHg/min), used as a metric for myocardial stress and energy consumption[211]; 8) myocardial oxygen supply:demand index (MO, calculated as the ratio of the diastolic pressure time interval to the systolic pressure time interval, DPTI/SPTI, no units)[372]; and 9) total peripheral resistance (TPR, mmHg.s/ml). Additionally, two body weight normalized indices were collected: 10) stroke index (SI, ml/m^2); and 11) cardiac index (CI, l/min/m^2).

Following the recommendations of the Task Force of the European Society of Cardiology and the North American Society of Pacing and Electrophysiology[213] we collected four time-domain autonomic indices and three frequency-domain autonomic indices. These measurements were: 1) the standard deviation of the NN intervals (SDNN, ms); 2) heart rate variability triangular index (HRVTi, no units); 3) the root mean square of direct differences of the NN interval (RMSDD); 4) baroreflex sensitivity (BRS, ms/mmHg); 5) normalized spectral power density in the low frequency (0.04–0.15 Hz) band (LFNorm, no units); 6) normalized spectral power density in the high frequency (0.15–0.4 Hz) band (HFNorm, no units); and 7) the ratio between low frequency and high frequency power spectral densities (LF/HF, no units). Interpretation of these measurements has been previously described in Section 4.2.3, however in brief SDNN and HRVTi represent heart rate variability incorporating sympathetic and parasympathetic effects, RMSDD and HFNorm are closely correlated with parasympathetic activity[214], LFNorm represents sympathetic activity, LF/HF represents sympathovagal balance, and BRS represents a measure of total autonomic control via the arterial baroreflex[213,216,217].

In relation to the head and neck, the following eight measurements were collected (or calculated): 1) intraocular pressure (IOP, mmHg); 2) ocular perfusion pressure (OPP, mmHg); 3) internal jugular vein cross-sectional area (A_{IJV}, mm^2); 4) internal jugular vein pressure (IJVP, mmHg);

5) internal jugular vein flow pattern (IJVF, grade – see discussion in Section 5.2.4 below); 6) common carotid artery cross-sectional area (A_{CCA}, mm^2); 7) common carotid artery peak systolic velocity (PSV, cm/s); and 8) common carotid artery end diastolic velocity (EDV, cm/s). Head and neck measurements were collected on both the right (Dexter) and left (Sinister) sides.

5.2.4 Instrumentation and Data Collection

Hemodynamic measurements were collected using two instruments, an Innocor inert gas re-breathing device (Cosmed: The Metabolic Company, Rome, Italy) and a Finapres NOVA (Finapres Medical Systems B.V., Enschede, the Netherlands). Full calibration was performed on devices daily, and ambient data calibrations were also performed prior to each subject test (mean ± SD: temperature 24.4 ± 1.2°C, relative humidity 46.7 ± 5.8%, pressure 753.6 ± 4.2 mmHg). Innocor rebreathes were performed at every pressure level in a manner identical to the procedure described in Section 4.2.4. Finapres data (finger arterial pulse contour waveform and 5-lead electrocardiogram) were collected continuously throughout the protocol with pressure corrected to heart level with a hydrostatic height sensor placed laterally on the mid-coronal plane at the fifth intercostal space. At each pressure level, the Finapres pressure waveform was calibrated with a discrete blood pressure measurement using a brachial sphygmomanometer. Autonomic indices were derived from the Finapres ECG trace and beat-to-beat RR interval as described in Section 4.2.4.

Measurements of intraocular pressure were obtained at each pressure level using a contact tonometer (IC200, iCare, Vantaa, Finland). Values presented are the mean of the central four of six measures (i.e., a trimmed mean) in order to account for arterial and respiratory fluctuation. Ocular perfusion pressure was manually calculated from the IOP and MAP measurements for each subject by correcting MAP to eye level (MAP_{eye}) as per the procedure described in Section 4.6.2.3, Figure 4.12, and Equation 4.4.

Internal jugular vein pressure, IJVP, was obtained by manually compressing the IJV with a VeinPress (Compremium, Bern, Switzerland) manometer attached to the head of an ultrasound probe (VScan Extend, GE Healthcare, Chicago, IL). The VeinPress device was zeroed prior to each measurement. Pressure was recorded at the point at which the walls of the IJV vessel were

just about to touch each other. When this occurred, the pressure reading was allowed to stabilize for two seconds to counter any inertial effects. Two IJVP measurements were collected at each LBNP-position-side combination, and the final IJVP in that condition was calculated as the average of the two measurements.

All other measurements of the carotid arteries and jugular veins were collected using a Butterfly iQ+ ultrasound device (Butterfly Network Inc., Burlington, MA). Four separate images were obtained from each side of the subject in each experimental condition (i.e., pressure-position combination). Two images captured a transverse view of the CCA and IJV, respectively, collected approximately 30 mm inferior to the CCA bifurcation point (around the C3 vertebral level) at end diastole. Two trained operators, acting independently, manually identified and circumscribed the CCA and IJV on each image to calculate A_{CCA} and A_{IJV} based on pixel count. If the two measured areas from the different operators differed by less than 10%, the final A_{IJV} in that condition was calculated as the average of the two independently measured areas. However, if the measured area differed by more than 10%, a third operator repeated the circumscription and the final A_{IJV} in that condition was calculated as the average of the three independently measured areas.

The final two images captured spectral pulse-wave Doppler flow of the CCA and IJV respectively. For the CCA flow, an envelope tracing algorithm was applied, modified from an algorithm developed by Wadehn and Heldt[373]. The output of this algorithm was used to calculate average peak systolic velocity (PSV) and end diastolic velocity (EDV). IJV was binned into categories representing four flow regimes as defined by Marshall-Goebel *et al.*[12]. These flow grades represent: Grade 1 – forward flow that never returns to zero; Grade 2 – forward flow that may return to zero; Grade 3 – stagnant flow characterized by equal forward and retrograde flow; and Grade 4 – predominantly retrograde flow. No instances of grade 4 flow were observed. Examples of grades 1, 2, and 3 flow are presented in Figure 5.1.

5.2.5 Statistical Analysis

In contrast to the tilt experiment(s) described in Section 4, for LBNP we implemented a fully Bayesian workflow. This was done for three main reasons. First, Bayesian analysis is less con-

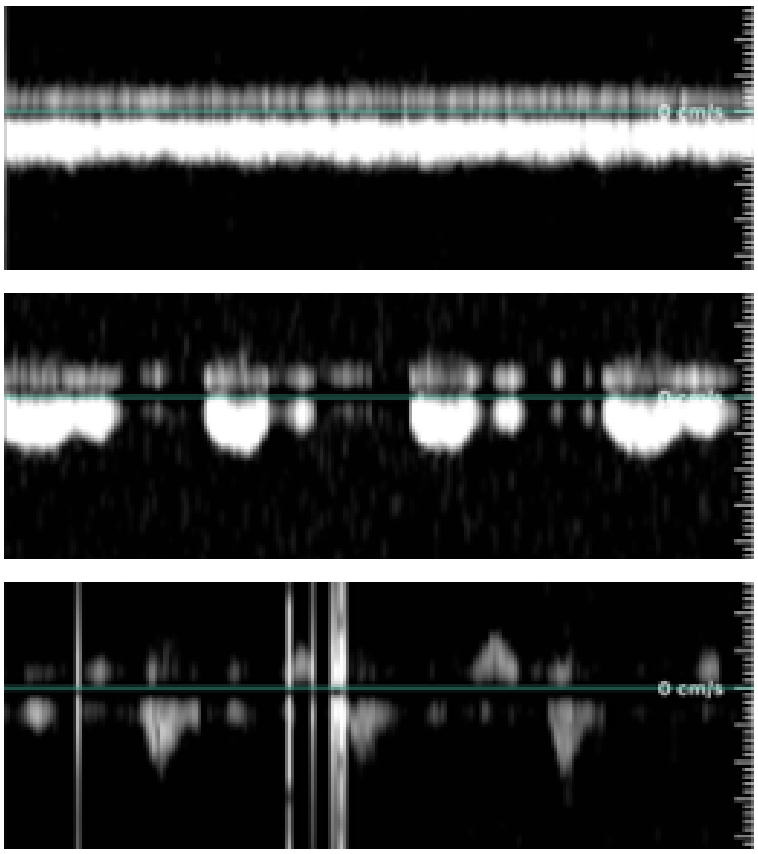

Figure 5.1: Internal jugular vein blood flow velocity waveform grades. **(Top)** Grade 1: forward flow that never returns to zero; **Middle** Grade 2: forward flow that may return to zero; and **Bottom** Grade 3: stagnant flow characterized by equal forward and retrograde flow. Flow grade regimes are as defined by Marshall-Goebel *et al.*[12].

strained by the problems of low sample size commonly found in spaceflight studies[374]. Since Bayesian analysis represents a continual updating of understanding based on evidence ("the posteriors of today are the priors of tomorrow"), this approach allows for the work to be taken and expanded on with future data availability. Second, we believe that the outputs of a Bayesian model are easier to interpret and understand in the context of dose-response curves. As an example, the estimate and 95% confidence interval for a dose-response curve, like the ones constructed in Section 4, formally represent the statement *"if we were to repeat this experiment 100 times, we would expect the estimated curve to appear in this interval 95 times out of 100"*. On the other hand, with a dose-response curve constructed using Bayesian posteriors and, say, an 89% credible interval

we are able to make the statement *"the true effect size has an 89% probability of sitting within this interval"*[375]. Third, the Bayesian methodology allows for the construction of more complicated regression models at the expense of computational time. As discussed in Section 5.1, we note that there is certainly a dependent structural relationship between all of the variables measured. By following a Bayesian methodology we are able to conduct a multivariate analysis with models an order of magnitude more complex than would be possible in a frequentist framework. This is primarily due to the fact that the implementation of the Bayesian methodology relies on a sampling framework, as opposed to a direct estimation of a prohibitively complex maximum likelihood function in the frequentist approach[376,377]. A multivariate analysis allows us to elucidate some insight into the nature of the structural relationships. We fully and comprehensively report the methodology following the Bayesian Analysis Reporting Guidelines (BARG) given by Kruschke[378].

All variables measured (with the exception of IJVF, described separately below) exhibited an approximately linear response to graded LBNP. A single Bayesian robust multivariate, hierarchical regression model was used to estimate the effects of sex, pressure, and position (0° supine or 15° HDT) on all dependent variables. The model is presented in Equation 5.2:

$$\begin{aligned} y_{ip} &\sim Student\left(\mu_p, \sigma_p, \nu_p\right) \\ \mu_p &= \beta_{p,0} + \beta_{p,LBNP}\left(Pressure\right) + \beta_{p,sex}\left(Sex\right) + \beta_{p,pos}\left(Position\right) + ... + \gamma_{ip} \\ \gamma_{ip} &\sim \mathcal{N}(0, \sigma_{up}) \end{aligned} \tag{5.2}$$

where for each dependent variable, p outlined in Section 5.2.3, y represents the standardized response, σ represents the population level standard deviation, ν represents the degrees of freedom, β_0, β_{LBNP}, β_{sex}, and β_{pos} represent the coefficients for the independent variables, and γ_i represents a group-level intercept for subject i distributed normally with mean 0 and standard deviation σ_u. $Pressure$ is an index variable representing the LBNP level, with 0 indicating 0 mmHg through to 5 indicating –50 mmHg, such that β_{LBNP} gives the effect size of a decrease in 10 mmHg. Sex

represents a contrast coded variable (-0.5 = Female, 0.5 = Male), such that β_{sex} gives the effect size of the increase in y_p for males over females. $Position$ is a categorical variable with 0 representing 0° supine and 1 representing 15° HDT, such that β_{pos} gives the effect size of a change from 0° supine to 15° HDT.

Prior to constructing the dose-response curves, all dependent variables (except IJVF) were standardized to have a mean of 0 and a standard deviation of 0.5. This was done for three principal reasons. First, the prior choice was greatly simplified, as priors on the same scale could be used for all dependent variables. Second, the computational efficiency of the Bayesian calculation was greatly improved. Finally and most importantly, this process allows for the comparison of the magnitude of the effect size across different variables. The results are presented both in this standardized form, and also back-transformed to the original scales of measurement.

Correlations were modeled to exist between the dependent variables, p, such that the covariance matrix of all the σ_u, $\boldsymbol{\Sigma}$, was described by a Cholesky decomposition as shown in Equation 5.3:

$$\begin{aligned} \boldsymbol{\Sigma} &= (\sigma_u \boldsymbol{I})\, \boldsymbol{R}\, (\sigma_u \boldsymbol{I}) \\ \boldsymbol{R} &= \boldsymbol{L}\boldsymbol{L}^T \end{aligned} \tag{5.3}$$

where $\boldsymbol{I}$ is the identity matrix, $\boldsymbol{R}$ is a Hermitian positive-definite matrix, and $\boldsymbol{L}$ is a lower triangular matrix.

For each dependent variable p, Bayes factors analysis of a simple univariate regression was used to determine any additional interaction effects that needed to be included in the model, with a Bayes factor of 3 (substantial evidence) used as the decision rule in favor of a more complicated model[379].

For the eight variables related to the head and neck, an additional independent contrast coded variable, $Side$ (and any appropriate interactions, determined using Bayes Factors), was included, such that β_{side} gives the effect size of the increase in y_p for the right side (Dexter) over the left side (Sinister). In the case of the dependent variable IJVP, in order to deal with significant heterogeneity (i.e., the variance of the data increasing with stronger LBNP), a distributional regression model was

used such that σ was allowed to vary with the pressure level:

$$\log\left(\sigma_{IJVP}\right) = \zeta_{0,IJVP} + \zeta_{LBNP,IJVP}\left(Pressure\right) \tag{5.4}$$

where $\zeta_{0,IJVP}$ and $\zeta_{LBNP,IJVP}$ are the intercept and slope of the $\log$ of the σ_{IJVP}, respectively.

In the case of IJVF we implemented an ordinal logistic regression model. For this model, the dependent variable was flow grade (from 1 to 3). The model used a binomial distribution with a logistic (logit) link, presented in Equation 5.5. *Pressure*, *Sex*, *Position*, and *Side* remained as the predictor variables and the group-level intercept was allowed to correlate with the remainder of the dependent variables. In this case, the coefficients, β, of the independent variables represent the log odds of either a grade 2 or grade 3 flow pattern with respect to a grade 1 pattern. e^{β} represents the odds ratio (OR).

$$\begin{aligned} y^{*}_{i,IJVF} &\sim Cumulative\left(\mu_{i,IJVF}\right) \\ \mathrm{logit}(\mu_{i,IJVF}) &= \beta_{IJVF,0} + \beta_{IJVF,LBNP}\left(Pressure\right) + \beta_{IJVF,sex}\left(Sex\right) \\ &\quad + \beta_{IJVF,pos}\left(Position\right) + \beta_{IJVF,side}\left(Side\right) + \gamma_{i,IJVF} \\ \gamma_{i,IJVF} &\sim \mathcal{N}(0, \sigma_{u,IJVF}) \end{aligned} \tag{5.5}$$

where $y^{*}_{i,IJVF}$ is the latent variable for the IJV blood flow velocity waveform pattern for subject i; $\mu_{i,IJVF}$ is the linear predictor (with a logit link function); $\beta_{IJVF,0}$, $\beta_{IJVF,LBNP}$, $\beta_{IJVF,sex}$, $\beta_{IJVF,pos}$, and $\beta_{IJVF,side}$ are the coefficients for the intercept, LBNP *Pressure*, *Sex* (male or female), *Position* (0° supine or 15° HDT), and *Side* (right or left), respectively; $\gamma_{i,IJVF}$ is the group-level intercept for subject i; and $\sigma_{u,IJVF}$ is the standard deviation of the group-level intercept.

Finally, in order to determine the multivariate relationship between the variables measured and the subject characteristics, standardized Age, $Height$, $Weight$, and BMI, were added to the multivariate regression model as dependent variables with only a group varying intercept in the form of Equation 5.6:

$$
\begin{aligned}
y_{i,chars} &= \gamma_{i,chars} \\
\gamma_{i,chars} &\sim \mathcal{N}(0, \sigma_{u,chars})
\end{aligned}
\tag{5.6}
$$

where $y_{i,chars}$ is the characteristic (Age, $Height$, $Weight$, or BMI) of subject i; and $\gamma_{i,chars}$ is a group-level intercept with standard deviation $\sigma_{u,chars}$.

Table 5.2 presents the form of the regression model for all dependent variables, p.

Weakly informative priors were chosen across all parameters; the summary of the priors used is presented in Table 5.3. Normal priors were used for all β and ζ. Following the recommendations of Gelman[380], half-Cauchy distributions were used for all σ and σ_u. Gamma priors were used for all ν. The covariance matrix, $\mathbf{\Sigma}$, was assigned a Lewandowski-Kurowicka-Joe (LKJ) prior[381,382]. Prior predictive checks were conducted to ensure that the priors generated credible estimates.

The model was fit via Markov Chain Monte Carlo (MCMC) using Stan version 2.26.1[383], R version 4.2.2[340], and the `brms` package[384–386]. Stan is a probabilistic programming platform for statistical modeling and high-performance statistical computation, where Hamilton Monte Carlo (HMC) sampling is performed using a no-U-turn sampler (NUTS) to efficiently explore posteriors in models. The model was sampled using 20,000 draws (1,000 burn-in) in each of four chains. In the fitted model, chain diagnostics were visually inspected to ensure good mixing, with all $\hat{R}$ values < 1.01 and all effective chain lengths > 5000[387]. Posterior predictive checks were conducted to ensure that the posterior estimates approximated the data distribution. Pareto-smoothed leave-one-out cross validation was conducted in order to ensure accurate model predictive power[388]. All posterior summaries are given using the maximum a-posteriori estimate and the 89% highest density interval (HDI, also known as the 89% credible interval – 89% CrI). Evidence for the existence of an effect is presented using the probability of direction (pd), which is the proportion of the posterior distribution that is of the same sign as the median (from 50% to 100%)[389]. Evidence for the significance of an effect is presented as the percentage of the full posterior inside the region of practical equivalence (ROPE). For the majority of parameters, the ROPE is defined as $[-0.05, 0.05]$ on a normalized scale (or $[-0.1sd(y_p), 0.1sd(y_p)]$ on the original scale of measurement)[371,390]. For

Table 5.2: Distributions, main effects, and additional effects (interactions or distributional parameters) for the Bayesian multivariate regression model used to construct the dose-response curves for the cardiovascular response to LBNP. All dependent variables are combined into a single matrix and analyzed using a single, large regression model as detailed in the text.

Measure	**Distribution**	**Main Effects**	**Additional Effects**[†]
HR	$Student$	$Pressure$, Sex, $Position$	—
SV	$Student$	$Pressure$, Sex, $Position$	$Pressure \times Sex$
CO	$Student$	$Pressure$, Sex, $Position$	—
VO2	$Student$	$Pressure$, Sex, $Position$	$Sex \times Position$
SBP	$Student$	$Pressure$, Sex, $Position$	—
DBP	$Student$	$Pressure$, Sex, $Position$	—
RPP[‡]	$\mathcal{N}$	$Pressure$, Sex, $Position$	—
MO	$Student$	$Pressure$, Sex, $Position$	—
TPR	$Student$	$Pressure$, Sex, $Position$	—
SI	$Student$	$Pressure$, Sex, $Position$	—
CI	$Student$	$Pressure$, Sex, $Position$	—
SDNN	$Student$	$Pressure$, Sex, $Position$	—
HRVTi	$Student$	$Pressure$, Sex, $Position$	—
RMSDD	$Student$	$Pressure$, Sex, $Position$	—
BRS	$Student$	$Pressure$, Sex, $Position$	—
LFNorm	$Student$	$Pressure$, Sex, $Position$	—
HFNorm	$Student$	$Pressure$, Sex, $Position$	—
LF/HF	$Student$	$Pressure$, Sex, $Position$	$Pressure \times Sex$
IOP	$Student$	$Pressure$, Sex, $Position$, $Side$	—
OPP	$Student$	$Pressure$, Sex, $Position$, $Side$	—
A_{IJV}	$Student$	$Pressure$, Sex, $Position$, $Side$	—
IJVP	$Student$	$Pressure$, Sex, $Position$, $Side$	$\log(\sigma) \sim Pressure$
IJVF[§]	$Cumulative$	$Pressure$, Sex, $Position$, $Side$	—
A_{CCA}	$Student$	$Pressure$, Sex, $Position$, $Side$	—
PSV	$Student$	$Pressure$, Sex, $Position$, $Side$	—
EDV	$Student$	$Pressure$, Sex, $Position$, $Side$	$Pressure \times Sex$, $Sex \times Position$, $Sex \times Side$
Age[‖]	—	—	—
Height[‖]	—	—	—
Weight[‖]	—	—	—
BMI[‖]	—	—	—

Notes:
[†]Interactions or distributional parameters.
[‡]Bayes Factor analysis strongly favored a Gaussian distribution over a robust Student distribution for RPP.
[§]As described in the main text, IJVF flow pattern was modeled as an ordinal logistic regression with a logit link.
[‖]Subject characteristics with only a group-level intercept.

Table 5.3: Weakly informative priors used for multivariate dose-response model. Note that the priors apply to all relevant standardized dependent variables, p, in line with the model formulae outlined in Table 5.2.

Group	Prior	Comment
β_0	$\mathcal{N}(0,1)$	Intercept
β	$\mathcal{N}(0,1)$	Slope[†]
ζ_0	$\mathcal{N}(0,1)$	Distributional intercept parameter
ζ_{LBNP}	$\mathcal{N}(0,1)$	Distributional slope parameter
ν	$\Gamma(2,0.1)$	Degrees of freedom
σ	$Cauchy^{+}(0,1)$	Population variance
σ_u	$Cauchy^{+}(0,1)$	Group variance
$\boldsymbol{L}$, $\boldsymbol{R}$	$\mathcal{LKJ}corr(1)$	Correlation structure[‡]

Notes:
[†]Applies to β_{LBNP}, β_{sex}, β_{pos}, β_{side} (where relevant), and any interactions.
[‡]Lewandowski-Kurowicka-Joe (LKJ) Cholesky correlation distribution with shape parameter $\eta = 1$.

the log odds parameters related to IJVF, the ROPE is defined as $[-0.1\pi/\sqrt{3}, 0.1\pi/\sqrt{3}]$[390].

5.3 Results

5.3.1 Systemic Hemodynamic Response

Figure 5.2 shows the evolution of systemic hemodynamic parameters (mean ± SE) as a function of LBNP pressure (the seated baseline has been removed for clarity). All measured variables follow an approximately linear trend with respect to LBNP.

In particular, in males heart rate (Figure 5.2A) increases from 67.5 ± 3.4 bpm at 0 mmHg to 87.6 ± 4.1 bpm at –50 mmHg in 0° supine and from 65.2 3.6 bpm at 0 mmHg to 79.9 ±2.8 bpm at –50 mmHg in 15° HDT. In general, female subjects have a heart rate 2.9 bpm (89% CrI: –3.4 to 10.1 bpm) higher than males ($pd = 77.83\%$, $\%_{ROPE} = 19.41\%$). Stroke volume (Figure 5.2B) and cardiac output (Figure 5.2C) fall at an average rate (males and females together) of 8.7 ml (89% CrI: 8.2 to 9.4 ml) and 0.46 l/min (89% CrI: 0.42 to 0.49 l/min) for every 10 mmHg increase in LBNP strength (more negative). In absolute values, stroke volume and cardiac output are higher in males by 24.9 ml (89% CrI: 16.9 to 33.6 ml) and 0.62 l/min (89% CrI: 0.21 to 1.06 l/min) respec-

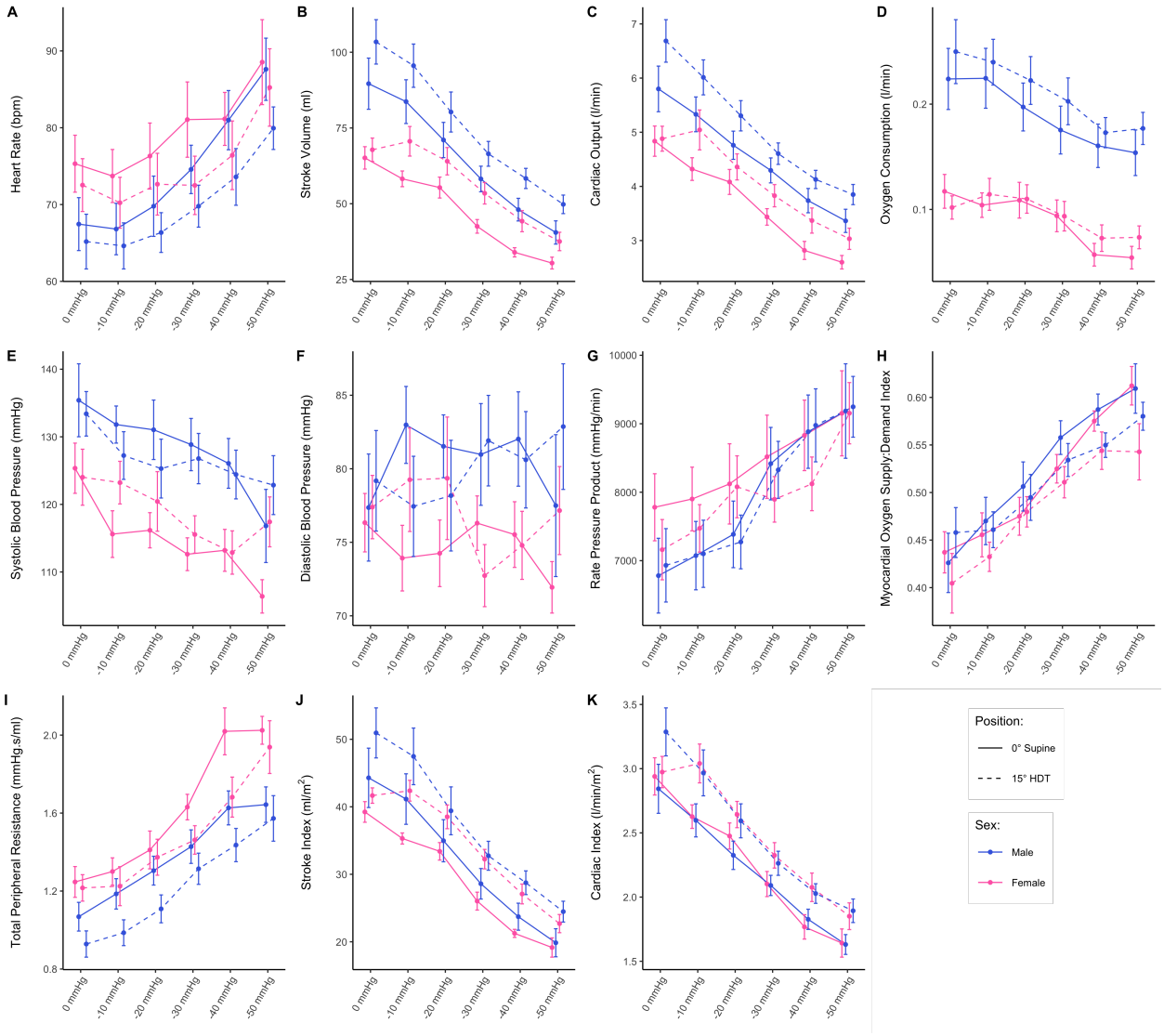

Figure 5.2: **(A-K)** Systemic hemodynamic variables as a function of LBNP in 0° supine (solid line) and 15° HDT (dashed line) positions, collected on 24 subjects (12 male, 12 female). Measurements were taken at 0 mmHg, –10 mmHg, –20 mmHg, –30 mmHg, –40 mmHg, and –50 mmHg. Data are presented as means ± SE at each pressure level. **(A)** HR, heart rate; **(B)** SV, stroke volume; **(C)** CO, cardiac output; **(D)** VO2, oxygen consumption; **(E)** SBP, systolic blood pressure; **(F)** DBP, diastolic blood pressure; **(G)** RPP, rate pressure product; **(H)** MO, myocardial oxygen supply:demand index; **(I)** TPR, total peripheral resistance; **(J)** SI, stroke index; **(K)** CI, cardiac index.

tively. However, when variables are indexed by body surface area, cardiac index (Figure 5.2K) is equivalent in males and females, decreasing by 0.26 l/min/m^2 (89% CrI: 0.24 to 0.28 l/min/m^2, males and females together) per 10 mmHg. On the other hand, stroke index (Figure 5.2J) is still

higher in male subjects by, on average, 4.3 ml/m^2 (89% CrI: 0.4 to 8.4 ml/m^2).

Systolic blood pressure (Figure 5.2E), which is higher in males by 7.4 mmHg (89% CrI: 0.9 to 13.8 mmHg), decreases slightly at an average rate of 1.9 mmHg (89% CrI: 1.3 to 2.6 mmHg) per 10 mmHg LBNP. However, diastolic blood pressure (Figure 5.2F) appears to hold a relatively constant value with no clear trend.

Rate pressure product (Figure 5.2G), myocardial oxygen supply:demand index (MO, Figure 5.2H), and total peripheral resistance (Figure 5.2I) all increase linearly across the range of LBNP values measured. There is no difference in MO between male and female subjects (0.01, 89% CrI: –0.04 to 0.05), however rate pressure product and total peripheral resistance appear slightly higher in females (for RPP: 270 mmHg/min higher, 89% CrI –600 to 1200 mmHg/min, $pd = 70.06\%$, $\%_{ROPE} = 22.47\%$; for TPR: 0.15 mmHg.s/ml higher, 89% CrI –0.01 to 0.30 mmHg.s/ml, $pd = 93.69\%$, $\%_{ROPE} = 10.02\%$). In RPP, this is most noticeable at lower pressure levels, and is likely driven by the higher resting heart rate in female subjects.

The largest difference between males and females appears in oxygen consumption, where males have around twice the consumption of females. Males have an average consumption of 0.22 ± 0.03 l/min at 0 mmHg, falling to 0.15 ± 0.02 l/min at –50 mmHg (in 0° supine); whilst females have an average consumption of 0.12 0.02 l/min at 0 mmHg, falling to 0.05 ± 0.01 l/min at –50 mmHg (0° supine). Relative to both a) the effect of LBNP, and b) the difference between the sexes, the effect of position (0° supine or 15° HDT) appears minimal. This is supported by evidence from Figure 4.2H in Section 4.3, which noted no effect of tilt angle on oxygen consumption.

5.3.2 Autonomic Response

Figure 5.3 shows the evolution of autonomic parameters (mean ± SE) as a function of LBNP pressure.

Broadly, there is minimal effect of LBNP on overall heart rate variability, as evidenced by minimal significant effect of LBNP on SDNN (Figure 5.3A) or HRVTi (Figure 5.3B). On the other hand, the overall balance of sympathetic and vagal activity is clearly altered by LBNP. In particular, RMSDD (Figure 5.3C), a marker of vagal activity, falls from 35.5 ± 3.0 ms at 0 mmHg

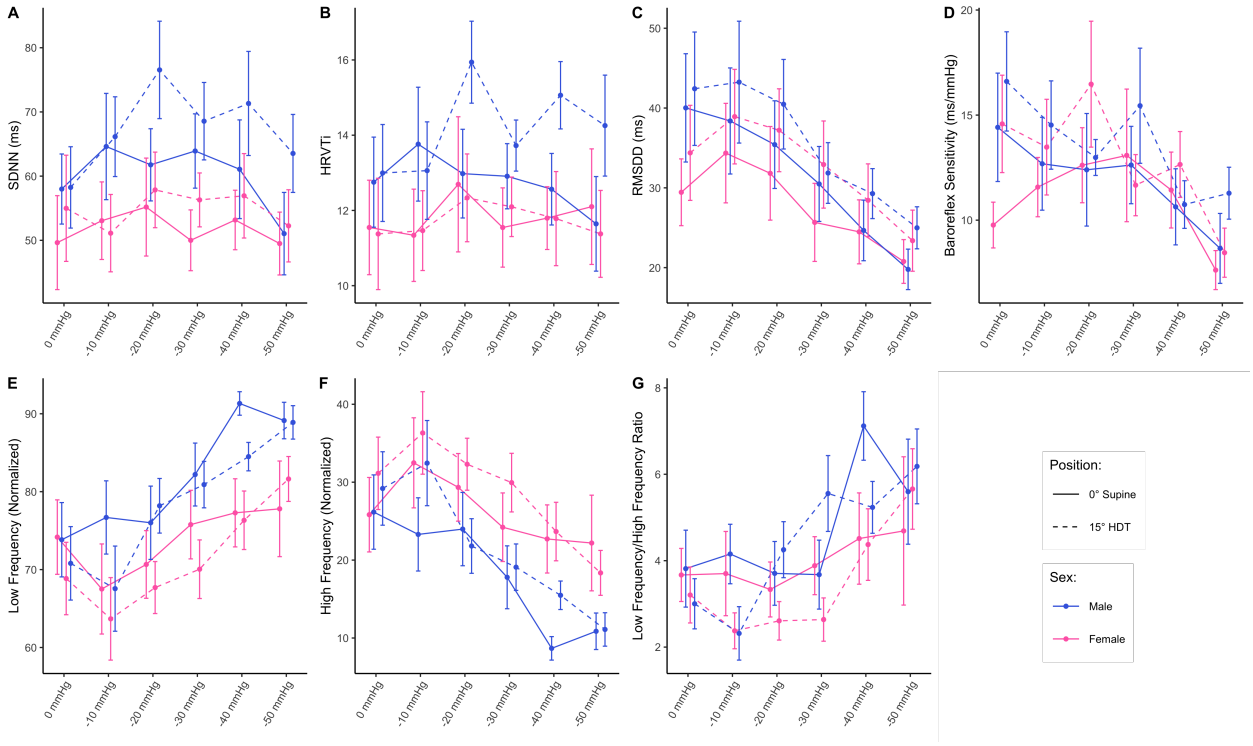

Figure 5.3: **(A-G)** Autonomic variables as a function of LBNP in 0° supine (solid line) and 15° HDT (dashed line) positions, collected on 24 subjects (12 male, 12 female). Measurements were taken at 0 mmHg, –10 mmHg, –20 mmHg, –30 mmHg, –40 mmHg, and –50 mmHg. Data are presented as means ± SE at each pressure level. **(A)** SDNN, standard deviation of NN intervals; **(B)** HRVTi, heart rate variability triangular index; **(C)** RMSDD, root mean square of direct differences of NN intervals; **(D)** BRS, baroreflex sensitivity; **(E)** LFNorm, normalized low frequency power spectral density; **(F)** HFNorm, normalized high frequency power spectral density; **(G)** LF/HF, low frequency to high frequency ratio.

to 22.4 ± 1.5 ms at –50 mmHg (average of both sexes and both positions), a fall of 2.8 ms (89% CrI: 2.1 to 3.5 ms) per 10 mmHg LBNP. This decrease in vagal activity is further supported by the fall in normalized high frequency power spectral density (Figure 5.3F) from 28.1 ± 2.3 at 0 mmHg to 14.5 ± 1.6 at –50 mmHg (average of both sexes and both positions). This fall in vagal activity is matched by a corresponding increase in sympathetic activity seen in the rise in normalized low frequency power spectral density (Figure 5.3E) and low/high frequency ration (Figure 5.3G, a marker of sympathovagal balance).

Finally, baroreflex sensitivity (Figure 5.3D) decreases slightly with LBNP, from 13.8 ± 1.1 ms/mmHg at 0 mmHg to 9.2 ± 0.7 ms/mmHg at –50 mmHg (average of both sexes and both

positions). This is an average decrease of 0.9 ms/mmHg (89% CrI: 0.6 to 1.2 ms/mmHg) per 10 mmHg LBNP. This reduction in sensitivity is likely related to a fall in blood flow and pressure in the carotid sinus and aortic arch as blood is pooled in the lower body.

5.3.3 Head/Neck Response

Figure 5.4 shows the evolution of head/neck parameters (mean ± SE), excluding IJVF, as a function of LBNP pressure. Figure 5.5 shows the change in IJV blood flow velocity waveform pattern as a function of LBNP.

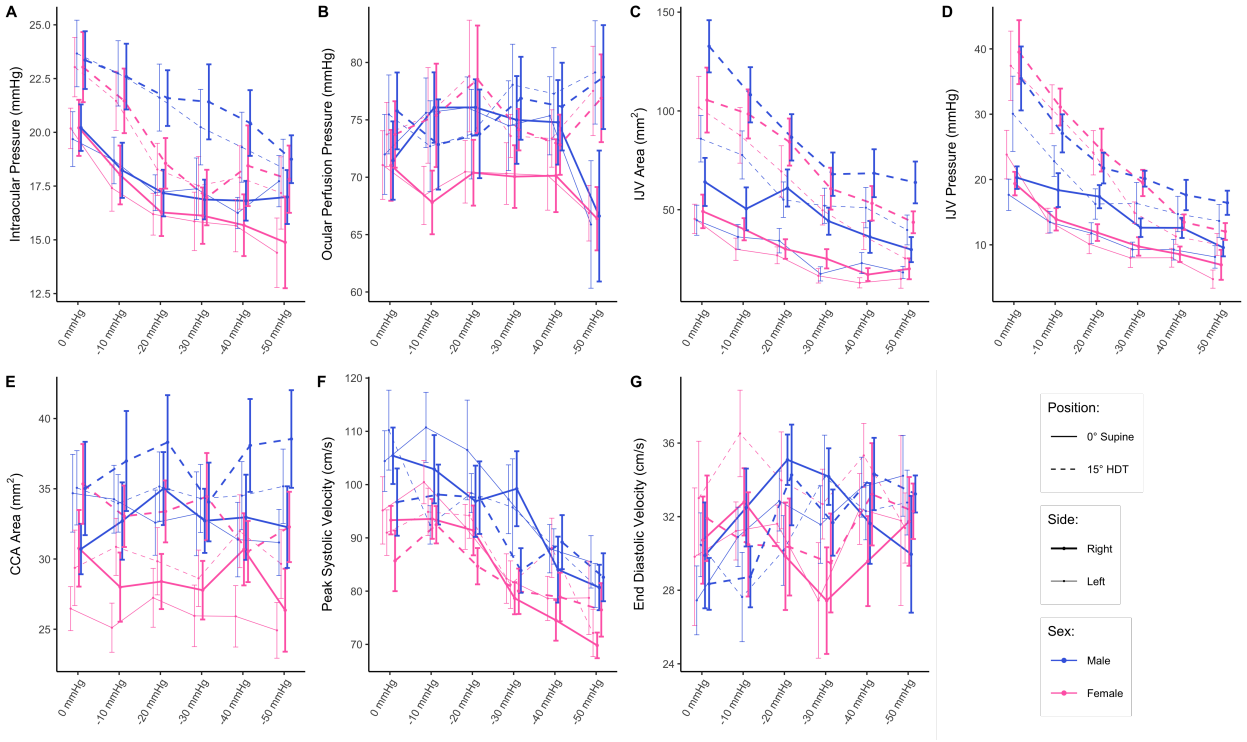

Figure 5.4: **(A-G)** Head/neck variables as a function of LBNP in 0° supine (solid line) and 15° HDT (dashed line) positions, collected on 24 subjects (12 male, 12 female). Thick lines represent the right side (Dexter) and thin lines represent the left side (Sinister). Measurements were taken at 0 mmHg, –10 mmHg, –20 mmHg, –30 mmHg, –40 mmHg, and –50 mmHg. Data are presented as means ± SE at each pressure level. **(A)** IOP, intraocular pressure; **(B)** OPP, ocular perfusion pressure; **(C)** A_{IJV}, internal jugular vein cross sectional area; **(D)** IJVP, internal jugular vein pressure; **(E)** A_{CCA}, common carotid artery area; **(F)** PSV, peak systolic velocity; **(G)** EDV, end diastolic velocity.

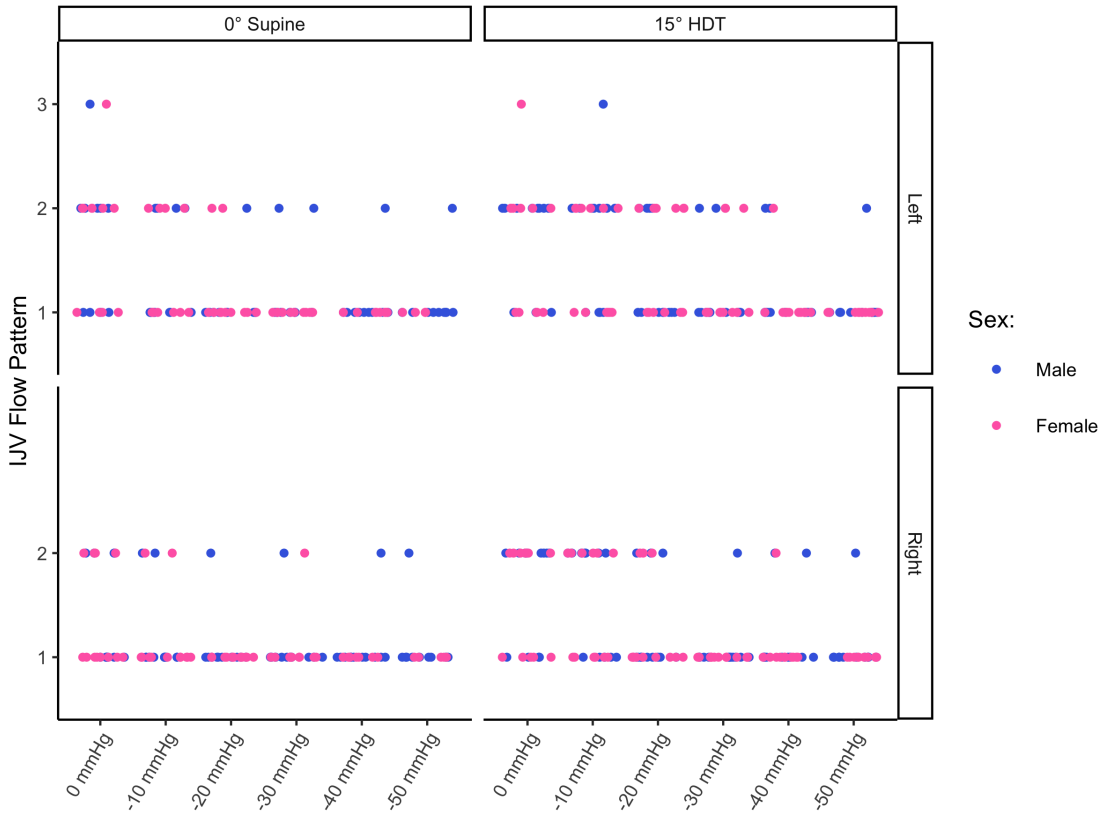

Figure 5.5: Internal jugular vein blood flow velocity waveform pattern as a function of LBNP in 0° supine (left column) and 15° HDT positions (right column), on the left (top row) and right (bottom row) sides, collected on 24 subjects (12 male, 12 female). Flow grade patterns are described in the main text, illustrated in Figure 5.1, and taken from Marshall-Goebel *et al.*[12].

There appears to be little difference between the right and left sides (thick and thin lines, respectively) in any of the variables considered. Intraocular pressure (Figure 5.4A) is higher in the 15° HDT position by 2.9 mmHg (89% CrI: 2.3 to 3.4 mmHg) and decreases linearly from 20.1 ± 0.6 mmHg at 0 mmHg to 16.4 ± 0.7 mmHg at –50 mmHg (0° supine, average of both sexes and both sides). In 15° HDT, IOP decreases from 23.3 ± 0.7 mmHg at 0 mmHg to 18.1 ± 0.7 mmHg at –50 mmHg. In contrast, there appears to be no significant effect of LBNP on ocular perfusion pressure (Figure 5.4B), with the response remaining relatively constant, there is even a slight increase in 15° HDT from 74.7 ± 1.5 mmHg at 0 mmHg LBNP to 78.1 ± 2.1 mmHg at –50 mmHg LBNP (male and female, both sides).

With common carotid artery area (Figure 5.4E), similar to the tilt response (Figure 4.7) we see no effect of LBNP, although we find a small effect of position. The average A_{CCA} at 0° supine is 30.3 ±0.5 mm^2, which increases to 33.7 ±0.6 mm^2 in 15° HDT (average of all pressure levels, sexes, and sides). There is minimal change in end diastolic velocity of the CCA (Figure 5.4G), however the peak systolic velocity (Figure 5.4F) falls from 97.7 ± 2.1 cm/s at 0 mmHg to 79.1 ± 1.7 cm/s at –50 mmHg (average of both side, both sexes, and both positions), indicating an overall decrease in the pulse velocity.

Finally, the internal jugular vein exhibits a strong response to LBNP, with decreases of 8.8 mm^2 (89% CrI: 7.3 to 10.2 mm^2) per 10 mmHg LBNP in area (Figure 5.4C) and 2.7 mmHg (89% CrI: 2.4 to 3.1 mmHg) per 10 mmHg in pressure (Figure 5.4D), respectively. As would be expected from Figure 4.8 and 4.9, both A_{CCA} and IJVP are higher in the 15° HDT position, by 40.1 mm^2 (89% CrI: 35.5 to 44.8 mm^2) and 7.9 mmHg (89% CrI: 6.9 to 9.0 mmHg) respectively. However, in contrast to Figure 4.8 we see no effect of side on IJV cross-sectional area. This is not necessarily surprising, since the larger changes in A_{IJV} in Figure 4.8 only really begin to appear in HDT and are amplified at larger tilt angles (30° HDT and 45° HDT). With respect to the IJV blood flow velocity waveform, Figure 5.5 reveals that, whilst the majority of observed flows are at Grade 1, at lower LBNP levels there appear to be more instances of Grade 2 flow (and even two cases of Grade 3 flow stagnation, both appearing in the left IJV). It appears that LBNP is effective at reducing the instances of Grade 2 flow.

5.3.4 Dose-Response

The Bayesian methodology allows us to gain deeper insight into the relative changes amongst all of the parameters considered. From the fitted dose-response model, we can extract and visualize the posterior draws, $\beta_{p,eff}$, for the effect size of each individual main effect, eff ($LBNP$, sex, pos, or $side$), on each dependent variable p. Since all dependent variables in the model were standardized, the effect sizes can be compared across different variables. In particular, we use the Bayesian concept of a region of practical equivalence (ROPE) as an analogy to a frequentist p-value. As discussed in Section 5.2.5, the ROPE is standardized as $[-0.05, 0.05]$ for all variables

(except IJVF, where $[-0.1\pi/\sqrt{3}, 0.1\pi/\sqrt{3}]$ is used due to the log odds interpretation). Thus, we can quantify the percentage of the full posterior distribution for any particular effect (*Pressure*, Sex, $Position$, or $Side$) inside the ROPE ($\%_{ROPE}$). In general, if greater than 95% of the full posterior distribution is inside the ROPE, this can be interpreted as strong evidence in favor of the null hypothesis (no effect), whilst less than 5% of the full posterior distribution inside the ROPE denotes strong evidence of an effect[391].

This interpretation must also be viewed in the context of the probability of direction (pd). For example, in all of the $Side$ effects considered, the posterior distribution is centralized about 0 but very wide, such that $\%_{ROPE}$ is low, whilst $pd \approx 50\%$. This implies that there is strong evidence of an effect, but little evidence as to whether that effect is positive or negative. Sections 5.3.4.1, 5.3.4.2, 5.3.4.2, and 5.3.4.2 below consider the effect sizes of $Pressure$, Sex, $Position$, and $Side$, respectively, from the fitted dose-response curves.

5.3.4.1 Pressure Effect

Figure 5.6 presents the effect sizes of $Pressure$ on the normalized responses of all variables considered. The variables are ordered from the largest positive effect size at the top to the largest negative effect size at the bottom, and IJVF is presented separately due to the differing ROPE range. Table 5.4 presents the fitted parameters from the dose-response curves, back-transformed from the standardized posterior distributions into their original units. Finally, Table 5.5 presents the pd and $\%_{ROPE}$ for each of the four main effects (β_{LBNP}, β_{sex}, β_{pos}, and β_{side}) for all dependent variables. pd and $\%_{ROPE}$ are invariant of the scale (normalized or original) used since the ROPE scales with the dependent variable.

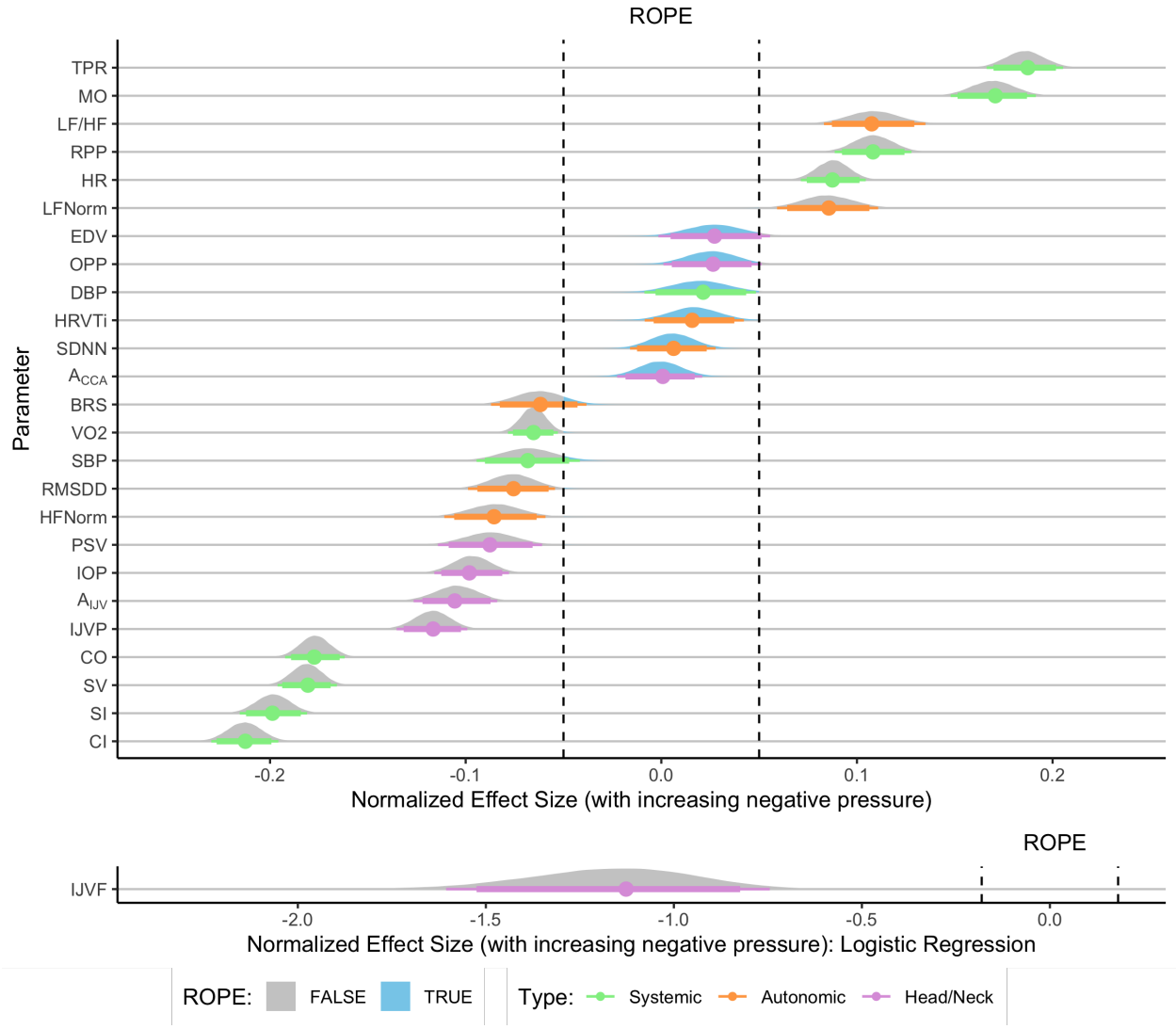

Figure 5.6: Normalized main effect of LBNP level on systemic (green), autonomic (orange), and head/neck (purple) variables. Variables are ordered from the largest positive effect size at the top to the largest negative effect size at the bottom. Data are presented as the posterior distributions from the Bayesian multivariate regression model. Distributions are colored gray when located outside of the ROPE, and they are colored blue when located inside the ROPE. Points and error bars underneath the distributions represent the maximum a-posteriori estimate along with the 89% (thick) and 95% (thin) highest density intervals. IJVF is presented separately below, since the ROPE is defined differently for a logistic regression model (see Section 5.2.5 for detail).

Table 5.4: Posterior estimates for dose-response curves fitted to all measured parameters. Data are presented as the maximum a-posteriori (89% CrI).

Parameter	β_0	β_{LBNP}[†]	β_{sex}[‡]	β_{pos}[§]	β_{side}[‖]	**Additional**[¶]	σ	σ_{u}	ν
HR (bpm)	69.7 (66.5, 72.6)	2.4 (2.0, 2.8)	–2.9 (–10.1, 3.4)	–3.4 (–4.6, –2.2)	—	—	5.0 (4.4, 5.5)	8.9 (7.4, 11.2)	10.5 (3.6, 35.7)
SV (ml)	79.7 (76.0, 83.4)	–8.7 (–9.4, –8.2)	24.9 (16.9, 33.6)	7.4 (5.7, 9.3)	—	–4.2 (–5.4, –3.0)[††]	6.8 (5.8, 8.1)	10.0 (8.2, 12.7)	4.3 (2.3, 11.2)
CO (l/min)	5.29 (5.11, 5.50)	–0.46 (–0.49, –0.42)	0.62 (0.21, 1.06)	0.35 (0.26, 0.46)	—	—	0.36 (0.31, 0.42)	0.55 (0.44, 0.69)	3.7 (2.4, 6.4)
VO2 (l/min)	0.17 (0.16, 0.19)	–0.01 (–0.01, –0.01)	0.07 (0.03, 0.11)	0.01 (0.01, 0.02)	—	0.02 (0.01, 0.03)[‡‡]	0.02 (0.02, 0.02)	0.05 (0.04, 0.06)	2.6 (1.9, 4.2)
SBP (mmHg)	127.9 (124.7, 131.1)	–1.9 (–2.6, –1.3)	7.4 (0.9, 13.8)	–0.3 (–2.4, 1.5)	—	—	8.2 (7.0, 9.2)	8.1 (6.3, 10.6)	6.7 (2.8, 26.9)
DBP (mmHg)	77.5 (74.9, 80.2)	0.5 (–0.1, 0.9)	3.4 (–2.0, 8.7)	–0.2 (–1.8, 1.4)	—	—	6.6 (5.7, 7.4)	6.6 (5.2, 8.7)	7.2 (3.2, 25.0)
RPP (mmHg/min)	7190 (6800, 7630)	390 (330, 450)	–270 (–1200, 600)	–230 (–400, –20)	—	—	840 (770, 910)	1130 (920, 1450)	—
MO (–)	0.44 (0.42, 0.46)	0.03 (0.03, 0.03)	0.01 (–0.04, 0.05	–0.01 (–0.02, 0.00)	—	—	0.04 (0.03, 0.04)	0.06 (0.04, 0.08)	3.9 (2.4, 7.4)
TPR (mmHg.s/ml)	1.11 (1.04, 1.19)	0.15 (0.13, 0.16)	–0.15 (–0.30, 0.01)	–0.12 (–0.16, –0.08)	—	—	0.16 (0.14, 0.18)	0.20 (0.16, 0.26)	7.9 (3.5, 30.6)
SI (ml/m^2)	42.7 (40.9, 44.7)	–4.6 (–4.9, –4.3)	4.3 (0.4, 8.4)	4.3 (3.3, 5.3)	—	—	4.1 (3.5, 4.7)	5.0 (4.0, 6.4)	5.1 (2.6, 17.2)
CI (l/min/m^2)	2.91 (2.81, 3.01)	–0.26 (–0.28, –0.24)	0.07 (–0.14, 0.29)	0.19 (0.14, 0.25)	—	—	0.20 (0.17, 0.23)	0.28 (0.22, 0.36)	4.5 (2.7, 9.0)
SDNN (ms)	56.1 (50.2, 61.5)	0.3 (–0.6, 1.0)	12.2 (0.9, 24.4)	4.0 (1.6, 6.6)	—	—	9.3 (7.9, 10.8)	15.1 (12.0, 19.1)	3.8 (2.4, 7.2)
HRVTi (–)	12.2 (11.1, 13.3)	0.1 (–0.0, 0.3)	1.8 (–0.5, 4.0)	0.3 (–0.3, 0.8)	—	—	2.3 (2.0, 2.5)	2.8 (2.2, 3.7)	8.5 (3.5, 28.4)
RMSDD (ms)	37.0 (32.6, 40.9)	–2.8 (–3.5, –2.1)	5.0 (–4.0, 14.1)	4.0 (2.0, 5.9)	—	—	7.2 (6.1, 8.6)	11.5 (9.3, 14.8)	3.9 (2.1, 8.7)
BRS (ms/mmHg)	13.2 (11.4, 14.9)	–0.9 (–1.2, –0.6)	1.0 (–3.0, 4.4)	2.0 (1.2, 3.0)	—	—	3.4 (2.9, 3.9)	4.5 (3.5, 6.2)	3.7 (2.4, 6.3)
LFNorm (–)	71.2 (67.7, 74.5)	2.6 (2.0, 3.3)	5.9 (–0.8, 12.7)	–2.6 (–4.7, –0.7)	—	—	7.8 (6.5, 9.1)	8.1 (6.6, 10.7)	4.5 (2.4, 17.5)
HFNorm (–)	28.9 (25.6, 32.4)	–2.6 (–3.3, –2.0)	–5.9 (–12.7, 0.7)	2.5 (0.7, 4.7)	—	—	7.9 (6.6, 9.2)	8.3 (6.6, 10.7)	4.7 (2.4, 17.4)
LF/HF (–)	3.38 (2.74, 3.98)	0.55 (0.45, 0.66)	–0.07 (–1.54, 1.20)	–0.61 (–0.95, –0.27)	—	0.49 (0.28, 0.72)[§§]	1.42 (1.22, 1.59)	1.58 (1.27, 2.06)	6.7 (3.2, 23.5)
IOP (mmHg)	20.0 (12.1, 26.6)	–1.0 (–1.1, –0.8)	0.3 (–3.3, 4.1)	2.9 (2.3, 3.4)	0.3 (–14.1, 14.3)	—	2.0 (1.7, 2.3)	4.7 (3.7, 6.3)	5.2 (2.4, 16.3)
OPP (mmHg)	72.9 (54.5, 89.1)	0.6 (0.1, 1.1)	1.4 (–4.7, 8.3)	2.4 (0.8, 4.0)	–2.4 (–34.7, 34.2)	—	6.0 (5.1, 7.1)	8.3 (6.7, 10.7)	4.4 (2.3, 11.8)
A_{IJV} (mm^2)	57.6 (–3.5, 117.5)	–8.8 (–10.2, –7.3)	15.4 (–8.7, 37.6)	40.1 (35.5, 44.8)	3.3 (–119.6, 119.9)	—	16.1 (13.5, 19.0)	30.3 (23.5, 40.0)	3.4 (2.1, 6.6)
IJVP (mmHg)	18.7 (2.6, 36.4)	–2.7 (–3.1, –2.4)	2.6 (–1.3, 6.3)	7.9 (6.9, 9.0)	1.4 (–32.8, 34.4)	–0.22 (–0.29, –0.14)[‖‖]	$\sigma_0 = 3.8$ (3.2, 4.5)	4.6 (3.5, 6.2)	3.0 (2.0, 5.1)
IJVF (–)[¶¶]	0.98 (–0.56, 2.28) 12.1 (7.5, 21.4)	–1.13 (–1.52, –0.82)	0.27 (–1.09, 1.54)	1.66 (0.91, 2.41)	–0.10 (–1.60, 1.57)	—	—	2.66 (1.68, 4.27)	—
A_{CCA} (mm^2)	30.4 (17.9, 44.1)	0.0 (–0.3, 0.3)	1.5 (–5.1, 8.4)	3.6 (2.5, 4.6)	–1.1 (–25.9, 25.8)	—	4.0 (3.4, 4.7)	8.8 (6.8, 11.5)	4.5 (2.4, 12.1)
PSV (cm/s)	97.3 (68.8, 125.3)	–3.5 (–4.3, –2.6)	10.7 (0.5, 19.8)	–3.1 (–5.9, –0.3)	3.7 (–53.0, 59.4)	—	11.7 (10.6, 13.0)	11.8 (9.1, 15.9)	11.3 (5.1, 39.7)
EDV (cm/s)	31.7 (20.0, 42.1)	0.4 (0.1, 0.8)	1.1 (–10.5, 12.4)	–0.9 (–2.1, 0.5)	–1.0 (–22.6, 21.2)	1.2 (0.5, 1.9)[†††] –4.6 (–7.1, –2.1)[‡‡‡] 2.3 (–21.3, 22.8)[§§§]	4.4 (3.7, 5.2)	4.2 (3.0, 5.9)	3.1 (1.9, 5.4)

Notes:
[†]Change per 10 mmHg increase in LBNP strength (more negative).
[‡]Change from females to males.
[§]Change from 0° supine to 15° HDT.
[‖]Change from left side to right side.
[¶]Interaction terms or distributional parameters.
[††]SV interaction: $Pressure \times Sex$.
[‡‡]VO2 interaction: $Sex \times Position$.
[§§]LF/HF interaction: $Pressure \times Sex$.
[‖‖]IJVP distributional parameter ($\log(\sigma) \sim Pressure$): ζ_{LBNP}. Such that $\sigma = \sigma_0 e^{(\zeta_{LBNP} \times Pressure)}$.
[¶¶]First intercept gives base log odds of grade 1 vs. grade 2 and 3 flow. Second intercept gives base log odds of grade 1 and 2 vs. grade 3 flow.
[†††]EDV interaction 1: $Pressure \times Sex$.
[‡‡‡]EDV interaction 2: $Sex \times Position$.
[§§§]EDV interaction 3: $Sex \times Side$.

Table 5.5: Existence and significance of main effects for dose-response model. Evidence for existence of effects is presented as probability of direction (pd). Evidence for significance of effects is presented as percentage of full posterior distribution in region of practical equivalence ($\%_{ROPE}$). See Section 5.2.5 for detail on the pd and ROPE range.

Parameter	$\beta_{\mathbf{LBNP}}$		$\beta_{\mathbf{sex}}$		$\beta_{\mathbf{pos}}$		$\beta_{\mathbf{side}}$	
	pd	$\%_{ROPE}$	pd	$\%_{ROPE}$	pd	$\%_{ROPE}$	pd	$\%_{ROPE}$
HR	100%	0%	77.83%	19.41%	100%	0.30%	—	—
SV	100%	0%	100%	0%	100%	0%	—	—
CO	100%	0%	98.95%	2.76%	100%	0.01%	—	—
VO2	100%	0.81%	99.61%	0.79%	99.91%	20.20%	—	—
SBP	100%	8.73%	96.22%	5.60%	63.28%	72.76%	—	—
DBP	91.38%	98.11%	85.80%	14.04%	58.30%	70.47%	—	—
RPP	100%	0%	70.06%	22.47%	96.34%	38.59%	—	—
MO	100%	0%	65.67%	23.91%	97.20%	30.62%	—	—
TPR	100%	0%	93.69%	10.02%	100%	0.05%	—	—
SI	100%	0%	95.86%	8.47%	100%	0%	—	—
CI	100%	0%	70.72%	30.82%	100%	0%	—	—
SDNN	69.18%	99.99%	95.76%	5.42%	99.46%	11.75%	—	—
HRVTi	90.29%	99.51%	89.01%	10.87%	78.78%	62.93%	—	—
RMSDD	100%	0.91%	81.00%	17.44%	99.93%	4.21%	—	—
BRS	100%	15.46%	62.06%	22.99%	99.98%	0.92%	—	—
LFNorm	100%	0.28%	91.85%	10.89%	98.28%	18.63%	—	—
HFNorm	100%	0.34%	91.93%	10.85%	98.42%	18.73%	—	—
LF/HF	100%	0%	56.70%	23.67%	99.71%	5.36%	—	—
IOP	100%	0%	56.96%	17.16%	100%	0%	51.25%	4.48%
OPP	97.77%	97.06%	66.81%	21.46%	99.35%	10.73%	51.62%	4.28%
A_{IJV}	100%	0%	85.52%	13.18%	100%	0%	51.39%	4.47%
IJVP	100%	0%	86.11%	21.65%	100%	0%	51.52%	4.47%
IJVF	100%	0%	61.21%	16.74%	100%	0.04%	50.10%	14.53%
A_{CCA}	52.12%	100%	64.46%	16.35%	100%	0%	51.23%	4.51%
PSV	100%	0.28%	95.60%	5.94%	96.03%	26.60%	53.70%	4.47%
EDV	97.12%	93.87%	55.09%	8.32%	84.96%	44.97%	50.77%	4.45%

Of the four main effects considered, the effect of LBNP presents the strongest evidence (narrowest posterior distributions), with the majority of parameters falling either fully inside or outside of the ROPE. The systemic hemodynamic variables are evidently those most influenced by LBNP, with a larger relative effect size (either positive or negative) than the autonomic or cephalad variables. In particular, the fall in SV/CO (and their indexed equivalents) and the corresponding rise

in TPR and MO. In contrast, there is strong evidence in favor of no effect of LBNP on five variables (A_{CCA}, SDNN, HRVTi, DBP, and OPP) and trending evidence of no effect in EDV ($\%_{ROPE}$: 93.87%). This informs us that a) overall heart rate variability is not influenced by LBNP, and b) most LBNP-related effects are related to the systolic ($\%_{ROPE} = 8.73\%$), as opposed to the diastolic ($\%_{ROPE} = 98.11\%$), part of the blood pressure waveform. In addition, related to the head/neck hemodynamics, it is insightful that there is strong evidence for an effect of LBNP on IOP, A_{IJV}, and IJVP, of approximately similar relative magnitude ($\%_{ROPE}$: 0% for all three), yet no effect on OPP ($\%_{ROPE}$: 97.06%). This has potential implications for the use of LBNP as a SANS countermeasure, discussed in Section 5.4 below.

Of the three groups (systemic hemodynamics, autonomic response, and head/neck), the autonomic variables are the least affected by LBNP, although there is still strong evidence of a decrease in parasympathetic activity (decrease in RMSDD and HFNorm; $\%_{ROPE}$: 0.91% and 0.34% respectively) matched by an increase in sympathetic activity (increase in LFNorm and LF/HF; $\%_{ROPE}$: 0.28% and 0% respectively). Finally, there is clearly an effect of LBNP on IJVF flow pattern ($\%_{ROPE}$: 0%), with the relative log odds of a higher grade (2 or 3) flow decreasing by 1.13 (89% CrI: 0.82 to 1.52) with each 10% mmHg increase in LBNP strength.

5.3.4.2 Sex Effect

Figure 5.7 presents the effect sizes of Sex on the normalized responses of all variables considered. The variables are ordered from the largest positive effect size at the top to the largest negative effect size at the bottom, and IJVF is presented separately due to the differing ROPE range. Due to the contrast coding in the model, a positive effect size represents an increase in male subjects with respect to female subjects. Tables 5.4 and 5.5 present the fitted parameters from the dose-response curves, and the pd and $\%_{ROPE}$, respectively.

In contrast to the effect of $Pressure$, the posteriors associated with the Sex effect are much wider. This is due to the fact that the magnitude of any sex effect between males and females is often dwarfed by the natural intersubject variability found across all subjects. We found strong evidence of significant effects of Sex in only three variables (SV, $\%_{ROPE} = 0\%$l CO, $\%_{ROPE} =$

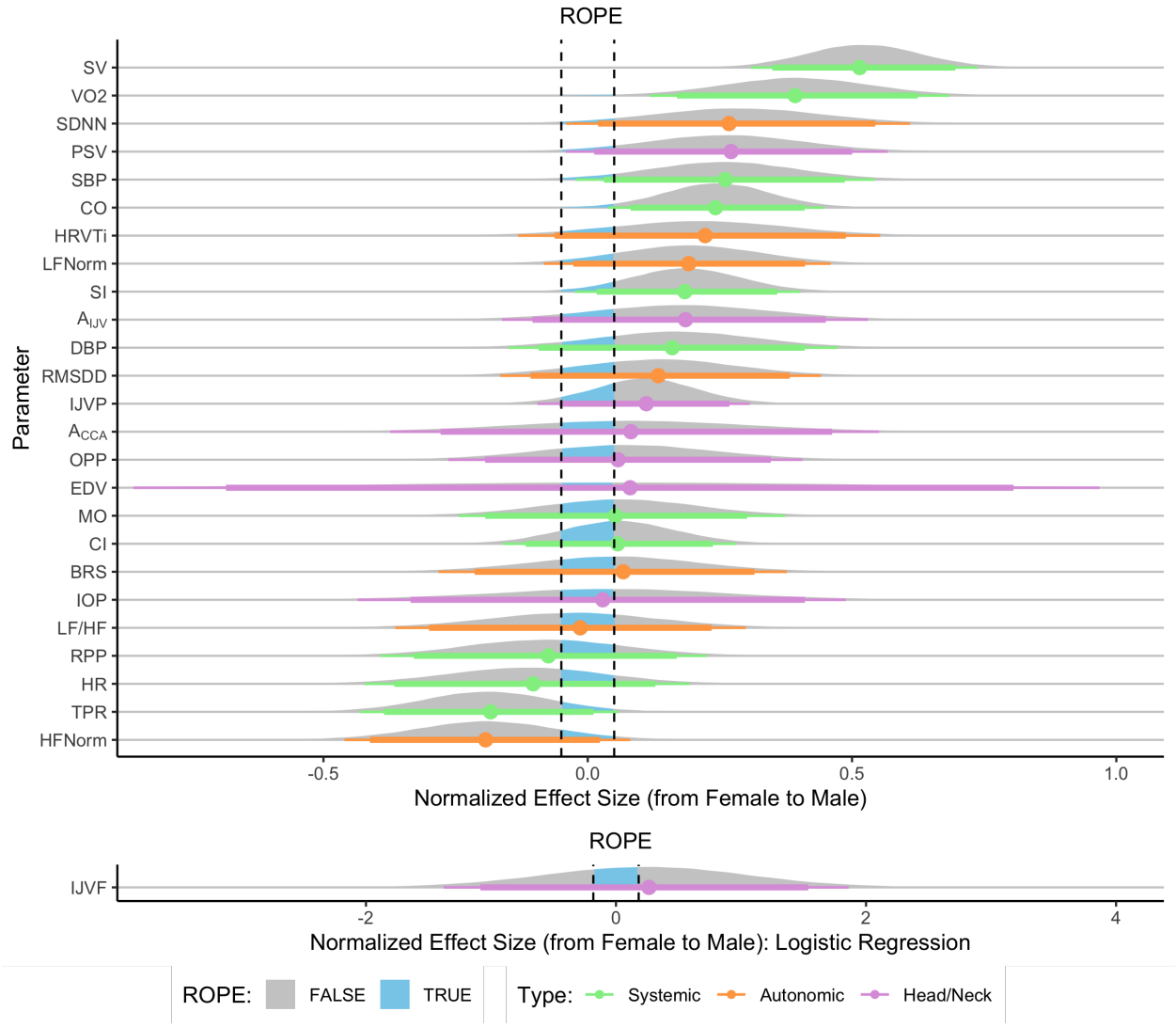

Figure 5.7: Normalized main effect of sex (male or female) on systemic (green), autonomic (orange), and head/neck (purple) variables. Variables are ordered from the largest positive effect size at the top to the largest negative effect size at the bottom. Data are presented as the posterior distributions from the Bayesian multivariate regression model. Distributions are colored gray when located outside of the ROPE, and blue when located inside the ROPE. Points and error bars underneath the distributions represent the maximum a-posteriori estimate along with the 89% (thick) and 95% (thin) highest density intervals. IJVF is presented separately below, since the ROPE is defined differently for a logistic regression model (see Section 5.2.5 for detail).

2.76%; and VO2, $\%_{ROPE} = 0.79\%$). With respect to the indexed variables, there is minimal evidence of a sex effect in CI ($pd = 70.72\%$, $\%_{ROPE} = 30.82\%$) but some evidence of a sex effect in SI ($pd = 95.86\%$, $\%_{ROPE} = 8.47\%$). The presence of an effect in the absolute variables (CO,

SV), and the lack of a significant effect in the indexed variables (and elsewhere) would appear to indicate that variation between males and females are principally the results of anthropometric differences (i.e., on average males are larger, with a higher total blood volume and a larger stroke volume).

In five variables, there is moderate evidence of the presence of a sex effect, even if it is not necessarily of significant magnitude. This is evidenced by variables with a pd greater than 90% and a $\_ROPE$ less than 10%. These variables are SDNN ($pd = 95.76\%$, $\%_{ROPE} = 5.42\%$), PSV ($pd = 95.60\%$, $\%_{ROPE} = 5.94\%$), SBP ($pd = 96.22\%$, $\%_{ROPE} = 5.60\%$), SI ($pd = 95.86\%$, $\%_{ROPE} = 8.47\%$), and TPR ($pd = 93.69\%$, $\%_{ROPE} = 10.02\%$). Similar to our results from the female subjects in tilt, presented in Section 4.7, the fact that SDNN appears larger in males (by, on average, 12.2 ms, 89% CrI: 0.9 to 24.4 ms) is likely explained by hormonal effects on the autonomic nervous system[347]. We do not, however, see a corresponding reduction in RMSDD in males which would be indicative of higher parasympathetic activity in females.

In summary, comparison between absolute variables (CO, SV) and indexed variables (CI, SI) suggest that sex differences in the data appear to be principally driven by anthropometric variation between males and females, however there is some evidence of increased sympathetic activity in male subjects.

5.3.4.3 Position Effect

The main effect of position is insightful as it relates to how LBNP acts in the presence of a cephalad fluid shift as experienced in microgravity. Figure 5.8 presents the effect sizes of $Position$ on the normalized responses of all variables considered. The variables are ordered from the largest positive effect size at the top to the largest negative effect size at the bottom, and IJVF is presented separately due to the differing ROPE range. Based on the way position has been captured in the model, a positive effect size represents an increase from 0° supine to 15° HDT. Tables 5.4 and 5.5 present the fitted parameters from the dose-response curves, and the pd and $\%_{ROPE}$, respectively.

A significant effect is seen in six of the 11 systemic hemodynamic parameters, two of the autonomic parameters, and five of the eight head/neck parameters. The largest effect sizes are

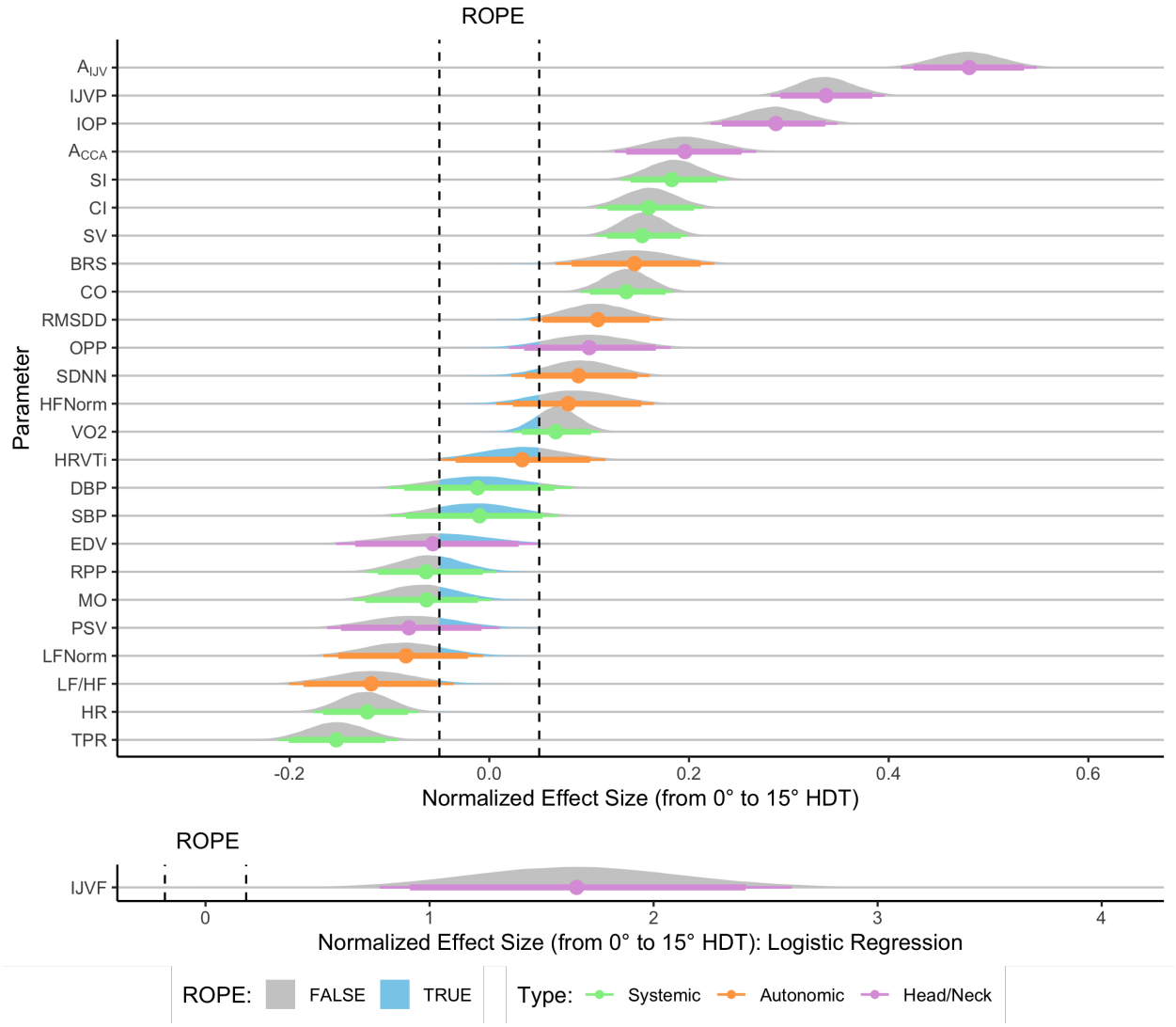

Figure 5.8: Normalized main effect of position (0° supine or 15° HDT) on systemic (green), autonomic (orange), and head/neck (purple) variables. Variables are ordered from the largest positive effect size at the top to the largest negative effect size at the bottom. Data are presented as the posterior distributions from the Bayesian multivariate regression model. Distributions are colored gray when outside of the ROPE, and blue inside the ROPE. Points and error bars underneath the distributions represent the maximum a-posteriori estimate along with the 89% (thick) and 95% (thin) highest density intervals. IJVF is presented separately below, since the ROPE is defined differently for a logistic regression model (see Section 5.2.5 for detail).

seen in the jugular vein response (area, pressure, and flow). This is congruent with our results in Section 4, which demonstrated the strong gravitational dependence of the jugular vein. In contrast to Figure 4.7, we also find a significant effect of Position on A_{CCA} ($pd = 100\%$,

$\%_{ROPE} = 0\%$), although it should be noted that we are only considering a single tilt angle here. Similar to Section 4, we also note significant increases in SV ($pd = 100\%$, $\%_{ROPE} = 0\%$), CO ($pd = 100\%$, $\%_{ROPE} = 0\%$) (and their indexed equivalents), IOP ($pd = 100\%$, $\%_{ROPE} = 0\%$), BRS ($pd = 99.98\%$, $\%_{ROPE} = 0.92\%$), and RMSDD ($pd = 99.93\%$, $\%_{ROPE} = 4.21\%$), along with significant decreases in HR ($pd = 100\%$, $\%_{ROPE} = 0.30\%$) and TPR ($pd = 100\%$, $\%_{ROPE} = 0.05\%$).

The RMSDD and BRS responses, combined with the decrease in heart rate indicate that the autonomic response is activated by the cephalad fluid shift, manifested principally by an increase in vagal activity lowering heart rate. This is combined with the reduced TPR promoting venous return leading to increased SV and CO through the Frank-Starling mechanism[188].

Finally, we note an increase in OPP in 15° HDT ($pd = 99.35\%$, $\%_{ROPE} = 10.73\%$), which is significant in direction and approaching significance in magnitude. This is congruent with our results in Section 4.6 demonstrating an increase in OPP in HDT. Analysis of the relative magnitudes of the effect sizes indicates that the increase in OPP is blunted by the constancy of blood pressure, where there is slight evidence in favor of the null hypothesis of no effect of position (($pd = 63.28\%$, $\%_{ROPE} = 72.76\%$ and $pd = 58.30\%$, $\%_{ROPE} = 70.47\%$ for SBP and DBP, respectively).

5.3.4.4 Side Effect

Figure 5.9 presents the effect sizes of $Side$ on the normalized responses of the head/neck variables considered. The variables are ordered from the largest positive effect size at the top to the largest negative effect size at the bottom, and IJVF is presented separately due to the differing ROPE range. Due to the contrast coding in the model, a positive effect size represents an increase from left to right side. Tables 5.4 and 5.5 present the fitted parameters from the dose-response curves, and the pd and $\%_{ROPE}$, respectively.

In all eight variables considered, we did not find an effect of *Side*. Whilst the $\%_{ROPE}$ is small ($< 5\%$) for all variables except IJVF, this is due to the broad spread of the posterior distributions. Taken in context with the pd (in the range 50% to 54% for all variables), there is no evidence of

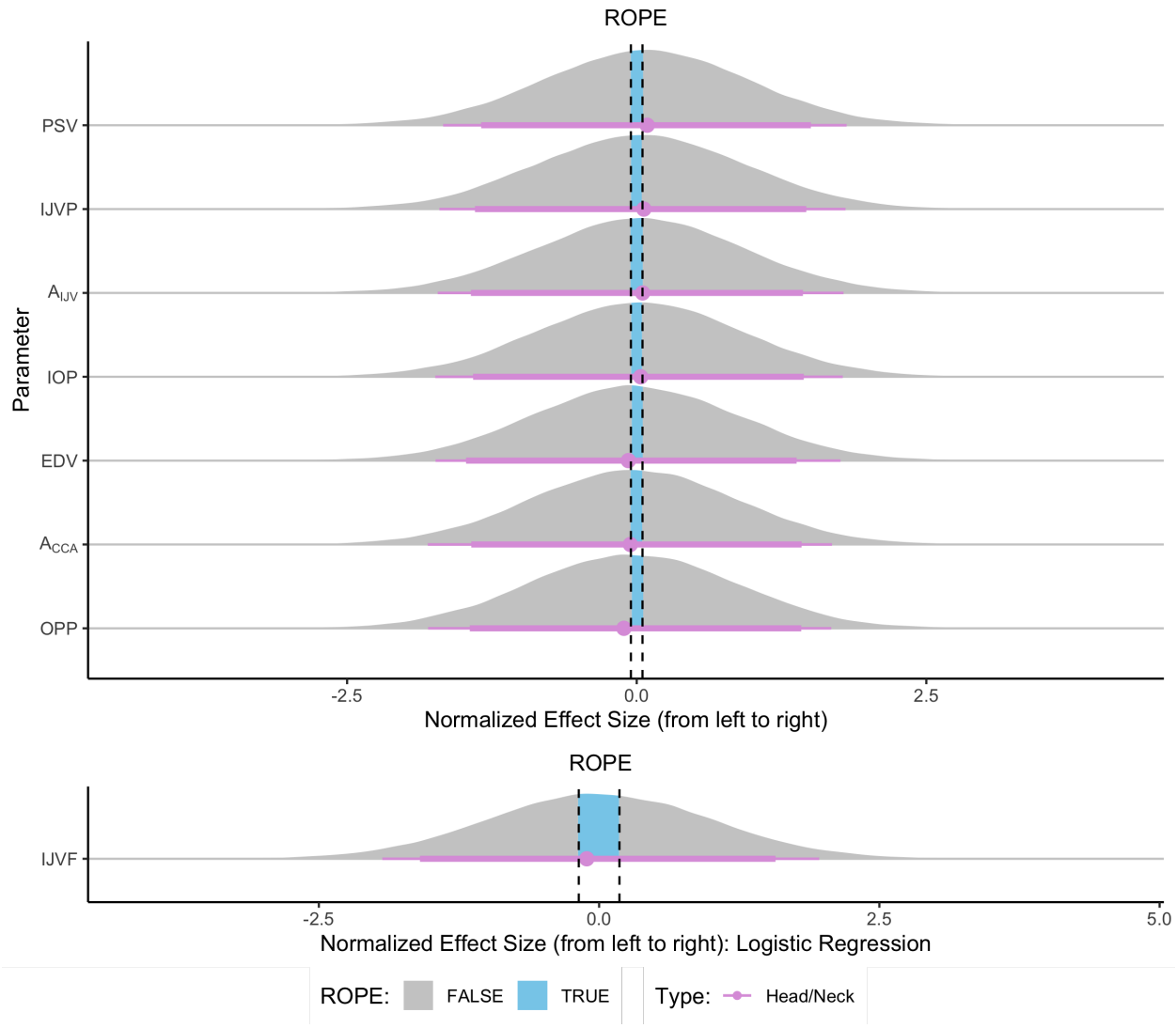

Figure 5.9: Normalized main effect of side (left or right) on head/neck (purple) variables. Variables are ordered from the largest positive effect size at the top to the largest negative effect size at the bottom. Data are presented as the posterior distributions from the Bayesian multivariate regression model. Distributions are colored gray when outside of the ROPE, and blue inside the ROPE. Points and error bars underneath the distributions represent the maximum a-posteriori estimate along with the 89% (thick) and 95% (thin) highest density intervals. IJVF is presented separately below, since the ROPE is defined differently for a logistic regression model (see Section 5.2.5 for detail).

an effect size in any particular direction. This is in contrast to our results from the tilt experiment, where we found differences in size between the left and right jugular veins. It would appear that this effect is only present in the amplified expansion of the jugular vein in extreme head-down tilt. Note that, in contrast to the frequentist methodology presented in Section 4, we are not constrained

to accept the null hypothesis in the absence of evidence to the contrary. In fact, here we can go further and say that there is no significant evidence either in favor of the null hypothesis (no effect), or the alternative (an existing effect). Aside from our findings on A_{IJV} in tilt discussed above, the rest of the results are congruent with the remainder of our tilt data, in that we found no effect of side on IOP, OPP, or IJVP.

5.3.4.5 IJV Flow

The majority of the variables are explained by linear models, whose interpretation is relatively straight forward. In contrast, the dose-response curve for the internal jugular vein blood velocity waveform flow pattern is based on an ordinal logistic regression, with a slightly more cryptic interpretation. Thus, it is insightful to plot this dose-response in full. Figure 5.10 presents this IJV flow pattern dose-response curve. Based on the effect sizes in Figures 5.6, 5.8, 5.9, and 5.7 (where there was evidence of $Pressure$ and $Position$ effects, but no evidence of Sex or $Side$ effects), we have grouped males and females, and left and right sides together. Whilst the response is ordinal, the figure shows the latent variable[1] given by the logit function[392]. Due to only a couple of instances of Grade 3 flow occurring (Figure 5.5), we have grouped the probabilities such that the Y axis in the curve represents the probability of "greater than Grade 1 flow" (i.e., Grade 2 or Grade 3 flow).

In 0° supine, the probability of greater than Grade 1 flow is 31.2% (89% CrI: 8.5% to 61.9%) at 0 mmHg. This is reduced by LBNP to 13.8% (89% CrI: 2.8% to 33.0%), 5.2% (89% CrI: 0.8% to 13.9%), 1.9% (89% CrI: 0.2% to 5.5%), 0.7% (89% CrI: 0.1% to 2.1%), and 0.2% (89% CrI: 0.0% to 0.8%) at –10 mmHg, –20 mmHg, –30 mmHg, –40 mmHg, and –50 mmHg, respectively. In 15° HDT, there is an increased probability of Grade 2 or higher flow of 65.4% (89% CrI: 33.8% to 89.8%) at 0 mmHg. This is reduced by LBNP to 40.9% (89% CrI: 14.3% to 71.3%), 19.8% (89% CrI: 4.7% to 43.3%), 8.0% (89% CrI: 1.3% to 20.6%), 3.0% (89% CrI: 0.3% to 8.6%), and 1.1% (89% CrI: 0.1% to 3.5%) at –10 mmHg, –20 mmHg, –30 mmHg, –40 mmHg, and –50 mmHg,

[1] In the context of a logistic regression, the latent unobserved variable, y^*, represents the probability of an observed binary variable, y. For an ordinal logistic regression, the ordinal responses are grouped to create binary categories (e.g., grade 1 versus grade 2 and 3 flow, or grade 1 and 2 versus grade 3 flow).

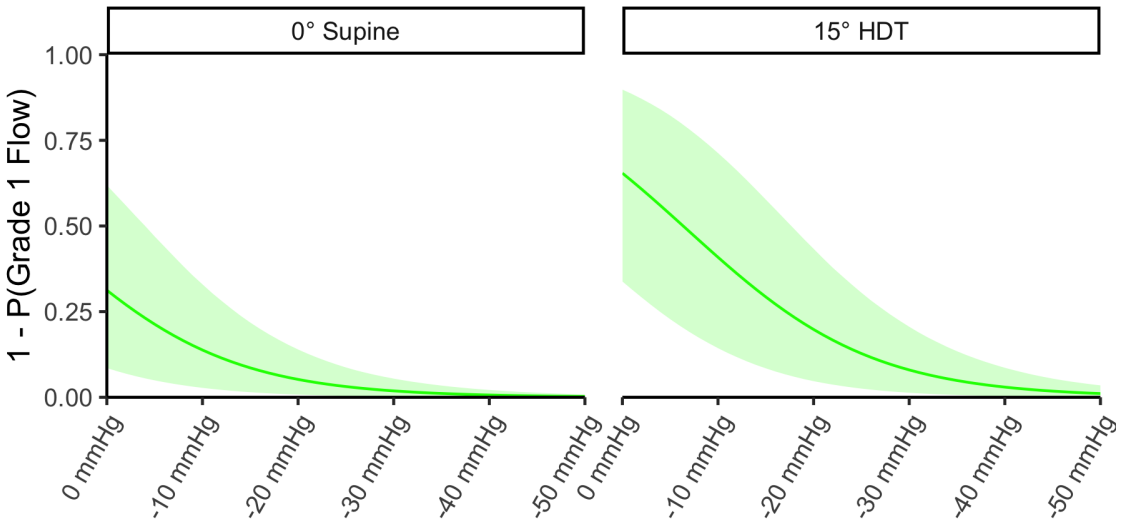

Figure 5.10: Dose-response curve for internal jugular vein blood flow velocity flow pattern. The y-axis represents the probability of having higher than grade 1 flow (i.e., grade 2 or grade 3 flow). Dose-response represents the fitted posterior draws from the multivariate regression model. Sex and $Side$ effects are pooled. $Position$ (0° supine or 15° HDT) is faceted. Dose-response is presented as the maximum a-posteriori estimate ± 89% CrI.

respectively.

The data highlight that LBNP is an effective tool for reducing flow stagnation in the internal jugular veins, suggesting its use as a potential countermeasure against the concern of VTE described in Section 2.2.3. The implications for this will be further discussed in Section 5.4 below.

5.3.5 Multivariate Relationships

Figure 5.11 presents the multivariate relationships amongst all of the variables considered, including the subject characteristics (Age, $Height$, $Weight$, and BMI). These relationships are derived from the correlation matrix between the group-level intercepts (γ_{ip} in Equation 5.2) modeled with an LKJ prior (Equation 5.3 and Table 5.3). Correlations are only displayed where there is significant evidence of an effect (in the Bayesian formulation, when the full posterior distribution does not encompass 0)[iv]. The inclusion of the subject characteristics also sheds light on

[iv]Compared to correlation in a frequentist framework, the maximum a-posteriori estimate is analogous the r-value, whilst the significance, i.e., whether the posterior distribution encompasses 0, is analogous to the p-value.

any relationships between the variables driven by anthropometric considerations such as height or weight.

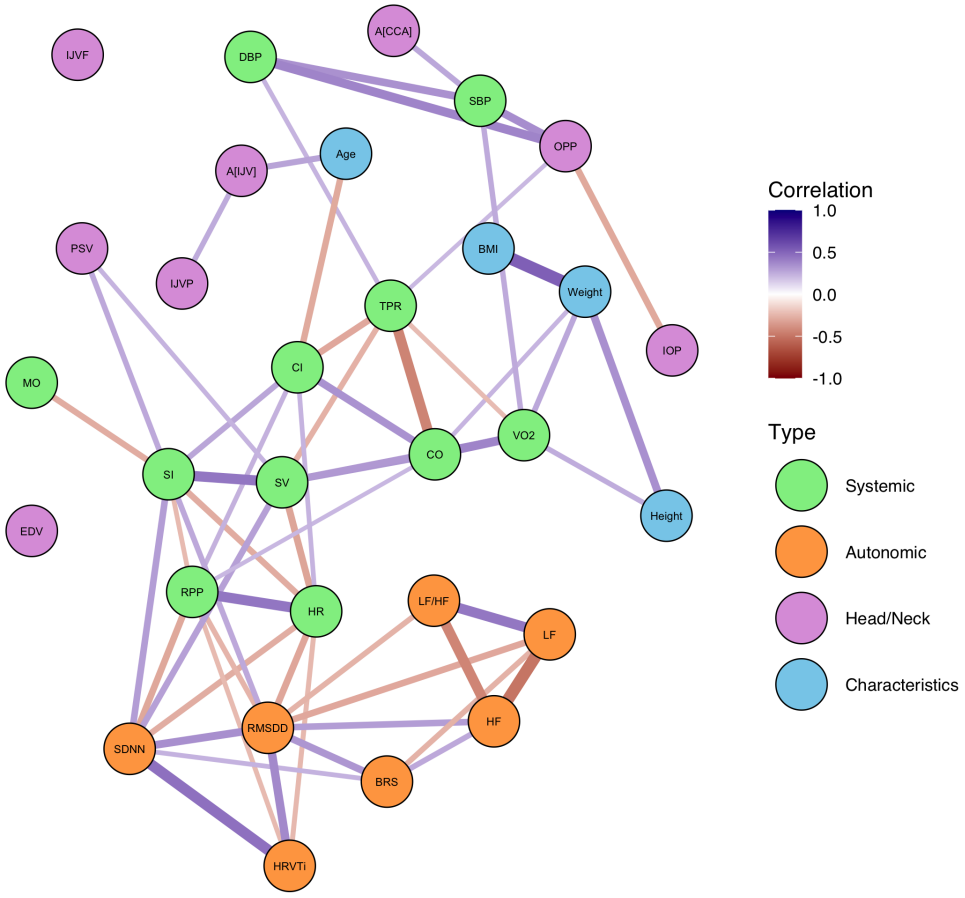

Figure 5.11: Graph structure representing the multivariate relationships amongst all of the measured variables (green: systemic, orange: autonomic; purple: head/neck; blue: subject characteristics). The direction of the correlations (positive or negative) are represented by the color of the edges, and the strength (the maximum a-posteriori estimate) is represented by the thickness of the edges. Only significant correlations are shown (see text for details).

Broadly, the graph structure appears to form two connected groups. All of the autonomic

parameters are strongly connected to one another, forming one group. Similarly, the systemic hemodynamics form a second connected group structure. HR is linked to the autonomic parameters through heart rate variability and parasympathetic activity (RMSDD), where higher heart rate is associated with lower variability and lower vagal activity. Similarly, increased HRV is associated with increased stroke volume, and reduced RPP.

OPP is associated with both blood pressure and IOP (which is natural given Equation 4.4), but increased OPP is also associated with increased TPR. The relationship with the subject characteristics is also insightful: in contrast to Buckey *et al.*[50,61], we do not find any association between IOP and body weight or BMI, however greater height and weight are associated with increased oxygen consumption. More interestingly, we see that Age is positively correlated with IJV cross-sectional area (and by extension pressure), and negatively correlated with CI. Finally, carotid hemodynamics are associated with systolic blood pressure (correlated with A_{CCA}) and stroke volume (correlated with PSV). There is no significant relationship between EDV or IJVF and any of the other metrics.

5.3.6 Relationship Between Change in IOP and Body Weight

In order to further investigate the relationship between IOP and body weight we are able to extract the specific increase in IOP between 0° supine and 15° HDT. In order to do this, we define a new variable, ΔIOP_{pos} such that:

$$\Delta IOP_{pos,ijk} = IOP_{15,ijk} - IOP_{0,ijk} \tag{5.7}$$

where IOP_{15} is the IOP in 15° HDT and IOP_0 is the IOP in 0° supine for each subject (i), pressure (j), and side (k) combination.

To assess the correlation between ΔIOP_{pos} and body weight, we will use a robust Bayesian methodology. Using MCMC sampling, and assuming weakly informative priors, we will fit a multivariate t-distribution to the two variables in order to estimate the correlation coefficient between them such that:

$$\begin{bmatrix} weight \\ \Delta IOP_{pos} \end{bmatrix} \sim Student\left(\boldsymbol{\mu}, \boldsymbol{\Sigma}, \nu\right)$$

$$\boldsymbol{\mu} = \begin{bmatrix} \mu_{weight} \\ \mu_{\Delta IOP_{pos}} \end{bmatrix} \tag{5.8}$$

$$\boldsymbol{\Sigma} = \begin{bmatrix} \sigma^2_{weight} & \rho \cdot \sigma_{weight} \cdot \sigma_{\Delta IOP_{pos}} \\ \rho \cdot \sigma_{weight} \cdot \sigma_{\Delta IOP_{pos}} & \sigma^2_{\Delta IOP_{pos}} \end{bmatrix}$$

where $\boldsymbol{\mu}$ is the vector of means, $\boldsymbol{\Sigma}$ is the covariance matrix, and ρ is the Bayesian correlation coefficient.

Figure 5.12A presents the data with 50%, 89%, and 95% density ellipses from the fitted multivariate t-distribution overlaid, whilst Figure 5.12B presents the posterior distribution of the fitted correlation coefficient, ρ. Using the same methodology, the analysis was repeated with BMI instead of weight, and with OPP (with ΔOPP_{pos} similarly defined as per Equation 5.7) instead of IOP. The resulting correlation estimates are presented in Table 5.6.

Table 5.6: Bayesian robust correlation between body weight/BMI and the change in IOP/OPP from 0° supine to 15° HDT. Correlation, ρ, is presented as the maximum a-posteriori estimate (89% HDI). Evidence for existence of correlations is presented as probability of direction (pd). Evidence for significance of correlations is presented as probability that $|\rho| > 0.1$ (i.e., probability that ρ is not small). See Section 5.2.5 for detail on the pd.

Parameter 1	**Parameter 2**	ρ	pd	$P\left(\lvert\rho\rvert > 0.1\right)$
$weight$	ΔIOP_{pos}	0.201 (0.100, 0.299)	99.9%	94.4%
BMI	ΔIOP_{pos}	0.165 (0.058, 0.266)	99.3%	83.0%
$weight$	ΔOPP_{pos}	–0.127 (–0.224, –0.028)	97.6%	65.5%
BMI	ΔOPP_{pos}	–0.103 (–0.206, –0.009)	96.2%	56.4%

Results show that a modest, but significant, positive correlation does exist between the increase in IOP with HDT and body weight, with an 89% probability that the correlation coefficient is in the range 0.100 to 0.299 (maximum a-posteriori estimate 0.201). It has been previously noted that

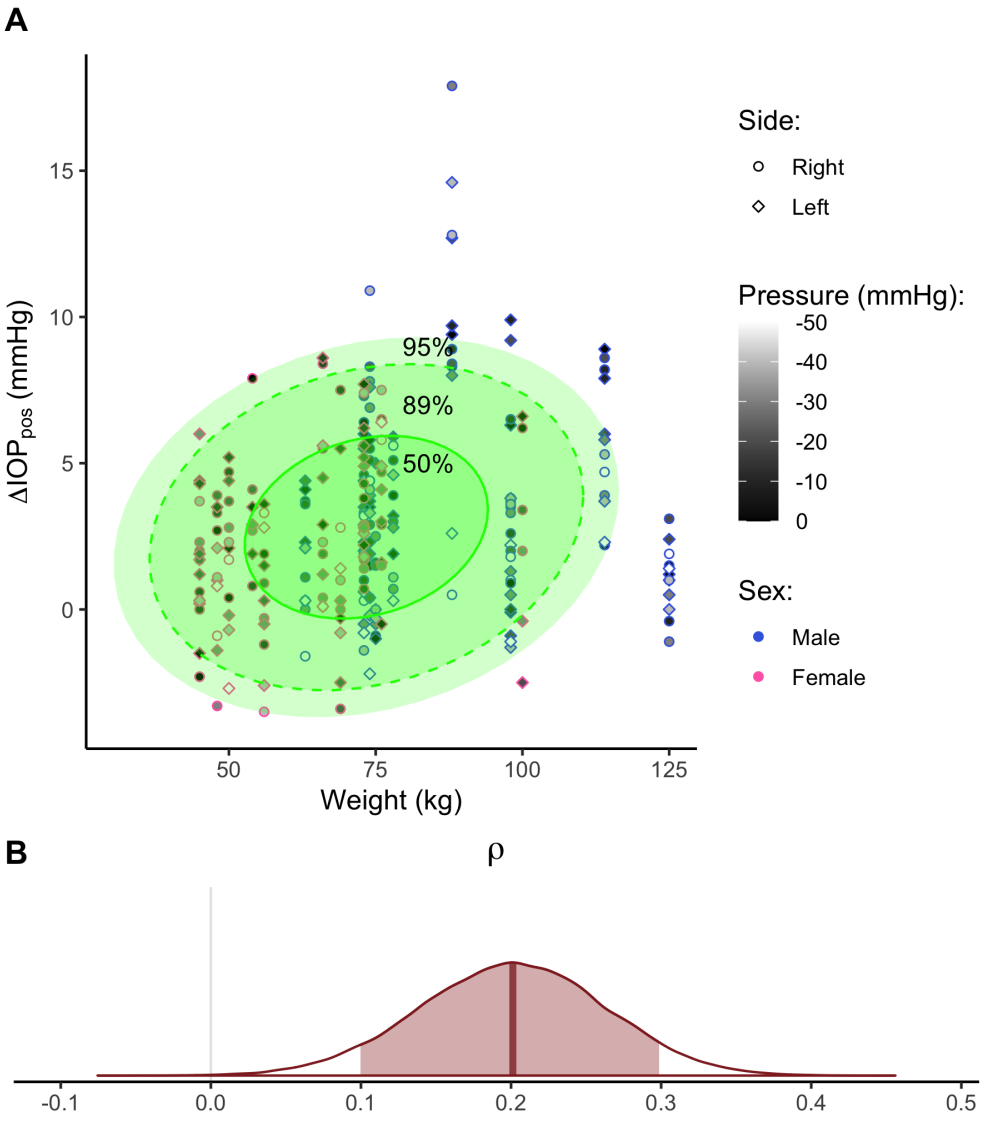

Figure 5.12: **(A-B)** Bayesian robust correlation between the change in IOP from 0° supine to 15° HDT, ΔIOP_{pos}, and body weight. **(A)** Raw data with 50%, 89%, and 95% density ellipses from a multivariate t-distribution overlaid; fitted via MCMC as per Equation 5.8. **(B)** Posterior distribution of the Bayesian correlation coefficient, ρ. The filled portion of the posterior distribution represents the 89% HDI.

there is an association between preflight body weight and the manifestation of SANS[61]. Buckey *et al.* more recently suggest that the removal of hydrostatic gradients in microgravity reduces transmural pressure posterior to the eye, and that this effect is more pronounced in individuals with a higher preflight body weight[50,393]. The direction of the change in IOP compared to the terrestrial supine position is opposite between HDT (positive) and microgravity (negative), however the association of the magnitude with body weight remains. They reconcile the fact that IOP appears reduced in microgravity compared to the supine position on Earth, with development of SANS by hypothesizing that removal of tissue weight reduces IOP at the back of the eye, whilst reducing ICP in the same location, leading to a decrease in transmural pressure (compared to the supine position) that is more pronounced in heavier individuals. This reduced transmural pressure promotes a shortening of the eye[50]. We also note some evidence of a correlation between ΔIOP_{pos} and BMI, although the significance is less compelling (an 83.0% probability that the correlation is not small). Regarding the association between ΔOPP_{pos} and body weight/BMI, data suggests a small negative correlation, although in frequentist terms this would likely not appear significant (given that $P(|\rho| > 0.1) = 65.5\%$ and 56.4% for body weight and BMI respectively). Given (1) the similarities in our work demonstrating the gravitational dependence of OPP (i.e., the importance of the relative pressure changes between IOP and MAP_{eye})[1] and the hypothesis of Buckey *et al.* highlighting the importance of the relative changes between IOP and head venous pressures related to body weight[50]; (2) the association between body weight and SANS[61]; and (3) the similarities between terrestrially elevated OPP and symptoms of SANS[60]; future work should systematically investigate the holistic relationship between changing vascular pressures in the ocular system (IOP, OPP, MAP_{eye}, and ICP), body weight, and the removal of tissue compressive forces in microgravity.

5.4 Discussion

This study investigated the acute effects of LBNP on the cardiovascular system. To our knowledge, this is the most comprehensive analysis of cardiovascular hemodynamics, autonomic, and cephalad response to LBNP. Further, we also introduce a new methodology for constructing dose-

response models from cardiovascular measurements, analyzing the multivariate structure through a Bayesian workflow. Our main findings show that: (1) there is a varying magnitude of the normalized effect sizes of responses to LBNP in different cardiovascular variables; (2) sex differences exist between the male and female response; however, these are principally driven by anthropometric considerations; (3) there is no evidence of a difference between the response in the left and right sides (in terms of the common carotid arteries, internal jugular veins, or eyes) to LBNP; and (4) there is an underlying multivariate structure with associations connecting all but two (EDV, IJVF) of the cardiovascular variables considered as well as subject characteristics such as age, height, weight, and BMI.

Multiple studies have investigated the effects of LBNP on cardiovascular hemodynamics; many of these are summarized in a comprehensive review article by Goswami *et al.*[73]. In a classic study by Blomqvist and Stone[309], the systemic hemodynamic responses to graded LBNP up to –40 mmHg were shown to be linear for TPR, HR, SV, CO, and MAP. Data from their study was compiled by Goswami *et al.* and part of one of their figures is presented for comparison in Figure 5.13 below. The slopes on these data show the relative effect size of the five variables considered with the application of LBNP. Our study, and in particular Figure 5.6, extend this work and increase the number of variables considered significantly. Our findings agree with the authors as to the relative magnitudes of the effects of TPR (large positive), HR (small positive), and CO and SV (large negative). We further find no decrease in DBP, and a small decrease in SBP, which corresponds well with the minimal decrease in MAP found by Goswami and colleagues. In Figure 5.6 we add the effect sizes of 17 new variables, and present the relative magnitudes of the LBNP-induced changes. Of note, we find that, whilst the TPR and SV/CO changes are the largest positive and negative effects, respectively, there are smaller, still significant, negative effects surrounding the jugular vein (A_{IJV}, IJVP, IJVF), IOP, and VO2, as well as positive effects on myocardial oxygen supply:demand index and rate pressure product.

Murray *et al.* investigated graded LBNP in four subjects and found a linear increase in heart rate from 59 ± 2.9 bpm at 0 mmHg to 90 ± 5.5 bpm at –50 mmHg. They further found changes in blood

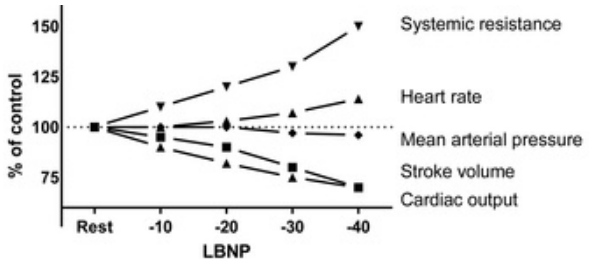

Figure 5.13: Hemodynamic responses to graded LBNP in the range 0 mmHg to –40 mmHg as collected by Blomqvist and Stone[309]. Figure reproduced from Goswami *et al.*[73].

pressure (SBP/DBP) from 125 ±6.7/71 ± 4.6 mmHg at 0 mmHg to 119 ± 4.3/81 ± 3.5 mmHg at –50 mmHg, and a decrease in stroke volume and cardiac output from 84 ± 6.0 ml and 4.9 ± 0.3 l/min at 0 mmHg to 39 ± 4.6 ml and 3.4 ± 0.2 l/min at –50 mmHg respectively[394]. Murray's increase in HR (31 bpm) is greater than the average increase that we find (12 bpm, 89% CrI: 10 to 14 bpm) over the same range, considering both positions and both sexes. Our SBP falls at a similar rate, from 129.5 ±2.2 mmHg at 0 mmHg to 117.2 ± 2.4 mmHg at –50 mmHg, but we do not see any corresponding increase in DBP (effect size of 0.5 mmHg, 89% CrI: –0.1 to 0.9 mmHg per 10 mmHg LBNP). Conversely, we find a larger decrease in stroke volume and cardiac output (effect sizes: -0.87 ml/mmHg, 89% CrI: –0.94 to –0.82 ml/mmHg; and –0.046 l/min/mmHg, 89% CrI: –0.049 to –0.042 l/min/mmHg, respectively). In general, our values fall within the confidence intervals found by Murray *et al.*. Further, this study by Murray is one of the few to investigate systemic vascular resistance or TPR. They found an increase from 1,415 ± 123 dyne-sec.cm^{-5} at 0 mmHg to 2,200 ± 132 dyne-sec.cm^{-5} at –50 mmHg (equivalent to 1.06 ± 0.09 mmHg.s/ml to 1.65 ± 0.10 mmHg.s/ml in peripheral resistance units, PRU). This closely matches the increase we found, from 1.11 ± 0.04 mmHg.s/ml at 0 mmHg to 1.75 ± 0.06 mmHg.s/ml at –50 mmHg; an effect size of 0.015 mmHg.s/ml/mmHg (89% CrI: 0.013 to 0.016 mmHg.s/ml/mmHg). Similarly, Levine *et al.* found an increase of 18 bpm in HR, and a decrease of 43 ml in SV at –40 mmHg LBNP in 13 subjects[395]. Finally, Hinojosa-Laborde *et al.* considered graded LBNP as an experimental model of hemorrhage[354]. The found a decrease in SBP from 121 to 80 mmHg, a decrease in SV from 59 to 41 ml, a decrease in CO from 5.1 to 4.2 l/min, and an increase in HR from 82 to 94 bpm from

0 mmHg to –40 mmHg LBNP. The decrease in SBP is much larger than the corresponding drop in our data, however all other measurements fall within the calculated confidence intervals of the dose-response.

Autonomic response to LBNP is principally mediated through the reduction in central blood volume lowering systemic flow and perfusion pressure, leading to stimulation of the arterial baroreflex[73,239,396,397]. Convertino *et al.* investigated the effect of LBNP on baroreflex sensitivity, finding that BRS decreased from 15 ± 1 ms/mmHg to 7 ± 1 ms/mmHg at presyncope in low-tolerance subjects and from 17 ± 2 ms/mmHg to 4 ± 0 ms/mmHg in high-tolerance subjects[398]. This matches well with our data, which found a reduction from 13.8 ± 1.1 ms/mmHg at 0 mmHg to 9.2 ± 0.7 ms/mmHg at –50 mmHg (average of both sexes and both positions). We did not deliberately take our subjects to the point of presyncope, but the decreasing trend is anticipated to continue to that point. This decrease in BRS, combined with the reduction in time- and frequency-derived HRV metrics (i.e., RMSDD and HFNorm) is indicative of progressive vagal withdrawal[399–401]. This vagal withdrawal is matched by a linear increase in sympathetic nervous activation with progressive LBNP. Our data demonstrate a linear increase in LFNorm, matched by a linear increase in LF/HF. These data are supported by multiple studies assessing either HRV metrics or muscle sympathetic nervous activity (MSNA) with LBNP[357,363,364,402–404]. Experiments using cholinergic blockade demonstrate the importance of both arms of the autonomic response to mediate cardiac function in LBNP[405,406]. The sympathetic response is also important for mediating vascular smooth muscle constriction in response to the reduction in central blood volume[398].

Regarding sex differences, Convertino investigated differences in autonomic function related to blood pressure regulation[353]. Our results are congruent with Convertino, who noted higher heart rate in female subjects, combined with a lower stroke volume during LBNP. Convertino took all subjects to presyncope, and noted a lower tolerance in females. Whilst we did not deliberately take our subjects to this level, the fact that many more female subjects reached presyncope in the 0 to –50 mmHg range would suggest a lower tolerance. This lower tolerance in females is well supported by multiple studies[353,358,366,367,407,408]. Convertino further derived the

effect size of the LBNP response in males and females with regard to HR, SV, CO, MAP, and TPR, noting that the difference in slope is non-significant ($p > 0.05$) in all cases except for TPR ($p = 0.0002$). In heart rate, he noted a 0.37 ± 0.05 bpm/mmHg increase in males and a 0.58 ± 0.10 bpm/mmHg increase in females. This is slightly higher than the 0.24 bpm/mmHg (89% CrI: 0.20 to 0.28 bpm/mmHg) that we derived. With regards to stroke volume, Convertino found a –1.06 ± 0.10 ml/mmHg change in males and a –1.23 ± 0.19 ml/mmHg change in females. This compares with our findings of –0.87 ml/mmHg (89% CrI: –0.94 to –0.82 ml/mmHg). In contrast, we also note a "significant" interaction effect, with males decreasing stroke volume 0.42 ml/mmHg (89% CrI: 0.30 to 0.54 ml/mmHg) faster than females. Finally, in cardiac output, we note a change of –0.046 l/min/mmHg (89% CrI: –0.049 to –0.042 l/min/mmHg). This fits in between his measured values of –0.03 ± 0.01 l/min/mmHg in males and –0.07 ± 0.01 l/min/mmHg in females. On the autonomic side, Convertino measured the baroreflex sensitivity, noting that the response was 1.32 ms/mmHg lower in females ($p = 0.047$). We found that BRS was potentially higher in males by 1.0 ms/mmHg (89% CrI: –3.0 to 4.4 ms/mmHg), though the difference was far from significant and outweight by intersubject variability ($pd = 62.06\%$, $\%_{ROPE} = 22.99\%$). Other studies have found potential differences in the autonomic response between men and women. Frey *et al.* and Evans *et al.* found that women have a more dominant vagal response, whilst men primarily demonstrate a greater sympathetic response[362,409]. In addition, Frey and Hoffler also found that men exhibited a larger increase in TPR[365]. By considering Figure 5.7, we likewise find evidence of a higher sympathetic response in males based on LFNorm ($pd = 91.85\%$, $\%_{ROPE} = 10.89\%$), however we find conflicting evidence of a higher vagal response in women. The two autonomic markers corresponding to vagal response trend in opposite directions, with HFNorm higher in females ($pd = 91.93\%$, $\%_{ROPE} = 10.85\%$), but RMSDD higher in males ($pd = 81.00\%$, $\%_{ROPE} = 17.44\%$). Further, we find that TPR is actually lower in males initially by 0.15 mmHg.s/ml (89% CrI: –0.01 to 0.30 mmHg.s/ml), with an similar magnitude in the response to LBNP. Further study is required to investigate these discrepancies in the sex-driven autonomic response. More recently, Patterson *et al.* measured A_{IJV} differences between men and

women in the range 0 to –40 mmHg[295]. They noted a significant effect of sex ($p < 0.001$) and LBNP ($p < 0.001$), but no significant interaction ($p = 0.066$), with A_{IJV} being larger in female subjects at 0 mmHg, –20 mmHg, and –30 mmHg. In contrast, we found a significant effect of LBNP of -0.88 mm^2/mmHg (89% CrI: –1.02 to –0.73 mm^2/mmHg) but no significant effect of sex. In fact, in our study we found trending evidence of a higher A_{IJV} in males by 15.4 mm^2 (89% CrI: –8.7 to 37.6 mm^2; $pd = 85.52\%$, $\%_{ROPE} = 13.18\%$. Our results match previous studies, for example Jeon *et al.* and Magnano *et al.* who found no difference in A_{IJV} between males and females[410,411].

The article by Magnano *et al.* is highly interesting in that they note a positive association between A_{IJV} and age in over 1000 subjects[411]. Using a totally different methodology, we also discovered this association in Figure 5.11. This finding lends support both to their conclusions and also to our Bayesian modeling workflow. The authors hypothesize that increased A_{IJV} is linked to inhibited central venous drainage as a result of raised intra-abdominal pressure with increased BMI, which trends higher in older individuals. By contrast, though admittedly in a far smaller study, we find no direct link between BMI (or weight) and A_{IJV}. This suggests that the association might be related to other factors outside of BMI. Magnano *et al.* posit on the role of endothelial progenitor cells (EPCs) in the vascular remodeling process, noting sex differences related to pregnancy hormones[412]. Given evidence that EPCs decrease with increasing age[413], we could support this as potentially one of the factors in the age related differences in A_{IJV}. Continuing our discussion of Figure 5.11, we also note the negative association between age and CI, which is supported by a number of studies[414,415]. Related to the head and neck variables, we do not see the association between body weight and IOP noted by Buckey *et al.*[61]. As discussed in Section 5.3.6 above, when we extract the change in IOP between 0° supine and 15° HDT, we do find small positive associations between the increase in IOP in HDT and both higher body weight and BMI. Further, we do find an association between OPP and total peripheral resistance. It is difficult to find evidence in the literature for similar relationships, although Fındıkoğlu *et al.* noted a decrease in OPP in 34 subjects after hot-water immersion, which was also matched by a decrease in TPR[416]. Samsudin *et*

al. noted a relationship between OPP and EDV (which we did not find), but noted no relationship between OPP and resistive index[417]. In this study, resistive index (RI) referred only to the specifics of the ocular vasculature and not on the total peripheral resistance, thus, it is difficult to draw comparisons. Future work should look more closely at the relationship between IOP, OPP, and body weight, given the evidence for the role of tissue weight in the pathogenesis of SANS[50].

The effect of position is important since it allows us to determine the relative magnitude of a fluid shift induced by HDT (and, by extrapolation, microgravity) compared to the LBNP effect. Of the three groups (systemic, autonomic, and cephalad), we note that the largest effect size increase is in head/neck parameters including A_{IJV}, IJVP, IOP, and IJVF. This supports our evidence from Section 4 that the jugular veins and eyes exhibit a non-linear response to HDT. Interestingly, in this experiment we also found evidence of an increase in A_{CCA}, which we did not see in the tilt study. This is only at a single tilt angle, and compensatory mechanisms may prevent this increase from progressing at more severe HDT angles. Aside from A_{CCA} there are no data that contradicts our results from Section 4, including evidence that blood pressure is maintained in tilt. By comparing the magnitude of the $Pressure$ effect and the $Position$ effect, we were able to estimate the pressure required to bring that variable back to a supine equivalent, calculated as Estimated LBNP $= -10\beta_{pos}/\beta_{LBNP}$. These results are presented in Table 5.7. These data show that for the systemic parameters, an LBNP strength of less than –15 mmHg is sufficient to return the values to equivalent to supine, whilst for the head and neck, much high strengths are required (e.g, around –30 mmHg for IOP and IJVP, around –45 mmHg for A_{IJV}).

We do not see any differences in any of the head/neck variables between the left and right side.

Looking back at our data from the tilt experiment in Section 4 would suggest that there is no difference in the pressures in the ocular system between the left and right (neither IOP, nor OPP). In our tilt experiment, we did not measure PSV or EDV, however we would anticipate that there is little difference between sides since the CCA branch is located just superior to the ascending aorta, such that arterial flow in the CCA is still approximately equivalent to aortic flow velocity. The only difference found between between the left and right sides in Section 4 occurred in the

Table 5.7: Estimated LBNP strength required to remove the effect caused by the fluid shift induced with 15° HDT for each variable considered. The first column presents the standardized effect size of $Pressure$ per mmHg LBNP, the second column presents the standardized effect size of $Position$, and the third column presents the ratio between the two (Estimated LBNP $= -10\beta_{pos}/\beta_{LBNP}$). Data are presented as the maximum a-posteriori estimate (89% CrI). Estimate not shown where the effects of $Pressure$ and $Position$ are in the same direction (i.e., no amount of LBNP would reverse the change in the variable back from 15° HDT to 0° supine).

Parameter	$\frac{\beta_{\mathbf{LBNP}}}{\mathbf{10}}$ *(mmHg^{-1})*	$\beta_{\mathbf{pos}}$	**Estimated LBNP** *(mmHg)*
HR	0.0087 (0.0074, 0.0101)	–0.1221 (–0.1666, –0.0812)	13.9 (10.9, 16.4)
SV	–0.0181 (–0.0194, –0.0169)	0.1536 (0.1177, 0.1921)	8.5 (7.0, 9.9)
CO	–0.0177 (–0.0189, –0.0164)	0.1371 (0.1008, 0.1766)	7.7 (6.1, 9.3)
VO2	–0.0065 (–0.0076, 0.0055)	0.0668 (0.0325, 0.1019)	10.2 (5.9, 13.4)
SBP	–0.0068 (–0.0090, –0.0047)	–0.0106 (–0.0834, 0.0535)	—
DBP	0.0021 (–0.0003, 0.0043)	–0.0115 (–0.0852, 0.0651)	—
RPP	0.0108 (0.0092, 0.0124)	–0.0629 (–0.1114, –0.0064)	5.8 (0.7, 8.9)
MO	0.0171 (0.0151, 0.0187)	–0.0636 (–0.1242, –0.0111)	3.7 (0.7, 6.6)
TPR	0.0187 (0.0170, 0.0202)	–0.1528 (–0.2009, –0.1039)	8.2 (6.1, 9.9)
SI	–0.0199 (–0.0212, –0.0184)	0.1833 (0.1415, 0.2283)	9.2 (7.7, 10.8)
CI	–0.0213 (–0.0227, –0.0199)	0.1597 (0.1183, 0.2051)	7.5 (5.9, 9.0)
SDNN	0.0006 (–0.0012, 0.0023)	0.0895 (0.0359, 0.1482)	—
HRVTi	0.0016 (–0.0004, 0.0037)	0.0327 (–0.0337, 0.1008)	—
RMSDD	–0.0075 (–0.0094, –0.0058)	0.1079 (0.0533, 0.1604)	14.3 (9.2, 17.1)
BRS	–0.0062 (–0.0083, 0.0043)	0.1450 (0.0825, 0.2117)	23.5 (19.3, 25.6)
LFNorm	0.0085 (0.0064, 0.0106)	–0.0836 (–0.1513, –0.0214)	9.8 (13.3, 14.2)
HFNorm	–0.0085 (–0.0106, –0.0064)	0.0807 (0.0236, 0.1522)	9.5 (3.7, 14.4)
LF/HF	0.0108 (0.0087, 0.0129)	–0.1184 (–0.1861, –0.0519)	11.0 (6.0, 14.4)
IOP	–0.0098 (–0.0112, –0.0081)	0.2870 (0.2331, 0.3364)	29.3 (28.7, 29.9)
OPP	0.0026 (0.0005, 0.0046)	0.1002 (0.0349, 0.1668)	—
A_{IJV}	–0.0105 (–0.0122, –0.0087)	0.4796 (0.4249, 0.5356)	45.5 (43.9, 48.7)
IJVP	–0.0117 (–0.0132, –0.0102)	0.3369 (0.2914, 0.3836)	28.9 (28.5, 29.1)
IJVF	–0.1128 (–0.1525, –0.0824)	1.6589 (0.9116, 2.4113)	14.7 (11.1, 15.8)
A_{CCA}	0.0000 (–0.0018, 0.0017)	0.1957 (0.1371, 0.2526)	—
PSV	–0.0088 (–0.0109, –0.0066)	–0.0795 (–0.1485, –0.0077)	—
EDV	0.0027 (0.0005, 0.0051)	–0.0559 (–0.1342, 0.0294)	—

A_{IJV}, and A_{CCA} when female subjects were included (Figure 4.23). We did not see any significant difference in IJVP between the left and right sides, hypothesized as due to the fact that both sides sit minimally above CVP.

Thus, the key difference between this LBNP experiment and the tilt study presented in Section 4 is that here we did not find any $Side$ effect on the cross-sectional area of the CCA or IJV. The main difficulty in detecting significance between the left and right sides is the large intersubject variability. Ogoh *et al.* assessed the difference between the left and right side A_{IJV} in two conditions: (1) 0° supine with –60 mmHg LBNP; and (2) 60° HUT with no LBNP[368]. This is one of the few studies that assessed both sides of the jugular veins. Similar to our data, they found large variability in their data. With the application of –60 mmHg LBNP, they measured a change in the right A_{IJV} of –45% ± 49%, and in the left A_{IJV} of –49% ± 27%. Here, as with our data, the standard deviation of the measurements is too large to draw significant conclusions. This gives us confidence that indeed natural variability between subjects is larger than intrasubject differences between the left and right side.

5.4.1 Implications for Countermeasure Design

This study has several implications for countermeasure design, but leads to important further questions that warrant future investigation. The key risks and concerns from the Human Research Roadmap that are addressed by this work were introduced in Section 2.2. They will be considered briefly in turn below:

5.4.1.1 Risk of Cardiovascular Adaptations Contributing to Adverse Mission Performance and Health Outcomes

Since this study only considered acute effects of LBNP, it is difficult to make solid recommendations about a long-term countermeasure for cardiovascular health. By considering the DAG in Figure 2.2, we can track that one of the routes of the cardiovascular risk is through fluid shifts leading to: (1) alterations in intravascular volume, (2) changes in cardiac and vascular structure/function, (3) oxidative stress, and (4) inflammation[34]. Reducing the headward fluid shift, or at least periodic unloading, would block these pathways in the DAG. The open questions are therefore the specific level and protocol of LBNP that are appropriate.

This study leads to two insights into these questions. First, we note the well-established differ-

ences in tolerance between males and females. Given that there is strong evidence of a difference between the male and female response in absolute variables (e.g., SV, CO) but not in indexed variables (e.g., SI, CI), it would appear that differences are principally anthropometrically driven. This places an upper limit on the level of LBNP that could be used in a spaceflight environment, particularly when the astronauts are in a deconditioned state. It appears, for example, that a strength of –50 mmHg is perhaps too strong for many female subjects. Further analysis may lead to the development of personalized protocols based on anthropometric considerations, rather than a "one size fits all" approach. Second, and most importantly, by considering Figure 5.6 in conjunction with Figure 5.8, we gain an insight into the relative magnitude of the LBNP $Pressure$ effect compared to a gravitationally induced fluid shift. We can used these differences to produce "Earth normal" conditions in the variables of interest. As one example, we note that a 15° HDT increases cardiac output by 0.35 l/min (89% CrI: 0.26 to 0.46 l/min). In contrast, LBNP reduces CO by 0.046 l/min/mmHg (89% CrI 0.042 to 0.049 l/min/mmHg). Thus it would appear that only –6 mmHg of LBNP is required to return CO to its normal, supine value. The amount of LBNP required depends on the variable, for example for IOP, approximately –29 mmHg are required. Thus, an analysis of which variables are most important to control, combined with further understanding of the long-duration effects, will allow us to target levels of LBNP for investigation. It should be noted that there are differences between the physiological response to spaceflight and HDT. In particular, as previously discussed, HDT replicates the fluid shifts but does not remove hydrostatic gradients or alter tissue weight. Thus, countermeasure development will require validation of the resultant protocols in microgravity conditions in addition to terrestrial development.

5.4.1.2 Risk of Spaceflight Associated Neuro-ocular Syndrome (SANS)

This study is insightful into the SANS risk for two reasons. First, as discussed, we do not find any evidence for an association between body weight and intraocular pressure[50]. In particular, the correlation between weight and IOP was calculated as 0.06 (89% CrI: –0.19 to 0.29, $pd = 63.28\%$). It must be stressed that we also do not find any evidence to the contrary (i.e., no association). Thus further investigation should consider more subjects (in LBNP) to determine

the true nature of the relationship. Second, we find that OPP is not influenced by LBNP in the range measured. A head-down tilt increases OPP (as also seen in Section 4.6), but there is significant evidence for no effect of $Pressure$ to subsequently reduce it ($\%_{ROPE} = 97.06\%$). Given the potential relationship between SANS and elevated OPP that we hypothesized in Section 4.6, and the symptomatic similarities between terrestrial traumatically elevated OPP and SANS[1,60], this could perhaps be a contraindication against LBNP as a SANS countermeasure. As previously discussed, the pathoetiology of SANS is currently unknown, but it is likely the result of multiple contributing factors. Related to fluid pressures, whilst OPP may be important, there are other pressure gradients that also likely play a role, including the translaminar pressure gradient (TLPG)[1]. An important missing piece of information for determining the complete hemodynamic environment of the ocular system is a measurement of intracranial pressure (ICP). Petersen *et al.* demonstrated that LBNP can reduce ICP in a study using 10 subjects with either parenchymal ICP-sensors or Ommaya-reservoirs fitted to the frontal horn of a lateral ventricle[88]. They found that graded LBNP (in the same range as our experiment) reduced ICP from 15 ± 2 mmHg (0 mmHg LBNP) to 14 ± 4 (–10 mmHg LBNP), 12 ± 5 (–20 mmHg LBNP), 11 ± 4 (–30 mmHg LBNP), 10 ± 3 (–40 mmHg LBNP), and 9 ± 4 mmHg (–50 mmHg LBNP) ($p < 0.0001$), but that cerebral perfusion pressure ($CPP = MAP_{mid-brain} - ICP$) was unchanged. It is difficult to obtain non-invasive measurements of ICP, but there are a number of existing techniques with varying degrees of accuracy including computed tomography and magnetic resonance imaging, transcranial Doppler, electroencephalography power spectrum analysis, and audiological and ophthalmological techniques[418]. Future work should assess the totality of hemodynamic measurements in the head and eyes, including IOP, OPP, ICP, and CPP.

5.4.1.3 Concern of Venous Thromboembolism

The key finding from this study is that we have quantified the changes in IJV blood flow velocity waveform pattern as a function of applied LBNP. In Figure 5.10 we demonstrated that increasing LBNP can decrease the probability of a Grade 2 or higher flow. Grade 1 and 2 flows are normal, whilst the risk of VTE is elevated when attaining Grade 3 and Grade 4 flows[12]. Since

this was an acute study, we only observed four instances of Grade 3 Flow in three subjects (two male, one female). In contrast, Marshall-Goebel *et al.* observed Grade 3 or higher flow in 7 of 11 subjects in flight. Thus, our data mainly demonstrates the ability of LBNP to change Grade 2 flow to Grade 1 flow. In order to further understand the suitability of LBNP as a countermeasure to mitigate the concern of VTE, future work should either focus on long duration head-down tilt bed rest (HDTBR) studies or spaceflight studies, where Grade 3 or higher flow is more likely to occur.

5.4.2 Discussion of the Bayesian Workflow Methodology

An important contribution of this research effort is the novel Bayesian workflow used to construct the dose-response curves. We believe that this methodology, which moves away from more common and traditional null hypothesis significance testing (NHST), is better suited to the analysis of both ground-based and spaceflight studies of physiological response, which are often plagued by a lower subject pool. In particular, by removing the reliance on a single value, e.g., $p = 0.05$, to make binary decisions about a null hypothesis, we are able to gather evidence both in favor of, and against, the null and alternative hypotheses. Similarly, whilst many spaceflight studies may find significance, they are often constrained by difficulty in obtaining sufficient power. In a Bayesian framework power constraints are less important, and we can find evidence even with a low subject pool. Increasing the amount of evidence available reduces the width of the posteriors, increasing our confidence in the estimates, but even a small amount of data are better than no data. Finally, we believe that the Bayesian methodology provides improved understanding of the dose-response parameters. Rather than an often misunderstood interpretation of a confidence interval, the Bayesian credible interval provides us with estimates as to where the effect sizes fall within the population.

The other benefit of the Bayesian workflow is that it allows us the ability to construct more complicated models since we are no longer constrained by the assumptions of (generalized) linear mixed-effects models. In this study, we used this feature for two purposes. First, by allowing the dependent variables to follow a Student, rather than a Gaussian distribution, we developed a model hierarchy more robust to outliers in the data. Second, rather than analyzing each variable independently, we were able to construct a single, highly complex regression model in order to de-

termine the multivariate structure of the response. The resulting output, in Figure 5.11, represents a novel understanding of the relationships between the variables, derived from the experimental data. When combined with theory, this allows us to draw further insights from the data.

One common criticism of the Bayesian methodology is a reliance on seemingly arbitrary priors as part of the workflow. However, on closer inspection selection of priors is just as much a natural part of scientific experiment design as determining null hypotheses in the first place[375]. We rarely go into an experiment with no knowledge about the expected outcomes, thus prior choice is seldom fully blind. Use of prior predictive checks and a sensitivity analysis allow us to overcome this complaint. For all variables in the model, we undertook a prior-predictive check in order to determine that the priors chosen led to reasonable values when placed in the model. In particular, the Gaussian weakly informative priors ($\mathcal{N}(0,1)$ for the slopes) allow an effect size centered around zero with a wide variance that exceeded the maximum a-posteriori estimate of any individual posterior effect. Further, we augmented our workflow with a sensitivity analysis in order to determine the influence of the prior choices on the results. For this sensitivity analysis, we fit the same multivariate regression model using completely uninformative flat priors of the form $\mathcal{U}_{[-3,3]}$ (which are viable, but often cautioned against in literature[380]), and more constrained Gaussian priors of the form $\mathcal{N}(0,0.1)$, with an order of magnitude reduction on the variance. In both cases, the choice of prior did not significantly alter the overall conclusions. The smallest change occurred in the $Pressure$ effect, which contained the narrowest Credible Intervals for the posterior effect size. The largest difference occurred in the $Side$ effect, where the strong priors narrowed the posterior distributions. This is due to the low weight of evidence supporting trends in either particular direction of $Side$, where intersubject variability far outweighs any intrasubject effect. Overall, the prior predictive checks and sensitivity analysis confirmed that the choice of priors were appropriate for this study. A great feature of the Bayesian workflow is that future studies can now build on our data, using the posteriors we have derived in order to inform more constrained prior choice.

We believe that this Bayesian workflow could be applied to spaceflight studies on physiological response outside of just the cardiovascular system. In particular, it is theoretically possible to

elicit the relationship between multiple different physiological systems. For example, it would allow us to answer questions such as "what is the relationship between cardiovascular degradation and musculoskeletal remodelling during long-duration spaceflight"? Even with the low number of subjects in spaceflight studies, evidence can be built up over time by replacing priors with posteriors from previous studies.

5.4.3 Limitations

There are a number of limitations in this study, some of which are the same as in Section 4.4.3. We overcome two identified limitations in the tilt study by integrating female subjects from the outset, and capturing detail on the common carotid artery and internal jugular vein flow velocity. However, like the tilt study, (1) we still only consider the acute response to LBNP and (2) we are limited to noninvasive measurements. Regarding the acute nature of the study, Lightfoot *et al.* have found that adaptation occurs with presyncopal symptom limited LBNP (PSL-LBNP) over the course of a nine day repeated exposure[419]. The authors note an increase in RPP and maximal heart rate by days 7 and 8, but no change in the mean arterial pressure response. They made no comment about changing cardiovascular parameters at less than presyncopal strength LBNP with adaptation, but their work notes that adaptation is possible. This indicates that subjects with a low tolerance to LBNP, for example some of our female subjects, may be able to adapt to –50 mmHg LBNP. However, in multiple other studies LBNP tolerance was found to be highly repeatable in any given individual[90,356,360,420]. In studies of graded LBNP prior to presyncope, multiple studies by Convertino and Goswami have confirmed that individual cardiovascular response is highly reproducible, even with rest periods as long as one year between tests[73,90,357,359]. This reproducability also supported our decision to progress, rather than randomize, the presentation of LBNP strength to each subject. In order to determine the utility of LBNP as a spaceflight countermeasure to mitigate SANS or VTE, long term studies must be conducted either in spaceflight or in HDTBR in order to determine whether periodically unloading the cephalad fluid shift is able to prevent the manifestation of symptoms. Finally, we previously discussed the limitations of noninvasive measurement in Section 4.4.3. The same constraints apply in this study as to the accuracy of non-

invasive cardiovascular measures[126,299]. The ability to obtain invasive measures would also allow us to gain an accurate measure of ICP[88]. Future studies should attempt to obtain some measure of ICP, which may be easier with advancing technology in the area[418].

5.5 Summary of Experiment 2

We subjected 24 male and female subjects to graded LBNP to investigate the acute changes in multiple hemodynamic parameters, autonomic indices, and head/neck hemodynamics across the range 0 to –50 mmHg LBNP in both 0° supine and 15° HDT positions. Our data revealed a linear dependence on pressure for all metrics considered, with varying effect sizes of response. Based on the experimental data collected, we conducted a Bayesian multivariate analysis to construct dose-response curves for all variables across the ranges considered. These dose-response curves demonstrated anthropometrically driven sex-dependent changes in some metrics related to the systemic hemodynamics, and supported evidence from previous studies regarding different autonomic activation between men and women. We calculated the relative effect size of a HDT induced cephalad fluid shift, and the LBNP required to counteract it in each variable considered. Further, we demonstrated the potential for LBNP to reduce jugular venous flow stagnation, and provided a logistic dose-response. Finally, we calculated the relationship structures between all of the variables considered, as well as subject characteristics, finding correlation structures between many groups of variables. These findings provide data to support spaceflight countermeasure development against cardiovascular degradation, spaceflight-associated neuro-ocular syndrome (although there are potential contraindications in the lack of effect of LBNP on ocular perfusion pressure), and venous thromboembolism events.

6. COMPUTATIONAL MODELING*

6.1 Outline

To further understand the human CV response to altered gravity environments, we can use computational approaches to simulate a variety of environmental conditions and scenarios. Since Guyton's early models[171,172], a variety of modeling techniques have been used to investigate various aspects of the cardiovascular system. These techniques cover a range of functions, including investigating the effects of exercise[154], microgravity[95,169,178], head-up tilt[173–175], lower-body negative pressure[173,176,177], and postural changes[179–181]. Thus, modeling techniques allow us to expand beyond the limits imposed by human experimentation and therefore, to make predictions on the risk of orthostatic intolerance, the efficacy of countermeasures, and the variation in responses elicited by different individuals.

Section 6.2 provides a comprehensive description of the baseline model used in this study. Section 6.3 considers a sensitivity analysis on the baseline model in order to determine which parameters exert the most influence on outcomes in constant gravity studies[188]. Section 6.4 presents improvements and updates to the model in line with the Research Aims described in Section 3. Finally, Section 6.5 presents results of simulations carried out on the updated model to a) simulate the experiments described in Sections 4 and 5 and b) consider the influence of Short-Radius Centrifugation and microgravity on cardiovascular parameters.

6.2 Baseline Model

Figure 6.1 shows a schematic of the baseline cardiovascular model originally developed by Heldt[168] and subsequently modified by Zamanian[185] and Diaz-Artiles[120]. The model consists of 21 compartments: 15 compartments represent the systemic circulation, four compartments repre-

*Part of this chapter is reprinted with permission from Whittle RS, Diaz-Artiles A. Modeling individual differences in cardiovascular response to gravitational stress using a sensitivity analysis. *J Appl Physiol.* 2021;130:1983–2001.[188]

sent the cardiac chambers (which include variable capacitors representing contractions and diodes representing the mitral, tricuspid, pulmonary, and aortic non-return valves), and two compartments represent the pulmonary circulation. Parameters associated with each compartment include the anatomical vertical length (superior-to-inferior extension of the vascular segment), a resistance, and a vascular compliance, and they were estimated from the literature[168]. Three venous compartments (legs, splanchnic, and abdominal veins) are modeled with a nonlinear pressure-volume relationship. The model also incorporates the two-major reflex mechanism concerning the short-term hemodynamic regulation response: the arterial baroreflex and the cardiopulmonary reflex. These are represented as feedback loop mechanisms using set-point controllers and reference pressures.

6.2.1 Systemic and Pulmonary Compartments

The physical properties of each compartment are characterized by an inflow resistance R_n, an outflow resistance $R_{n+1)}$, a capacitive element representing the pressure-volume relationship $V_n(P_n - P_e)$, and two pressure sources: P_h represents the hydrostatic pressure associated with the compartment, whilst P_e represents the external pressure acting on the compartment. The flows assigned to the nth compartment, q_n, the $n + 1$th compartment, q_{n+1}, and the capacitive element, q_c, are defined as follows:

$$q_n = \frac{P_{n-1} - P_n + P_h)}{R_n} \tag{6.1}$$

$$q_{n+1} = \frac{P_n - P_{n+1}}{R_{n+1}} \tag{6.2}$$

$$q_c = \frac{d}{dt}V_n = \frac{dV_n}{dt}(P_n - P_e) \tag{6.3}$$

Combining the constitutive relationships for the flow in the compartment gives an expression for the rate of change of luminal pressure:

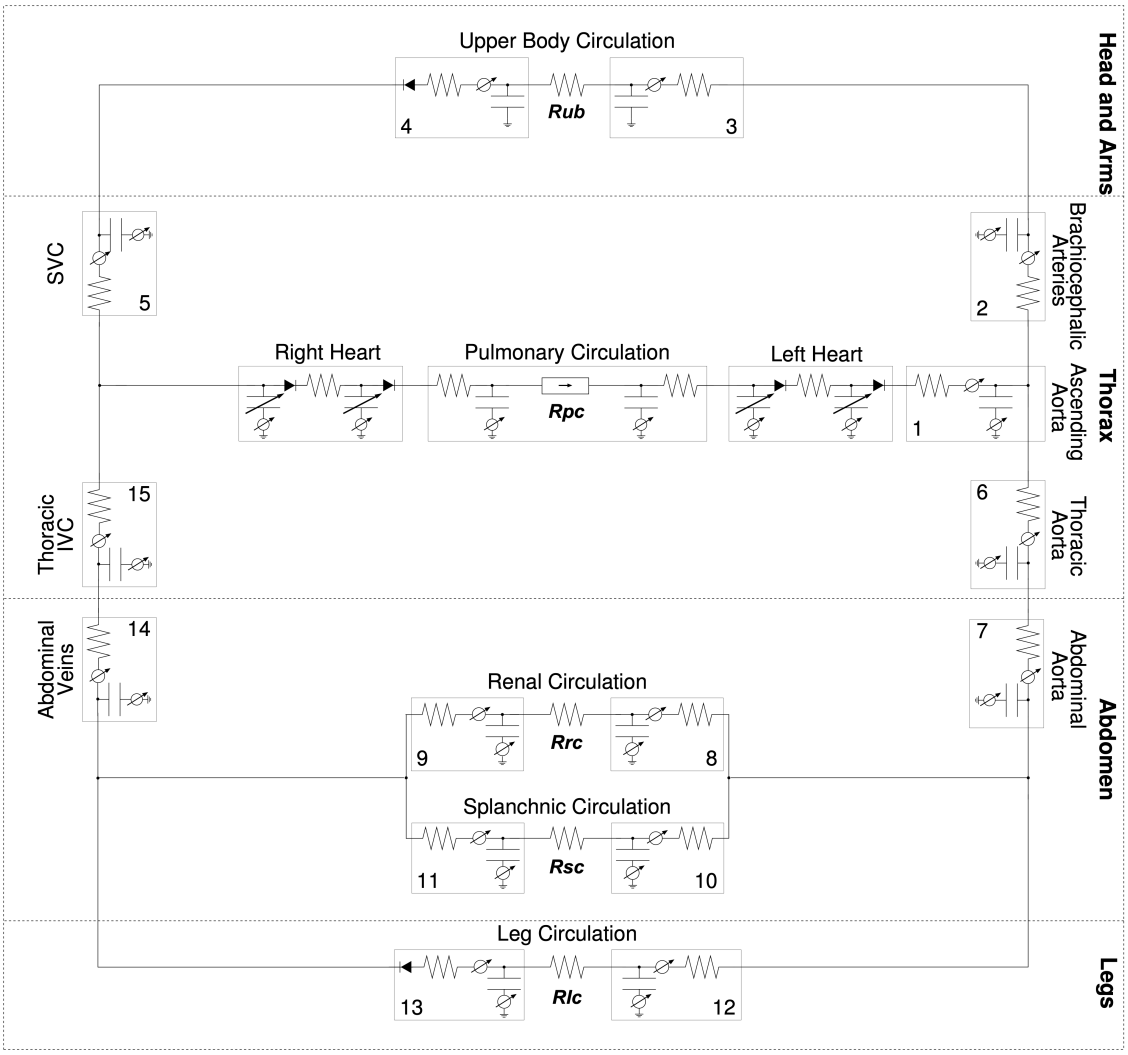

Figure 6.1: Circuit representation of the 21-compartment cardiovascular model, composed of 4 sections: head and arms, thorax, abdomen, and legs. The 15 systemic compartments are numbered as followed: 1, proximal aorta; 2, brachiocephalic arteries; 3, upper body arteries and 4, veins; 5, superior vena cava; 6, thoracic aorta; 7, abdominal aorta; 8, renal arteries and 9, veins; 10, splanchnic arteries and 11, veins; 12, leg arteries and 13, veins; 14, abdominal veins; and 15, inferior vena cava. Capillary beds are represented by four microvascular resistances: upper body R_{ub}, kidneys R_{rc}, splanchnic R_{sc}, and legs R_{lc}. Pulmonary circulation is represented by R_{pc}. Reproduced from Whittle and Diaz-Artiles[188].

$$q_n = q_c + q_{n+1} \tag{6.4}$$

$$\frac{d}{dt}P_n = \frac{P_{n-1} - P_n + P_h}{C_n R_n} - \frac{P_n - P_{n+1}}{C_n R_{n+1}} + \frac{d}{dt}P_e \tag{6.5}$$

with $C_n = dV_n/d(P_n - P_e)$ representing the incremental vascular compliance (capacitance). The entire system is thus defined by a set of coupled first-order differential equations with pressure as the principal variable of interest. These equations are solved iteratively by a 4th Order Runge-Kutta algorithm. In three of the venous compartments (11 – splanchnic, 13 – legs, and 14 – abdominal) a non-linear pressure volume relationship is implemented as follows[168,173]:

$$V_{t,n} = V_{0,n} + \frac{2V_{max,n}}{\pi} \cdot \arctan\left(\frac{\pi C_{0,n}}{2V_{max,n}} \cdot \Delta P_n\right) \text{ for } \Delta P > 0,\ n = 11, 13, 14 \tag{6.6}$$

where $V_{t,n}$ denotes the total volume in compartment n, $V_{0,n}$ denotes the zero-pressure filling volume, $V_{max,n}$ denotes the distending volume limit (1500 ml, 1000 ml, and 650 ml for compartments 11, 13, and 14 respectively), $C_{0,n}$ denotes the vascular compliance at zero transmural pressure, and ΔP_n denotes the transmural pressure. Total blood volume is the sum of the volumes in all compartments and is modified to account for transcapillary flow[173,185,421]. The pulmonary circulation is represented by two compartments (pulmonary arteries and veins, respectively) and a resistor representing the pulmonary capillaries.

Note that the compartments neglect all inertial effects. This was a computational choice since the model was primarily designed to analyze cycle-to-cycle changes in blood flow and pressure. In our case we are primarily concerned with steady state outcomes and the contribution of inertial effects to pressure and flow is highest within a heartbeat rather than on a beat-to-beat scale. Defares *et al.* estimate that less than 1% of stroke volume and mean arterial pressure are due to inertial effects[422] such that their inclusion would serve only as cosmetic refinement of the arterial waveform, which we are not concerned with in this proposed study.

6.2.2 Microvascular Resistances

Capillary flow is modeled by four resistors representing flow in the upper body, renal, splanchnic, and lower body circulations, respectively. As such, the capillary flows are modeled as non-distending volumes with no associated compliance.

6.2.3 Cardiac Chambers

Each of the four cardiac chambers is simulated using a time-varying elastance model[173,421]. The elastance $E(t)$ is defined by a piecewise function of the diastolic and end-systolic elastances (E_d and E_es respectively) such that the time of diastolic relaxation is half of the systolic time interval T_s:

$$E(t) = \begin{cases} E_d + \frac{E_{es}-E_d}{2} \cdot \left(1 - \cos\left(\pi \frac{t}{T_s}\right)\right) & 0 \leq t \leq T_s \\ E_d + \frac{E_{es}-E_d}{2} \cdot \left(1 + \cos\left(2\pi \frac{t}{T_s}\right)\right) & T_s < t \leq \frac{3}{2}T_s \\ E_d & \frac{3}{2}T_s < t \end{cases} \tag{6.7}$$

Relative timing between the chambers is characterized by the atrial and ventricular systole durations (T_s^a and T_s^v), and the PR interval represents the delay between the onset of atrial and ventricular depolarizations[173,421], T_{a-v}. These are all assumed to be proportional to the square root of the RR interval with:

$$T_s^a = 0.2\sqrt{T_{RR}} \tag{6.8}$$

$$T_s^v = 0.3\sqrt{T_{RR}} \tag{6.9}$$

$$T_{a-v} = 0.12\sqrt{T_{RR}} \tag{6.10}$$

The cardiac pacemaker is represented by an Integral Pulse Frequency Modulation (IPFM)

model[173,185,421,423]:

$$M(t) = \int_{t_{k-1}}^{t} m(t)\,dt = \int_{t_{k-1}}^{t} m_0 + m_r(t)\,dt \tag{6.11}$$

where $M(t)$ represents the behavior of the sinoatrial node transmembrane potential as a function of a constant cumulative automaticity, m_0, and the combination of neural control input from either sympathetic or parasympathetic activity since the end of the last heartbeat, $m_r(t)$. A new heartbeat occurs at time t_k when both $M(t)$ reaches a predefined threshold potential, $\Gamma = 1$, and the time since the previous heartbeat is at least one fifth of the preceding cycle length:

$$\{M(t_k) \geq \Gamma\} \text{ and } \{t_k - t_{k-1} \geq 0.2(t_{k-1} - t_{k-2})\} \tag{6.12}$$

After this time, $M(t)$ is reset and the integration process repeats. We define $m(t)$ as the inverse of the instantaneous RR interval, $I(t)$, which is the sum of the nominal RR interval, I_0 (the inverse of I_0 is the nominal heart rate), and the control input from the arterial baroreflex control system, $\Delta I_{AB}(t)$:

$$m(t) = \frac{1}{I(t)} = \frac{1}{(I_0 + \Delta I_{AB}(t)}(13) \tag{6.13}$$

Figure 6.2 shows the beat-to-beat response of the blood pressure waveform during a four-beat simulation cycle. This figure shows the pressure waveform in the descending aorta, the left ventricle, and the left atrium over a period of four heartbeats.

6.2.4 Control Systems

Two control systems, the arterial baroreflex and cardiopulmonary reflex are modeled using negative feedback loops. The feedback error signals are described by:

$$\delta P_{AB}[n] = 18 \cdot \arctan\left(\frac{\frac{1}{2}\left(\Delta P_{AA} + \Delta P_{CS}\right) - P_A^{sp}}{18}\right) \tag{6.14}$$

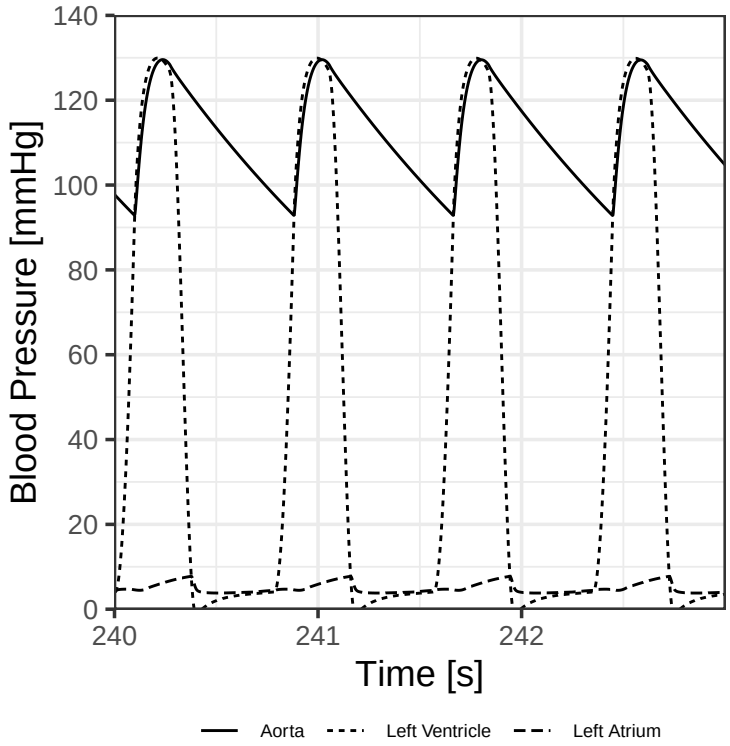

Figure 6.2: Pressure waveform of the descending aorta (solid), left ventricle (short dashes), and left atrium (long dashes) over a four-beat simulation cycle. Reproduced from Whittle and Diaz-Artiles[188].

$$\delta P_{CP}[n] = 5 \cdot \arctan\left(\frac{\Delta P_{CS} P_{RA} - P_{CP}^{sp}}{5}\right) \tag{6.15}$$

where $\delta P_{AB}[n]$ and $\delta P_{CP}[n]$ represent the error signals to the arterial baroreflex and cardiopulmonary reflex loops respectively; P_A^{sp} and P_{CP}^{sp} are the respective pressure set-points; ΔP_{CS} is the carotid sinus pressure defined as located 25 cm superior to the heart; ΔP_{AA} is the aortic arch pressure; and ΔP_{RA} is the transmural pressure in the right atrium. The transfer functions $\Delta X[n]$ for the sympathetic and parasympathetic arcs are modeled as static gains G_X^s and G_X^p multiplied by impulse response functions $s[n]$ and $p[n]$ with associated delays, peaks, and ends:

$$\Delta X_{Y-AB}[n] = \left(G_Y^{A,S} s[n] + G_Y^{A,P} p[n]\right) * \delta P_{AB}[n] \tag{6.16}$$

$$\Delta X_{Y-CP}[n] = \left(G_Y^{CP,S} s[n] + G_Y^{CP,P} p[n]\right) * \delta P_{CP}[n] \tag{6.17}$$

where in the transfer functions superscript A refers to the arterial baroreflex, superscript CP refers to the cardiopulmonary reflex, superscript S refers to the sympathetic arc, superscript P refers to the parasympathetic arc, and subscript Y refers to the effector. The model includes separate impulse responses to represent the parasympathetic, β-sympathetic, and α-sympathetic response for each reflex, and static gains (subscript Y) associated with loops to each effector separately. The effectors for the arterial baroreflex are RR interval (sympathetic and parasympathetic), left and right ventricular contractility (sympathetic only), systemic microvascular resistances (sympathetic only), and venous unstressed volume (sympathetic only). The effectors for the cardiopulmonary reflex are systemic microvascular resistances and venous unstressed volume (both sympathetic only).

6.2.5 Transcapillary Flow and the Interstitial Fluid Volume

Orthostatic stress causes an increase in transcapillary flow to the dependent vasculature leading to a decrease in intravascular volume[173,185,421]. In the model this is represented using additional RC compartments. The transcapillary flow is computed analytically and subtracted from the venous return in the splanchnic, leg, and abdominal venous compartments (compartments 11, 13, and 14). The total intercapillary flow $q(t)$ and interstitial volume change $V(t)$ is characterized by two parameters: the time constant $\tau = RC = 4.6$ min[173,421] and the maximum interstitial volume change V_{max}.

6.2.6 Modeling Orthostatic Stress

The effects of gravitational stress are particularly important in this modeling effort. These are represented using three mechanisms: 1) changes in hydrostatic pressure, a term included in all systemic compartments; 2) changes in intrathoracic pressure due to the weight of the liver being pulled down in the thoracic compartment[185,424,425]; and 3) changes in total blood volume due to the increase in transcapillary fluid flow from the intravascular volume into the dependent

vasculature[154,426].

6.2.6.1 Tilt

Gravitational stress expressions for simulating tilt are summarized in Table 6.1. For each compartment, we define an "effective" vertical length, h_n, equivalent to half of the anatomical length. In the leg compartments (12 and 13) the effective length is assumed to be one third of the anatomical length.

Table 6.1: Mathematical expressions used to simulate gravitational stress via tilt with tilt angle θ.

Gravitational Effect	**Expression**
Hydrostatic pressure (mmHg)	$P_{h,n} = \rho g_c h_n \sin(\theta)$
Intrathoracic pressure (mmHg)	$P_{th} = P_{th_0} - 3.5\frac{g_c}{g_E}\sin(\theta)$
Max. blood lost from intravascular vol. (ml)	$V_{max} = \frac{700}{\sin(85°)}\frac{g_c}{g_E}\sin(\theta)$

Notes:
$P_{h,n}$, hydrostatic pressure in compartment n; ρ, density of blood (7.95 mmHg.s^2/m^2); g_c, gravitational acceleration in constant gravity field; h_n, effective length of compartment n (defined as half of the anatomical length, except of the leg compartments where the effective length is assumed to be one third of the anatomical length); θ, tilt angle from supine; P_{th}, intrathoracic pressure; P_{th_0}, nominal intrathoracic pressure (–4 mmHg); g_E, gravitational acceleration on Earth (9.81 m/s^2); V_{max}, maximal blood volume lost from intravascular volume into the interstitial space.

6.2.6.2 LBNP

Lower body negative pressure is modeled using two separate mechanisms: 1) an external pressure on the leg compartments (compartments 12 and 13) and 2) changes in total blood volume due to blood pooling in the lower body[73,168]. Expressions for simulating LBNP are summarized in Table 6.2.

6.2.6.3 Short-Radius Centrifugation

Gravitational stress expressions for simulating short-radius centrifugation are summarized in Table 6.3.

Table 6.2: Mathematical expressions used to simulate gravitational stress via LBNP with pressure p_{LBNP}.

Gravitational Effect	**Expression**
External pressure (mmHg)	$P_{e,n} = p_{LBNP} \ \forall\, n \in [12, 13]$
Max. blood lost from intravascular vol. (ml)	$V_{max} = \frac{982\,\text{ml}}{70} p_{LBNP}$

Notes:
$P_{e,n}$, external pressure on compartment n; p_{LBNP}, lower body negative pressure; V_{max}, maximal blood volume lost from intravascular volume into the interstitial space.

Table 6.3: Mathematical expressions used to simulate gravitational stress via short-radius centrifugation with angular speed ω.

Gravitational Effect	**Expression**
Hydrostatic pressure (mmHg)	$P_{h,n} = \frac{1}{2}\rho\left(\left(d + \frac{r_{o,n}-r_{i,n}}{2^*}\right)^2 - \left(d + r_{i,n}\right)^2\right)\omega^2$
Intrathoracic pressure (mmHg)	$P_{th} = P_{th_0} - 3.5\frac{\left(d+r_{i_{10}}\right)\omega^2}{g_E}$
Max. blood lost from intravascular vol. (ml)	$V_{max} = \frac{700}{\sin(85^\circ)}\frac{\left(d+r_{i_{10}}\right)\omega^2}{g_E}$

Notes:
$P_{h,n}$, hydrostatic pressure in compartment n; ρ, density of blood (7.95 mmHg.s^2/m^2); d, distance of top of head from center of rotation; $r_{o,n}$, outer radius of compartment n; $r_{i,n}$, inner radius of compartment n; ω, angular speed; P_{th}, intrathoracic pressure; P_{th_0}, nominal intrathoracic pressure (–4 mmHg); $r_{i_{10}}$, inner radius of the liver (splanchnic arteries); g_E, gravitational acceleration on Earth (9.81 m/s^2); V_{max}, maximal blood volume lost from intravascular volume into the interstitial space. *For the majority of compartments, the effective length is assumed to be one half of the anatomical length. For the leg compartments (12 and 13), the effective length is assumed to be one third of the anatomical length.

6.2.6.4 Gravitational Fields

In the baseline model, we are also able to simulate altered gravity fields by changing the value of g_c in Table 6.1. As can be seen from the equations is Table 6.1, in the baseline model altering g_c is mathematically identical to changing the tilt angle. Thus, in the baseline version of the model, there is no physiological difference between HDT and a reduction in gravity. Our model demonstrates an acute increase in central venous pressure with increasing HDT and similarly with reducing gravity. This is in agreement with terrestrial studies in which an acute increase in gravity in the head-to-toe

direction through tilt causes a decrease in central venous pressure[427,428]. However, these trends contrast with spaceflight and parabolic flight evidence[3,22,206,429]. Buckey *et al.* suggest that this unexpected decrease in central venous pressure occurs as a result of the loss of tissue compressive forces produced by tissue weight[61,430]. The baseline model does not capture changes in tissue weight, and therefore, any simulations on reduced gravity could also be interpreted as a partial tilt on Earth (including supine position representing 0g, and upright position representing 1g). This differentiation will be addressed in Section 6.4.

6.3 Sensitivity Analysis

One of the challenges of computational approaches is linking the models with experimental data. This includes both the process of assigning values to simulated physiological parameters, and also the validation of the model[431]. Often, fitting experimental data requires a significant degree of processing, estimating values from related physiological measurements, or scaling from non-human studies[173]. When using a model to predict individual responses, rather than general trends, this challenge is compounded by the necessity to know the specific measurements for that specific individual. Thus, the following section describes an initial sensitivity analysis that was carried out on the baseline model in order to determine the most influential parameters.

6.3.1 Motivation

Complex systemic models can have hundreds of parameters[154,173], and it would be too resource-intensive, and in many cases impossible, to determine every single parameter for an individual. However, we can overcome this limitation by performing sensitivity analyses[432]. Thus, once an appropriate and reasonable range of variation for all parameters has been determined, sensitivity analysis techniques identify the most important parameters that dominate the physiological response in the specific context being modeled, i.e., parameters that we need to determine accurately for the individual in order to get accurate results (as opposed to parameters where using a population mean will not adversely affect the predictive power of the model).

We conducted a comprehensive Latin Hypercube Sampling/Partial Rank Correlation Coef-

ficient (LHS/PRCC) sensitivity analysis on the baseline 21-compartment lumped-parameter CV model[120,153,154,168,173,185] to determine the sensitivity of various physiological model parameters to variation within their normal non-pathological range. Simulations capture short-term cardiovascular responses of healthy subjects during an acute (600 seconds) tilt test (from supine to upright posture) at various constant gravitational conditions. Similar to Monte Carlo analysis, the proposed technique involves a large number of simulations in which model parameters are selected randomly (within the appropriate constraints). Therefore, each one of the simulations include a different combination of parameters, thus representing a different individual subject. Moreover, we used a range of gravitational conditions (from 0g to 1g, in 0.25g increments) to further determine whether the most relevant physiological features differ with the strength of the gravitational field.

6.3.2 Methods

6.3.2.1 Parameter Groups

The cardiovascular system and thus, our model have a small number of global key parameters which, based on previous simulations[168] and a preliminary analysis, cause larger variation in the outcome measures than the rest of the parameters. Examples of these are total blood volume or resting arterial pressure set-point. It was assumed that any future model simulations to determine individual differences between individuals would necessarily involve the accurate measurement or determination of these parameters using allometric scaling laws[433–435] and data given from reference sources such as Leggett and Williams[436]. As such, they were not included in the detailed LHS/PRCC sensitivity analysis presented herein, which aimed to determine the most important of the remaining limited (i.e., non-global) parameters. A discussion of these global parameters is given in Section 6.3.4.4. In all our simulations presented in the rest of this paper, the subject was modeled with a height of 169.3 cm, a weight of 70 kg, a total blood volume of 5625 ml[173,437,438], a nominal heart rate of 70 bpm, a resting arterial set point of 91 mmHg, and a resting cardiopulmonary reflex set point of 8 mmHg.

We divided the cardiovascular parameters of interest into three groups: compartments (includes parameters related to the systemic circulation: resistances, compliances, and anatomical lengths), controls (includes parameters related to the baroreceptors and the cardiopulmonary reflex: gains for resistances, volumes, and ventricular contractility), and heart and lungs (includes parameters related to the cardiac and pulmonary systems: resistances and compliances).

Table 6.4 shows the 45 parameters of the compartments group, comprising 15 resistances, 15 compliances, and 15 anatomical lengths. Anatomical length was defined as the vertical distance from the superior to the inferior end of the vascular segment. The control parameters, shown in Table 6.5, corresponded to the gains of the control system feedback signals in the baroreflex and cardiopulmonary reflex. Finally, Table 6.6 shows the heart and lungs group parameters. These were the compliances and resistances corresponding to the pulmonary arteries and veins, and the compliances and resistances corresponding to the four cardiac chambers.

As the exact distributions of many physiological parameters are relatively unknown, we assumed that they are represented by truncated Gaussian distributions (i.e., they follow a standard normal distribution where the two ends are modified to include lower and upper bounds. Thus, values outside the defined range are not included in the simulations)[432,439,440]. The ranges were chosen based on extensive literature reviews[168] to capture the total variation in a normal, non-pathological population. The LHS was set up to capture 90% of this population (i.e., mean ± 1.64 standard deviations).

6.3.2.2 Simulation Profile and Gravity Levels Investigated

We simulated cardiovascular responses when subjected to a constant gravitational field. During simulations the subject model was initially in a supine position during 60 s before being tilted to an upright position. Five levels of constant gravity were used: 0g, 0.25g, 0.5g, 0.75g, and 1g. Since we are concerned with steady state outcomes, the simulations were run until all transients had vanished and the model had reached stability. In all cases this occurred within 300 s of tilt). All outcomes were averaged across the final 60 seconds of the simulation, with stability assured by comparing means and variances with the preceding 240 seconds (giving a total 660 s run time

Table 6.4: Compartment parameters and their associated values (range for the sensitivity analysis: mean ± 1.64 standard deviations). Values taken from Heldt *et al.* and Diaz-Artiles *et al.* [154,173].

Parameter	**Symbol**	**Mean**	**SD**
Anatomical length 1 (Ascending Aorta)	l_{v1} [*cm*]	10.0	0.5
Anatomical length 2 (Brachiocephalic Arteries)	l_{v2} [*cm*]	4.5	0.5
Anatomical length 3 (Upper Body Arteries)	l_{v3} [*cm*]	20.0	1.0
Anatomical length 4 (Upper Body Veins)	l_{v4} [*cm*]	20.0	1.0
Anatomical length 5 (Superior Vena Cava)	l_{v5} [*cm*]	14.5	0.5
Anatomical length 6 (Thoracic Aorta)	l_{v6} [*cm*]	16.0	0.8
Anatomical length 7 (Abdominal Aorta)	l_{v7} [*cm*]	14.5	0.5
Anatomical length 8 (Renal Arteries)	l_{v8} [*cm*]	0.0	0.0
Anatomical length 9 (Renal Veins)	l_{v9} [*cm*]	0.0	0.0
Anatomical length 10 (Splanchnic Arteries)	l_{v10} [*cm*]	5.0	0.5
Anatomical length 11 (Splanchnic Veins)	l_{v11} [*cm*]	5.0	0.5
Anatomical length 12 (Leg Arteries)	l_{v12} [*cm*]	106.0	6.0
Anatomical length 13 (Leg Veins)	l_{v13} [*cm*]	106.0	6.0
Anatomical length 14 (Abdominal Veins)	l_{v14} [*cm*]	14.5	1.5
Anatomical length 15 (Thoracic IVC)	l_{v15} [*cm*]	6.0	0.5
Compliance 1 (Ascending Aorta)	C_1 [*ml/mmHg*]	0.28	0.04
Compliance 2 (Brachiocephalic Arteries)	C_2 [*ml/mmHg*]	0.13	0.02
Compliance 3 (Upper Body Arteries)	C_3 [*ml/mmHg*]	0.20	0.10
Compliance 4 (Upper Body Veins)	C_4 [*ml/mmHg*]	7.00	2.00
Compliance 5 (Superior Vena Cava)	C_5 [*ml/mmHg*]	1.30	0.10
Compliance 6 (Thoracic Aorta)	C_6 [*ml/mmHg*]	0.10	0.03
Compliance 7 (Abdominal Aorta)	C_7 [*ml/mmHg*]	0.10	0.01
Compliance 8 (Renal Arteries)	C_8 [*ml/mmHg*]	0.21	0.05
Compliance 9 (Renal Veins)	C_9 [*ml/mmHg*]	5.00	1.00
Compliance 10 (Splanchnic Arteries)	C_{10} [*ml/mmHg*]	0.20	0.10
Compliance 11 (Splanchnic Veins)	C_{11} [*ml/mmHg*]	60.00	7.50
Compliance 12 (Leg Arteries)	C_{12} [*ml/mmHg*]	0.20	0.10
Compliance 13 (Leg Veins)	C_{13} [*ml/mmHg*]	20.00	3.00
Compliance 14 (Abdominal Veins)	C_{14} [*ml/mmHg*]	1.30	0.10
Compliance 15 (Thoracic IVC)	C_{15} [*ml/mmHg*]	0.50	0.10
Resistance 1 (Ascending Aorta)	R_1 [*ml/mmHg*]	0.007	0.002
Resistance 2 (Brachiocephalic Arteries)	R_2 [*ml/mmHg*]	0.003	0.001
Resistance 3 (Upper Body Arteries)	R_3 [*ml/mmHg*]	0.014	0.004
Resistance 4 (Upper Body Veins)	R_4 [*ml/mmHg*]	0.110	0.050
Resistance 5 (Superior Vena Cava)	R_5 [*ml/mmHg*]	0.028	0.014
Resistance 6 (Thoracic Aorta)	R_6 [*ml/mmHg*]	0.011	0.002
Resistance 7 (Abdominal Aorta)	R_7 [*ml/mmHg*]	0.010	0.003
Resistance 8 (Renal Arteries)	R_8 [*ml/mmHg*]	0.100	0.050
Resistance 9 (Renal Veins)	R_9 [*ml/mmHg*]	0.110	0.050
Resistance 10 (Splanchnic Arteries)	R_{10} [*ml/mmHg*]	0.070	0.040
Resistance 11 (Splanchnic Veins)	R_{11} [*ml/mmHg*]	0.070	0.040
Resistance 12 (Leg Arteries)	R_{12} [*ml/mmHg*]	0.090	0.050
Resistance 13 (Leg Veins)	R_{13} [*ml/mmHg*]	0.100	0.050
Resistance 14 (Abdominal Veins)	R_{14} [*ml/mmHg*]	0.019	0.007
Resistance 15 (Thoracic IVC)	R_{15} [*ml/mmHg*]	0.008	0.003

for each simulation). In each of the three groups (compartments, controls, and heart and lungs) and at each of the five gravitational conditions, we conducted a separate sensitivity analysis using

Table 6.5: Control parameters and their associated values (range for the sensitivity analysis: mean ± 1.64 standard deviations). Values taken from Heldt *et al.* and Diaz-Artiles *et al.* [154,173].

Parameter	**Symbol**	**Mean**	**SD**
ABR R-R interval sympathetic gain	$G^{A,S}_{R-R}$	0.012	0.004
ABR left ventricular contractility gain	$G^{A,S}_{Clv}$	0.014	0.001
ABR right ventricular contractility gain	$G^{A,S}_{Crv}$	0.021	0.003
ABR upper body arterial resistance gain	$G^{A,S}_{Rub}$	–0.13	0.05
ABR renal circulation arterial resistance gain	$G^{A,S}_{Rrc}$	–0.13	0.05
ABR splanchnic circulation arterial resistance gain	$G^{A,S}_{Rsc}$	–0.13	0.05
ABR leg circulation arterial resistance gain	$G^{A,S}_{Rlc}$	–0.13	0.05
ABR upper body venous unstressed volume gain	$G^{A,S}_{Vub}$	5.30	0.85
ABR renal venous unstressed volume gain	$G^{A,S}_{Vrc}$	1.30	0.20
ABR splanchnic venous unstressed volume gain	$G^{A,S}_{Vsc}$	13.30	2.10
ABR leg venous unstressed volume gain	$G^{A,S}_{Vlc}$	6.70	1.10
ABR R-R interval parasympathetic gain	$G^{A,P}_{R-R}$	0.009	0.004
CPR upper body arterial resistance gain	G^{CP}_{Rub}	–0.30	0.05
CPR renal circulation arterial resistance gain	G^{CP}_{Rrc}	–0.30	0.05
CPR splanchnic circulation arterial resistance gain	G^{CP}_{Rsc}	–0.30	0.05
CPR leg circulation arterial resistance gain	G^{CP}_{Rlc}	–0.30	0.05
CPR upper body venous unstressed volume gain	G^{CP}_{Vub}	13.5	2.7
CPR renal venous unstressed volume gain	G^{CP}_{Vrc}	2.7	0.5
CPR splanchnic venous unstressed volume gain	G^{CP}_{Vsc}	64.0	12.8
CPR leg venous unstressed volume gain	G^{CP}_{Vlc}	30.0	6.0

LHS/PRCC techniques. When analyzing one of the groups, the other two were held constant, generating 15 independent sensitivity analysis datasets. Figure 6.3 shows examples of our tilt test simulations, including blood pressure (at 1g), and heart rate (at multiple g levels: 0g, 0.25g, 0.5g, 0.75g, and 1g).

6.3.2.3 Outcome Measures

The primary outcome measures considered were the following CV variables: heart rate, stroke volume, central venous pressure, mean arterial pressure, systolic blood pressure, and diastolic blood pressure. We further considered two secondary outcome measures calculated from the primary measures: cardiac output and pulse pressure.

Table 6.6: Heart and lungs parameters and their associated values (range for the sensitivity analysis: mean ± 1.64 standard deviations). Values taken from Heldt *et al.* and Diaz-Artiles *et al.* [154,173].

Parameter	**Symbol**	**Mean**	**SD**
Pulmonary arterial compliance	C_{pa} [*ml/mmHg*]	3.4	1.8
Pulmonary venous compliance	C_{pv} [*ml/mmHg*]	9.0	3.7
Right ventricular outflow resistance	R_{pa} [*PRU*]	0.006	0.003
Pulmonary venous outflow resistance	R_{pv} [*PRU*]	0.006	0.003
Pulmonary microvascular resistance	R_{pc} [*PRU*]	0.070	0.040
Right atrial end-systolic compliance	$C_{es,ra}$ [*ml/mmHg*]	1.35	0.18
Right ventricular end-systolic compliance	$C_{es,rv}$ [*ml/mmHg*]	1.30	0.47
Left atrial end-systolic compliance	$C_{es,la}$ [*ml/mmHg*]	1.64	0.19
Left ventricular end-systolic compliance	$C_{es,lv}$ [*ml/mmHg*]	0.40	0.10
Right atrial diastolic compliance	$C_{d,ra}$ [*ml/mmHg*]	3.33	0.56
Right ventricular diastolic compliance	$C_{d,rv}$ [*ml/mmHg*]	19.29	5.00
Left atrial diastolic compliance	$C_{d,la}$ [*ml/mmHg*]	2.00	0.40
Left ventricular diastolic compliance	$C_{d,lv}$ [*ml/mmHg*]	9.69	1.18
Tricuspid valve resistance	R_{tri} [*PRU*]	0.006	0.003
Mitral valve resistance	R_{mit} [*PRU*]	0.010	0.001

6.3.2.4 Latin Hypercube Sampling / Partial Rank Correlation Coefficient (LHS/PRCC)

We adopted a Latin Hypercube Sampling / Partial Rank Correlation Coefficient (LHS/PRCC) approach to examine the effects of varying model parameters on the outputs listed above (i.e., heart rate, stroke volume, central venous pressure, mean arterial pressure, systolic blood pressure, and diastolic blood pressure). This method is a combination of an ordered sampling method (i.e., Latin Hypercube Sampling)[441] followed by a correlation method (Partial Rank Correlation Coefficient)[442,443], both of which are briefly described below.

Latin Hypercube Sampling (LHS) – LHS was introduced by McKay *et al.*[444] and developed by Conover[445], and was initially created to characterize the uncertainty in inputs to computer models[439]. It is a stratified Monte Carlo sampling scheme to achieve maximal coverage of an input space. The "stratified sampling" scheme divides the distribution of a random variable X_j into n non-overlapping intervals of equal-probability. Then, a random sample is selected from each of the n intervals. This is repeated for each of k variables of interest[440,441,446–448]. This method has

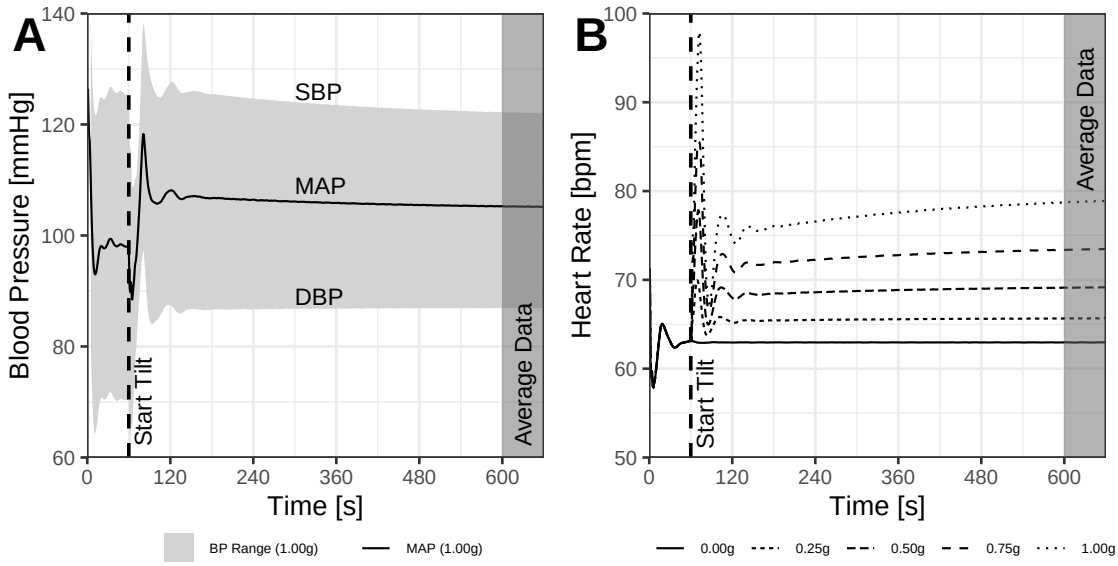

Figure 6.3: Examples of model outcome responses during the tilt test simulations. A) Blood pressure evolution over time for a single simulation run at 1g. The grey ribbon shows the blood pressure range (with systolic, mean, and diastolic blood pressures labeled). The tilt maneuver from 0° to 90° occurs at 60 s (dashed line), and model outcomes were averaged during the final 60 s of the simulation (shaded area starting at 600 s). B) Heart rate evolution over time for five simulations at the five levels of constant gravity used (0g, 0.25g, 0.5g, 0.75g, and 1g).

two main advantages: first, it ensures that samples are taken from the entire distribution, with more samples taken from closer to the probability peak of the distribution; and second, it is more computationally efficient than Monte Carlo methods, while ensuring that every interval in the $n \times k$ space is included in the experiment.

The LHS method ensured that we sampled over the entire distribution of each parameter. However, it is important to generate a sufficient number of intervals, since too few divisions could lead to an erroneous representation of the parameter space. According to Khan *et al.*[439], the recommended number of divisions when the number of variables is large falls between $4N/3$ and $5N$ for N total parameters. Our three groups (compartments, controls, and heart and lungs) had 45, 20, and 15 parameters, respectively. To be consistent, we took the same number of divisions, 100, for each of the three groups. This number of divisions lies on Khan's range for the compartments and controls groups[439], but is higher for the heart and lungs group, leading to a longer computational time but ensuring a large enough sampling size.

Furthermore, within each group and gravity condition, the entire LHS method described above was applied three times, resulting in 300 simulations per group and per gravity condition. Thus, the total experiment space was given by:

$$\textit{100 simulations} \times \textit{3 trials} \times \textit{3 variable groups} \times \textit{5 gravity conditions}$$

resulting in a total of 4,500 runs of the model. Each run of the model could be considered as representing a separate subject with a unique combination of individual physiological parameters (all within a normal physiological range).

Partial Rank Correlation Coefficient (PRCC) – PRCC is a non-linear correlation method used to interpret the association between a parameter and an outcome measure after removing the effects of all other parameters on that outcome[432]. This method allows quantification of the relationship between each pairing of a parameter and an outcome measure by a rank correlation coefficient between –1 (perfect inverse relationship) and +1 (perfect direct relationship), with 0 indicating no relationship[442,449–451]. Since this is a rank methodology, the linearity of the relationship is not determined or quantified.

6.3.2.5 Data Analysis

Cumulative Influence Factor – Every parameter was related to each of the six primary outcome measures by a PRCC coefficient, generating six PRCCs for each parameter, at each gravity condition. After those coefficients were calculated, they were normalized to obtain, for every parameter, a single value (the Cumulative Influence Factor) that quantifies its overall influence on the outcome measures. Thus, the "Cumulative Influence Factor" is calculated as follows:

$$CIF_j = \sum_{l=1}^{5} \frac{\sum_{k=1}^{6} |r_{jkl}|}{6 \times 5} \tag{6.18}$$

where $|r_{jkl}|$ is the absolute value of the PRCC between parameter j and outcome measure k at gravity level l, which is then averaged across all six outcome measures and all five gravity levels to calculate CIF_j. Each CIF had a value between 0 and 1, where 0 indicates no influence of the parameter on the outcome measures, and 1 indicates a very strong influence. For the compartments

group, we further grouped and normalized the influence of the three parameter types (resistance, compliance, and anatomical length) that represent a systemic compartment, giving a single numerical value representing the overall influence of each compartment on the outcome measures[440].

Cumulative Distribution Function and Coefficient of Variation – To quantitatively compare the variation of the outcome measures as a function of the gravity condition, and to compare between groups of parameters (i.e., compartments vs. controls vs. heart and lungs), we generated cumulative distribution functions (CDFs) for each of the three groups of parameters at each of the five gravity conditions[440,452,453]. To quantify these differences, we used the coefficient of variation (COV) to describe the spread of each CDF. Coefficient of variation is defined by:

$$COV_{k,lm} = \frac{\sigma_{k,lm}}{\mu_{k,lm}} \tag{6.19}$$

where $\sigma_{k,lm}$ and $\mu_{k,lm}$ represent the standard deviation and mean, respectively, of the outcome measure k, from group m (compartments, controls, or heart and lungs) at gravity level l. We further calculated the CDF and COV of the two secondary outcome measures (cardiac output and pulse pressure).

6.3.3 Results

Figure 6.4 shows the CIF of the compartments (A), controls (B), and heart and lungs (C) groups.

Figure 6.4 shows that within the compartments group, most influence comes from varying parameters in the splanchnic (Spl), lower body (LB), and abdominal (Abd) veins (Ve). Within each compartment, in the majority of cases the compliance is the dominant parameter, although towards the end of the venous segment (i.e., the abdominal vein and inferior and superior venae cavae) the resistance exerts the most influence. Within the controls group, the arterial baroreflex sympathetic arc resistance gains to the lower systemic circulation ($G^{A,S}_{Rrc}$, $G^{A,S}_{Rsc}$, $G^{A,S}_{Rlc}$), along with the cardiopulmonary reflex volume gains to the splanchnic ($G_{V\,sc^C P}$) and lower body (G^{CP}_{Vlc}) circulations, show the largest CIF. Both arcs of the arterial baroreflex (sympathetic and parasympathetic) related to R-R interval ($G^{A,S}_{R-R}$, $G^{A,P}_{R-R}$), also have a high (> 0.6) CIF. Finally, within the heart and lungs

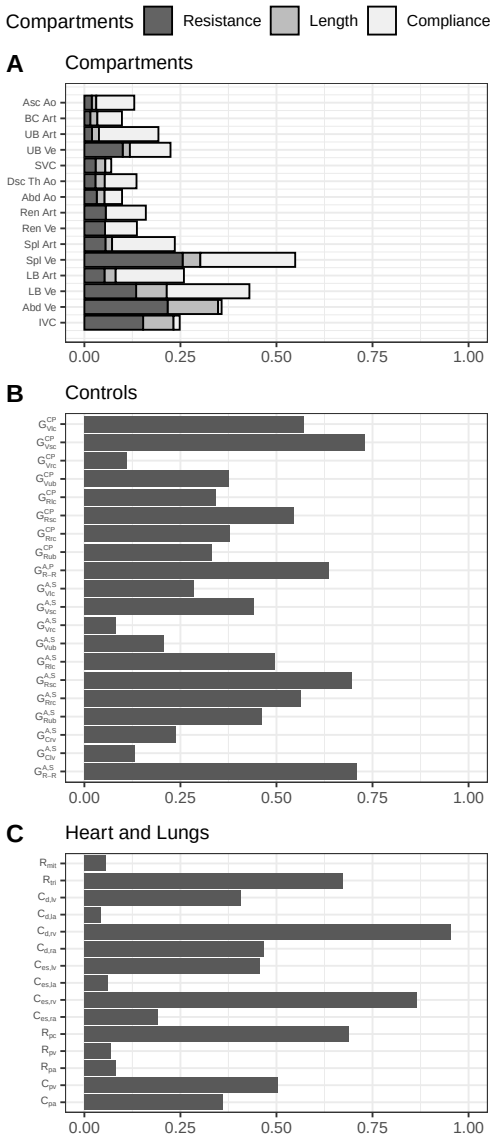

Figure 6.4: Cumulative influence factor (CIF) for compartments (A), controls (B), and heart and lungs (C) groups. In the compartment group (A), the CIF is further divided to show the individual contributions of the different parameters forming a compartment (resistance, length, and compliance). CIF takes a value between 0 and 1, where a higher value represents greater influence on the outcome measures. Abbreviations: Ao, aorta; Art, arteries; Ve, veins; Asc, ascending; Dsc, descending; BC, brachiocephalic; UB, upper body; SVC, superior vena cava; Th, thoracic; Abd, abdominal; Ren, renal; Spl, splanchnic; LB, lower body; IVC, inferior vena cava; G, gain; A, arterial baroreflex; CP, cardiopulmonary reflex; S, sympathetic; P, parasympathetic; R-R, R-R interval; C, compliance; lv, left ventricle; rv, right ventricle; R, resistance; ub, upper body microcirculation; rc, renal microcirculation; sc, splanchnic microcirculation; lc, lower body microcirculation; V, unstressed Volume; pa, pulmonary arteries; pv, pulmonary veins, pc, pulmonary microcirculation; es, end-systolic; ra, right atrium; la, left atrium; d, diastolic; tri, tricuspid valve; mit, mitral valve.

group, parameters related to the right ventricle have the largest CIF. These include end-systolic and diastolic compliances ($C_{es,rv}$, $C_{d,rv}$) and the tricuspid valve resistance (R_{tri}).

Figure 6.5 shows the cumulative distribution functions for all six primary outcome measures (heart rate, stroke volume, central venous pressure, mean arterial pressure, systolic blood pressure, and diastolic blood pressure) and the two secondary outcome measures (cardiac output and pulse pressure). Each plot shows the CDF for all five gravity levels (0g, 0.25g, 0.50g, 0.75g, 1g) and all three parameter groups (compartments, controls, and heart and lungs). These plots allow for comparison between the three groups showing the overall variation of the outcome measures as a function of the variation of the model parameters.

Figure 6.5 shows a decrease in stroke volume and central venous pressure, along with an increase in heart rate and diastolic blood pressure with increasing gravity level. There is also a small increase in mean arterial pressure. Systolic blood pressure is largely held constant. Both cardiac output and pulse pressure decrease with increasing gravity level. All parameters stay within a normal physiological range. For most of the outcome measures, the largest variation (i.e., largest spread of the CDFs) occurs in the heart and lungs group except for diastolic blood pressure and pulse pressure, where the largest variation occurs in the compartments group.

Figure 6.6 shows the coefficient of variation (COV) for each of the three parameter groups (compartments, controls, and heart and lungs) and each outcome measure, at each gravity level simulated. These figures highlight the change in the relative influence of each group as the gravity level changes from 0g to 1g.

Overall, the largest COVs (~ 0.1) are found in the heart and lungs group for stroke volume, central venous pressure, and pulse pressure, and in the compartments group for pulse pressure. The remaining COVs are 0.05 or lower. For heart rate, stroke volume, central venous pressure, and mean arterial pressure the heart and lungs group has the largest COV at all gravity levels and it is significantly higher (around twice the value) than the COV of the other two groups. These results suggest that variation of the heart and lungs parameters has significantly more effect on heart rate, stroke volume, central venous pressure, and mean arterial pressure than variation of

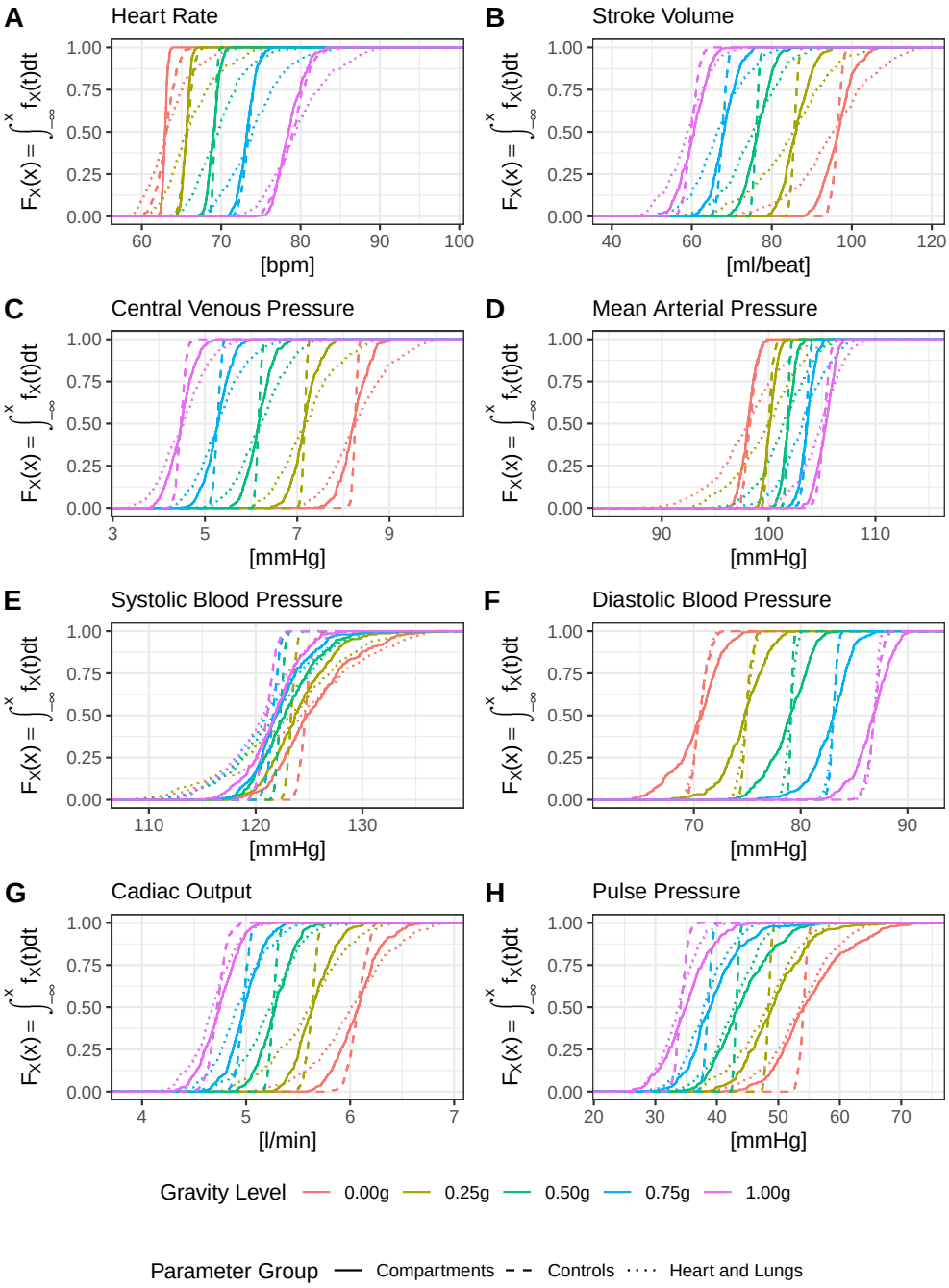

Figure 6.5: Cumulative distribution function (CDF) of all outcome measures under multiple gravity conditions. Each plot shows the total variation of the outcome measure across the entire range of model parameters in each one of the five gravity conditions (0g, 0.25g, 0.5g, 0.75g, and 1g). A: heart rate (HR); B: stroke volume (SV); C: central venous pressure (CVP); D: mean arterial pressure (MAP); E: systolic blood pressure (SBP); F: diastolic blood pressure (DBP); G: cardiac output (CO); and H: pulse pressure (PP).

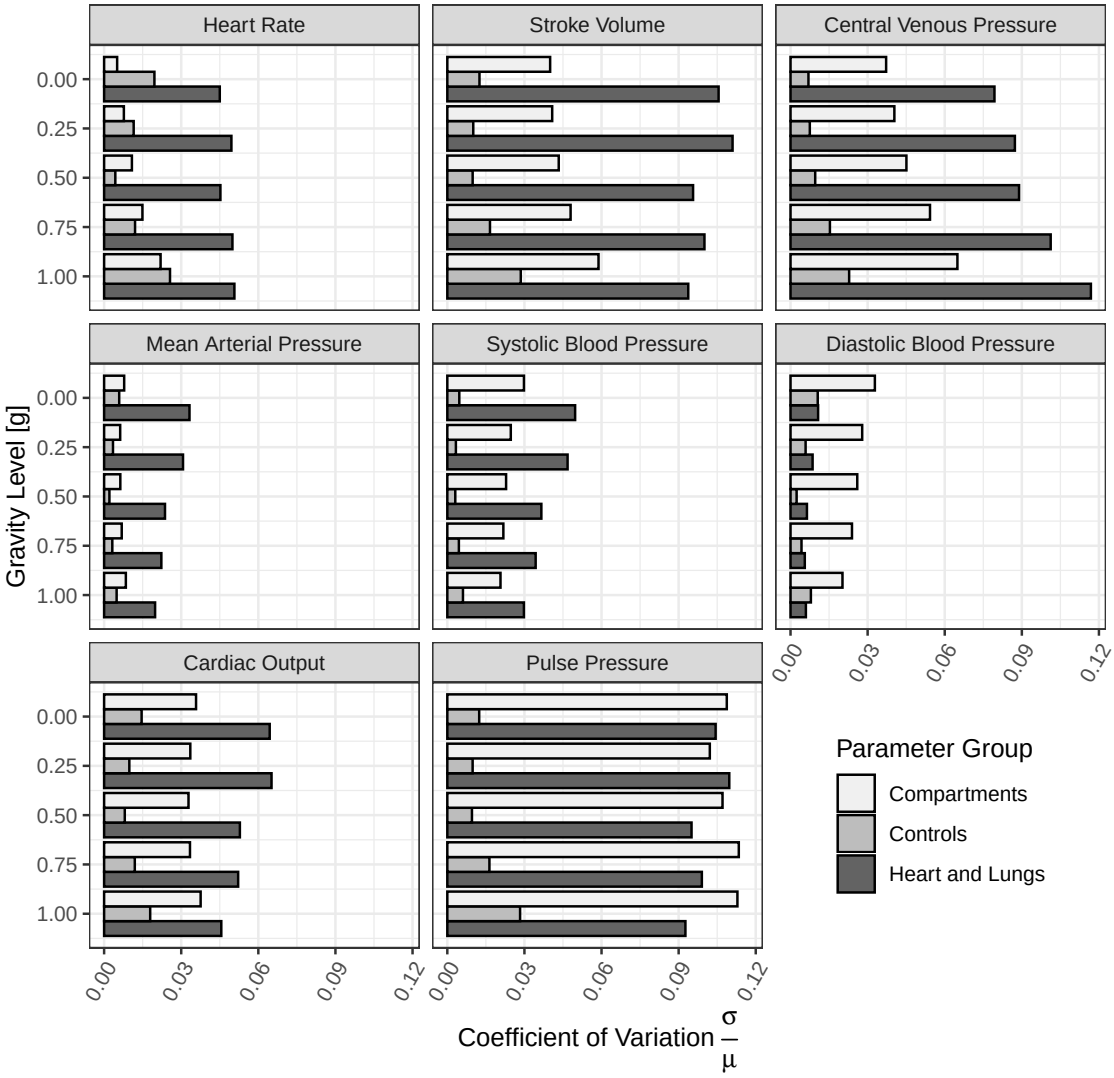

Figure 6.6: Coefficient of variation (COV) for each outcome measure and parameter group at each gravity level simulated. Each plot shows a single outcome measure, the gravity levels are on the y-axis and COV on the x-axis. All plots have the same scale.

either the compartments or controls parameters. For systolic blood pressure, the heart and lungs group still has the largest COV, but with increasing gravity the difference between COVs from heart and lungs and compartments groups decreases. In relation to diastolic blood pressure, the compartments group has the largest COV. In regards to the secondary outcome measures, cardiac output follows a similar trend to systolic blood pressure: the heart and lungs group has the largest COV but the COV of the compartment group is also high, particularly at higher gravity levels. The

COV of pulse pressure is equally high in both the compartments and heart and lungs groups.

6.3.4 Discussion

By varying parameter values across a normal physiological range and considering changes in systemic outcomes, we have identified a subset of parameters that have most influence on cardiovascular response to orthostatic stress in a number of gravitational conditions. We have also identified the parameters within our three chosen parameter groups with the most cumulative influence in constant gravitational fields. We have further compared these groups to one another, identifying the extent to which parameter variation within the group affects the overall systemic outcomes. Finally, we have quantified changes in the influence of each group with increasing gravity level.

6.3.4.1 Within Group Influence

Figure 6.4A shows that the largest influence in the compartments group comes from the splanchnic, abdominal, and lower body venous compartments. From a systemic perspective this is unsurprising, since at rest, 70% of blood is contained in the venous system at any instant, and these three compartments account for 47% of all circulating blood[168]. Together, this represents the total venous outflow from the gastrointestinal tract, all of the pelvic organs, two thirds of the skin, one half of the skeleton, 90% of the skeletal muscle, and nearly all of the adipose tissue[153,154,168].

Based on physiological principles, total venous return is expected to match cardiac output, both at rest and during exercise. The lower body venous compartment must be responsible for returning any blood from the legs back to the heart primarily through a combination of muscle pump and sympathetic nervous system stimulated venoconstriction[454,455]. The lower body microcirculation is predominantly supplying oxygen to skeletal muscle. Hyperemia to skeletal muscle can be up to 100-fold[456], particularly during high intensity exercise. Hence, the resistance of the lower body veins must ordinarily swing through a large range to promote effective venous return. It is therefore unsurprising that varying the resistance of the lower limb veins compartment in the absence of exercise causes large changes in hemodynamic parameters. As an example, Skoog *et*

al.[457] found reduced venous compliance to be an important determinant of orthostatic intolerance in some populations.

Within the majority of the compartments, compliance is the dominant influencing factor, with resistance being the second most influential parameter, particularly in the venous system. These findings confirm the decision to model the higher fidelity nonlinear relationship between pressure and volume in the large veins (details can be found in Section 6.2). In addition, the majority of the total blood volume at any instant resides in relatively compliant venous compartments and therefore, it is reasonable that the pressure-volume relationship of these compartments exerts the most influence on model outcomes. Some alternative models (for example Coats and Sharp or Blanco *et al.*[458,459]) choose to control compliance directly rather than controlling unstressed venous volume. Our results show that compliance is a key parameter for global outcomes and therefore the set points for these control systems should be carefully selected. Finally, the importance of accurate measures of compliance is underscored. This is particularly relevant when applying the model to simulate individual subjects, since studies have shown trends in compliance varying with age[460] and also deconditioning (for example time in bed rest[461] or microgravity[192]).

With respect to the abdominal and splanchnic venous compartments, these are the large venous compartments directly before the right atrium – excluding the thoracic inferior vena cava. The role of the venous components of circulation is to return blood to the heart. Hence, the large venous compartments are naturally compliant in order to accommodate a large variation in cardiac output whilst protecting systemic mean arterial pressure. As indicated in Table 2, these compliance values also present a fairly wide range (e.g., 47.7 to 72.3 ml/mmHg for the splanchnic veins compared to 0.04 to 0.36 ml/mmHg for the splanchnic arteries). Our modeling exercise demonstrates that varying the large range of compliance parameters in compartments associated with a high percentage of blood flow accounts for the largest changes to the systemic outcomes that the large venous compartments are partially responsible for regulating.

Finally, when considering the heart and lungs group, Figure 6.4C shows that the right ventricular compliance, both end-systolic and diastolic (along with the tricuspid valve resistance), exerts

the most influence on systemic outcome measures out of all the parameters studied. This may seem counter-intuitive, since we usually associate left ventricular function or degradation with many cardiovascular adaptation and pathologies (for example left ventricular hypertrophy is associated with both the physiological response to training and as a marker for cardiovascular disease associated with hypertrophic cardiomyopathy[462]). The left ventricle pumps blood around the entire system accommodating a wide range of preloads (determined principally by cardiac output matched to venous return) and afterloads (determined principally by peripheral resistance and the range of normal mean arterial pressures throughout the systemic system). From a resting baseline, mean arterial pressure rises only moderately in dynamic exercise scenarios, primarily due to significant vasodilation as a result of functional sympatholysis[463]. However, the same mean arterial pressure increases dramatically during isometric exercise as a result of the pressor response[464]. As a consequence, in a model simulation that involves no exercise response, the left ventricle is over-designed and underutilized, and therefore adjusting its parameters will not greatly affect the systemic response. By contrast, the right ventricle must only accommodate a narrower range of afterloads, determined by the limits of systolic pressure in the lower pressure pulmonary circulation. As such, the right ventricle becomes a systemic bottleneck, and varying these parameters can dramatically affect the flow of blood arriving at the left chambers, amplifying the impact of the right heart parameters in the system response.

6.3.4.2 Between Group Influence

The CIFs displayed in Figure 6.4 show the relative influence of each parameter within each group, but do not provide any information about the relative importance of one group with respect to the others. To investigate this relative importance, we must also consider the CDFs and COV (Figure 6.5 and Figure 6.6) Qualitatively, the CDFs follow the expected acute physiological response to changing the gravity level: when gravity level decreases there is an increase in cardiac output primarily due to an increased stroke volume as a result of increased preload[6], blunted by increased vagal modulation (seen as a fall in heart rate)[465]. The expected increase in pulse pressure[465] as a result of increased stroke volume is also well simulated.

Quantitatively, our models show a 1.34 l/min (Welch two sample t-test, $t(1537) = 128.8$, $p < 0.0005$, 95% CI: 1.32 to 1.36 l/min) increase in cardiac output between 1g and 0g, from 4.71 ± 0.17 l/min to 6.05 ± 0.26 l/min. This is closely matched to the 1.6 l/min acute increase found on entering microgravity reported by Norsk *et al.*[466], although their absolute cardiac output values are higher (6.6 ± 0.7 in 1g to 8.4 ± 0.9 l/min in 0g). The same study found no change in mean arterial pressure or heart rate. Our model shows a small decrease in mean arterial pressure of 6.98 mmHg (Welch two sample t-test, $t(1598) = -87.9$, $p < 0.0005$, 95% CI: 6.83 to 7.14 mmHg), and a decrease in heart rate of 15.98 bpm (Welch two sample t-test, $t(1532) = -142.2$, $p < 0.0005$, 95% CI: 15.76 to 16.20 bpm). It should be noted that Norsk's experimental values are taken after a week in space, when adaptation has already begun. Also, we note that we expect to see less variation in our population at a given condition since we are not varying parameters such as height, weight, and total blood volume that grossly impact our systemic CV outcomes (Section 6.3.4.4). Varying these parameters would lead to larger standard deviations such that, for example, our decrease in mean arterial pressure may not be significant in a global population. By comparison, Mukai *et al.*[467] found a decrease in heart rate of 22 ± 7 bpm in microgravity induced by parabolic flight, which is entirely consistent with our acute simulations.

Finally, visual inspection of the CDFs shows that for the majority of the parameters, the spread of the CDFs (which is a measure of the absolute variance) in the heart and lungs group (dotted lines) is often larger than the other two groups. This is most noticeable in mean arterial pressure, heart rate, and stroke volume. Based on these results, we preliminarily conclude that the heart and lungs group exerts the major influence on the outcome measures. In certain parameters (most noticeably stroke volume, central venous pressure, cardiac output, and pulse pressure), we further note that the absolute variation in the heart and lungs group appears to increase with decreasing gravity. We hypothesize that this model effect is related to decreased regulatory control in lower gravity, a finding supported by tilt studies showing reduced baroreflex sensitivity when decreasing orthostatic stress[468,469].

Further insight into the relative influence of the groups can be seen through the coefficient of

variation shown in Figure 6.6. In all outcome measures at all gravity levels, the controls group of parameters exerts the least variation on outcome measures. In five of the outcome measures, the heart and lung parameters provided the most variation, whilst in diastolic blood pressure it was the compartments parameters. Taking into context our understanding of the relative influence of the parameters within the groups, our results suggest that the right ventricular elastances are the key parameters that must be accurately determined for accurate system response, due to the bottleneck effect described above.

Interestingly, with increasing gravity levels, the influence of both the compartments group and the controls group slightly increase. However, the COV of the controls group never matches the COV of the heart and lungs group, and only in heart rate does it present a higher COV than the compartments group. We hypothesize that the increased influence of the controls group is due to the fact that, as the primary regulator of blood pressure, the arterial baroreflex is increasingly stressed at higher gravity levels. We further posit that the increased influence of the compartments stems from increased blood pooling in the large veins at higher gravity levels, leading to greater importance of their parameters in promoting effective venous return in order to allow regulated circulation; a change in these parameters will cause large scale changes in blood flow, which the already stressed control system is attempting to regulate. Aside from the aforementioned trends, it is important to note that in general, the COV of the different groups is similar across gravity levels. First, this underscores that our cardiovascular model (and more generally the cardiovascular system) behaves similarly across the 0g to 1g gravitational range. From the modeling perspective, these results specifically mean that the important set of parameters that must be accurately selected to simulate the behavior of a subject on Earth remain constant across reduced gravity conditions. This in itself is an important finding, stated simply that "if you can select precisely the necessary parameters to accurately model a subject on Earth, you can also accurately model the same subject in reduced gravity".

6.3.4.3 Recommendations

Our simulations suggest that a small subset of parameters exert a large influence on CV regulation. Thus, more effort should go into determining the specific value of these parameters for individuals whose physiological responses we intend to simulate. Specifically, we have determined that the most important physiological characteristics to be described are those related to the large veins (lower body, splanchnic, and abdominal), and the right ventricle. To give examples of how these could be measured, right ventricular function can be accurately estimated non-invasively using biplanar contrast cineangiography[470], and venous characteristics (at least in the lower body) can be readily determined using a combination of allometric scaling and water-displacement plethysmography[471] to determine the appropriate pressure-volume relationships.

To highlight the potential impact of these findings with a short case study, numerous studies[162,472–475] have found significant differences in CV responses to orthostatic stress based on gender. Aside from the global key parameters, many of which will be different between men and women (most notable those, such as total blood volume (TBV), linked to allometric scaling), there have also been studies noting gender differences in many of our important parameters. Maffessanti *et al.*[160] found that gender was highly significant ($p < 0.01$) in studies of right ventricular parameters. Similarly, it is expected that vascular length will be different in men and women based on allometry, but Monahan and Ray[161] also found gender differences in venous compliance (specifically in the leg, one of our influential compartments). All in all, our sensitivity analysis results suggest that accurately valuing differences in this subset of parameters, along with the global key parameters, could provide more accurate predictions of the CV responses of men and women, and more broadly, of specific individuals, to gravitational stress.

6.3.4.4 Global Parameters

Our model includes a small number of "global" parameters that cause larger variation in the outcome measures than the rest of the parameters. In particular, the four parameters that have the largest effect on one or more outcomes measures are total blood volume (V_{tot}), the arterial

baroreflex and cardiopulmonary reflex set points (P_{aspa}, P_{aspc}), and nominal heart rate (HR_{nom}). The aim of this study was to determine other influential parameters besides these four, so they were not included in the main sensitivity analysis. However, we did conduct a simple sensitivity analysis varying each of these four parameters in turn uniformly ± 2SD from the mean (ranges taken from Heldt[168]), in order to capture their influence on systemic outcomes. More detail on how these global parameters fit into the model can be found in Section 6.2.

Figure 6.7 shows the result of varying each of these four parameters (one at a time) on the six primary and two secondary outcome measures at each one of the five gravity levels simulated. The simulations had the same profile as described in the main text. All other parameters were held constant at their mean value.

Figure 6.7A shows that total blood volume has a large effect on all outcome measures except diastolic blood pressure. In particular, at 1.0g, a 203 ml increase in V_{tot} (1 SD from the mean of 5625 ml) leads to a 4.4 bpm drop in heart rate, an 8.4 ml increase in stroke volume, a 0.6 mmHg increase in central venous pressure, a 2.3 mmHg increase in central venous pressure, a 4.6 mmHg increase in systolic blood pressure, a 0.1 mmHg drop in diastolic blood pressure, a 0.4 l/min increase in cardiac output, and a 4.7 mmHg increase in pulse pressure. Figure 6.7B shows that the arterial baroreflex set point has an effect on blood pressure. In particular, at 1.0g, a 3.0 mmHg increase of P_{aspa} (1 SD) leads to a 2.5 mmHg increase in mean arterial pressure, systolic blood pressure, and diastolic blood pressure, but doesn't significantly change other outcomes. In contrast, the cardiopulmonary reflex set point (Figure 6.7C) also has an influence on heart rate. A 1.0 mmHg (1 SD) increase in P_{aspc} at 1.0g leads to a 2.9 bpm decrease in heart rate, a 1.5 mmHg increase in mean arterial pressure, and a 2.4 mmHg increase in systolic blood pressure. Finally, nominal heart rate (HR_{nom}) obviously has a significant influence on heart rate (Figure 6.7D) with a 3.3 bpm increase (1 SD) leading to a 3.5 bpm increase in outcome heart rate.

It is unsurprising that the amount of blood circulating in the body has a large influence on all hemodynamic outcome measures. Similarly, the primary function of the arterial baroreflex and cardiopulmonary reflex is to provide blood pressure regulation, so changing the set point has a

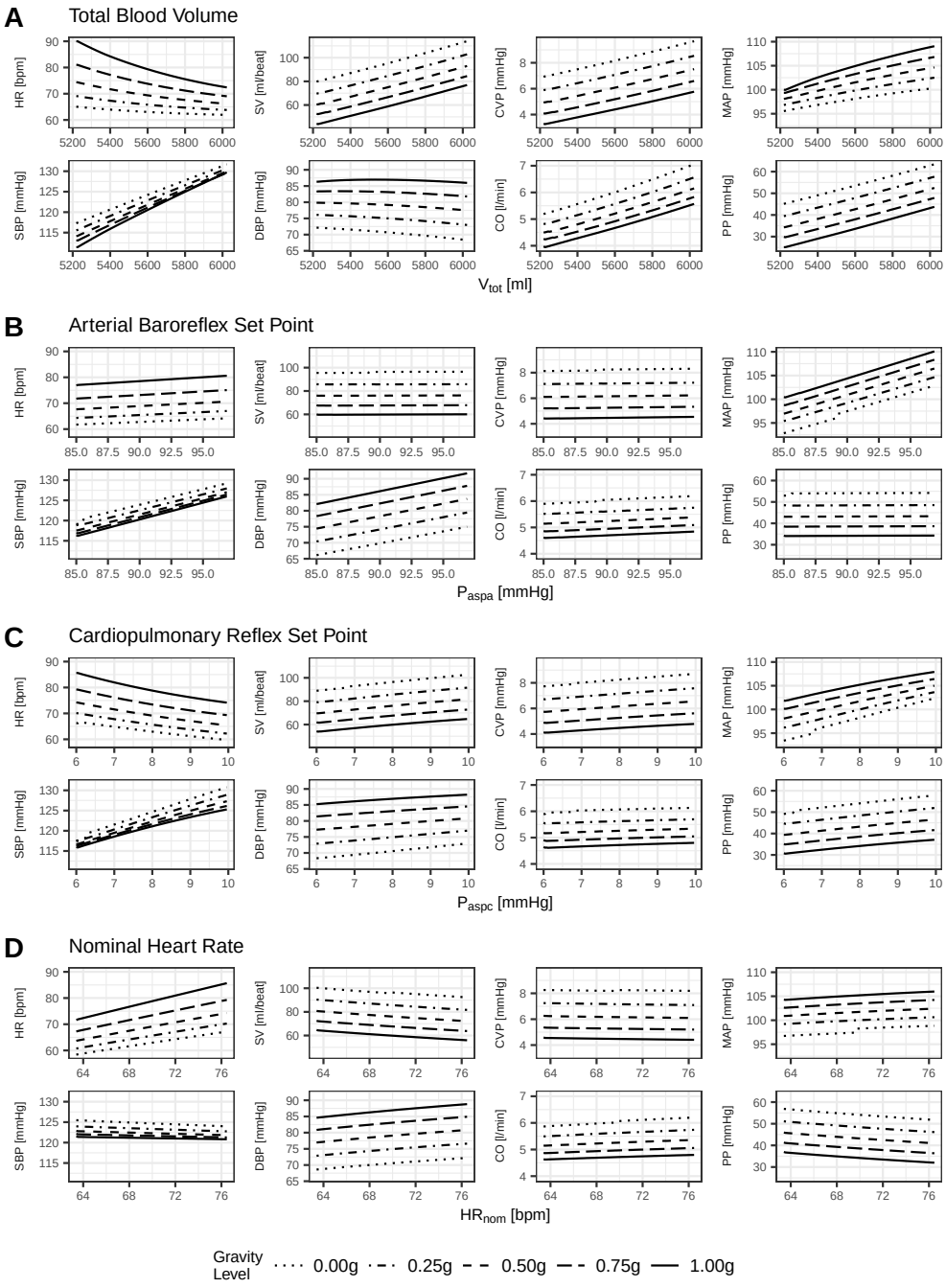

Figure 6.7: Change in outcome measures as a result of varying each of four key global parameters by ± 2SD with respect to baseline. A, total blood volume (V_{tot}), mean = 5625.0 ml, SD = 203.0 ml; B, arterial baroreflex set point (P_{aspa}), mean = 91.0 mmHg, SD = 3.0 mmHg; C, cardiopulmonary reflex set point (P_{aspc}), mean = 8.0 mmHg, SD = 1.0 mmHg; and D, nominal heart rate (HR_{nom}), mean = 70.0 bpm, SD = 3.3 bpm. Graphs showing the same outcome measure have the same y-axis scale.

direct influence on blood pressure. All of these parameters can be easily measured in an individual. As discussed in the main text, the aim of this study was to determine the other model parameters with large influence. As such, these four global parameters were excluded from the sensitivity analysis, but must be considered when applying the model to an individual.

6.3.4.5 Limitations

Diaz-Artiles *et al.* examined in detail some of the physiological limitations in the model in a previous publication[154]. This included limitations of lumped-parameter modeling to determine pulse wave propagation, and intra-beat changes, along with assumed linearities in the systolic and diastolic pressure-volume relationships, and lack of viscoelastic stress-relaxation effects of the systemic veins. Inertial effects are also not included, since this model was primarily designed to analyze cycle-to-cycle cardiovascular changes in blood flow and pressure when exposed to orthostatic stress. In our case, we are primarily concerned with steady state outcomes, and the contribution of inertial effects to pressure and flow is largest within the cardiac cycle (i.e., intra-beat changes) rather than on a beat-to-beat scale. Defares *et al.* estimated that less than 1% of stroke volume and mean arterial pressure are due to inertial effects[422]. Thus, their inclusion would only serve as a slight refinement of the arterial waveform at a higher computational cost. Diaz-Artiles *et al.* further commented on the difficulty of assigning numerical values to model parameters, and how a sensitivity analysis could help determine the subset of important parameters – this study intends to answer that limitation.

Similarly, the decision not to include compliances for the microvasculature, which are modeled as pure lumped resistances, was a modeling choice designed to limit the number of systemic compartments for computational efficiency. Literature on compliance of capillary beds, or their natural variation is scarce. Gallo *et al.* modeled all capillary compliances in the order of 0.03 ml/mmHg in a similar 0D lumped-parameter model[178]. This is at least an order of magnitude smaller than our arterial compliances, and two to three orders of magnitude smaller than our venous compliances. As such, any minute variation in distension in the microvasculature is unlikely to have a significant impact on outcome measures.

Other models found in the literature incorporate additional features not included in our model, but we expect to find our results applicable. For example, both Blanco *et al.*[459] and Coats and Sharp[458] developed models using arterial baroreflex control systems involving varying compliance, as opposed to the varying unstressed volume found in our model. In both of these models, we expect that the parameters with the highest sensitivity (aside from the heart and lung parameters, which are modeled similarly) are the ones related to the large venous compartments (for example venous resistance in the Coats and Sharp model), the compliance set points in these compartments, and the gains from the sympathetic arc of the arterial baroreflex.

With regards to the design of the sensitivity analysis, the full model contains in excess of 150 parameters. We selected a subset of parameters that we considered most likely to have large influence on the model outcomes, however there are others (such as time constants for the reflex arcs) that were not varied. The model outcomes only measured the average steady state response after acute transients had settled, such that the impact of variation on the time response of the system was untested. Since we are considering steady-state cardiovascular responses to resting conditions, we also neglected the impact of exercise on the system. This adds an entirely new set of variables that could be separately analyzed using the same methodology as an additional group.

The simulations varied the chosen model parameters within predefined ranges. These ranges were chosen based on an extensive literature review as detailed by Heldt[168], and were designed to capture the majority of individual variation within a non-pathological population. The influence of each parameter is valid only within the ranges given, and caution should be taken extrapolating the results outside of these ranges. In particular, extrapolation to populations with pathological indications, such as acute ventricular hypertrophy, should be avoided. In addition, since the exact distribution of the selected parameters is largely unknown, we assumed that they followed truncated normal distributions. However, these underlying distributions could be slightly different for certain parameters and reflect, for example, lognormal distributions, or have a bimodal behavior driven by gender differences. By dividing the subset of varied parameters into three separate groups, we are potentially losing some influence due to a potential complex interaction of param-

eters from different groups. We have considered the relative importance of the groups using CDFs and COVs, but we recognize there could be a certain amount of information lost. Additionally, our methodology assumes that all parameters are independently sampled. This was a choice to capture the largest range of possible variation. In reality, some parameters are certainly correlated, and this additional correlation could influence the PRCC used in the sensitivity analysis. A refined analysis using, for example, Copula models[476], could allow for more realistic selection of parameter combinations. The associated correlations and allometric scaling could be applied to both the local and global parameters together, as there is a relationship between body type/size and the homeostatic set point of an individual. This approach is dependent on identifying the potential correlations between parameter variables, and whilst the results may vary slightly in the details, due to the underlying physiological reasoning we anticipate the same underlying findings, namely high sensitivity from the large venous compartments and right ventricular parameters.

The parameter ranges chosen represent the individual variation found within healthy subjects in terrestrial conditions during a tilt test. As such, the model represents the acute response to changing gravitational conditions in the head-to-toe direction, as opposed to the response after deconditioning caused by a period spent in reduced gravity. It should be noted that this deconditioning causes a very specific trend in a subset or parameters, as opposed to the random variation assigned by the LHS/PRCC methodology. There are recently published models[178] that investigate long duration deconditioning due to microgravity, and combining the sensitivity analysis described in this paper with long duration trends could provide further insight into individual deconditioning responses.

As detailed in Section 6.2.6.4, the baseline model used for the sensitivity analysis does not differentiate between tilt and reduced gravity. The consequences are that we do not find reductions in CVP evidenced in spaceflight but instead, our results show an increase in CVP with reducing tilt angle supported by findings from tilt maneuvers on Earth. Whilst this is an inherent limitation of the baseline model, our findings related to the sensitivity of physiological parameters with respect to general hemodynamic response to orthostatic stress are not invalidated by this limitation. This limitation is addressed in Section 6.4 below.

6.3.5 Summary of Sensitivity Analysis

We have conducted a thorough sensitivity analysis of a lumped-parameter model of the cardiovascular system in a range of constant gravity conditions. Model simulations compared well qualitatively and quantitatively to expected changes based on physiological principles. We have determined a subset of model parameters, including those related to the large venous compartments and the right ventricle, that have the largest influence on model outcomes. The purpose of this sensitivity analysis was to determine the most important model parameters that must be accurately valued in order to model and predict the responses of individuals to gravitational environments. By effectively measuring those influential parameters (i.e., characteristics of the leg, abdominal, and splanchnic veins, and the right ventricle) in addition to the important global parameters, we can more accurately simulate and predict acute response to changing gravitational conditions. This allows for the design of more effective countermeasures and protocols.

6.4 Model Development

As part of this modeling effort, we incorporate three separate mechanisms into the model: (1) we separate the upper body branch into two separate branches, one representing the brachial circulation, and one representing just the head and neck; (2) the original model was not designed to simulate head-down tilt, we rectify this omission; (3) we include a simulation of body weight in order to differentiate between a tilt in a constant gravity field and a removal of all hydrostatic gradients[50,61,95,430]. Finally, we further develop a standalone ocular model, which could be incorporated into the full systemic model[1]. These additions are described in detail below.

6.4.1 Head Branch

The baseline upper body circulation is shown in detail in Figure 6.8. It consists of two compartments and a single microvascular resistance. Compartment 3 represents the upper body arteries, whilst compartment 4 represents the upper body veins.

In order to examine cephalad blood flow in more detail, we expand this branch into two parallel branches. The original branch, containing compartments 3 and 4 remains architecturally the same;

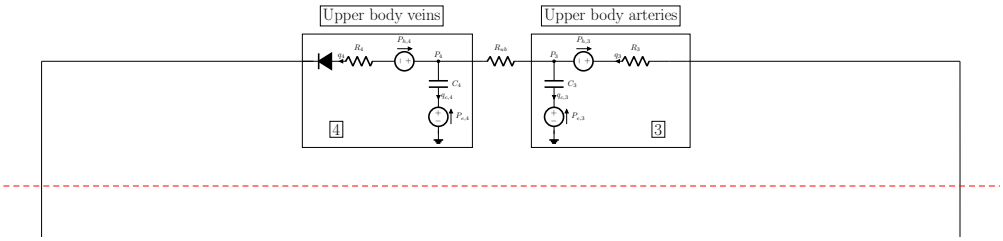

Figure 6.8: Detail of baseline model upper body branch showing two compartments (upper body arteries and veins) and the upper body microcirculation.

however, we reassign the parameter values to reflect an updated definition of the compartments. Thus, compartment 3 now represents the brachial arteries, compartment 4 represents the brachial veins, and the microvascular resistance, r_{arm}, now represents the arm microcirculation. In parallel, we add a new branch containing four new compartments and two new microcirculations.

In the updated architecture, shown in Figure 6.9, compartment H1 represents the lumped carotid arteries (common carotid arteries, external and internal carotid arteries), compartment H2 represents the cerebral arteries, compartment H3 represents the cerebral veins (including, but not limited to, the superior sagittal sinus, the straight sinus, the transverse sinuses, the superior and middle cerebral veins, and the cavernous sinuses), and r_{ceph} represents the cerebral microvasculature. There are two principal drainage pathways from the head: the jugular veins and the vertebral plexus[477]. The vertebral plexus is highly non-distendable due to its anatomical location along the spine. Thus, we model two parallel drainage pathways from H3: compartment H4 represents the internal and external jugular veins, whilst a fixed resistance, r_{vp} represents the vertebral plexus. The updated architecture of the new branch is presented in Figure 6.9.

6.4.1.1 Parameter Assignment

Parameter assignment covers both the reassignment of the parameters for compartments 3 and 4 to reflect their updated definition and also the assignment of parameters for the four new compartments and microvasculature. For all other compartments, we retain the values derived by Heldt and validated by Zamanian and Diaz-Artiles[120,185].

In the baseline model, Heldt used 4.9 PRU to represent the microvascular resistance of the

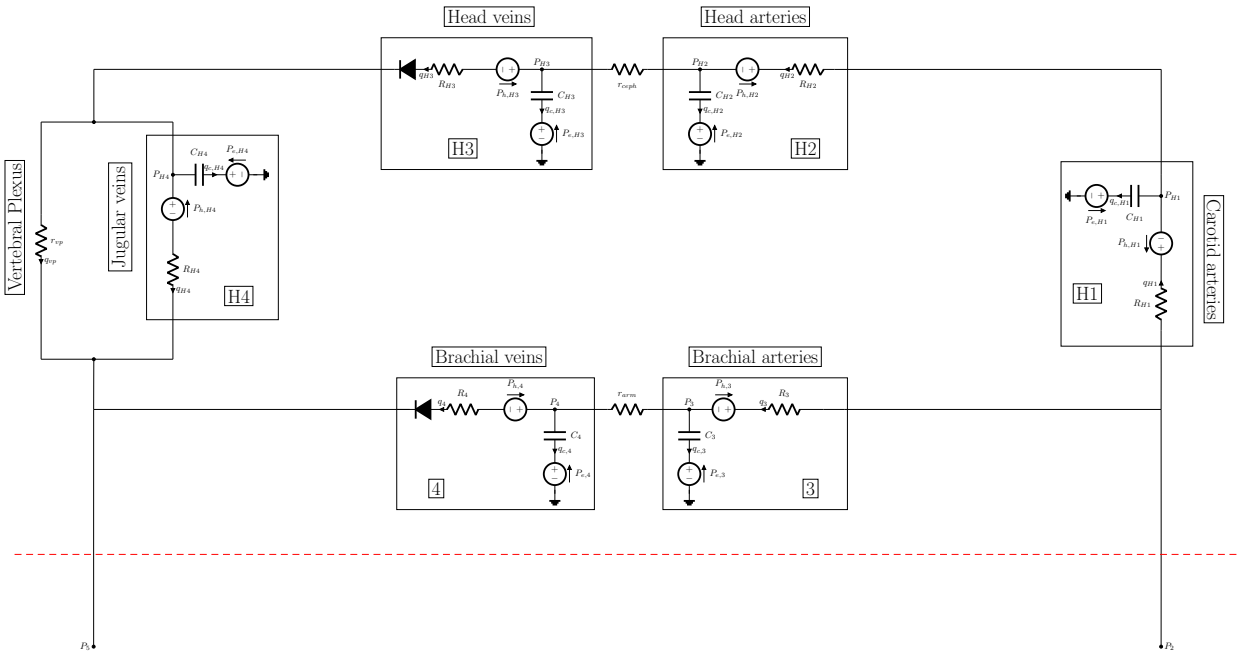

Figure 6.9: Lumped parameter representation of the new upper body incorporating a brachial branch and a head branch. Compartments H1 to H4 represent the carotid arteries, the cerebral arteries, the cerebral veins, and the jugular veins, respectively. r_{ceph} represents the cerebral microvasculature and r_{vp} represents the vertebral plexus.

upper body, based on a division of blood flow throughout the body such that 22% (15% to 29%) of resting cardiac output supplies the upper body[168,173]. We redivide the flow such that 12% (8% to 16%) of blood flows to the head[478], and the remainder of the flow goes to the upper body, keeping the overall systemic vascular resistance unchanged. Based on studies by Cirovic *et al.* and Gisolf *et al.*, we further assign a small value of 0.068 PRU to the fixed resistance of the vertebral plexus, r_{vp}[477,479]. New parameter values are shown in Table 6.7.

Table 6.7: Parameter assignments for systemic microvascular resistances.

		Microcirculation					
		head	arms	renal	splanchnic	legs	vertebral plexus
r	PRU	9.0	10.8	5.2	3.3	4.5	0.068

Regarding vascular length, the carotid arteries and jugular veins stretch from just above the aortic arch to just behind the jaw line. From this point, the major cerebral arteries and veins extend throughout the majority of the head. Following data from Gray[480], we assign 20 cm for the vertical length of each of compartments H1 to H4. We further lengthen compartments 3 and 4 to represent the full brachial system, based on a study by Singh *et al.* on 50 cadavers, we assign a value of 66 cm to the length of each compartment[481]. Since the majority of the blood volume is situated in the upper portion of arms, we define the effective length of compartments 3 and 4 to be one third of the anatomical length, similar to compartments 12 and 13 for the legs[168]. Table 6.8 presents the compartment lengths for compartments 3, 4, and H1–4.

Table 6.8: Parameter assignments for anatomical vertical length.

		Vertical Length					
		3	4	H1	H2	H3	H4
l_v	cm	66*	66*	20	20	20	20

Notes:
*Effective length defined as 1/3 anatomical length for compartments 3 and 4.

On the arterial side of the body, we assign values for the compliance per unit length of the brachial and cerebral arteries of 0.004 ml/mmHg/cm, giving values of 0.26 ml/mmHg and 0.08 ml/mmHg respectively for compartments 3 and H2[168,173]. The carotid artery has been studied extensively in the literature; thus, based on a study of the arterial stiffness in 584 subjects by Vriz *et al.* and 26 subjects by Gamble *et al.*, both using M-mode echocardiography, we derive a compliance of 1.226e-6 m^2/kPa for each of the two carotid arteries. Thus, we assign a value of 0.07 ml/mmHg to account for both vessels in compartment H1[482,483]. On the venous side, Heldt assigned a value of 7 ml/mmHg for compartment 4, derived from a compliance of 1.2 ml/mmHg for the arms, and the remainder for the cerebral sinuses and the jugular veins. We reassign this value of 1.2 ml/mmHg to compartment 4 alone, and split the remainder between compartments

H3 and H4. Based on supplemental data from Tarnoki *et al.* on 170 adult Caucasian twins, we are able to derive an estimate of the compliance of the jugular veins as being 2.6 ± 0.2 ml/mmHg on the right and 3.9 ± 0.2 ml/mmHg on the left[277]. Lumping these results together gives a value slightly above data recorded by Amelard *et al.* using optical hemodynamic imaging[484]. Thus, we assign 2.45 ml/mmHg to compartment H4, leaving 3.35 ml/mmHg to compartment H3. Table 6.9 presents the compliances for compartments 3, 4, and H1–4.

Table 6.9: Parameter assignments for vascular compliance.

		Compliance					
		3	4	H1	H2	H3	H4
C	ml/mmHg	0.26	1.2	0.07	0.08	3.35	2.45

We assume a reduction in mean arterial pressure of 2 ± 1 mmHg over the length of the upper body arteries, assigning a resistance value of 0.014 PRU to compartment 3. Heldt suggests an arterial resistance of (7.0 ± 2.0) $\cdot 10^{-4}$ PRU/cm in the lumped upper body arteries, thus we also assign a resistance of 0.014 PRU to each of compartments H1 and H2. On the venous side, Heldt assigns resistances of 0.07 ± 0.04 PRU, 0.11 ± 0.06 PRU, and 0.11 ± 0.05 PRU to the outflow resistances of the splanchnic, renal, and upper body compartments based on data from Barratt-Boyes and Wood[485]. Using the same source, we maintain the resistance in compartment 4 and also assign 0.05 PRU to the resistances of each of compartments H3 and H4 respectively[168]. Table 6.10 presents the resistances for compartments 3, 4, and H1–4.

Table 6.10: Parameter assignments for compartment resistances.

		Resistance					
		3	4	H1	H2	H3	H4
R	PRU	0.014	0.11	0.014	0.014	0.05	0.05

In order to derive and assign zero-pressure volumes for the new compartments, we begin with the estimates given by Heldt of 200 ml to compartment 3 and 645 ml to compartment 4. Rescaling these values to account for 12% of total blood flow to the head and 10% to the arms, whilst maintaining the same fractions of blood in the arterial and venous sides of the circulation, we arrive at 72 ml for compartment 3 and 360 ml for compartment 4. This leaves 128 ml on the arterial side, which we split between compartments H1 and H2. Based on our own experimental data from Sections 4 and 5, we take the cross-sectional area of the carotid artery to be 36 mm^2. Given a vascular length of 20 cm and two vessels, we conservatively assign 20 ml to compartment H1, leaving 108 ml to compartment H2. On the venous side, we split 285 ml between compartments H3 and H4. Lan *et al.* use a value of 35 ml for the zero-pressure volume of the jugular veins, likely a low estimate[95]. Thus we assign 250 ml to compartment H3, and 35 ml to H4. Table 6.11 presents the zero-pressure filling volumes for compartments 3, 4, and H1–4.

Table 6.11: Parameter assignments for zero-pressure filling volumes.

		Zero-Pressure Filling Volume					
		3	4	H1	H2	H3	H4
ZV	ml	72	360	20	108	250	35

The baseline model incorporates two control systems, the arterial baroreflex and the cardiopulmonary reflex. The efferent arm of each of these control systems influence systemic vascular resistance as well as venous unstressed volume. In order to incorporate the new head branch into these control systems, we adjust the values of the static gains to the upper body (now arms only) and assign new values to the static gains corresponding to the head branch. For resistance gains from both arcs, we maintain the values given by Heldt across all microvascular resistances of –0.05 PRU/mmHg, applying this to r_{ceph}. For the venous unstressed volumes, Heldt assigns 6 ml/mmHg to the volume gain from the arterial baroreflex for the upper body. We split this into 4 ml/mmHg to the arms, and 2 ml/mmHg to the head. Similarly, for the cardiopulmonary reflex,

we split Heldt's value of 13 ml/mmHg into 9.5 ml/mmHg for the upper body, and 3.5 ml/mmHg for the head[168]. Finally, the external pressure on compartments H2 and H3 is modeled as a constant intracranial pressure, P_{icp}, of 10 mmHg[124].

6.4.2 Head-Down Tilt

The baseline model developed by Heldt was validated on a standing test in which a subject was tilted from supine to a steep angle of HUT. One of the key mechanisms acting during this process is the decrease in intravascular volume as a result of transcapillary flow to the dependent vasculature. As described in Section 6.2.5, this is modeled as a single RC compartment with a time constant of 4.6 min. The flow is subtracted or added analytically to the splanchnic, leg, and abdominal venous compartments based on the instantaneous V_{max} given in Tables 6.1, 6.2, and 6.3. In the original model, this created problems during head-down tilt, since the negative value of $\sin(\theta)$ led to a negative V_max, implying that circulating blood volume is increased beyond the total blood volume.

In reality, during head-down tilt, blood is pooled in the upper body, principally in the arms and head. The volume of blood pooled in extravascular spaces in HDT is considerable less than in HUT[486]. Thus, we set the minimum value of V_{max} (which removes blood from the lower body and is activated during HUT) to be zero, and created a second RC compartment, with the same time constant, activated during HDT only (i.e., when $\sin(\theta) < 0$), with maximum blood pooling in the upper body $V_{max_{ub}}$. The upper body interstitial flow was analytically subtracted from compartments 4 and H3. Literature on blood pooling during HDT proved scarce; thus, we initially assigned a value of 200 ml to account for this blood pooling in HDT. This is likely an overestimate, and future work should be undertaken in order to refine this value[486].

6.4.3 Body Weight

One limitation of the current model (discussed in Section 6.2.6.4) is that there is no difference between a tilt and changes in the overall gravitational field strength. This is a reasonable assumption for many applications; however, there has been much literature published on the dif-

ferences between tilt and microgravity. One of the key differences in the physiological response can be found in central venous pressure[3,186]. CVP is observed to increase in HDT, but to decrease in microgravity. Recent literature has identified that this difference may be related to hydrostatic gradients caused by body tissue weight, which are removed in microgravity[95]. Questions related to removal of tissue weight in microgravity may also be linked to the pathoetiology of SANS[50]. In order to solve this issue, we propose to include the effects of tissue weight in each compartment, in the form of an additional pressure term, P_t. This mechanism was previously implemented by Lan *et al.* in a model used to predict reduced jugular vein flow in microgravity[95], and we implement a similar architecture here. The revised architecture for a single compartment is presented in Figure 6.10.

In the revised model, we further give the tissue weight a postural dependence, such that the full force is exerted when supine and there is no component acting on an upright vessel, such that $P_{t,n}$ is given by Equation 6.20:

$$P_{t,n} = \rho_t g_c h_{t,n} \left|\cos\left(\theta\right)\right| \tag{6.20}$$

where ρ_t is the density of fat-free tissue (1.10 g/cm^3)[487], g_c is the gravitational acceleration in a constant gravity field, $h_{t,n}$ is the radius of the body at that compartment, and θ is the angle of tilt from supine.

6.4.3.1 Parameter Assignment

In order to finalize this addition to the model it is necessary to assign a body radius, h_t, to each systemic compartment. Lan *et al.* split the body into four segments: the head, neck, chest and waist[95]. Modifying their procedure to our model, we elect to split the 19 systemic compartments of the body into six segments: head (compartments H2 and H3), neck (compartments H1 and H4), arms (compartments 3 and 4), thorax (compartments 1, 2, 5, 6, and 15), abdomen (compartments 7, 8, 9, 10, 11, and 14), and legs (compartments 12 and 13). We performed measurements on four volunteers and initially assigned the median values as baselines for each segment radius. At

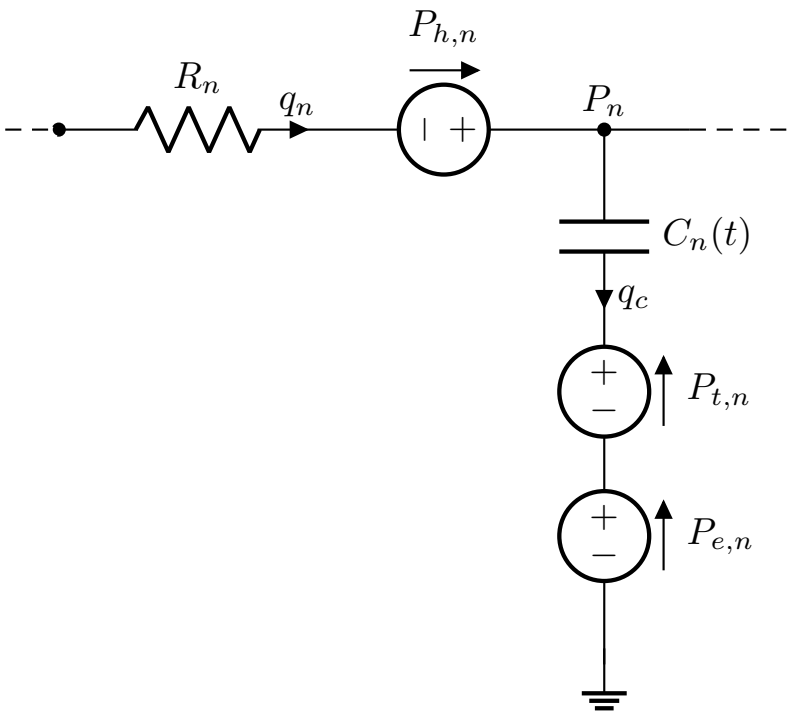

Figure 6.10: Revised schematic of a single compartment, n, incorporating a term to account for tissue weight, $P_{t,n}$. All other elements including vascular resistance (R_n), vascular compliance (C_n), hydrostatic pressure as a result of vascular length ($P_{h,n}$, and external pressure ($P_{e,n}$) are unchanged. q_n represents blood flow and P_n represents transmural pressure.

this time, we do not apply the body weight correction to the four cardiac chambers or the two pulmonary chambers. The values used are presented in Table 6.12.

Table 6.12: Parameter assignments for tissue weight body radii.

		Body Radii					
		head	neck	arms	thorax	abdomen	legs
h_t	cm	10	7	7	14	12	10

A complete schematic of the final updated model is included in Appendix A along with tabu-

lations of all of the parameters in the updated baseline.

6.4.4 Ocular Model

As part of our model development, we developed a standalone model of the eye and ocular hemodynamics. This model was validated independently using the experimental data obtained in Section 4.6. The validation results are presented in Section 6.5.2.5. Future work will integrate this standalone ocular model into the full model of systemic hemodynamics.

Our lumped-parameter model is a modified version of the model developed by Nelson *et al.*[24,488] with the addition of an extra hydrostatic column representing the eccentric placement of the eye from the mid-coronal plane. The original model is described in Nelson *et al.*[24] and our modifications are further detailed in Petersen *et al.*[1]. For completeness we have reproduced the key equations below. Figure 6.11 presents a schematic representation of the model.

6.4.4.1 Compartments

The model is represented by six compartments that interact with each other via a series of linked differential equations. The aqueous humor compartment represents both the anterior and posterior chambers of the eye. It has a volume V_{aq}, pressure IOP, and has an inflow and outflow represented by $Q_{aq,in}$ and $Q_{aq,out}$. Three blood compartments connected in series represent the arteries, veins, and capillaries in the eye (both the choroid and the retina). These compartments have volumes V_a, V_c, and V_v respectively. Blood flow to the arterial side of the eye is represented by $Q_{b,in}$ at pressure P_a (also referred to as MAP_{eye}). Blood flow leaving the venous side is represented by $Q_{b,out}$ at pressure P_v. The capillary compartment is modeled as a rigid bed with fixed resistance; thus it plays no part in the governing equations. These aqueous humor and blood compartments reside within a passive compartment. The passive compartment represents all the isovolumetric intraocular components including the lens and vitreous humor. The passive compartment has volume V_p and pressure IOP. The term "globe" is used to represent the combination of the aqueous humor compartment, the three blood compartments, and the passive compartment. Finally, the globe sits anterior to the retrobulbar subarachnoid space (rSAS) with pressure P_{csf}. The rSAS compartment

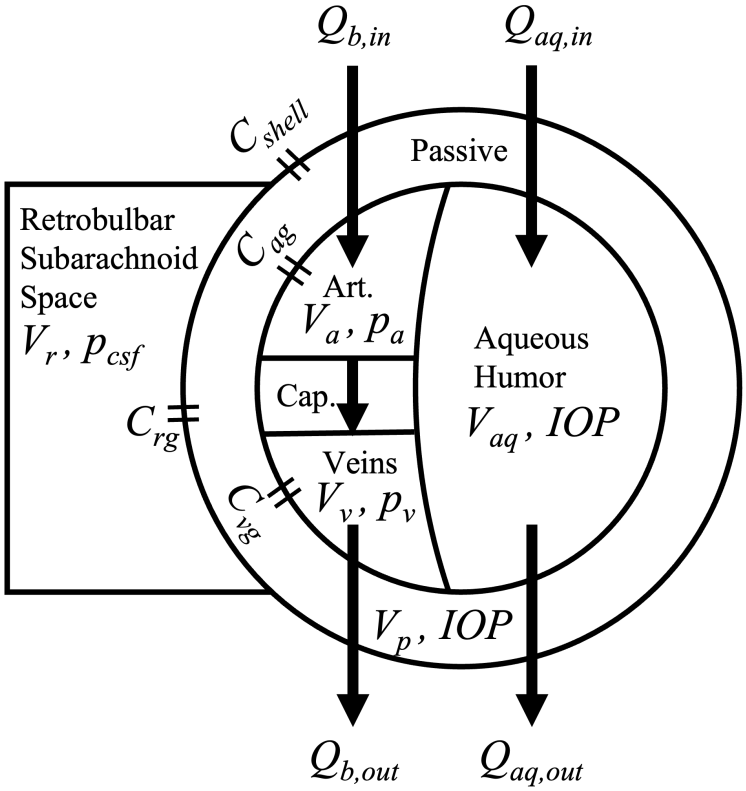

Figure 6.11: Standalone six-compartment lumped parameter model of the eye, modified from Nelson *et al.*[24]. Compartments:1) Aqueous humor with volume V_{aq} and pressure IOP. 2) Art., arteries with volume V_a and pressure p_a (equivalent to MAP_{eye}). 3) Cap., capillaries, non-distending. 4) Veins, with volume V_v and pressure p_v. 5) Passive (isovolumetric components) with volume V_p and pressure IOP. 6) Retrobulbar subarachnoid space (rSAS) with exchange volume V_r and pressure p_{csf}. Flows: $Q_{b,in}$, blood flow in; $Q_{b,out}$, blood flow out; $Q_{aq,in}$, aqueous humor inflow; $Q_{aq,out}$, aqueous humor outflow. Compliances: C_{ag}, arterial blood-to-globe compliance; C_{vg}, venous blood-to-globe compliance; C_{rg}, rSAS-to-globe compliance; C_{shell}, corneoscleral shell compliance.

does not exchange fluid with the globe but can exert influence through pressure difference acting via an exchange volume V_r.

Volume distension is represented by a series of compliances, $C = dV/dP$, between the various compartments: C_{ag} and C_{vg} are the arterial and venous blood-to-globe compliances (with the net blood-to-globe compliance $C_{bg} = C_{ag} + C_{vg}$ since the capillaries are non-distending with $C_{cg} = 0$); C_{rg} is the rSAS-to-globe compliance; and C_{shell} is the compliance of the corneoscleral shell. Extraorbital pressure is assumed constant.

6.4.4.2 *Transient Equations for Compartment Volumes*

Flow through the aqueous compartment is represented using unsteady mass conservation for an incompressible fluid, such that volume in the aqueous humor compartment, V_{aq}, is given by:

$$\frac{dV_{aq}}{dt} = Q_{aq,in} - Q_{aq,out} \tag{6.21}$$

where $Q_{aq,in}$ and $Q_{aq,out}$ represent the aqueous humor formation rate and outflow rate respectively. V_b, the volume in the blood compartments are given in terms of the compartmental compliances (capillaries are modeled as non-distending, $dV_c/dt = 0$), such that:

$$\frac{dV_b}{dt} = \frac{dV_a}{dt} + \frac{dV_v}{dt} = C_{ag}\frac{d}{dt}\left(P_a - IOP\right) + C_{vg}\frac{d}{dt}\left(P_v - IOP\right) \tag{6.22}$$

Similarly, exchange volume in the rSAS compartment, V_r, is given by:

$$\frac{dV_r}{dt} = C_{rg}\frac{d}{dt}\left(P_{csf} - IOP\right) \tag{6.23}$$

where the pressure in the rSAS compartment, P_{csf}, is the cerebrospinal fluid pressure.

The total volume of the globe, V_g, can be given either as the sum of the volumes of the blood compartments and the aqueous humor compartment (the passive compartment is isovolumetric, $dV_p/dt = 0$):

$$\frac{dV_g}{dt} = \frac{dV_b}{dt} + \frac{dV_{aq}}{dt} \tag{6.24}$$

or as a single object which can change volume either through expansion of the corneoscleral shell, or through volume exchange with the rSAS:

$$\frac{dV_g}{dt} = C_{shell}\frac{dIOP}{dt} - \frac{dV_r}{dt} \tag{6.25}$$

6.4.4.3 *Governing Equation for Intraocular Pressure (IOP)*

Equating Equations 6.24 and 6.25 gives:

$$\begin{aligned}(C_{shell} + C_{rg})\frac{dIOP}{dt} - C_{rg}\frac{dP_{csf}}{dt} = C_{ag}\frac{d}{dt}(P_a - IOP) \\ + C_{vg}\frac{d}{dt}(P_v - IOP) + Q_{aq,in} - Q_{aq,out}\end{aligned} \tag{6.26}$$

which can be rearranged to give:

$$(C_{shell} + C_{rg} + C_{bg})\frac{dIOP}{dt} = C_{rg}\frac{dP_{csf}}{dt} + C_{ag}\frac{dP_a}{dt} + C_{vg}\frac{dP_v}{dt} + Q_{aq,in} - Q_{aq,out} \tag{6.27}$$

where $C_bg = C_ag + C_vg$ is the net blood-to-globe compliance.

$Q_{aq,out}$ can be further defined as a combination of pressure-dependent outflow through the trabecular network and uveoscleral outflow, Q_{uv}, such that:

$$Q_{aq,out} = C_{tm}(IOP - EVP) + Q_{uv} \tag{6.28}$$

where C_{tm} is the aqueous outflow facility through the trabecular meshwork and EVP is episcleral venous pressure.

Substituting Equation 6.28 into Equation 6.27, rearranging, and simplifying to combine all terms not including IOP gives the governing equation for IOP:

$$\frac{dIOP}{dt} = \frac{1}{C_{g,in\,vivo}}F_g - \frac{1}{C_{g,in\,vivo}}C_{tm}IOP \tag{6.29}$$

where $C_{g,in\,vivo}$ represents the total globe compliance and F_g is a forcing function defined by grouping all of the terms which do not include IOP.

6.4.4.4 *Modeling Elements of the Governing Equation*

$C_{g,in\,vivo}$ is given by the sum of C_{shell}, C_{rg}, and C_{bg}. This is modeled using empirical constants derived by Nelson *et al.*[24], such that:

$$C_{g,in\,vivo} = C_{shell} + C_{rg} + C_{bg} = V_{g0}\left(\frac{C_1}{IOP} + C_2\right) \tag{6.30}$$

where $C_1 = 4.87 \cdot 10^{-3}$ mmHg^{-1}, $C_2 = 3.90 \cdot 10^{-5}$ mmHg^{-1}, and V_{g0} is the initial globe volume 6500 μl.

Aqueous outflow operates via a one-way valve preventing blood reflux into the eye if EVP is greater than IOP. This is modeled by a piecewise function, C_{tm}, such that:

$$C_{tm} = \begin{cases} C_{tm,normal}, & EVP \leq IOP \\ 0, & EVP > IOP \end{cases} \tag{6.31}$$

where $C_{tm,normal} = 0.30$ μl·min^{-1}·mmHg^{-1}.

The forcing function, F_g, is defined by collecting all of the terms from Equation 6.27 which do not involve IOP:

$$F_g = C_{rg}\frac{dP_{csf}}{dt} + C_{ag}\frac{dP_a}{dt} + C_{vg}\frac{dP_v}{dt} + Q_{aq,in} + C_{tm}EVP - Q_{uv} \tag{6.32}$$

Here, C_{rg}, P_{csf}, $Q_{aq,in}$, and Q_{uv} are modeled as constants: $C_{rg} = 1.1 \cdot 10^{-3}$ μl/mmHg, $P_{csf} = 13$ mmHg, $Q_{aq,in} = 2.4$ μl/min, and $Q_{uv} = 0.4$ μl/min. C_{ag} and C_{vg} are given by fractional division of the net blood-to-globe compliance, such that:

$$C_{ag} = (1 - \xi)\, C_{bg} \quad \text{and} \quad C_{vg} = \xi C_{bg} \tag{6.33}$$

where $\xi = 0.7$ (the fraction of blood distal to the arteries, approximately at venous pressure). C_{bg} is modeled similarly to $C_{g,in\,vivo}$ using empirical constants C_1 and C_2 such that:

$$C_{bg} = V_{g0}\left(\frac{C_1}{IOP} + C_2 - \frac{1}{k \cdot IOP}\right) \tag{6.34}$$

with k, the nondimensional globe stiffness, found by multiplying Friedenwald's ocular rigidity coefficient (45) $K = 0.048\ \mu\text{l}^{-1}$ by V_{g0} such that $k = 312$.

6.4.4.5 Pressures

Nelson's model uses two different approaches to account for the difference between central venous pressure (CVP) and episcleral venous pressure (EVP). Their theoretical approach uses a simple hydrostatic column to account for the pressure differential between the heart and the eye level, whilst their empirical approach more closely models experimental data to account for otherwise unmodeled autoregulatory processes. We adopt their second approach, modeling EVP as an empirically derived piecewise function given by Equation 6.35):

$$\begin{aligned} EVP &= 9\,\text{mmHg} - \alpha \sin(\theta) - \frac{h_1}{h}\alpha\cos(\theta) \\ \alpha &= \begin{cases} 2.23\,\text{mmHg}, & 0^\circ < \theta_{crit} < 180^\circ \text{ (HUT)} \\ 22.1\,\text{mmHg}, & 180^\circ \leq \theta_{crit} \leq 360^\circ \text{ (Horizontal/HDT)} \end{cases} \end{aligned} \tag{6.35}$$

where the critical angle θ_{crit} represents the point at which eye level is below heart level calculated as $\arctan(h_1/h)$. To further account for prone versus supine hydrostatic differences, we also add an additional hydrostatic column representing the perpendicular distance between the globe and the mid-coronal plane (h_1 in Figure 4.12)[142]. The additional hydrostatic column is modeled as the third term in Equation 6.36:

$$MAP_{eye} = MAP - \rho g h \sin(\theta) - \rho g h_1 \cos(\theta) - \Delta P_{a,losses} \tag{6.36}$$

where MAP_{eye} is the inflow arterial pressure at the level of the eye; MAP is the mean arterial pressure at the heart; ρ is the density of blood; g is the acceleration due to gravity; h is the distance from the aortic root to eye level along the mid-coronal plane; h_1 is the perpendicular distance from

the mid-coronal plane to the globe; θ is the tilt angle from horizontal supine; and $\Delta P_{a,losses}$ is a term representing viscous flow losses.

Venous pressure, P_v, is constrained such that it cannot drop below central venous pressure, CVP (7 mmHg):

$$P_v = \max \begin{cases} CVP \\ EVP \end{cases} \tag{6.37}$$

We make no changes to the parameter values given by Nelson *et al.*[24] with the exception of mean arterial pressure at eye level (MAP_{eye}). In this case, we adjust MAP_{eye} to represent our study population, varying with tilt angle. At each tilt angle, we obtain the steady state response after all transients have settled. We further use the mean h and h_1 values derived from our experimental subjects. As such, three parameters (MAP_{eye}, h, and h_1) are used to fit the model.

6.4.4.6 Solving the Equations

Thus, with all model parameters defined, the governing Equation 6.29 was solved for IOP at each tilt angle θ using a pseudo-implicit time marching series as described in Nelson *et al.*[24]. At each tilt angle, the model was allowed to run for a simulated time of five-minutes, by which time the IOP value had reached steady state. This steady state IOP value was taken as the simulation output for each tilt angle.

6.5 Validation

This section details a number of simulations used to validate the performance of the updated and expanded models in realistic scenarios.

6.5.1 Methods

6.5.1.1 Subjects

We simulate two subjects, a 50th percentile male and a 50th percentile female. In order to simplify the anatomical differences between male and female subjects, we scale our model based

on three parameters: total blood volume (ml), height (cm), and the location of the center of mass (CoM). In particular, we use 0.560 as the average ratio of CoM to height in males and 0.543 as the average ratio of CoM to height in females[489]. These scaling variables are presented in Table 6.13.

Table 6.13: Parameters used to scale the model to represent a 50th percentile male and 50th percentile female subject. Median height and blood volume data are sourced from Ogden[490] and Jain[491], respectively.

		50% Male	**50% Female**
Total Blood Volume	*ml*	5372.5	3972.5
Height	*cm*	178.1	163.2
CoM Ratio*	—	0.560	0.543

Notes:
*Ratio of center of mass to height.

Using these three parameters, we then scale a number of other variables in the model. In particular, using height we scale the vascular lengths (and the associated inner and outer radii of each compartment) and using total blood volume we further scale: (1) the zero-pressure filling volumes for each compartment and (2) the maximum volume in the nonlinear compartments 11, 13, and 14. The baseline values, along with the scaled values for the male and female subjects are presented in Table 6.14.

All other parameters are kept at their baseline values.

In order to test the standalone eye model we adopt a different methodology. Since this model does not incorporate the systemic circulation, we fit it to the experimental data collected in Section 4.6. Specifically, we use the mean MAP_{eye} measured from our 13 subjects at each tilt angle, combined with the mean values h (distance from heart to eye level along mid-coronal plane) and h_1 (perpendicular distance from mid-coronal plane to the globe of the eye) collected prior to the start of the experiment. See Figure 4.12 for a schematic of these measurements. Thus, three parameters are used to "fit" the model.

Table 6.14: Scaled zero-pressure volume and vascular length based on Table 6.13.

		Baseline	**50% Male**	**50% Female**
ZV_1	*ml*	21	22	16
ZV_2	*ml*	5	5	4
ZV_3	*ml*	72	75	56
ZV_4	*ml*	360	376	278
ZV_5	*ml*	16	17	12
ZV_6	*ml*	16	17	12
ZV_7	*ml*	10	10	8
ZV_8	*ml*	20	21	15
ZV_9	*ml*	30	31	23
ZV_{10}	*ml*	300	313	231
ZV_{11}	*ml*	1146	1196	884
ZV_{12}	*ml*	200	209	154
ZV_{13}	*ml*	716	747	552
ZV_{14}	*ml*	79	82	61
ZV_{15}	*ml*	33	34	25
ZV_{H1}	*ml*	20	21	15
ZV_{H2}	*ml*	108	113	83
ZV_{H3}	*ml*	250	261	193
ZV_{H4}	*ml*	35	37	27
$Vmax_{sp}$	*ml*	1500	1565	1157
$Vmax_{ll}$	*ml*	1000	1043	771
$Vmax_{ab}$	*ml*	650	678	501
l_{v1}	*cm*	10.0	10.2	9.4
l_{v2}	*cm*	4.5	4.6	4.2
l_{v3}	*cm*	66.0	67.2	61.6
l_{v4}	*cm*	66.0	67.2	61.6
l_{v5}	*cm*	14.5	14.8	13.6
l_{v6}	*cm*	16.0	16.3	15.0
l_{v7}	*cm*	14.5	14.7	13.5
l_{v8}	*cm*	0.0	0.0	0.0
l_{v9}	*cm*	0.0	0.0	0.0
l_{v10}	*cm*	10.0	10.2	9.3
l_{v11}	*cm*	10.0	10.2	9.3
l_{v12}	*cm*	105.0	106.9	97.9
l_{v13}	*cm*	105.0	106.9	97.9
l_{v14}	*cm*	14.5	14.7	13.5
l_{v15}	*cm*	6.0	6.1	5.6
l_{vH1}	*cm*	20.0	20.3	18.6
l_{vH2}	*cm*	20.0	20.3	18.6
l_{vH3}	*cm*	20.0	20.3	18.6
l_{vH4}	*cm*	20.0	20.3	18.6

6.5.1.2 Validation Scenarios

We validate the model using five scenarios:

1. **Tilt.** In this scenario we perform a graded tilt identical to that performed in Section 4. I.e., we progress from 45° HUT through to 45° HDT in 15° increments. We hold the simulation at each tilt angle, allow transients to settle for seven minutes in order to obtain the steady state response, and record the mean value of each parameter/compartment in the next five minutes. **Note:** the systemic model does not currently distinguish between supine and prone, thus these differences are not captured.

2. **LBNP.** In this scenario we perform a graded LBNP identical to that performed in Section 5. We progress from 0 mmHg LBNP through to –50 mmHg LBNP in 10 mmHg increments in a 0° supine position. We hold the simulation at each pressure level, allow transients to settle for seven minutes in order to obtain the steady state response, and record the mean value of each parameter/compartment in the next five minutes.

3. **SRC.** In this scenario we simulate graded artificial gravity on a short-radius centrifuge. We measure the level of artificial gravity generated as the level at the subject's center of mass, progressing from 0g through to 1.75g in 0.25g increments. Again, we hold the simulation at each g level, allow transients to settle for seven minutes in order to obtain the steady state response, and record the mean value of each parameter/compartment in the next five minutes. In order to determine the centrifugation speeds, both subjects were position such that their feet were at 230 cm (such that the head of the 50% male subject was closer to the center of rotation than the head head of the 50% female subject) and speeds calculated to give the required g-level at each subject's center of mass, g_{CoM}. As such, both subjects were subject to slightly different sets of speeds, and thus, both subjects experienced a different gravity level at the feet, g_{feet}. The relevant speeds and g-levels are presented in Table 6.15.

4. **Change in gravity level**. In this scenario, we progress the subjects through four different

Table 6.15: Speeds for the short-radius centrifugation simulations. Both male and female subjects were positioned with their feet at 230 cm, speeds were set to give 0.00g to 1.75g (in 0.25g increments) at the subject's center of mass.

		50% Male		**50% Female**	
r_{head}		51.9 cm		66.8 cm	
r_{feet}		230 cm		230 cm	
Level	g_{CoM}	rpm	g_{feet}	rpm	g_{feet}
1	0.00g	0.00	0.00g	0.00	0.00g
2	0.25g	13.10	0.44g	12.58	0.41g
3	0.50g	18.53	0.88g	17.79	0.81g
4	0.75g	22.69	1.32g	21.78	1.22g
5	1.00g	26.21	1.77g	25.15	1.63g
6	1.25g	29.30	2.21g	28.12	2.03g
7	1.50g	32.10	2.65g	30.81	2.44g
8	1.75g	34.67	3.09g	33.28	2.85g

gravity levels: Earth gravity (1g), Martian gravity (0.379g), Lunar gravity (0.166g) and Microgravity. This is repeated twice, once in the 0° supine position and once in an upright position. By maintaining the subject in a 0° supine posture, we isolate the effect of body weight (as opposed to hydrostatic gradients due to vascular length) in order to examine the changes compared to experimental spaceflight studies and capture the difference from a tilt response.

5. **Ocular model in tilt.** In this final scenario we switch to the ocular model. This model does not capture systemic changes but is able to measure IOP and OPP in tilt and also to capture the differences between a supine and a prone subject. We simulate the experiment performed in Section 4.6, progressing a subject through a complete 360° range of tilt angles in 15° increments. At each tilt angle, the IOP was allowed to reach steady state over five minutes before the final value was recorded.

6.5.2 Results and Discussion

Select results from the modeling simulations are presented below. Where relevant (simulations 1, 2, and 5), the results are displayed in conjunction with experimental data collected in Sections 4,

5, and 4.6, respectively. Model outputs include the pressures, volumes, and flows in every compartment. Thus, it would be impractical to present the complete set of output data. In order to provide comparisons between the scenarios, and the experimental data, we elect to present nine outputs for each simulation:

- Heart Rate (HR)
- Stroke Volume (SV)
- Cardiac Output (CO)
- Systolic Blood Pressure (SBP)
- Diastolic Blood Pressure (DBP)
- Total Peripheral Resistance (TPR)
- Cerebral Blood Flow (CBF)
- Central Venous Pressure (CVP)
- Jugular Vein Pressure (JVP)

6.5.2.1 Scenario 1: Tilt

Figure 6.12 presents the results of the tilt simulation. Where relevant (i.e., for all measures except CBF and CVP) the dose-response curves found in Section 4 (Mean ± 95% CI) are shown on top of the simulation results.

Results from the tilt simulations are mixed. We see good agreement with SV, CO, and TPR in terms of the slopes predicting the change with tilt, although the simulation results overestimate SV and CO by 20%, and underestimate TPR by 25%. This is likely due to a mismatch in the initial simulation parameters. Further, with blood pressure we see a large deviation from the experimental data.

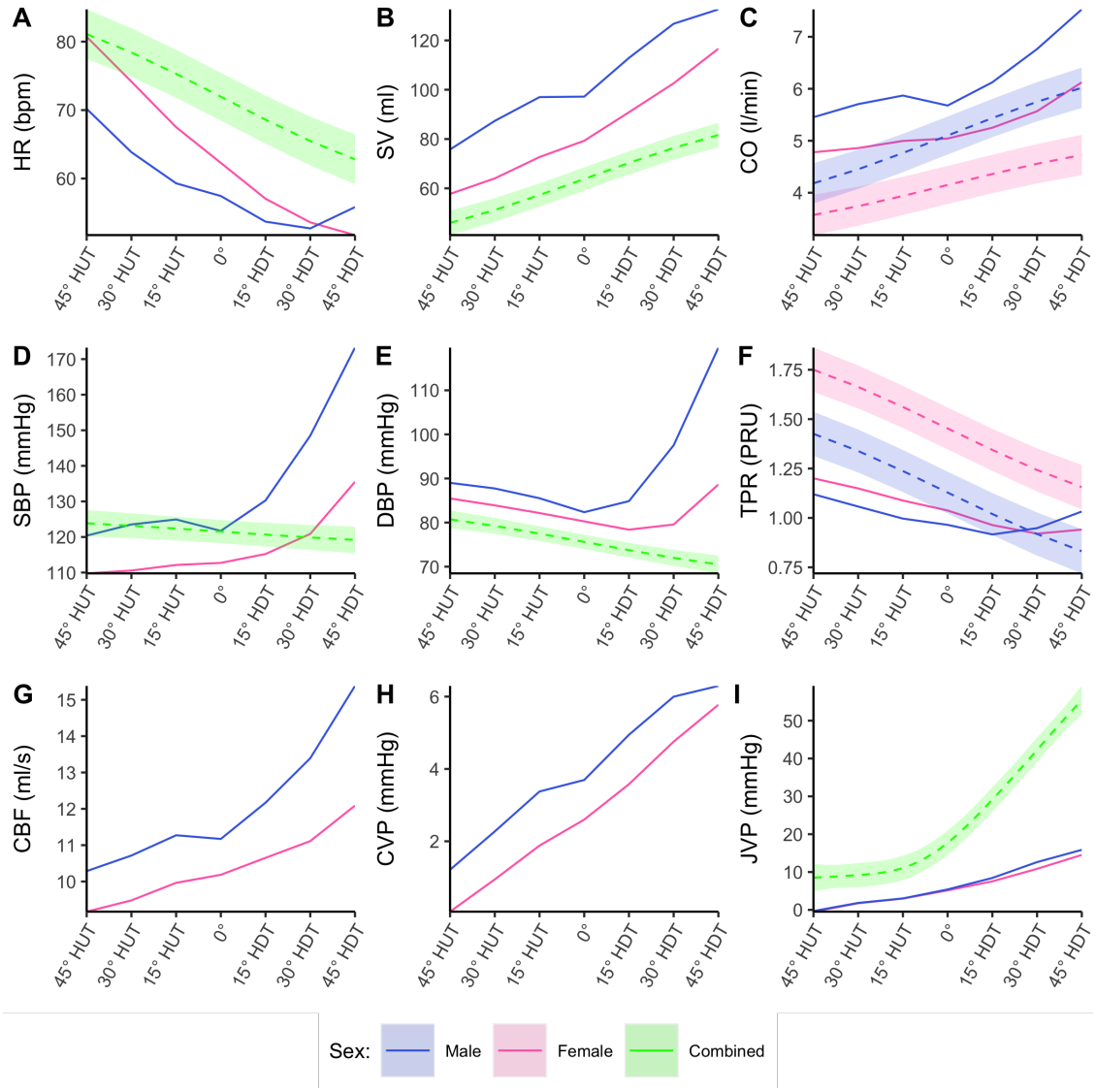

Figure 6.12: **(A-I)** Model outcomes as a function of tilt angle for 50th percentile male (blue) and 50th percentile female (pink) subjects. **(A)** HR, heart rate; **(B)** SV, stroke volume; **(C)** CO, cardiac output; **(D)** SBP, systolic blood pressure; **(E)** DBP, diastolic blood pressure; **(F)** TPR, total peripheral resistance; **(G)** CBF, cerebral blood flow; **(H)** CVP, central venous pressure; **(I)** JVP, jugular venous pressure.

6.5.2.2 Scenario 2: LBNP

Figure 6.13 presents the results of the LBNP simulation. Where relevant (i.e., for all measures except CBF and CVP) the dose-response curves found in Section 5 (MAP ± 89% CrI) are plotted on top of the simulation results.

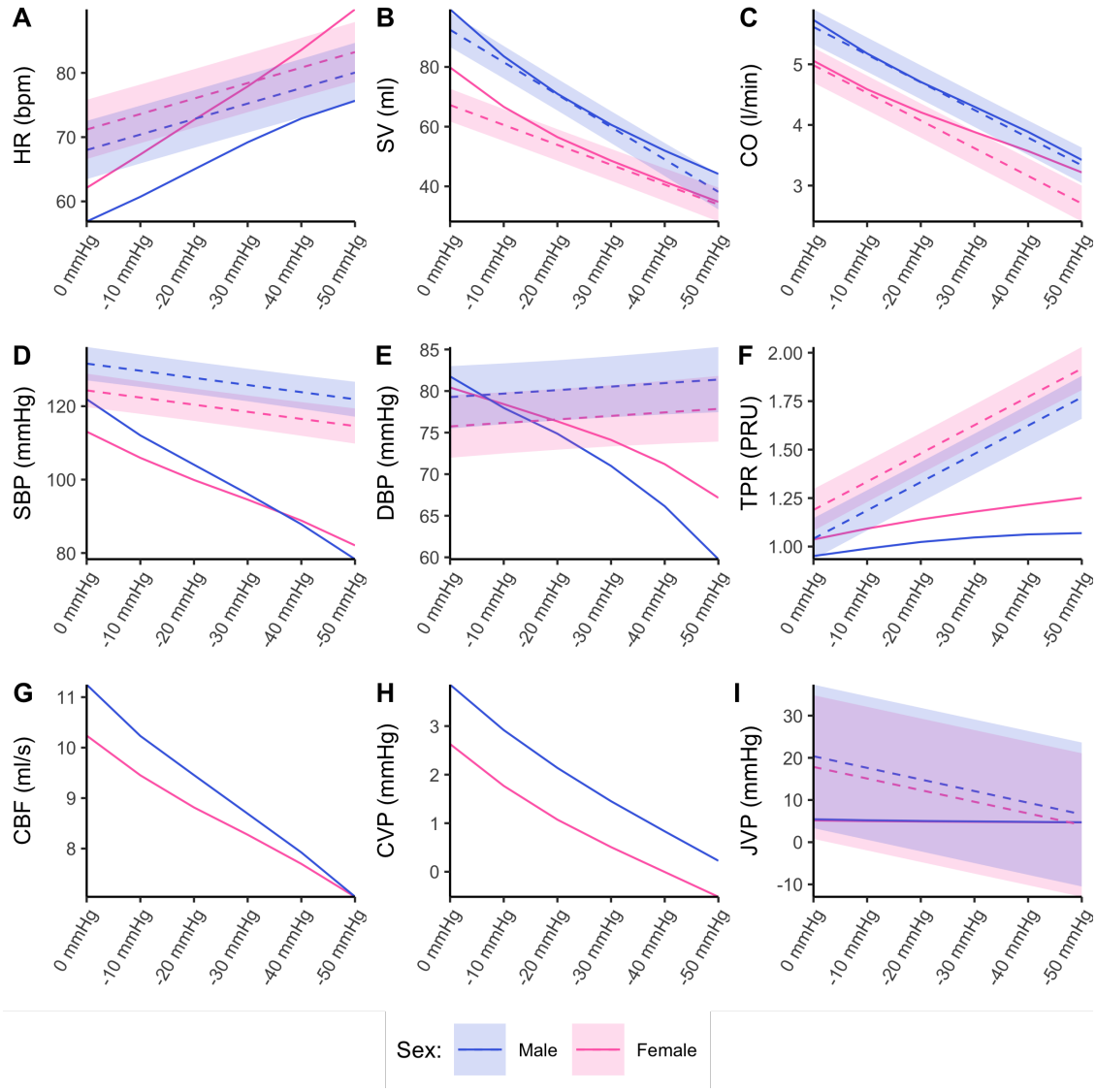

Figure 6.13: **(A-I)** Model outcomes as a function of LBNP for 50th percentile male (blue) and 50th percentile female (pink) subjects. Where appropriate, dose-response curves from Section 5 (MAP ± 89% CrI) are overlayed on the data (dashed line and ribbon). **(A)** HR, heart rate; **(B)** SV, stroke volume; **(C)** CO, cardiac output; **(D)** SBP, systolic blood pressure; **(E)** DBP, diastolic blood pressure; **(F)** TPR, total peripheral resistance; **(G)** CBF, cerebral blood flow; **(H)** CVP, central venous pressure; **(I)** JVP, jugular venous pressure.

The data show excellent agreement with the experimental dose-response curves for HR, SV, and CO. For SV and CO, the model follows almost the exact experimental response. Regarding blood pressure, our experimental data show that SBP decreases slightly whilst DBP is maintained during LBNP. This is in contrast to the simulation results, which predict a steady decrease in both

SBP and DBP. This is likely due to unmodeled systemic regulatory effects in play in addition to the modeled ABR and CPR. The simulation predicts and increase in TPR, but it is significantly underestimated compared to the experimental response. This is likely due to the differences in the blood pressure response, and were blood pressure maintained we would see good agreement between the model and the experimental data.

The model shows a drop in CBF and CVP. We did not measure these variables in our experimental studies, however the predicted values are in good agreement with literature. Hinojosa-Laborde *et al.* recorded a 4 mmHg drop in CVP between 0 and –54 mmHg LBNP in male subjects with CVP reaching 0 mmHg at –54 mmHg LBNP and dropping to –2 mmHg at –71 mmHg LBNP[354]. We see an almost identical response, with CVP falling from 3.9 mmHg at 0 mmHg LBNP to 0.2 mmHg at –50 mmHg LBNP. Regarding CBF, it is difficult to make comparisons as most studies measure cerebral blood velocity (CBV) in one or more major arteries as a surrogate for CBF[492,493]. In one of the few studies that directly measure CBF, Neumann *et al.* found a 14.6% drop in CBF between 0 mmHg and –50 mmHg LBNP[494]. However, this study had a wide dispersion and our modeled decreases of 37.3% in males and 31.2% in females are well within their experimental confidence intervals.

Finally, similarly as for the tilt simulation, the model underestimates the JVP response. The same explanation applies, although it should be noted that the simulation response falls firmly within the Bayesian credible interval across the entire range. Altogether, with the exception of blood pressure and TPR, the LBNP model simulation is an excellent predictor of the experimental dose-response.

6.5.2.3 Scenario 3: SRC

Figure 6.14 presents the model response to short-radius centrifugation. In this simulation, the model behaves as expected up to 1.00g at the center of mass (1.77g at the feet for males and 1.63g at the feet for females). Above 1.00g, systolic and diastolic blood pressure, which are relatively stable until that point, begin to drop rapidly until blood pressure is 12.7/7.1 mmHg at 1.75g (clearly unrealistic). Likewise, CBF hits 0 ml/s at 1.75g. Examining the simulation in

more details shows that at 1.75g, the vasculature in the head branch are entirely collapsed as a result of the low transmural pressures throughout the system (compared to the pressures due to the hydrostatic forces induced by centrifugation). Thus, no blood is flowing through the head branch. This is also observed in the marked increase in TPR at 1.75g, as the autonomic system attempts to maintain systemic blood pressure.

One area in the model that is potentially responsible for this unrealistic response in hypergravity conditions is the blood lost to the interstitial space, V_{int}. The instantaneous value is set by a transfer function built around an RC circuit with a time-constant of 276 s, however the maximum value is defined in Table 6.3 as:

$$V_{max} = \frac{700}{\sin(85^\circ)} \frac{(d + r_{i_{10}})\,\omega^2}{g_E} \tag{6.38}$$

such that V_{int} is given by:

$$V_{int}(t) = \mathcal{L}^{-1}\left\{\frac{1}{276s + 1}\right\} * V_{max}(t) \tag{6.39}$$

where $*$ is a convolution. The instantaneous value V_{max} was originally defined empirically by Zamanian[185] and Diaz-Artiles[120] based on experimentation using the Massachusetts Institute of Technology (MIT) Compact Radius Centrifuge, which has a maximum radius of 1.4 m. In the validation experiments, the subject was in a seated position with their feet 1.09 m from the center of rotation, with a maximum exposure level of 1.4g *at the feet*[120]. In this scenario a 50$^{\text{th}}$ percentile male subject would only experience 1.01g at the center of mass. V_{max} was set such that 700 ml of blood would be lost at a speed generating 0.996g at the liver (equivalent to an 85° HUT). Thus, the model has not been validated in hypergravity conditions.

In order to validate the model in hypergravity conditions, first it is necessary to collect experimental data against which to compare the model. This was precluded in this study by the unavailability of a human rated centrifuge, and is discussed in Sections 7.2.1 and 7.2.2. Based on the centrifuge experimental data, it may be necessary to adjust certain parameters in the model

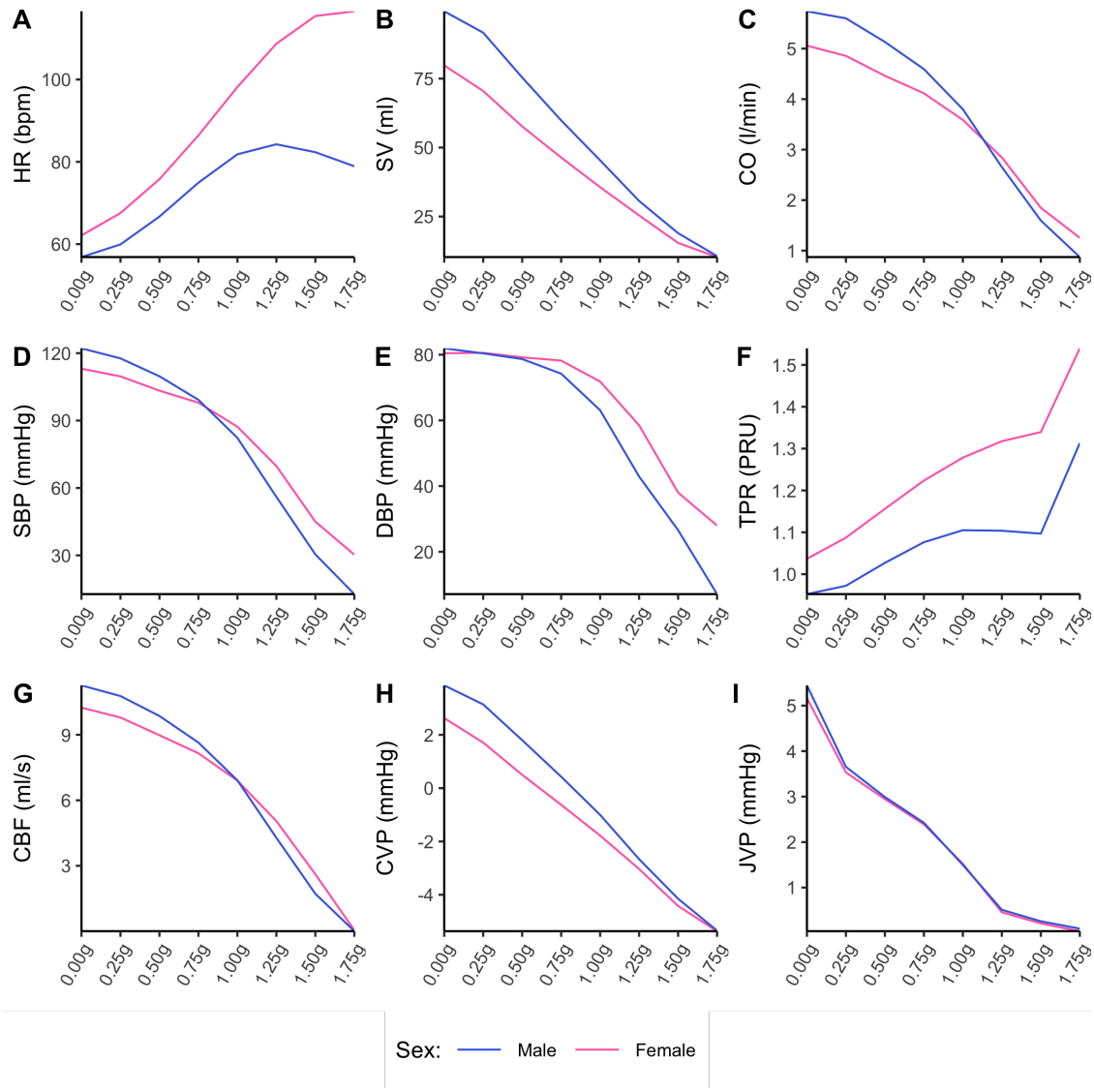

Figure 6.14: **(A-I)** Model outcomes as a function of short-radius centrifugation for 50th percentile male (blue) and 50th percentile female (pink) subjects. The x-axis presents g-level at the subject's center of mass, g_{CoM}. **(A)** HR, heart rate; **(B)** SV, stroke volume; **(C)** CO, cardiac output; **(D)** SBP, systolic blood pressure; **(E)** DBP, diastolic blood pressure; **(F)** TPR, total peripheral resistance; **(G)** CBF, cerebral blood flow; **(H)** CVP, central venous pressure; **(I)** JVP, jugular venous pressure.

to account for changes in circulating blood volume with centrifugation. It is likely that the value of V_{max} should be altered. Second, even with adjusted model parameters, the model architecture may not accurately represent the physiology of a hypergravity spin. In high-performance aviation, pilots use a mixture of technology (e.g., anti-g pants, positive pressure regulators) and techniques

(e.g., an anti-g straining maneuver, AGSM) to increase systemic vascular resistance, raise intrathoracic pressure, and maintain cerebral blood flow during high-g maneuvers. Since this is the first time that the model has been used in hypergravity conditions, it may be necessary to model some of these effects. For example we could model an AGSM as an increase in P_{th} in hypergravity. Finally, as discussed in Section 6.4.1, the model does not currently incorporate any of the cerebral autoregulation mechanisms. Adding these mechanisms may help to maintain cerebral blood flow, but would do little to influence overall SBP/DBP.

6.5.2.4 Scenario 4: Change in Gravity Level

Figure 6.15 presents the model response to reducing gravity from 1g to microgravity through Martian and Lunar gravity. The simulation is repeated twice, once with the subjects in a supine position, and once in a standing position. In 1g, whilst supine there is an effect of tissue weight but no effect of vascular length, whilst the opposite is true in a standing position.

Figure 6.15 shows that the model now correctly follows the expected response to entry to microgravity. In particular, our data closely match Norsk *et al.*[466] who noted that CO in spaceflight was decreased slightly (nonsignificant) from a supine position but increased significantly by 1.0 l/min from seated ($p = 0.021$). This closely matches the increase we see of 1.2 l/min in male subjects. Similarly, Norsk *et al.* noted a nonsignificant increase in TPR from supine to microgravity, but a significant decrease from standing to microgravity of 2.5 mmHg.min/l (equivalent to 0.15 PRU). Again this is similar to the reduction we find of 0.27 PRU in males and 0.25 PRU in females. The data from Norsk *et al.* is presented in Figure 6.16 for comparison.

Importantly, we can now capture the correct trend in CVP: a decrease in spaceflight compared to the terrestrial supine position[3] whilst heart rate remains relatively constant[495]. This demonstrates that, even with the very rough estimates for body radius in Table 6.12, the body weight augmentations to the model are effective at capturing the effects of microgravity. This supports the conclusions of Lan *et al.* and Buckey *et al.* on the importance of tissue weight[50,95]. By incorporating our standalone ocular model into the complete lumped-parameter model, future work will enable us to draw more conclusions as to the influence of body weight on IOP and OPP.

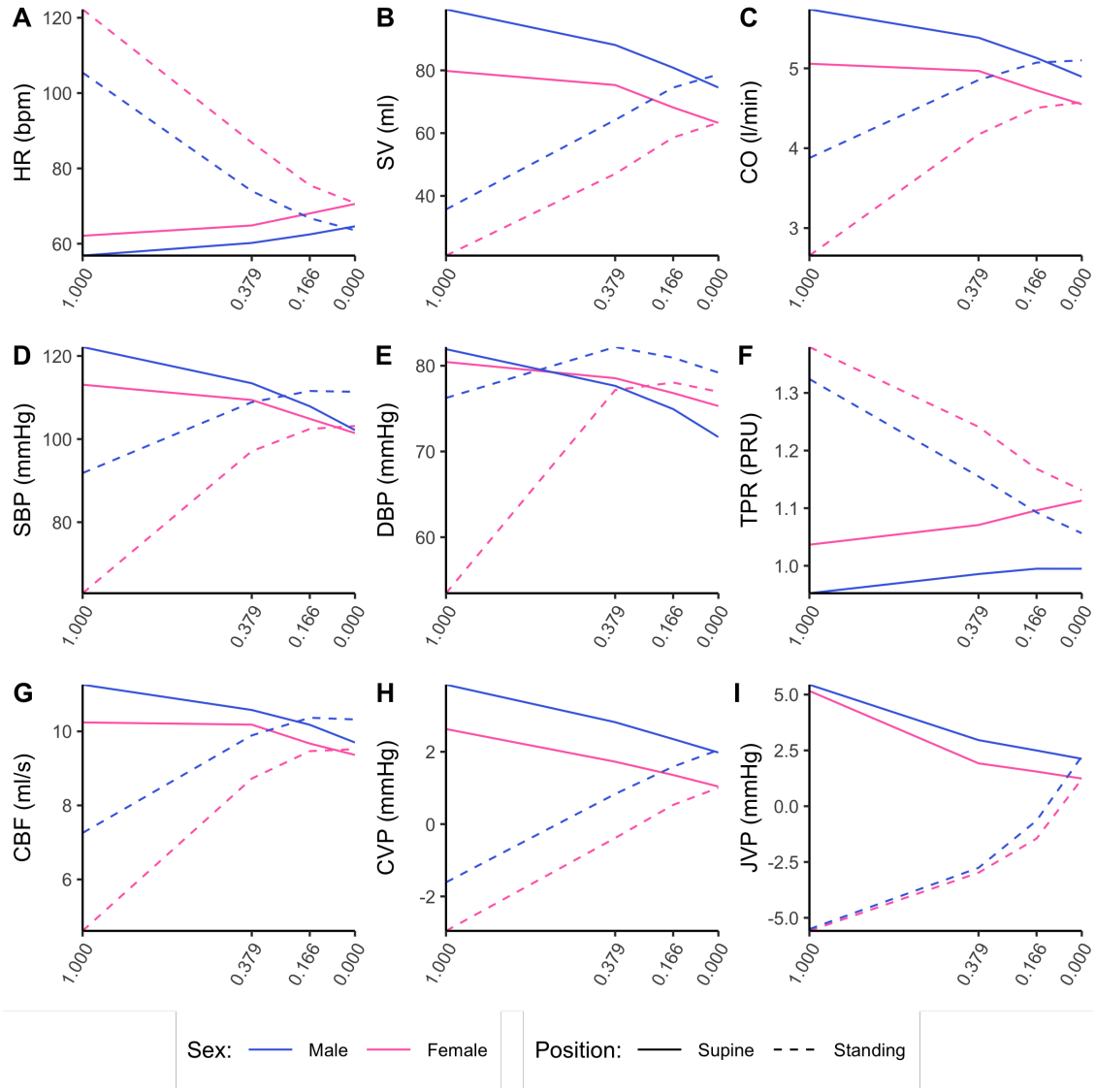

Figure 6.15: **(A-I)** Model outcomes as a function of gravitational field strength for 50th percentile male (blue) and 50th percentile female (pink) subjects in supine (solid) and standing (dashed) postures. The x-axis represents gravitational field strength in Earth-g, with marks at Lunar (0.166g) and Martian (0.379g) gravity levels. **(A)** HR, heart rate; **(B)** SV, stroke volume; **(C)** CO, cardiac output; **(D)** SBP, systolic blood pressure; **(E)** DBP, diastolic blood pressure; **(F)** TPR, total peripheral resistance; **(G)** CBF, cerebral blood flow; **(H)** CVP, central venous pressure; **(I)** JVP, jugular venous pressure.

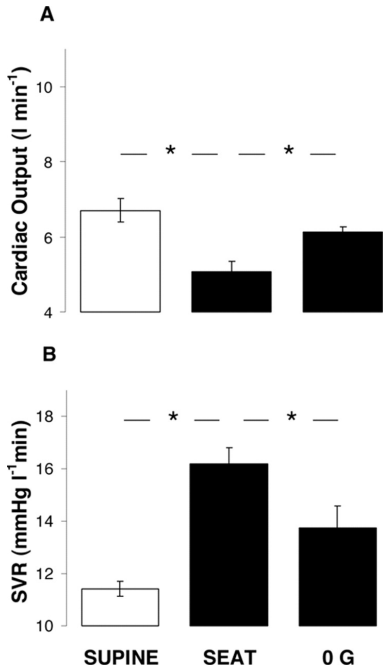

Figure 6.16: **(A-B)** Data reproduced from Norsk *et al.*[466] showing cardiac output and systemic vascular resistance (cf. TPR) in spaceflight compared to preflight measurements in the supine and seated positions. **(A)** cardiac output, **(B)** systemic vascular resistance. Image modified from Norsk *et al.*[466].

6.5.2.5 Scenario 5: Ocular Model in Tilt

For the final simulation we use the standalone ocular model. The simulation outputs are IOP and OPP (calculated using Equation 4.4). As discussed in Section 6.5.1.1, for this validation scenario we use the experimental data collected in Section 4.6. Figure 6.17 presents the model outputs overlaid on the experimental data collected for IOP (Figure 4.16, Figure 6.17A) and OPP (Figure 4.15, Figure 6.17B).

Three parameters were used to fit the lumped parameter model to the experimental data: MAP_{eye}; h, the mean distance from the aortic root to eye level along the mid-coronal plane; and h_1, the mean perpendicular distance from the mid-coronal plane to the globe. Model fit was assessed by comparing normalized squared residuals from the experimental data with a reduced chi-square statistic $\chi^2_{red} \approx 1$ with $p > 0.05$ indicating good fit. The resulting value of $\chi^2_{red}(532) = 1.04$, $p = 0.254$ indicates an excellent fit to the experimental data as can be seen in Figure 6.17. The

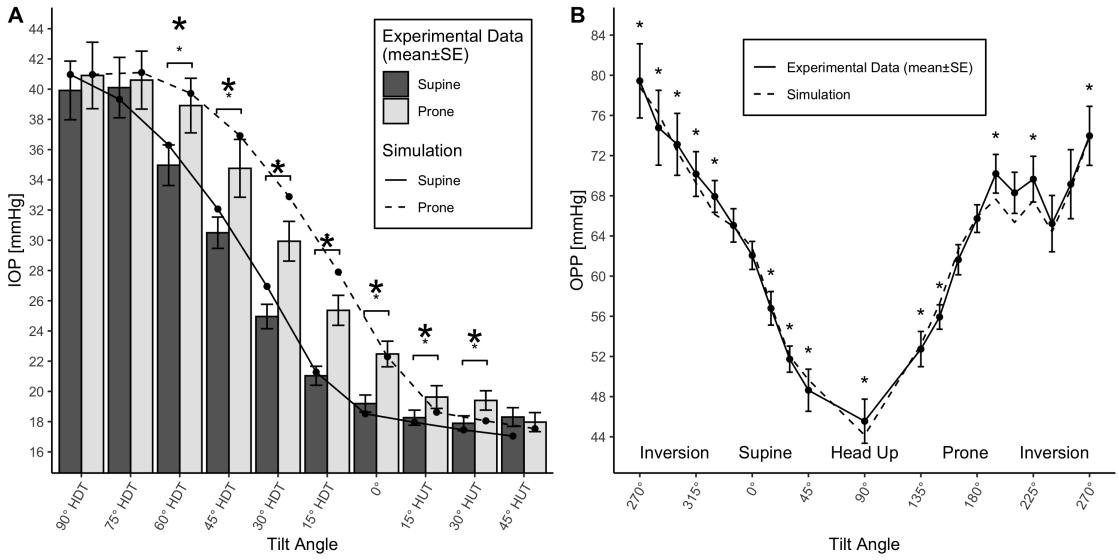

Figure 6.17: **(A-B)** Simulation outputs for the standalone ocular model compared to the experimental data collected in Section 4.6 and presented in Figures 4.15 and 4.16. **(A)** IOP, **(B)** OPP.

original model by Nelson *et al.*[24], was more recently validated using a set of 36 studies measuring the effect of postural changes on IOP with good result[488]. Our additions to the model and the design of our experiment bring two additional contributions. First, we validate the range of the model across the entire 360° orientation space using a single dataset including 13 subjects. Second, our addition of the secondary hydrostatic column in the G_x plane allows the model to capture the differences between prone and supine posture, extending the use cases and predictive power.

6.5.3 Limitations

Computational modeling is not without limitations, many of which have already been addressed in Section 6.3.4.5. Related specifically to the model development that we have presented in Section 6.4, the limitations are presented below.

First, the model does not include any specific cerebral autoregulation. Cerebral autoregulation is a highly complex mechanism involving the complex interaction of four separate processes: myogenic, neurogenic, endothelial, and metabolic[496]. Much is still unknown about these mechanisms, and the relative influence of each is controversial[497]. In the current model it is not possible to directly incorporate the endothelial and metabolic processes as we do not currently model blood gas

concentrations[209]. We note that, even without this extra control system, the model performs well in tilt, LBNP, and microgravity maintaining CBF within a reasonable range, although jugular venous pressure is underestimated in HDT. The key area where it appears that this additional autoregulation would be required is in high speed SRC, where the equivalent gravity in greater than Earth (i.e., hypergravity conditions). Without experimental data to compare the model against for this simulation it is difficult to determine the magnitude of the regulation that should be included. For these simulations it may be necessary to incorporate additional effects of hypergravity including things like AGSM and changes in intrathoracic pressure.

Second, in any modeling effort parameter assignment is a critical part of the model development that is highly dependent on the literature sources chosen. Many parameters in a lumped-parameter model cannot be directly measured and must be estimated from a range of sources including but not limited to animal studies and supplementary data from studies where the variable is not the variable of interest. In the original model development, Heldt did an excellent job of assigning the baseline model parameters[168]. We have attempted to follow his example in assigning parameters for the new branches of the model developed, but every single parameter could be argued differently. The criticality of parameter assignment is somewhat offset by the performance of a comprehensive sensitivity analysis, such as the one presented in Section 6.3. However it should be noted that we performed this sensitivity analysis on the baseline model prior to any model development. Future work should apply this same methodology to the updated model in order to determine the sensitivity of the new parameters.

Third, modeling gives us access to so much data that it is not practical to present every variable measured in every scenario. This is further complicated by the ability to vary the input parameters to represent different subjects. The simulations captured the output of 150 direct variables from the model (including the pressures, volumes, and flows for all compartment) as well as many other derived quantities. For ease of comparison between the scenarios, we elected to present the same 9 variables for each simulation, and to use the same two subjects (an idealized 50^{th} percentile male and female) in order to provide an overall picture of the cardiovascular response. On closer

inspection, it may become apparent that certain aspects of the model do not behave as they should and must be adapted. However, it is clear from the data presented that overall, the models largely behave as expected.

Finally, we created our idealized subjects by modifying only a small subset of the input parameters based on height and total blood volume. As the data from Sections 4 and 5, as well as literature, show, there are deeper physiological differences between males and females that could further be incorporated into creating male and female subjects. In particular, the sensitivity analysis highlighted the influence of the heart and lungs parameters, which we elected not to change in these subject simulations. Overall, based on the limited number of parameters we do change, the simulations capture the differences between males and females well, as shown by the general agreement with the dose-response curves for tilt and LBNP.

6.6 Summary of Modeling

In this Section we augmented an existing lumped-parameter model in order to incorporate (1) a separate branch for cephalad blood flow, (2) a simulation of the effects of body weight, and (3) the effects of head-down tilt. We further developed a standalone ocular model that can account for the effects of posture in simulations of IOP. Using the baseline model, we conducted a comprehensive sensitivity analysis using a LHS-PRCC methodology in order to determine which parameters have the most influence on model outcomes. Having developed the models and assigned parameters from a combination of literature and our experimental data, we conducted five short validation studies testing the systemic model on 50^{th} percentile males and females in tilt, LBNP, SRC, and microgravity, and the ocular model in 360° of tilt. Simulation results show that: (1) the updated model can capture the effects of microgravity well; (2) the systemic lumped-parameter model is able to effectively recreate the dose-response curves from tilt and LBNP in most parameters, although underestimates jugular venous pressure in HDT; (3) the model is able to predict the effects of SRC but does not capture hypergravity conditions well (i.e., when $g_{CoM} > 1\text{g}$); and (4) the ocular model is able to accurately predict IOP and OPP across a full 360° range of tilt angles. This model development expands our understanding of the cardiovascular effects of altered-gravity

by allowing us to measure the pressures, volumes, and flows throughout the body rather than just overall systemic measurements. Theoretically we could use these models to construct dose-response curves for every compartment in the model.

7. CONCLUSION

Future exploratory class spaceflight will require development of new countermeasures in order to counteract the effects of cardiovascular deconditioning and reduce the risk of SANS and VTE. LBNP and short-radius centrifugation are promising countermeasures for reducing the cephalad fluid shift; however, we still do not have a complete understanding of the dose-response of the cardiovascular system to altered-gravity or to differing levels of LBNP/SRC. This research effort aimed to generate the acute dose-response curves for the CV system in graded tilt as a terrestrial analog for altered-gravity, and LBNP. These results provide a baseline from which to investigate protocols for long-duration use.

Three specific areas were targeted, using complementary methods. In Section 4 we developed comprehensive dose-response curves for the acute cardiovascular response to graded head-up and head-down tilt. In Section 5 we used a different statistical approach to develop dose-response curves for the cardiovascular response to lower body negative pressure as a potential spaceflight countermeasure, using the power of Bayesian modeling to draw additional insights from the relationships between measured variables. Finally, in Section 6 we used a modeling approach to support the conclusions derived experimentally and expand our scenarios to consider short-radius centrifugation as an alternative countermeasure as well as capture specific changes related to an external gravity field. The specific aims and hypotheses tested in this dissertation are reproduced below:

1. To empirically investigate the acute cardiovascular response to graded head-up and head-down tilt. In particular, the specific objectives are:

    1.1 To generate dose-response curves for cardiovascular parameters, including the systemic circulation, the autonomic response, and head and neck hemodynamics over the range 45° head-up tilt (HUT) to 45° head-down tilt (HDT).

    - *Hypothesis 1.1: Systemic hemodynamics will follow an approximately linear re-*

sponse to HUT and HDT in the range observed. The response of the autonomic system and head/neck will be non-linear.

1.2 To quantify the differences between the supine (face-up) and prone (face-down) response to graded tilt as an analog to consider the influence of body weight on cardiovascular hemodynamics.

- *Hypothesis 1.2: Altered body positioning will influence cardiovascular response. In particular, the additional pressures due to body weight on the thoracic cavity in the prone position will impair baroreflex function and venous return.*

1.3 To quantify the difference between the male and female response to graded tilt.

- *Hypothesis 1.3: Anthropometric considerations will be the principal driving force between differences between males and females in cardiovascular response.*

2. To empirically investigate the acute cardiovascular response to graded lower body negative pressure (LBNP). In particular, the specific objectives are:

2.1 To generate dose-response curves for cardiovascular parameters, including the systemic circulation, the autonomic response, and head and neck hemodynamics over the range 0 mmHg to –50 mmHg of LBNP.

- *Hypothesis 2.1: Systemic hemodynamics will follow an approximately linear response to graded LBNP. The response of the autonomic system and head/neck will be non-linear..*

2.2 To quantify the multivariate relationship between systemic, autonomic, and head/neck cardiovascular parameters in graded LBNP.

- *Hypothesis 2.2: Cardiovascular variables should not be considered in isolation. In particular, a network structure exists between the parameters and latent subject characteristics (for example body weight) such that there is a relationship connecting all of the variables.*

2.3 To quantify the difference between the male and female response to graded LBNP.

- *Hypothesis 2.3: Anthropometric considerations will be the principal driving force between differences between males and females in cardiovascular response.*

3. To develop a cardiovascular model to capture the effects of tilt, LBNP, short-radius centrifugation (SRC), and microgravity on cardiovascular hemodynamics. In particular, the specific objectives are:

   3.1 To expand an existing cardiovascular model to incorporate detailed modeling of blood flow through the head and eyes.

   3.2 To incorporate the effects of tissue weight into a cardiovascular model in order to determine the influence of its removal in microgravity on cardiovascular hemodynamics.

   3.3 To validate the cardiovascular model with dose-response curves generated from experimental measurements of subjects in tilt and LBNP.

   3.4 To investigate the effects of SRC and microgravity on representative subjects.

A summary of the results, main conclusions, contributions, and associated publications is presented in Section 7.1 below, along with suggestions for further research in Section 7.2.

7.1 Summary and Contributions

The first experimental study exposed 12 male subjects to a graded tilt profile in the range 45° HUT to 45° HDT whilst obtaining measurements of systemic hemodynamics, autonomic response, and head/neck parameters. From these measurements dose-response curves were generated *(Aim 1.1)*. These dose-response curves followed a linear structure for the systemic hemodynamics, a generalized linear form for the autonomic response, and a highly non-linear form for the head and neck *(Hypothesis 1.1 confirmed)*. The study was repeated twice, once in the supine position and once in the prone position, and the generated dose-response curves captured the effect of compression of the thorax in the prone position *(Aim 1.2)*, inhibiting baroreflex function, increasing

sympathetic activity, and raising central venous pressure *(Hypothesis 1.2 confirmed)*. In an addendum to the study, we subsequently performed the same experiment of 12 female subjects *(Aim 1.3)*. Thus, we were able to construct dose-response curves capturing the sex-dependent difference in the cardiovascular response *(Hypothesis 1.3 confirmed)*.

The second experimental study exposed 24 subjects (12 male, 12 female; most previously participated in Experiment 1) to graded LBNP in the range 0 mmHg to –50 mmHg. We measured the same set of cardiovascular parameters along with two additional measurements related to jugular vein flow pattern and carotid artery flow velocity. We adopted a Bayesian workflow to construct a single multivariate dose-response model *(Aim 2.1)*, which took a linear form for all variables considered *(Hypothesis 2.1 partially confirmed)*. The use of a single multivariate regression model allowed us to construct a network diagram for the relationship between the cardiovascular measures as well as subject characteristics *(Aim 2.2)*. The network structure revealed an association structure between most of the cardiovascular variables and highlighted some previously unforeseen linkages such as the association between Age and A_{IJV} *(Hypothesis 2.2 confirmed)*. Unexpectedly, there was no association between IOP and body weight. From the dose-response model, we were able to extract the effect sizes of the sex difference *(Aim 2.3)*, as well as the effect of posture. As expected, anthropometric considerations were the principal driver between male and female differences, although there remained an effect of sex even in some indexed variables (e.g., SI) *(Hypothesis 2.3 partially confirmed)*. From the effect size of position (0° vs. 15° HDT), we were able to predict the strength of LBNP required to "correct" the effect of a headward fluid shift in each variable.

Finally, the computational approach involved the expansion and further development of an existing cardiovascular lumped-parameter model. We added a new branch to the model allowing simulation of cephalad blood flow. This was augmented by a standalone eye model with the ability to capture supine vs. prone differences in tilt *(Aim 3.1)*. We further added a simulation of tissue weight to each compartment in the model. This addition enabled the model to correctly replicate the effects of microgravity, in particular with relation to the direction of the change in CVP with

respect to HDT *(Aim 3.2)*. We simulated the augmented model using four scenarios: tilt, LBNP, SRC, and a gravity change *(Aim 3.3)*. Further, we validated the standalone eye model using a simulation of 360° of tilt. In the cases of tilt and LBNP, the models accurately replicated the dose-response curves for some of the variable measured; however, it underestimated others (for example jugular venous pressure in HDT) *(Aim 3.4)*. Finally, in the SRC simulations, the model performed well up to 1.00g at the center of mass, but was unable to maintain cerebral blood flow in hypergravity simulations, likely due to missing autoregulation in the head loop.

7.1.1 List of Associated Publications

7.1.1.1 Journal Articles

1. Whittle RS, Diaz-Artiles A. Gravitational effects on jugular and carotid characteristics in graded head-up and head-down tilt. *J Appl Physiol*. 2023;134:217–229. doi: 10.1152/japplphysiol.00248.2022.[187]

2. Whittle RS, Keller N, Hall EA, Vellore HS, Stapleton LM, Findlay KH, Dunbar BJ, Diaz-Artiles A. Gravitational dose response curves for acute cardiovascular hemodynamics in a tilt paradigm. *J Am Heart Assoc*. 2022;11:e024175. doi: 10.1161/JAHA.121.024175.[186]

3. Petersen LG, Whittle RS, Lee JH, Sieker J, Carlson J, Finke C, Shelton CM, Petersen JCG, Diaz-Artiles A. Gravitational effects on intraocular pressure and ocular perfusion pressure. *J Appl Physiol*. 2022;132:24–35. doi: 10.1152/japplphysiol.00546.2021.[1]

4. Whittle RS, Stapleton LM, Petersen LG, Diaz-Artiles A. Indirect measurement of absolute cardiac output during exercise in simulated altered gravity is highly dependent on the method. *J Clin Monit Comput*. 2022;36:1355–1366. doi: 10.1007/s10877-021-00769-y.[126]

5. Whittle RS, Diaz-Artiles A. Modeling individual differences in cardiovascular response to gravitational stress using a sensitivity analysis. *J Appl Physiol*. 2021;130:1983–2001. doi: 10.1152/japplphysiol.00727.2020.[188]

7.1.1.2 Conference Papers

1. Whittle RS, Diaz-Artiles A. Metabolic Modeling in Altered Gravity. In: *IEEE Aerospace Conference*. Big Sky, MT. 2020; 1–17. doi: 10.1109/AERO47225.2020.9172582.[209]

7.1.1.3 Oral Papers

1. Diaz-Artiles A, Whittle RS. Quantification of the internal jugular vein characteristics during fluid shift induced by lower body negative pressure. In: *International Society of Gravitational Physiology Meeting*. Antwerp, Belgium. 2023.

2. Whittle RS, Dunbar BJ, Diaz-Artiles A. Acute dose-response of the internal jugular vein to graded head up and head down tilt. *Aerosp Med Hum Perform*. 2023;94:327.[498]

3. Hall EA, Whittle RS, Diaz-Artiles A. Effect of lower body negative pressure on ocular perfusion pressure. *Aerosp Med Hum Perform*. 2023;94:311.[499]

4. Whittle RS. Quantifying and modeling the acute cardiovascular response to altered-gravity and spaceflight countermeasures. In: *2022 Rising Stars in Aerospace Symposium*. Boulder, CO. 2022; 1–14.[500]

5. Whittle RS, Keller N, Hall EA, Vellore HS, Stapleton LM, Findlay KH, Dunbar BJ, Diaz-Artiles A. Hemodynamic and autonomic response of the cardiovascular system to tilt: gravitational dose-response curves. In: *NASA Human Research Program Investigators Workshop*. Virtual. 2022; 1–32.[501]

6. Whittle RS, Petersen LG, Lee JH, Sieker J, Petersen JCG, Diaz-Artiles A. Modeling changes in intraocular pressure associated with the physiological response to changes in the gravitational vector. *Aerosp Med Hum Perform*. 2021;92:512.[502]

7. Whittle RS, Keller N, Stapleton LM, Hall EA, Dunbar BJ, Diaz-Artiles A. Acute gravitational dose-response curves in hemodynamic and ocular variables induced by tilt. In:

Proceedings of the 2021 International Society of Gravitational Physiology (ISGP) Meeting, edited by Bagher P, Bloomfield S, Diaz-Artiles A, Custaud MA. 2021; 234–239. doi: 10.3389/978-2-88971-011-9.[503]

7.1.1.4 Posters

1. Whittle RS, Keller N, Dunbar BJ, Diaz-Artiles A. Sex differences in cardiovascular response to lower body negative pressure. In: *poster session presented at the NASA Human Research Program Investigators Workshop*. Galveston, TX. 2023; 1.[504]

2. Diaz-Artiles A, Whittle RS, Keller N, Hall EA, Dunbar BJ. Predicting acute cardiovascular and ocular changes due to tilt, LBNP, and centrifugation: Status report and next steps. In: *poster session presented at the NASA Human Research Program Investigators Workshop*. Galveston, TX. 2023; 1.[505]

3. Whittle RS, Real Fraxedas F, Keller N, Dunbar BJ, Diaz-Artiles A. Quantifying the cardiovascular response to fluid shifts induced by graded lower body negative pressure (LBNP). In: *poster session presented at the American Society for Gravitational and Space Research (ASGSR) 2022 Meeting*. Houston, TX. 2022; 1.[506]

4. Diaz-Artiles A, Whittle RS, Real Fraxedas F, Hall EA, Vellore HS, Dunbar BJ. Gravitational dose-response curves during tilt, LBNP, and centrifugation. In: *poster session presented at the NASA Human Research Program Investigators Workshop*. Virtual. 2022; 1.[507]

5. Real Fraxedas F, Whittle RS, Diaz-Artiles A. Modeling gravitational dose-response curves during tilt, LBNP, and centrifugation. In: *poster session presented at the NASA Human Research Program Investigators Workshop*. Virtual. 2022; 1.[508]

6. Diaz-Artiles A, Whittle RS, Stapleton L, Keller N, Dunbar BJ. Predicting acute CV and ocular changes due to changes in the gravitational vector. In: *poster session presented at the NASA Human Research Program Investigators Workshop*. Virtual. 2021; 1.[509]

7. Whittle RS, Diaz-Artiles A. A multidisciplinary approach to characterizing the long duration impact of hypogravity exposure on the cardiovascular system. In: *poster session presented at the NASA Human Research Program Investigators Workshop*. Galveston, TX. 2020; 1.[510]

8. Lee J, Whittle RS, Diaz-Artiles A, Sieker J, Petersen JCG, Petersen LG. Gravitational effects on ocular perfusion pressure. In: *poster session presented at the NASA Human Research Program Investigators Workshop*. Galveston, TX. 2020; 1.[511]

9. Whittle RS, Diaz-Artiles A. Understanding cardiovascular changes on long duration spaceflight. In: *poster session presented at Paving the Road to Living in Space: Asgardia's First Space Science and Investment Congress*. Darmstadt, Germany. 2019; 1.[512]

10. Whittle RS, Alonso DA, Diaz-Artiles A. Individual differences in cardiovascular responses to orthostatic stress. In: *poster session presented at the NASA Human Research Program Investigators Workshop*. Galveston, TX. 2019; 1.[513]

7.2 Suggestions for Further Research

This section contains some suggestions for future research based on this work.

7.2.1 Further Experimental Studies

In the experimental portion of this research effort, dose-response curves were generated for two separate interventions: tilt and LBNP. As discussed, the tilt study provides a baseline from which to compare the efficacy of various countermeasures, whilst also having terrestrial use cases. LBNP is a potential countermeasure to mitigate multiple degrading effects of spaceflight and our dose-response curves enhance the understanding of the levels that should be targeted for different protocols. Below, we detail one further study and two measurement enhancements that could be incorporated into future work:

- **Short-radius centrifugation:** In Section 6 we incorporated a simulation of the effects of short-radius centrifugation on cardiovascular function. The Texas A&M University Aerospace Engineering Centrifuge is currently under construction. Once complete, this will allow us

to experimentally conduct the protocol described in Table 6.15. This procedure should be performed, ideally using the same subjects as were used in the experiments described in Sections 4 and 5. This would allow dose-response curves for SRC to be constructed in the same manner as they have been for tilt and LBNP. The Bayesian workflow presented in Section 5 could be used for this in order to capture the relationships between the measured variables.

- **Measurement of total blood volume changes:** Orthostatic stress (tilt, LBNP, or centrifugation) alters the amount of blood in circulation. In addition, one of the early effects of entry to microgravity is a reduction in circulating blood volume mediated via the RAAS system due to the cephalad fluid shift[5]. In our cardiovascular model we capture this effect through flow into two interstitial compartments (one for the upper body and one for the lower body). Future experimental studies should measure the circulating blood volume during the course of orthostatic interventions in order to determine the accuracy of the modeling. One method of performing this measurement would be using an abbreviated carbon monoxide (CO) rebreathing method (aCORM), which has been validated in multiple studies[514–516].

- **Noninvasive measurement of intracranial pressure changes:** During our experimental studies into tilt and LBNP, we were able to capture multiple metrics related to the head and neck. These included IOP, OPP, A_{CCA}, A_{IJV}, IJVP, IJVF, PSV, and EDV. One important omission was a measurement of ICP. It has been noted throughout this work that a measurement of ICP is important for understanding the complete hemodynamic picture of the head. Unfortunately, ICP is a very difficult measurement to accurately capture, particularly using a non-invasive method. Previous work by Petersen *et al.* captured ICP using invasive methods in subjects with pre-existing conditions that allowed measurement through an Ommaya reservoir or similar[88]. Noninvasive techniques to measure ICP are in existing, although with varying accuracy. Khan *et al.*[517] provide a review of existing modalities. Of the 15 techniques they examine, they highlight optic nerve sheath diameter (ONSD) and pupillometry as the two most promising methods. These, and other methods, should be further investi-

gated to determine whether they could be incorporated into future experimental studies.

7.2.2 Further Modeling Analysis

The modeling analysis performed in this research effort significantly enhanced the existing capabilities of the lumped-parameter cardiovascular model through (1) the addition of a head and neck branch to the model (2) allowing the accurate simulation of head-down tilt, and (3) incorporating the effects of body weight. However, below are listed some further improvements to the model that could be incorporated into future work:

- **Incorporating the eye model into the systemic model:** The current model architecture comprises two separate models, a systemic model and a standalone ocular model. The next stage of work is to incorporate this standalone ocular model into the complete model of the systemic circulation. Whilst the standalone model is very effective at predicting ocular changes in tilt[1], this extension would allow for more complex simulations of IOP and OPP. In particular, this would be a useful step to comparing our experimental findings from Section 5. It would also allow us to predict ocular changes in SRC prior to the completion of the Texas A&M Aerospace Engineering Centrifuge and validation of the systemic modeling results for SRC.

- **Incorporating a model of ICP:** At present, the lumped-parameter model uses a highly simplified model of intracranial pressure, keeping it at a fixed value of 10 mmHg. In reality, ICP has a postural dependence and can also be influenced by external manipulation such as LBNP[88]. More comprehensive simulations of ICP could be incorporated into the model, for example those used by Lan *et al.*[95], Fois *et al.*[518], or Ursino and Giannessi[519].

- **Incorporating cerebral autoregulation:** Similar to the ICP above, at present cerebral autoregulation is only performed with the existing control loops representing the arterial baroreflex and the cardiopulmonary reflex. As observed in Section 6, this works well in hypogravity conditions, but begins to perform poorly in hypergravity. This was most clearly

observed during the SRC simulations when $g_{CoM} > 1\mathrm{g}$. In reality, the additional cerebral autoregulation mechanisms (myogenic, neurogenic, endothelial, and metabolic) should engage in these hypergravity conditions in order to maintain cerebral blood flow within a normative range. Cerebral autoregulation is difficult to model in a mechanistic, bottom-up fashion as we have done for the arterial baroreflex and cardiopulmonary reflex, since there is still much unknown about the relative influence of the specific mechanisms. However, by incorporating methods similar to those found in Ursino and Giannessi[519], it should be possible to better maintain CBF in hypergravity scenarios.

- **Understanding the underestimate of jugular venous pressure in head-down tilt:** In Section 6 it was noted that, whilst the head branch generally performs well, it tends to underestimate jugular venous pressure in a head-down tilt scenario. Further work should focus on understanding why this occurs, and correcting as necessary in order to rectify the model and allow it to better follow the dose-response curves developed in Sections 4 and 5.

- **Incorporating long duration changes:** The current model is limited to simulation of acute changes. As discussed in Section 2, in reality chronic effects play an important role in cardiovascular degradation during spaceflight. Further, for the development of countermeasures it is vital to understand the effects of potential protocols such as LBNP or SRC on a deconditioned CV system. Experimental studies such as long duration HDTBR can allow us to simulate protocols on deconditioned physiology. However, there is utility in a predictive model to understand the changes in the cardiovascular system during long duration spaceflight. Modeling efforts have had some success in this area already, for example Gallo *et al.*[178]. In Whittle and Diaz-Artiles[512], we outlined how the model could be adapted to incorporate chronic changes by creating a separate 'long duration' loop, which would alter the baseline parameters based on data from long-duration spaceflight studies incorporated via a machine-learning architecture. This would allow us to propagate the model through a long period in spaceflight conditions (e.g., a Mars transit) with or without a range of potential

countermeasures. Once the long-duration loop had been propagated, we would then be able to run an acute simulation in order to analyze the differences between an intervention (e.g., a gravity transition) on a "healthy" subject and the same intervention on a deconditioned subject.

- **Expansion to include metabolic transport:** At present, the model only focuses on the cardiovascular system. However, lumped parameter modeling has also been successfully applied to the pulmonary system and metabolic transport of gases[520]. In Whittle and Diaz-Artiles[209] we detailed how the model could be expanded in order to allow prediction of blood gases throughout the cardiovascular system. By expanding the model in this direction, we would enable two novel use cases. First, we would be able to simulate the effects of cabin atmospheres, including compositions and pressures, on the cardiovascular system. This would allow us to simulate a range of different nominal and off-nominal spaceflight scenarios, and the cardiopulmonary effects of actions such as extravehicular activity (EVA). Second, such an expanded model could be easily combined with a model of bubble formation in reduced gravity in order to provide an individualized risk model of decompression sickness (DCS).

REFERENCES

[1] Petersen LG, Whittle RS, Lee JH, Sieker J, Carlson J, Finke C, Shelton CM, Petersen JCG, Diaz-Artiles A. Gravitational effects on intraocular pressure and ocular perfusion pressure. *J Appl Physiol*. 2022;132:24–35. doi:10.1152/JAPPLPHYSIOL.00546.2021.

[2] Hughson RL, Helm A, Durante M. Heart in space: effect of the extraterrestrial environment on the cardiovascular system. *Nat Rev Cardiol*. 2017;15:167–180. doi:10.1038/nrcardio.2017.157.

[3] Buckey JC, Gaffney FA, Lane LD, Levine BD, Watenpaugh DE, Wright SJ, Yancy CW, Meyer DM, Blomqvist CG. Central venous pressure in space. *J Appl Physiol*. 1996;81:19–25. doi:10.1152/jappl.1996.81.1.19.

[4] Eckberg DL, Halliwill JR, Beightol LA, Brown TE, Taylor JA, Goble R. Human vagal baroreflex mechanisms in space. *J Physiol*. 2010;588:1129–1138. doi:10.1113/jphysiol.2009.186650.

[5] Buckey JC. *Space Physiology*. Oxford University Press; 2006.

[6] Norsk P, Asmar A, Damgaard M, Christensen NJ. Fluid shifts, vasodilatation and ambulatory blood pressure reduction during long duration spaceflight. *J Physiol*. 2015;593:573–584. doi:10.1113/jphysiol.2014.284869.

[7] Hargens AR, Richardson S. Cardiovascular adaptations, fluid shifts, and countermeasures related to space flight. *Respir Physiol Neurobiol*. 2009;169:S30–S33. doi:10.1016/j.resp.2009.07.005.

[8] Nelson ES, Mulugeta L, Myers JG. Microgravity-induced fluid shift and ophthalmic changes. *Life*. 2014;4:621–665. doi:10.3390/life4040621.

[9] Auñón-Chancellor SM, Pattarini JM, Moll S, Sargsyan A. Venous Thrombosis during Spaceflight. *N Engl J Med*. 2020;382:89–90. doi:10.1056/NEJMc1905875.

[10] Limper U, Tank J, Ahnert T, Maegele M, Grottke O, Hein M, Jordan J. The thrombotic risk of spaceflight: has a serious problem been overlooked for more than half of a century? *Eur*

Heart J. 2021;42:97–100. doi:10.1093/EURHEARTJ/EHAA359.

[11] Zwart SR, Auñón-Chancellor SM, Heer M, Melin MM, Smith SM. Albumin, Oral Contraceptives, and Venous Thromboembolism Risk in Astronauts. *J Appl Physiol*. 2022; doi:10.1152/JAPPLPHYSIOL.00024.2022.

[12] Marshall-Goebel K, Laurie SS, Alferova IV, Arbeille P, Auñón-Chancellor SM, Ebert DJ, Lee SM, MacIas BR, Martin DS, Pattarini JM, Ploutz-Snyder R, Ribeiro LC, Tarver WJ, Dulchavsky SA, Hargens AR, Stenger MB. Assessment of Jugular Venous Blood Flow Stasis and Thrombosis During Spaceflight. *JAMA Netw Open*. 2019;2. doi:10.1001/JAMANETWORKOPEN.2019.15011.

[13] Harris KM, Weber T, Greaves D, Green DA, Goswami N, Petersen LG. Going against the flow: are venous thromboembolism and impaired cerebral drainage critical risks for spaceflight? WHAT HAPPENED? *J Appl Physiol*. 2022;132:270–273. doi:10.1152/japplphysiol.00425.2021.

[14] Compton WD. *Where No Man Has Gone Before: A History of Apollo Lunar Exploration Missions - NASA SP-4214*. NASA Office of Management; 1989.

[15] Wooster PD, Braun RD, Ahn J, Putnam ZR. Trajectory Options for Human Mars Missions. In: *AIAA/AAS Astrodynamics Specialist Conference and Exhibit*. 2006; 1–17. doi:10.2514/6.2006-6308.

[16] Seedhouse E. Launch and Re-Entry. In: *Pulling G*. Springer Praxis; 2013. doi:10.1007/978-1-4614-3030-8_7.

[17] Buckner J, Walker J, Clark C, Orleans N, Bucknera JK, Walker JE, Clark CK, Buckner JK, Manager E. The Design of the F-16 High-Alpha Flight Control Characteristics and Control System Concept. In: *17th Aerospace Sciences Meeting*. 1979; 1–8. doi:10.2514/6.1979-403.

[18] Hall JE. *Guyton and Hall Textbook of Medical Physiology*. Elsevier; 2016.

[19] Yang JQ, Jiang N, Li ZP, Guo S, Chen ZY, Li BB, Chai SB, Lu SY, Yan HF, Sun PM, Zhang T, Sun HW, Yang JW, Zhou JL, Yang HM, Cui Y. The effects of microgravity on the digestive system and the new insights it brings to the life sciences. *Life Sci Space Res*. 2020;

27:74–82. doi:10.1016/J.LSSR.2020.07.009.

[20] Whitson PA, Pietrzyk RA, Pak CY. Renal stone risk assessment during space shuttle flights. *J Urol*. 1997;158:2305–2310. doi:10.1016/S0022-5347(01)68240-5.

[21] Diedrich A, Paranjape SY, Robertson D. Plasma and Blood Volume in Space. *Am J Med Sci*. 2007;334:80–86. doi:10.1097/MAJ.0b013e318065b89b.

[22] Lawley JS, Petersen LG, Howden EJ, Sarma S, Cornwell WK, Zhang R, Whitworth LA, Williams MA, Levine BD. Effect of gravity and microgravity on intracranial pressure. *J Physiol*. 2017;595:2115–2127. doi:10.1113/JP273557.

[23] Chung KY, Woo SJ, Yi S, Choi GH, Ahn CH, Hur GC, Lim JG, Kim TW. Diurnal pattern of intraocular pressure is affected by microgravity when measured in space with the pressure phosphene tonometer (PPT). *J Glaucoma*. 2011;20:488–491. doi:10.1097/IJG.0B013E3181F464D2.

[24] Nelson ES, Mulugeta L, Feola A, Raykin J, Myers JG, Samuels BC, Ethier CR. The impact of ocular hemodynamics and intracranial pressure on intraocular pressure during acute gravitational changes. *J Appl Physiol*. 2017;123:352–363. doi:10.1152/japplphysiol.00102.2017.

[25] Tanaka K, Nishimura N, Kawai Y. Adaptation to microgravity, deconditioning, and countermeasures. *J Physiol Sci*. 2017;67:271–281. doi:10.1007/S12576-016-0514-8.

[26] Navasiolava N, Yuan M, Murphy R, Robin A, Coupé M, Wang L, Alameddine A, Gauquelin-Koch G, Gharib C, Li Y, Custaud MA. Vascular and Microvascular Dysfunction Induced by Microgravity and Its Analogs in Humans: Mechanisms and Countermeasures. *Front Physiol*. 2020;11. doi:10.3389/FPHYS.2020.00952/FULL.

[27] Baevsky RM, Baranov VM, Funtova II, Diedrich A, Pashenko AV, Chernikova AG, Drescher J, Jordan J, Tank J. Autonomic cardiovascular and respiratory control during prolonged spaceflights aboard the International Space Station. *J Appl Physiol*. 2007;103:156–161. doi:10.1152/JAPPLPHYSIOL.00137.2007.

[28] Fritsch-Yelle JM, Charles JB, Jones MM, Beightol LA, Eckberg DL. Spaceflight alters

autonomic regulation of arterial pressure in humans. *J Appl Physiol*. 1994;77:1776–1783. doi:10.1152/JAPPL.1994.77.4.1776.

[29] Levine BD, Pawelczyk JA, Ertl AC, Cox JF, Zuckerman JH, Diedrich A, Biaggioni I, Ray CA, Smith ML, Iwase S, Saito M, Sugiyama Y, Mano T, Zhang R, Iwasaki K, Lane LD, Buckey JC, Cooke WH, Baisch FJ, Robertson D, Eckberg DL, Blomqvist CG. Human muscle sympathetic neural and haemodynamic responses to tilt following spaceflight. *J Physiol*. 2002;538:331–340. doi:10.1113/jphysiol.2001.012575.

[30] Mandsager KT, Robertson D, Diedrich A. The Function of the Autonomic Nervous System during Spaceflight. *Clin Auton Res*. 2015;25:141–151. doi:10.1007/s10286-015-0285-y.

[31] Watenpaugh DE, Hargens AR. The Cardiovascular System in Microgravity. In: *Handbook of Physiology, Section 4 - Environmental Physiology*, edited by Fregly MJ, Blatteis CM. Oxford University Press; 1996.

[32] Perhonen MA, Franco F, Lane LD, Buckey JC, Blomqvist CG, Zerwekh JE, Peshock RM, Weatherall PT, Levine BD. Cardiac atrophy after bed rest and spaceflight. *J Appl Physiol*. 2001;91:645–653. doi:10.1152/jappl.2001.91.2.645.

[33] Buckey JC, Lane LD, Levine BD, Watenpaugh DE, Wright SJ, Moore WE, Gaffney FA, Blomqvist CG. Orthostatic intolerance after spaceflight. *J Appl Physiol*. 1996;81:7–18. doi:10.1152/JAPPL.1996.81.1.7.

[34] Antonsen EL, Monti A, Charvat J, Connell ES, Reynolds RJ, HSRB Risk Custodian Team Collaborators, Abukmail A, Marotta K, Brown C. Directed Acyclic Graphs: A Tool for Understanding the NASA Human Spaceflight System Risks. *Tech. rep.*, NASA Johnson Space Center, Houston, TX. 2022.

[35] Convertino VA. Consequences of cardiovascular adaptation to spaceflight: Implications for the use of pharmacological countermeasures. *Gravit Space Biol Bull*. 2005;18:59.

[36] Downs M, Moore A, Lee SMC, Ploutz-Snyder L, Stenger M, Phillips T, Summers R, Feeback D, Platts SH. Evidence Report: Risk of Reduced Physical Performance Capabilities Due To Reduced Aerobic Capacity Human Research Program Human Health Countermea-

sures Element, NASA-HRP-47072. *Tech. rep.*, National Aeronautics and Space Administration (NASA). 2015. Publication Title: Human Research Program: Human Health Countermeasures Element.

[37] Perusek G, Lewandowski BE, Nall M, Norsk P, Linnehan R, Baumann D. Advanced Exercise Concepts (AEC) Overview. In: *Human Research Program Investigator's Workshop*. Galveston, TX, USA. 2015; 1–15.

[38] Moore AD, Lee SM, Stenger MB, Platts SH. Cardiovascular exercise in the U.S. space program: Past, present and future. *Acta Astronaut*. 2010;66:974–988. doi:10.1016/J.ACTAASTRO.2009.10.009.

[39] Bogomolov VV, Castrucci F, Comtois JM, Damann V, Davis JR, Duncan JM, Johnston SL, Gray GW, Grigoriev AI, Koike Y, Kuklinski P, Matveyev VP, Morgun VV, Pochuev VI, Sargsyan AE, Shimada K, Straube U, Tachibana S, Voronkov YV, Williams RS. International Space Station medical standards and certification for space flight participants. *Aviat Space Environ Med*. 2007;78:1162–1169. doi:10.3357/ASEM.2175.2007.

[40] Aerospace Medical Association Task Force on Space Travel. Medical guidelines for space passengers. Aerospace Medical Association Task Force on Space Travel. *Aviat Space Environ Med*. 2001;72:948–950.

[41] Hodkinson PD, Anderton RA, Posselt BN, Fong KJ. An overview of space medicine. *Br J Anaesthesia*. 2017;119:i143–i153. doi:10.1093/BJA/AEX336.

[42] Mader TH, Gibson CR, Pass AF, Kramer LA, Lee AG, Fogarty J, Tarver WJ, Dervay JP, Hamilton DR, Sargsyan A, Phillips JL, Tran D, Lipsky W, Choi J, Stern C, Kuyumjian R, Polk JD. Optic Disc Edema, Globe Flattening, Choroidal Folds, and Hyperopic Shifts Observed in Astronauts after Long-duration Space Flight. *Ophthalmol*. 2011;118:2058–2069. doi:10.1016/J.OPHTHA.2011.06.021.

[43] Paez YM, Mudie LI, Subramanian PS. Spaceflight Associated Neuro-Ocular Syndrome (SANS): A Systematic Review and Future Directions. *Eye Brain*. 2020;12:105. doi:10.2147/EB.S234076.

[44] Macias BR, Patel NB, Gibson CR, Samuels BC, Laurie SS, Otto C, Ferguson CR, Lee SM, Ploutz-Snyder R, Kramer LA, Mader TH, Brunstetter T, Stenger MB. Association of Long-Duration Spaceflight With Anterior and Posterior Ocular Structure Changes in Astronauts and Their Recovery. *JAMA Ophthalmol*. 2020;138:553–559. doi:10.1001/JAMAOPHTHALMOL.2020.0673.

[45] Laurie SS, Lee SM, Macias BR, Patel N, Stern C, Young M, Stenger MB. Optic Disc Edema and Choroidal Engorgement in Astronauts During Spaceflight and Individuals Exposed to Bed Rest. *JAMA Ophthalmol*. 2020;138:165–172. doi:10.1001/JAMAOPHTHALMOL.2019.5261.

[46] Wojcik P, Kini A, Al Othman B, Galdamez LA, Lee AG. Spaceflight associated neuro-ocular syndrome. *Curr Opin Neurol*. 2020;33:62–67. doi:10.1097/WCO.0000000000000778.

[47] Stenger MB, Tarver WJ, Brunstetter T, Gibson CR, Laurie SS, Lee SMC, Macias BR, Mader TH, Otto C, Smith SM, Zwart SR. Evidence Report: Risk of Spaceflight Associated Neuro-ocular Syndrome (SANS). *Tech. rep.*, Human Research Program, Houston, TX. 2017.

[48] Laurie SS, Macias BR, Pardon LP, Brunstetter T, Tarver WJ, Gibson CR, Greenwald SH, Marshall-Goebel K, Jasien JV, Mason S, Tsung A. Evidence Report: Risk of Spaceflight Associated Neuro-ocular Syndrome (SANS). *Tech. rep.*, Human Research Program, Houston, TX. 2022.

[49] Jóhannesson G, Eklund A, Lindén C. Intracranial and Intraocular Pressure at the Lamina Cribrosa: Gradient Effects. *Curr Neurol Neurosci Rep*. 2018;18:1–10. doi:10.1007/S11910-018-0831-9.

[50] Buckey JC, Lan M, Phillips SD, Archambault-Leger V, Fellows AM. A theory for why the spaceflight-associated neuro-ocular syndrome develops. *J Appl Physiol*. 2022; doi:10.1152/JAPPLPHYSIOL.00854.2021.

[51] Smith SM, Zwart SR. Spaceflight-related ocular changes: The potential role of genetics, and the potential of B vitamins as a countermeasure. *Curr Opin Clin Nutr Metab Care*. 2018;21:481–488. doi:10.1097/MCO.0000000000000510.

[52] Zwart SR, Gibson CR, Mader TH, Ericson K, Ploutz-Snyder R, Heer M, Smith SM. Vision Changes after Spaceflight Are Related to Alterations in Folate–and Vitamin B-12–Dependent One-Carbon Metabolism. *J Nutr*. 2012;142:427–431. doi:10.3945/JN.111.154245.

[53] Zwart SR, Gibson CR, Gregory JF, Mader TH, Stover PJ, Zeisel SH, Smith SM. Astronaut ophthalmic syndrome. *FASEB J*. 2017;31:3746–3756. doi:10.1096/FJ.201700294.

[54] Laurie SS, Macias BR, Dunn JT, Young M, Stern C, Lee SM, Stenger MB. Optic Disc Edema after 30 Days of Strict Head-down Tilt Bed Rest. *Ophthalmol*. 2019;126:467–468. doi:10.1016/J.OPHTHA.2018.09.042.

[55] Ong J, Lee AG, Moss HE. Head-Down Tilt Bed Rest Studies as a Terrestrial Analog for Spaceflight Associated Neuro-Ocular Syndrome. *Front Neurol*. 2021;12:648958. doi:10.3389/FNEUR.2021.648958.

[56] Kebukawa Y, Ly V, Rao Velichala S, Hargens AR. Cardiovascular, Lymphatic, and Ocular Health in Space. *Life*. 2022;12:268. doi:10.3390/LIFE12020268.

[57] Lee AG, Mader TH, Gibson CR, Tarver W, Rabiei P, Riascos RF, Galdamez LA, Brunstetter T. Spaceflight associated neuro-ocular syndrome (SANS) and the neuro-ophthalmologic effects of microgravity: a review and an update. *npj Microgravity*. 2020;6:1–10. doi:10.1038/s41526-020-0097-9.

[58] Aleci C. From international ophthalmology to space ophthalmology: the threats to vision on the way to Moon and Mars colonization. *Int Ophthalmol*. 2020;40:775–786. doi:10.1007/S10792-019-01212-7.

[59] McGregor HR, Lee JK, Mulder ER, De Dios YE, Beltran NE, Kofman IS, Bloomberg JJ, Mulavara AP, Smith SM, Zwart SR, Seidler RD. Ophthalmic changes in a spaceflight analog are associated with brain functional reorganization. *Hum Brain Mapp*. 2021;42:4281–4297. doi:10.1002/HBM.25546.

[60] Albano de Guimarães J, Carneiro Teixeira G, Lima da Silva TK, Castelo Moura F. Optic Disc Edema and Posterior Globe Flattening Secondary to Ocular Hypotony: Case Re-

port and Discussion Regarding Pathophysiology and Clinical Findings. *J Neuroophthalmol*. 2021;41:e220–e222. doi:10.1097/WNO.0000000000001095.

[61] Buckey JC, Phillips SD, Anderson AP, Chepko AB, Archambault-Leger V, Gui J, Fellows AM. Microgravity-induced ocular changes are related to body weight. *Am J Physiol Regul Integr Comp Physiol*. 2018;315:R496–R499. doi:10.1152/ajpregu.00086.2018.

[62] Simka M, Latacz P, Redelbach W. Blood flow in the internal jugular veins during the spaceflight – Is it actually bidirectional? *Life Sci Space Res*. 2020;25:103–106. doi:10.1016/J.LSSR.2020.03.005.

[63] Kim DS, Vaquer S, Mazzolai L, Roberts LN, Pavela J, Watanabe M, Weerts G, Green DA. The effect of microgravity on the human venous system and blood coagulation: a systematic review. *Exp Physiol*. 2021;106:1149–1158. doi:10.1113/EP089409.

[64] Jennings RT, Murphy DMF, Ware DL, Aunon SM, Moon RE, Bogomolov VV, Morgun VV, Voronkov YI, Fife CE, Boyars MC, Ernst RD. Medical qualification of a commercial spaceflight participant: not your average astronaut. *Aviat Space Environ Med*. 2006;77:475–484.

[65] Blue RS, Jennings RT, Antunano MJ, Mathers CH. Commercial spaceflight: Progress and challenges in expanding human access to space. *REACH*. 2017;7-8:6–13. doi:10.1016/J.REACH.2018.08.001.

[66] Stepanek J, Blue RS, Parazynski S. Space Medicine in the Era of Civilian Spaceflight. *N Engl J Med*. 2019;380:1053–1060. doi:10.1056/NEJMra1609012.

[67] Moore AD, Downs ME, Lee SM, Feiveson AH, Knudsen P, Ploutz-Snyder L. Peak exercise oxygen uptake during and following long-duration spaceflight. *J Appl Physiol*. 2014; 117:231–238. doi:10.1152/JAPPLPHYSIOL.01251.2013.

[68] Trappe S, Costill D, Gallagher P, Creer A, Peters JR, Evans H, Riley DA, Fitts RH. Exercise in space: Human skeletal muscle after 6 months aboard the International Space Station. *J Appl Physiol*. 2009;106:1159–1168. doi:10.1152/JAPPLPHYSIOL.91578.2008.

[69] Robertson D, Davis TL. Recent advances in the treatment of orthostatic hypotension. *Neu-*

rol. 1995;45:S26–32.

[70] Benditt DG, Fahy GJ, Lurie KG, Sakaguchi S, Fabian W, Samniah N. Pharmacotherapy of neurally mediated syncope. *Circulation*. 1999;100:1242–1248. doi:10.1161/01.CIR.100.11.1242.

[71] Vernikos J, Convertino VA. Advantages and disadvantages of fludrocortisone or saline load in preventing post-spaceflight orthostatic hypotension. *Acta Astronaut*. 1994;33:259–266. doi:10.1016/0094-5765(94)90133-3.

[72] Bungo MW, Charles JB, Johnson PC. Cardiovascular deconditioning during space flight and the use of saline as a countermeasure to orthostatic intolerance. *Aviat Space Environ Med*. 1985;56:985–990.

[73] Goswami N, Blaber AP, Hinghofer-Szalkay H, Convertino VA. Lower body negative pressure: Physiological effects, applications, and implementation. *Physiol Rev*. 2019;99:807–851. doi:10.1152/PHYSREV.00006.2018.

[74] Stevens PM, Lamb LE. Effects of lower body negative pressure on the cardiovascular system. *Am J Cardiol*. 1965;16:506–515. doi:10.1016/0002-9149(65)90027-5.

[75] Gilbert CA, Stevens PM. Forearm vascular responses to lower body negative pressure and orthostasis. *J Appl Physiol*. 1966;21:1265–1272. doi:10.1152/jappl.1966.21.4.1265.

[76] Berry CA. Medical legacy of Apollo. *Aerosp Med*. 1974;45:1046–1057.

[77] Johnson RL, Hoffler GW, Nicogossian AE, Bergman Jr SA, Jackson MM. Lower body negative pressure - third manned Skylab mission. In: *Biomedical Results from Skylab*, edited by Johnston RS, Dietlein LF. NASA STI Program Office; 1977.

[78] Johnson RL, Hoffler GW, Nicogossian AE, Bergman Jr SA. Skylab experiment M-092: results of the fi rst manned mission. *Acta Astronaut*. 1975;2:265–296. doi:10.1016/0094-5765(75)90096-X.

[79] Charles JB, Lathers CM. Summary of Lower Body Negative Pressure Experiments During Space Flight. *J Clin Pharmacol*. 1994;34:571–583. doi:10.1002/J.1552-4604.1994.TB02009.X.

[80] Campbell MR, Charles JB. Historical review of lower body negative pressure research in space medicine. *Aerosp Med Hum Perform*. 2015;86:633–640. doi:10.3357/AMHP.4246.2015.

[81] Gazenko OG, Genin AM, Egorov AD. Summary of medical investigations in the U.S.S.R. manned space missions. *Acta Astronaut*. 1981;8:907–917. doi:10.1016/0094-5765(81)90061-8.

[82] Garshnek V. Soviet space flight: The human element. *Aviat Space Environ Med*. 1989; 60:695–705.

[83] Murthy G, Watenpaugh DE, Ballard RE, Hargens AR. Exercise against lower body negative pressure as a countermeasure for cardiovascular and musculoskeletal deconditioning. *Acta Astronaut*. 1994;33:89–96. doi:10.1016/0094-5765(94)90112-0.

[84] Lee SM, Schneider SM, Boda WL, Watenpaugh DE, Macias BR, Meyer RS, Hargens AR. Supine LBNP exercise maintains exercise capacity in male twins during 30-d bed rest. *Med Sci Sports Exerc*. 2007;39:1315–1326. doi:10.1249/MSS.0B013E31806463D9.

[85] Watenpaugh DE, O'Leary DD, Schneider SM, Lee SM, Macias BR, Tanaka K, Hughson RL, Hargens AR. Lower body negative pressure exercise plus brief postexercise lower body negative pressure improve post-bed rest orthostatic tolerance. *J Appl Physiol*. 2007; 103:1964–1972. doi:10.1152/JAPPLPHYSIOL.00132.2007.

[86] Hisdal J, Toska K, Flatebø T, Walløe L. Onset of mild lower body negative pressure induces transient change in mean arterial pressure in humans. *Eur J Appl Physiol*. 2002;87:251–256. doi:10.1007/S00421-002-0630-4.

[87] Marshall-Goebel K, Terlević R, Gerlach DA, Kuehn S, Mulder E, Rittweger J. Lower body negative pressure reduces optic nerve sheath diameter during head-down tilt. *J Appl Physiol*. 2017;123:1139–1144. doi:10.1152/JAPPLPHYSIOL.00256.2017.

[88] Petersen LG, Lawley JS, Lilja-Cyron A, Petersen JC, Howden EJ, Sarma S, Cornwell WK, Zhang R, Whitworth LA, Williams MA, Juhler M, Levine BD. Lower body negative pressure to safely reduce intracranial pressure. *J Physiol*. 2019;597:237–248.

doi:10.1113/JP276557.

[89] Pynn HJ, Smith JE. The Compensatory Reserve Index – potential uses in a military context. *J Royal Nav Med Serv*. 2018;104:120–123. doi:10.1136/JRNMS-104-120.

[90] Convertino VA. Lower body negative pressure as a tool for research in aerospace physiology and military medicine. *J Gravit Physiol*. 2001;8:1–14.

[91] Korn C, Hollinger M, Henderson S. Pediatric Head Injury in an Urban Level 1 ED. *Ann Emerg Med*. 2005;46:67. doi:10.1016/J.ANNEMERGMED.2005.06.250.

[92] Harris KM, Petersen LG, Weber T. Reviving lower body negative pressure as a countermeasure to prevent pathological vascular and ocular changes in microgravity. *npj Microgravity*. 2020;6:1–8. doi:10.1038/s41526-020-00127-3.

[93] Scott JM, Tucker WJ, Martin D, Crowell JB, Goetchius E, Ozgur O, Hamilton S, Otto C, Gonzales R, Ritter M, Newby N, Dewitt J, Stenger MB, Ploutz-Snyder R, Ploutz-Snyder L, Morgan WH, Haykowsky MJ. Association of Exercise and Swimming Goggles With Modulation of Cerebro-ocular Hemodynamics and Pressures in a Model of Spaceflight-Associated Neuro-ocular Syndrome. *JAMA Ophthalmol*. 2019;137:652. doi:10.1001/JAMAOPHTHALMOL.2019.0459.

[94] Scott JM, Tucker WJ, Haykowsky MJ. Lamina Cribrosa Pore Diameter and Spaceflight-Associated Neuro-ocular Syndrome. *JAMA Ophthalmol*. 2019;137:1331. doi:10.1001/JAMAOPHTHALMOL.2019.3322.

[95] Lan M, Phillips SD, Archambault-Leger V, Chepko AB, Lu R, Anderson AP, Masterova KS, Fellows AM, Halter RJ, Buckey JC. Proposed mechanism for reduced jugular vein flow in microgravity. *Physiol Rep*. 2021;9:e14782. doi:10.14814/PHY2.14782.

[96] Clément GR, Bukley AP, Paloski WH. Artificial gravity as a countermeasure for mitigating physiological deconditioning during long-duration space missions. *Front Syst Neurosci*. 2015;9:92. doi:10.3389/fnsys.2015.00092.

[97] Czysz PA, Bruno C, Chudoba B. *Future Spacecraft Propulsion Systems and Integration*. Springer Berlin Heidelberg; 2018.

[98] Clément G, Bukley A, eds. *Artificial Gravity*. Springer; 2007.

[99] Clarke AC. *2001: A Space Odyssey*. Hutchinson; 1968.

[100] Kubrick S. 2001: A Space Odyssey. 1968. Place: USA.

[101] Johnson RD, Holbrow C, Holbrow C. *Space Settlements: A Design Study*. NASA STI Program Office; 1977.

[102] Clément G, Traon APL. Centrifugation as a countermeasure during actual and simulated microgravity: A review. *Eur J Appl Physiol*. 2004;92:235–248. doi:10.1007/S00421-004-1118-1/TABLES/2.

[103] Clément G. International roadmap for artificial gravity research. *npj Microgravity*. 2017; 3:1–7. doi:10.1038/s41526-017-0034-8.

[104] Horie K, Kato T, Kudo T, Sasanuma H, Miyauchi M, Akiyama N, Miyao T, Seki T, Ishikawa T, Takakura Y, Shirakawa M, Shiba D, Hamada M, Jeon H, Yoshida N, Inoue Ji, Muratani M, Takahashi S, Ohno H, Akiyama T. Impact of spaceflight on the murine thymus and mitigation by exposure to artificial gravity during spaceflight. *Sci Rep*. 2019;9:1–10. doi:10.1038/s41598-019-56432-9.

[105] Benson AJ, Guedry FE, Parker DE, Reschke MF. Microgravity Vestibular Investigations: Perception of Self-Orientation and Self-Motion. *J Vestib Res*. 1997;7:453–457. doi:10.3233/VES-1997-7604.

[106] Kreitenberg A, Baldwin KM, Bagian JP, Cotten S, Witmer J, Caiozzo VJ. The "Space Cycle" Self Powered Human Centrifuge: a proposed countermeasure for prolonged human spaceflight. *Aviat Space Environ Med*. 1998;69:66–72.

[107] Kuebler U, Grinberg A, Kern P. Concept for a short arm human centrifuge onbord ISS. In: *38th COSPAR Scientific Assembly*, vol. 38. 2010; 4.

[108] Shimada K, Kasai Y, Yuasa T. International Space Station (ISS) Intelligent Human Centrifuge. *J Mech Electr Intell Syst*. 2020;3.

[109] Shipov AA, Kotovskaya AR, Galle RR. Biomedical aspects of artificial gravity. *Acta Astronaut*. 1981;8:1117–1121. doi:10.1016/0094-5765(81)90087-4.

[110] Bukley A, Lawrence D, Clément G, Bukley A, Lawrence D, Clément G. Generating artificial gravity onboard the Space Shuttle. *Acta Astronaut*. 2007;60:472–478. doi:10.1016/J.ACTAASTRO.2006.09.013.

[111] Stone Jr RW. An overview of artificial gravity. In: *Fifth symposium on the role of the vestibular organs in space exploration*, edited by Graybiel A. 1973; 23–34.

[112] Young LR, Hecht H, Lyne LE, Sienko KH, Cheung CC, Kavelaars J. Artificial gravity: head movements during short-radius centrifugation. *Acta Astronaut*. 2001;49:215–226. doi:10.1016/S0094-5765(01)00100-X.

[113] Bretl KN, McCusker AT, Sherman SO, Mitchell TR, Dixon JB, Clark TK. Tolerable acclimation to the cross-coupled illusion through a 10-day, incremental, personalized protocol. *J Vestib Res*. 2019;29:97–110. doi:10.3233/VES-190656.

[114] Bretl KN, Clark TK. Improved feasibility of astronaut short-radius artificial gravity through a 50-day incremental, personalized, vestibular acclimation protocol. *npj Microgravity*. 2020; 6:1–8. doi:10.1038/s41526-020-00112-w.

[115] Bretl KN, Clark TK. Predicting individual acclimation to the cross-coupled illusion for artificial gravity. *J Vestib Res*. 2022;32:305–316. doi:10.3233/VES-210019.

[116] Clark TK. Effects of Spaceflight on the Vestibular System. In: *Handbook of Space Pharmaceuticals*, edited by Pathak YV, Araújo dos Santos M, Zea L. Springer International Publishing; 2022. doi:10.1007/978-3-030-05526-4_2.

[117] Lackner JR, DiZio P. Human orientation and movement control in weightless and artificial gravity environments. *Exp Brain Res*. 2000;130:2–26. doi:10.1007/S002210050002.

[118] Lackner JR, Dizio P. Artificial gravity as a countermeasure in long-duration space flight. *J Neurosci Res*. 2000;62:169–176. doi:10.1002/1097-4547(20001015)62:2<169::AID-JNR2>3.0.CO;2-B.

[119] Diaz-Artiles A, Heldt T, Young LR. Short-Term Cardiovascular Response to Short-Radius Centrifugation With and Without Ergometer Exercise. *Front Physiol*. 2018;9:1492. doi:10.3389/fphys.2018.01492.

[120] Diaz-Artiles A. Exercise under Artificial Gravity - Experimental and Computational Approaches. 2015.

[121] Frett T, Green DA, Mulder E, Noppe A, Arz M, Pustowalow W, Petrat G, Tegtbur U, Jordan J. Tolerability of daily intermittent or continuous short-arm centrifugation during 60-day 6o head down bed rest (AGBRESA study). *PLOS ONE*. 2020;15:e0239228. doi:10.1371/JOURNAL.PONE.0239228.

[122] Shiraishi M, Schou M, Gybel M, Christensen N, Norsk P. Comparison of acute cardiovascular responses to water immersion and head-down tilt in humans. *J Appl Physiol*. 2002; 92:264–268. doi:10.1152/JAPPL.2002.92.1.264.

[123] Marshall-Goebel K, Ambarki K, Eklund A, Malm J, Mulder E, Gerlach D, Bershad E, Rittweger J. Analogs of Microgravity: Space Research without Leaving the Planet: Effects of short-term exposure to head-down tilt on cerebral hemodynamics: a prospective evaluation of a spaceflight analog using phase-contrast MRI. *J Appl Physiol*. 2016;120:1466. doi:10.1152/JAPPLPHYSIOL.00841.2015.

[124] Marshall-Goebel K, Mulder E, Bershad E, Laing C, Eklund A, Malm J, Stern C, Rittweger J. Intracranial and intraocular pressure during various degrees of head-down tilt. *Aerosp Med Hum Perform*. 2017;88:10–16. doi:10.3357/AMHP.4653.2017.

[125] Diaz-Artiles A, Navarro Tichell P, Perez F. Cardiopulmonary Responses to Sub-Maximal Ergometer Exercise in a Hypo-Gravity Analog Using Head-Down Tilt and Head-Up Tilt. *Front Physiol*. 2019;10:720. doi:10.3389/fphys.2019.00720.

[126] Whittle RS, Stapleton LM, Petersen LG, Diaz-Artiles A. Indirect measurement of absolute cardiac output during exercise in simulated altered gravity is highly dependent on the method. *J Clin Monit Comput*. 2022;36:1355–1366. doi:10.1007/s10877-021-00769-y.

[127] Shankhwar V, Singh D, Deepak KK, Shankhwar V, Singh D, Deepak KK. Immediate changes in cardiac autonomic tone and stroke volume during microgravity simulation using head-down tilt. *Indian J Physiol Pharmacol*. 2021;65:86–93. doi:10.25259/IJPP_2_2021.

[128] Kim Prisk G, Fine JM, Elliott AR, West JB. Effect of 6 degrees head-down tilt on car-

diopulmonary function: comparison with microgravity. *Aviat Space Environ Med*. 2002; 73:8–16.

[129] Amirova L, Navasiolava N, Rukavishvikov I, Gauquelin-Koch G, Gharib C, Kozlovskaya I, Custaud MA, Tomilovskaya E. Cardiovascular System Under Simulated Weightlessness: Head-Down Bed Rest vs. Dry Immersion. *Front Physiol*. 2020;0:395. doi:10.3389/FPHYS.2020.00395.

[130] Meck JV, Dreyer SA, Warren LE. Long-Duration Head-Down Bed Rest: Project Overview, Vital Signs, and Fluid Balance. *Aviat Space Environ Med*. 2009;80:A01–A08. doi:10.3357/ASEM.BR01.2009.

[131] Marshall-Goebel K, Mulder E, Donoviel D, Strangman G, Suarez JI, Rao CV, Frings-Meuthen P, Limper U, Rittweger J, Bershad EM. An international collaboration studying the physiological and anatomical cerebral effects of carbon dioxide during head-down tilt bed rest: the SPACECOT study. *J Appl Physiol*. 2017;122:1398–1405. doi:10.1152/JAPPLPHYSIOL.00885.2016.

[132] Basner M, Stahn AC, Nasrini J, Dinges DF, Moore TM, Gur RC, Mühl C, Macias BR, Laurie SS. Effects of head-down tilt bed rest plus elevated CO2 on cognitive performance. *J Appl Physiol*. 2021;130:1235–1246. doi:10.1152/JAPPLPHYSIOL.00865.2020.

[133] Laurie SS, Christian K, Kysar J, Lee SM, Lovering AT, Macias BR, Moestl S, Sies W, Mulder E, Young M, Stenger MB. Unchanged cerebrovascular CO2 reactivity and hypercapnic ventilatory response during strict head-down tilt bed rest in a mild hypercapnic environment. *J Physiol*. 2020;598:2491–2505. doi:10.1113/JP279383.

[134] Zhang R, Zuckerman JH, Pawelczyk JA, Levine BD. Effects of head-down-tilt bed rest on cerebral hemodynamics during orthostatic stress. *J Appl Physiol*. 1997;83:2139–2145. doi:10.1152/JAPPL.1997.83.6.2139.

[135] Vijayalakshmi P, Madanmohan. Acute effect of 30 degrees, 60 degrees and 80 degrees head-down tilt on blood pressure in young healthy human subjects. *Indian J Physiol Pharmacol*. 2006;50:28–32.

[136] Nagaya K, Wada F, Nakamitsu S, Sagawa S, Shiraki K. Responses of the circulatory system and muscle sympathetic nerve activity to head-down tilt in humans. *Am J Physiol Regul Integr Comp Physiol*. 1995;268:R1289–R1294. doi:10.1152/AJPREGU.1995.268.5.R1289.

[137] Zaidi A, Benitez D, Gaydecki PA, Vohra A, Fitzpatrick AP. Haemodynamic effects of increasing angle of head up tilt. *Heart*. 2000;83:181–184. doi:10.1136/HEART.83.2.181.

[138] Hainsworth R, Al-Shamma YMH. Cardiovascular responses to upright tilting in healthy subjects. *Clin Sci*. 1988;74:17–22. doi:10.1042/CS0740017.

[139] Lieshout JJV, Harms MPM, Pott F, Jenstrup M, Secher NH. Stroke volume of the heart and thoracic fluid content during head-up and head-down tilt in humans. *Acta Anaesthesiol Scand*. 2005;49:1287–1292. doi:10.1111/J.1399-6576.2005.00841.X.

[140] Convertino VA, Doerr DF, Eckberg DL, Fritsch JM, Vernikos-Danellis J. Head-down bed rest impairs vagal baroreflex responses and provokes orthostatic hypotension. *J Appl Physiol*. 1990;68:1458–1464. doi:10.1152/JAPPL.1990.68.4.1458.

[141] Prisk GK, Paiva M, West JB. *Gravity and the Lung: Lessons from Microgravity*. Marcel Dekker, Inc.; 2001.

[142] Anderson AP, Swan JG, Phillips SD, Knaus DA, Kattamis NT, Toutain-Kidd CM, Zegans ME, Fellows AM, Buckey JC. Acute effects of changes to the gravitational vector on the eye. *J Appl Physiol*. 2016;120:939–946. doi:10.1152/japplphysiol.00730.2015.

[143] Tugrul M, Camci E, Pembeci K, Al-Darsani A, Telci L. Relationship between peripheral and central venous pressures in different patient positions, catheter sizes, and insertion sites. *J Cardiothorac Vasc Anesth*. 2004;18:446–450. doi:10.1053/J.JVCA.2004.05.022.

[144] Roth C, Ferbert A, Deinsberger W, Kleffmann J, Kästner S, Godau J, Schüler M, Tryba M, Gehling M. Does Prone Positioning Increase Intracranial Pressure? A Retrospective Analysis of Patients with Acute Brain Injury and Acute Respiratory Failure. *Neurocrit Care*. 2014;21:186–191. doi:10.1007/S12028-014-0004-X.

[145] Nekludov M, Bellander BM, Mure M. Oxygenation and cerebral perfusion pressure improved in the prone position. *Acta Anaesthesiol Scand*. 2006;50:932–936.

doi:10.1111/J.1399-6576.2006.01099.X.

[146] Kim SY, Park SJ. The Effect of the Lithotomy-Trendelenburg Position on Respiratory and Hemodynamic Changes during General Anesthesia. *Korean J Anesthesiol*. 2002;42:722. doi:10.4097/KJAE.2002.42.6.722.

[147] Reuter DA, Felbinger TW, Schmidt C, Moerstedt K, Kilger E, Lamm P, Goetz AE. Trendelenburg positioning after cardiac surgery: effects on intrathoracic blood volume index and cardiac performance. *Eur J Anaesthesiol*. 2003;20:17–20. doi:10.1017/S0265021503000036.

[148] Arvizo C, Mehta ST, Yunker A. Adverse events related to Trendelenburg position during laparoscopic surgery: Recommendations and review of the literature. *Curr Opin Obstet Gynecol*. 2018;30:272–278. doi:10.1097/GCO.0000000000000471.

[149] Dharmavaram S, Jellish WS, Nockels RP, Shea J, Mehmood R, Ghanayem A, Kleinman B, Jacobs W. Effect of prone positioning systems on hemodynamic and cardiac function during lumbar spine surgery: An echocardiographic study. *Spine*. 2006;31:1388–1393. doi:10.1097/01.BRS.0000218485.96713.44.

[150] DePasse JM, Palumbo MA, Haque M, Eberson CP, Daniels AH. Complications associated with prone positioning in elective spinal surgery. *World J Orthop*. 2015;6:351. doi:10.5312/WJO.V6.I3.351.

[151] Rozet I, Vavilala MS. Risks and Benefits of Patient Positioning During Neurosurgical Care. *Anesthesiol Clin*. 2007;25:631–653. doi:10.1016/J.ANCLIN.2007.05.009.

[152] Steris Healthcare. Surgical Table Accessories for Trendelenburg Positioning. 2023. URL `https://www.steris.com/healthcare/products/surgical-table-accessories/trendelenburg-position-accessories`

[153] Diaz Artiles A, Heldt T, Young LR. Effects of artificial gravity on the cardiovascular system: Computational approach. *Acta Astronaut*. 2016;126:395–410. doi:10.1016/j.actaastro.2016.05.005.

[154] Diaz-Artiles A, Heldt T, Young LR. Computational Model of Cardiovascular Response to

Centrifugation and Lower-body Cycling Exercise. *J Appl Physiol*. 2019;127:1453–1468. doi:10.1152/japplphysiol.00314.2019.

[155] Merz AA, Cheng S. Sex differences in cardiovascular ageing. *Heart*. 2016;102:825–831. doi:10.1136/HEARTJNL-2015-308769.

[156] Lash SJ, Gillespie BL, Eisler RM, Southard DR. Sex differences in cardiovascular reactivity: effects of the gender relevance of the stressor. *Health Psychol*. 1991;10:392–398. doi:10.1037/0278-6133.10.6.392.

[157] Hastrup JL, Light KC. Sex differences in cardiovascular stress responses: Modulation as a function of menstrual cycle phases. *J Psychosom Res*. 1984;28:475–483. doi:10.1016/0022-3999(84)90081-3.

[158] Parker BA, Kalasky MJ, Proctor DN. Evidence for sex differences in cardiovascular aging and adaptive responses to physical activity. *Eur J Appl Physiol*. 2010;110:235–246. doi:10.1007/S00421-010-1506-7.

[159] Wheatley CM, Snyder EM, Johnson BD, Olson TP. Sex differences in cardiovascular function during submaximal exercise in humans. *SpringerPlus*. 2014;3:1–13. doi:10.1186/2193-1801-3-445/TABLES/6.

[160] Maffessanti F, Muraru D, Esposito R, Gripari P, Ermacora D, Santoro C, Tamborini G, Galderisi M, Pepi M, Badano LP. Age-, body size-, and sex-specific reference values for right ventricular volumes and ejection fraction by three-dimensional echocardiography: a multicenter echocardiographic study in 507 healthy volunteers. *Circ Cardiovasc Imaging*. 2013;6:700–10. doi:10.1161/CIRCIMAGING.113.000706.

[161] Monahan KD, Ray CA. Gender affects calf venous compliance at rest and during baroreceptor unloading in humans. *Am J Physiol Heart Circ Physiol*. 2004;286:H895–H901. doi:10.1152/ajpheart.00719.2003.

[162] Platts SH, Bairey Merz CN, Barr Y, Fu Q, Gulati M, Hughson R, Levine BD, Mehran R, Stachenfeld N, Wenger NK. Effects of Sex and Gender on Adaptation to Space: Cardiovascular Alterations. *J Womens Health*. 2014;23:950–955. doi:10.1089/JWH.2014.4912.

[163] Arzeno NM, Stenger MB, Lee SMC, Ploutz-Snyder R, Platts SH. Sex differences in blood pressure control during 6° head-down tilt bed rest. *J Appl Physiol*. 2013;304:1114–1123. doi:10.1152/AJPHEART.00391.2012.

[164] Patel K, Rössler A, Lackner HK, Trozic I, Laing C, Lorr D, Green DA, Hinghofer-Szalkay H, Goswami N. Effect of postural changes on cardiovascular parameters across gender. *Med*. 2016;95. doi:10.1097/MD.0000000000004149.

[165] Lee AG, Mader TH, Gibson CR, Brunstetter TJ, Tarver WJ. Space flight-associated neuro-ocular syndrome (SANS). *Eye*. 2018;doi:10.1038/s41433-018-0070-y.

[166] Adhikari A, Shet RV, Mandal R, Vaghela Y. Variations in Intraocular Pressure During Different Phases of Menstrual Cycle. *J Ophthalmol Res*. 2021;4:183–191. doi:10.26502/fjor.2644-00240036.

[167] Qureshi IA, Xi XR, Wu XD, Pasha N, Huang YB. Variations in Ocular Pressure During Menstrual Cycle. *J Pak Med Assoc*. 1998;48:37–40.

[168] Heldt T. Computational models of cardiovascular response to orthostatic stress. 2004.

[169] Summers R, Coleman T, Meck J. Development of the Digital Astronaut Project for the analysis of the mechanisms of physiologic adaptation to microgravity: Validation of the cardiovascular system module. *Acta Astronaut*. 2008;63:758–762. doi:10.1016/j.actaastro.2007.12.054.

[170] Levine BD, Lane LD, Watenpaugh DE, Gaffney FA, Buckey JC, Blomqvist CG. Maximal exercise performance after adaptation to microgravity. *J Appl Physiol*. 1996;81:686–94. doi:10.1152/jappl.1996.81.2.686.

[171] Guyton AC, Lindsey AW, Kaufmann BN. Effect of mean circulatory filling pressure and other peripheral circulatory factors on cardiac output. *Am J Physiol*. 1955;180:463–468. doi:10.1152/ajplegacy.1955.180.3.463.

[172] Guyton AC, Coleman TG, Granger HJ. Circulation: Overall Regulation. *Annu Rev Physiol*. 1972;34:13–44. doi:10.1146/annurev.ph.34.030172.000305.

[173] Heldt T, Shim EB, Kamm RD, Mark RG. Computational modeling of car-

diovascular response to orthostatic stress. *J Appl Physiol*. 2002;92:1239–1254. doi:10.1152/japplphysiol.00241.2001.

[174] Van Heusden K, Gisolf J, Stok WJ, Dijkstra S, Karemaker JM. Mathematical modeling of gravitational effects on the circulation: Importance of the time course of venous pooling and blood volume changes in the lungs. *Am J Physiol Heart Circ Physiol*. 2006;291:H2152–65. doi:10.1152/ajpheart.01268.2004.

[175] Lim E, Chan GS, Dokos S, Ng SC, Latif LA, Vandenberghe S, Karunanithi M, Lovell NH. A cardiovascular mathematical model of graded head-up tilt. *PLOS ONE*. 2013;8. doi:10.1371/journal.pone.0077357.

[176] Melchior FM, Srinivasan RS, Thullier PH, Clere JM. Simulation of cardiovascular response to lower body negative pressure from 0 to -40 mmHg. *J Appl Physiol*. 1994;77:630–640. doi:10.1152/jappl.1994.77.2.630.

[177] Hao WY, Bai J, Wu XY, Zhang LF. Simulation study of the effects of hypovolaemia on cardiovascular response to orthostatic stress. *Med Biol Eng Comput*. 2003;41:44–51. doi:10.1007/BF02343538.

[178] Gallo C, Ridolfi L, Scarsoglio S. Cardiovascular deconditioning during long-term spaceflight through multiscale modeling. *npj Microgravity*. 2020;6:1–14. doi:10.1038/s41526-020-00117-5.

[179] Olufsen M, Tran H, Ottesen J. Modeling cerebral blood flow control during posture change from sitting to standing. *Cardiovasc Eng*. 2004;4:47–58. doi:10.1023/B:CARE.0000025122.46013.1a.

[180] Olufsen MS, Ottesen JT, Tran HT, Ellwein LM, Lipsitz LA, Novak V. Blood pressure and blood flow variation during postural change from sitting to standing: Model development and validation. *J Appl Physiol*. 2005;99:1523–1537. doi:10.1152/japplphysiol.00177.2005.

[181] Ellwein LM, Tran HT, Zapata C, Novak V, Olufsen MS. Sensitivity analysis and model assessment: Mathematical models for arterial blood flow and blood pressure. *Cardiovasc Eng*. 2008;8:94–108. doi:10.1007/s10558-007-9047-3.

[182] Melchior FM, Srini Srinivasan R, Charles JB. Mathematical modeling of human cardiovascular system for simulation of orthostatic response. *Am J Physiol Heart Circ Physiol*. 1992; 262:H1920–H1933. doi:10.1152/ajpheart.1992.262.6.H1920.

[183] Croston RC, Rummel JA, Kay FJ. Computer Model of Cardiovascular Control System Responses to Exercise. *J Dyn Syst Meas Control*. 1973;September:301–307. doi:10.1115/1.3426719.

[184] Peterson K, Ozawa ET, Pantalos GM, Sharp MK. Numerical Simulation of the Influence of Gravity and Posture on Cardiac Performance. *Ann Biomed Eng*. 2002;30:247–259. doi:10.1114/1.1451075.

[185] Zamanian S. Modeling and simulating human cardiovascular response to acceleration. 2007.

[186] Whittle RS, Keller N, Hall EA, Vellore HS, Stapleton LM, Findlay KH, Dunbar BJ, Diaz-Artiles A. Gravitational dose-response curves for acute cardiovascular hemodynamics and autonomic responses in a tilt paradigm. *J Am Heart Assoc*. 2022;11:e024175. doi:10.1161/JAHA.121.024175.

[187] Whittle RS, Diaz-Artiles A. Gravitational effects on carotid and jugular characteristics in graded head-up and head-down tilt. *J Appl Physiol*. 2023;134:217–229. doi:10.1152/japplphysiol.00248.2022.

[188] Whittle RS, Diaz-Artiles A. Modeling individual differences in cardiovascular response to gravitational stress using a sensitivity analysis. *J Appl Physiol*. 2021;130:1983–2001. doi:10.1152/japplphysiol.00727.2020.

[189] Verheyden B, Liu J, Beckers F, Aubert AE. Adaptation of heart rate and blood pressure to short and long duration space missions. *Respir Physiol Neurobiol*. 2009;169:S13–S16. doi:10.1016/J.RESP.2009.03.008.

[190] Karemaker JM, Berecki-Gisolf J. 24-h blood pressure in Space: The dark side of being an astronaut. *Respir Physiol Neurobiol*. 2009;169:S55–S58. doi:10.1016/J.RESP.2009.05.006.

[191] Limper U, Moestl S, Tank J, Prisk GK, Heusser K, Hoffmann F, Goßmann A, Migeotte PF, Gauger P, Beck LEJ, Schlegel HW, Levine BD, Jordan J. A 20-year evolution of car-

diac performance in microgravity in a male astronaut. *Clin Auton Res*. 2020;31:139–141. doi:10.1007/S10286-019-00657-1.

[192] Iwase S, Nishimura N, Tanaka K, Mano T. Effects of Microgravity on Human Physiology. In: *Beyond LEO - Human Health Issues for Deep Space Exploration [Working Title]*. IntechOpen; 2020. doi:10.5772/intechopen.90700.

[193] Schroeder C, Tank J, Boschmann M, Diedrich A, Sharma AM, Biaggioni I, Luft FC, Jordan J. Selective Norepinephrine Reuptake Inhibition as a Human Model of Orthostatic Intolerance. *Circulation*. 2002;105:347–353. doi:10.1161/HC0302.102597.

[194] Lee SM, Martin DS, Miller CA, Scott JM, Laurie SS, Macias BR, Mercaldo ND, Ploutz-Snyder L, Stenger MB. Venous and Arterial Responses to Partial Gravity. *Front Physiol*. 2020;11:863. doi:10.3389/FPHYS.2020.00863/BIBTEX.

[195] David J, Scheuring RA, Morgan A, Olsen C, Sargsyan A, Grishin A. Comparison of Internal Jugular Vein Cross-Section Area During a Russian Tilt-Table Protocol and Microgravity. *Aerosp Med Hum Perform*. 2021;92:207–211. doi:10.3357/AMHP.5600.2021.

[196] Watenpaugh DE. Analogs of microgravity: Head-down tilt and water immersion. *J Appl Physiol*. 2016;120:904–914. doi:10.1152/JAPPLPHYSIOL.00986.2015.

[197] Taibbi G, Young M, Vyas RJ, Murray MC, Lim S, Predovic M, Jacobs NM, Askin KN, Mason SS, Zanello SB, Vizzeri G, Theriot CA, Parsons-Wingerter P. Opposite response of blood vessels in the retina to 6° head-down tilt and long-duration microgravity. *npj Microgravity*. 2021;7:1–11. doi:10.1038/s41526-021-00165-5.

[198] London G, Levenson J, Safar M, Simon A, Guerin A, Payen D. Hemodynamic effects of head-down tilt in normal subjects and sustained hypertensive patients. *Am J Physiol*. 1983; 245. doi:10.1152/AJPHEART.1983.245.2.H194.

[199] Clenaghan S, McLaughlin RE, Martyn C, McGovern S, Bowra J. Relationship between Trendelenburg tilt and internal jugular vein diameter. *Emerg Med J*. 2005;22:867–868. doi:10.1136/EMJ.2004.019257.

[200] Garcia-Leal M, Guzman-Lopez S, Verdines-Perez AM, de Leon-Gutierrez H,

Fernandez-Rodarte BA, Alvarez-Villalobos NA, Martinez-Garza JH, Quiroga-Garza A, Elizondo-Omaña RE. Trendelenburg position for internal jugular vein catheterization: A systematic review and meta-analysis. *J Vasc Access*. 2021;24:338–347. doi:10.1177/11297298211031339.

[201] Zuñiga WF, Sanabria FR, de Mejía CN, Hermida E, Sánchez JA, Solórzano MC, Rodriguez RHP, Nuñez LJL. Internal jugular vein cannulation: How much safety can we offer? *Rev Col Anest*. 2015;43:76–86. doi:10.1016/j.rcae.2014.10.001.

[202] Lorchirachoonkul T, Kah Ti L, Manohara S, Teng Lye S, Tan SA, Shen L, Song Chua Kang D, Lian Kah T. Anatomical variations of the internal jugular vein: implications for successful cannulation and risk of carotid artery puncture. *Singapore Med J*. 2012;53:325–328.

[203] Lobato EB, Sulek CA, Moody RL, Morey TE. Cross-sectional area of the right and left internal jugular veins. *J Cardiothorac Vasc Anesth*. 1999;13:136–138. doi:10.1016/S1053-0770(99)90075-7.

[204] Lee JG, Park HB, Shin HY, Kim JD, Yu SB, Kim DS, Ryu SJ, Kim GH. Effect of Trendelenburg position on right and left internal jugular vein cross-sectional area. *Korean J Anesthesiol*. 2014;67:305. doi:10.4097/KJAE.2014.67.5.305.

[205] Marshall-Goebel K, Stevens B, Rao CV, Suarez JI, Calvillo E, Arbeille P, Sangi-Haghpeykar H, Donoviel DB, Mulder E, Bershad EM, Basner M, Becker C, Clark J, Damani R, Doering W, Dohmen C, Frings-Meuthen P, Gauger P, Gerlach D, Hand O, Hasan K, Huth E, Johannes B, Kramer L, Kraus G, Limper U, Mittag U, Muller K, Nasrini J, Niederberger B, Poddig D, Putzke M, Rittweger J, Sagner M, Schrage-Knoll I, Sies W, Stern C, Stetefeld H, Strangman G, von Waechter A, Weber T, Wittkowski M, Gerzer R, Do J, Sutton J. Internal Jugular Vein Volume During Head-Down Tilt and Carbon Dioxide Exposure in the SPACECOT Study. *Aerosp Med Hum Perform*. 2018;89:351–356. doi:10.3357/AMHP.4934.2018.

[206] Videbaek R, Norsk P. Atrial distension in humans during microgravity induced by parabolic flights. *J Appl Physiol*. 1997;83:1862–1866. doi:10.1152/jappl.1997.83.6.1862.

[207] Arbeille P, Provost R, Zuj K, Vincent N. Measurements of jugular, portal, femoral, and

calf vein cross-sectional area for the assessment of venous blood redistribution with long duration spaceflight (Vessel Imaging Experiment). *Eur J Appl Physiol*. 2015;115:2099–2106. doi:10.1007/S00421-015-3189-6/TABLES/1.

[208] Lippi G, Favaloro EJ, Cervellin G. Prevention of venous thromboembolism: Focus on mechanical prophylaxis. *Semin Thromb Hemost*. 2011;37:237–251. doi:10.1055/S-0031-1273088/ID/34.

[209] Whittle RS, Diaz-Artiles A. Metabolic Modeling in Altered Gravity. In: *IEEE Aerospace Conference*. Big Sky, MT. 2020; 1–17. doi:10.1109/AERO47225.2020.9172582.

[210] Diaz A, Trigg C, Young LR. Combining ergometer exercise and artificial gravity in a compact-radius centrifuge. *Acta Astronaut*. 2015;113:80–88. doi:10.1016/j.actaastro.2015.03.034.

[211] Ansari M, Javadi H, Pourbehi M, Mogharrabi M, Rayzan M, Semnani S, Jallalat S, Amini A, Abbaszadeh M, Barekat M, Nabipour I, Assadi M. The association of rate pressure product (RPP) and myocardial perfusion imaging (MPI) findings: a preliminary study:. *Perfusion*. 2012;27:207–213. doi:10.1177/0267659112436631.

[212] Widjaja D, Vandeput S, Van Huffel S, Aubert AE. Cardiovascular autonomic adaptation in lunar and martian gravity during parabolic flight. *Eur J Appl Physiol*. 2015;115:1205–1218. doi:10.1007/S00421-015-3118-8.

[213] TFESCNASPE. Task Force of the European Society of Cardiology and the North American Society of Pacing and Electrophysiology: Heart Rate Variability - Standards of measurement, physiological interpretation, and clinical use. *Circulation*. 1996;93:1043–1065. doi:10.1161/01.CIR.93.5.1043.

[214] Berntson GG, Lozano DL, Chen YJ. Filter properties of root mean square successive difference (RMSSD) for heart rate. *Psychophysiology*. 2005;42:246–252. doi:10.1111/J.1469-8986.2005.00277.X.

[215] Swenne CA. Baroreflex sensitivity: mechanisms and measurement. *Neth Heart J*. 2013;21:58. doi:10.1007/S12471-012-0346-Y.

[216] Eckberg DL, Sleight P. *Human baroreflexes in health and disease*. Clarendon Press; 1992.

[217] Rovere MTL, Pinna GD, Raczak G. Baroreflex Sensitivity: Measurement and Clinical Implications. *Ann Noninvasive Electrocardiol*. 2008;13:191–207. doi:10.1111/J.1542-474X.2008.00219.X.

[218] Westerhof B, Gisolf J, Stok W, Wesseling K, Karemaker J. Time-domain cross-correlation baroreflex sensitivity: performance on the EUROBAVAR data set. *J Hypertension*. 2004; 22:1371–1380. doi:10.1097/01.HJH.0000125439.28861.ED.

[219] Otsu N. A Threshold Selection Method from Gray-Level Histograms. *IEEE Trans Syst Man, Cybern*. 1979;9:62–66. doi:10.1109/TSMC.1979.4310076.

[220] Failmezger H, Yuan Y, Rueda O, Markowetz F. CRImage: CRImage a package to classify cells and calculate tumour cellularity. 2021.

[221] Fernández E, Neto ES, Abry P, Macchiavelli R, Balzarini M, Cuzin B, Baude C, Frutoso J, Gharib C. Assessing erectile neurogenic dysfunction from heart rate variability through a Generalized Linear Mixed Model framework. *Comput Meth Programs Biomed*. 2010; 99:49–56. doi:10.1016/J.CMPB.2009.11.001.

[222] Oh DY, Park SM, Choi SW. Daytime Neurophysiological Hyperarousal in Chronic Insomnia: A Study of qEEG. *J Clin Med*. 2020;9:3425. doi:10.3390/JCM9113425.

[223] Park SM, Jung HY. Respiratory sinus arrhythmia biofeedback alters heart rate variability and default mode network connectivity in major depressive disorder: A preliminary study. *Int J Psychophysiology*. 2020;158:225–237. doi:10.1016/J.IJPSYCHO.2020.10.008.

[224] Barbeau DY, Krueger C, Huene M, Copenhaver N, Bennett J, Weaver M, Weiss MD. Heart rate variability and inflammatory markers in neonates with hypoxic-ischemic encephalopathy. *Physiol Rep*. 2019;7. doi:10.14814/PHY2.14110.

[225] Bates D, Mächler M, Bolker B, Walker S. Fitting Linear Mixed-Effects Models Using lme4. *J Stat Softw*. 2015;67:1–48. doi:10.18637/JSS.V067.I01.

[226] Dunnett CW. A Multiple Comparison Procedure for Comparing Several Treatments with a Control. *J Am Stat Assoc*. 1955;50:1096–1121. doi:10.1080/01621459.1955.10501294.

[227] Benjamini Y, Hochberg Y. Controlling the False Discovery Rate: A Practical and Powerful Approach to Multiple Testing. *J Royal Stat Soc Ser B: Stat Methodol*. 1995;57:289–300. doi:10.1111/J.2517-6161.1995.TB02031.X.

[228] László Z, Rössler A, Hinghofer-Szalkay HG. Cardiovascular and Hormonal Changes with Different Angles of Head-up Tilt in Men. *Physiol Res*. 2001;50:71–82.

[229] R Core Team. R: A Language and Environment for Statistical Computing, version 4.1.0. 2021.

URL `https://www.r-project.org/`

[230] Brooks ME, Kristensen K, van Benthem KJ, Magnusson A, Berg CW, Nielsen A, Skaug HJ, Mächler M, Bolker BM. glmmTMB balances speed and flexibility among packages for zero-inflated generalized linear mixed modeling. *R J*. 2017;9:378–400. doi:10.32614/RJ-2017-066.

[231] Wood SN. Fast stable restricted maximum likelihood and marginal likelihood estimation of semiparametric generalized linear models. *J Royal Stat Soc Ser B: Stat Methodol*. 2011; 73:3–36. doi:10.1111/j.1467-9868.2010.00749.x.

[232] Kuznetsova A, Brockhoff PB, Christensen RHB. lmerTest Package: Tests in Linear Mixed Effects Models. *J Stat Softw*. 2017;82:1–26. doi:10.18637/JSS.V082.I13.

[233] Hartig F. DHARMa: Residual Diagnostics for Hierarchical (Multi-Level / Mixed) Regression Models. 2021.

URL `https://cran.r-project.org/package=DHARMa`

[234] Lenth RV. emmeans: Estimated Marginal Means, aka Least-Squares Means. 2021.

URL `https://cran.r-project.org/package=emmeans`

[235] Porta A, Tobaldini E, Guzzetti S, Furlan R, Montano N, Gnecchi-Ruscone T. Assessment of cardiac autonomic modulation during graded head-up tilt by symbolic analysis of heart rate variability. *Am J Physiol Heart Circ Physiol*. 2007;293:702–708. doi:10.1152/AJPHEART.00006.2007.

[236] Yamazaki F, Matsumura N, Nagata J, Ando A, Imura T. Spontaneous arterial baroreflex

control of the heart rate during head-down tilt in heat-stressed humans. *Eur J Appl Physiol*. 2001;85:208–213. doi:10.1007/S004210100482.

[237] Tuckman J, Shillingford J. Effect of different degrees of tilt on cardiac output, heart rate, and blood pressure in normal man. *Br Heart J*. 1966;28:32. doi:10.1136/HRT.28.1.32.

[238] Bundgaard-Nielsen M, Sørensen H, Dalsgaard M, Rasmussen P, Secher NH. Relationship between stroke volume, cardiac output and filling of the heart during tilt. *Acta Anaesthesiol Scand*. 2009;53:1324–1328. doi:10.1111/J.1399-6576.2009.02062.X.

[239] Rowell LB. *Human Cardiovascular Control*. Oxford University Press; 1993.

[240] Olufsen MS, Alston AV, Tran HT, Ottesen JT, Novak V. Modeling Heart Rate Regulation—Part I: Sit-to-stand Versus Head-up Tilt. *Cardiovasc Eng*. 2007;8:73–87. doi:10.1007/S10558-007-9050-8.

[241] Mukai S, Hayano J. Heart rate and blood pressure variabilities during graded head-up tilt. *J Appl Physiol*. 1995;78:212–216. doi:10.1152/JAPPL.1995.78.1.212.

[242] Mosqueda-Garcia R, Furlan R, Fernandez-Violante R, Desai T, Snell M, Jarai Z, Ananthram V, Robertson RM, Robertson D. Sympathetic and baroreceptor reflex function in neurally mediated syncope evoked by tilt. *J Clin Investig*. 1997;99:2736–2744. doi:10.1172/JCI119463.

[243] Printz MP, Jaworski RL. Hypertension; Overview. In: *Encyclopedia of Endocrine Diseases*, vol. 3. Elsevier, 2nd ed.; 2018. doi:10.1016/B978-0-12-801238-3.03801-0.

[244] Silvani A. Sleep disorders, nocturnal blood pressure, and cardiovascular risk: A translational perspective. *Auton Neurosci Basic Clin*. 2019;218:31–42. doi:10.1016/J.AUTNEU.2019.02.006.

[245] Prisk GK, Elliott AR, Guy HJ, Kosonen JM, West JB. Pulmonary gas exchange and its determinants during sustained microgravity on Spacelabs SLS-1 and SLS-2. *J Appl Physiol*. 1995;79:1290–1298. doi:10.1152/JAPPL.1995.79.4.1290.

[246] Sharma P, Paudel B, Singh P, Linmbu P. Heart rate variability: Response to graded head up tilt in healthy men. *Kathmandu Univ Med J*. 2009;7:252–257.

doi:10.3126/KUMJ.V7I3.2733.

[247] Malhotra V, Thakare AE, Hulke SM, Wakode SL, Parashar R, Ravi N. Effect of head down tilt on heart rate variability. *J Fam Med Prim Care*. 2021;10:439. doi:10.4103/JFMPC.JFMPC_1642_20.

[248] Saito M, Foldager N, Mano T, Iwase S, Sugiyama Y, Oshima M. Sympathetic control of hemodynamics during moderate head-up tilt in human subjects. *Environ Med Annu Rep Res Inst Environ Med Nagoya Univ*. 1997;41:151–155.

[249] O'Leary DD, Kimmerly DS, Cechetto AD, Shoemaker JK. Differential effect of head-up tilt on cardiovagal and sympathetic baroreflex sensitivity in humans. *Exp Physiol*. 2003; 88:769–774. doi:10.1113/EPH8802632.

[250] Vettorello M, Colombo R, De Grandis C, Costantini E, Raimondi F. Effect of fentanyl on heart rate variability during spontaneous and paced breathing in healthy volunteers. *Acta Anaesthesiol Scand*. 2008;52:1064–1070. doi:10.1111/J.1399-6576.2008.01713.X.

[251] Cozanitis D, Pouttu J, Rosenberg P. Bradycardia associated with the use of vecuronium. A comparative study with pancuronium with and without glycopyrronium. *Anaesthesia*. 1987; 42:192–194. doi:10.1111/J.1365-2044.1987.TB02998.X.

[252] Sharma S, Nair P, Murgai A, Selvaraj R. Transient bradycardia induced by thiopentone sodium: a unique challenge in the management of refractory status epilepticus. *BMJ Case Rep*. 2013;2013. doi:10.1136/BCR-2013-200484.

[253] Ma M, Noori S, Maarek J, Holschneider D, Rubinstein E, Seri I. Prone positioning decreases cardiac output and increases systemic vascular resistance in neonates. *J Perinatol*. 2015; 35:424–427. doi:10.1038/JP.2014.230.

[254] Pump B, Talleruphuus U, Christensen NJ, Warberg J, Norsk P. Effects of supine, prone, and lateral positions on cardiovascular and renal variables in humans. *Am J Physiol Regul Integr Comp Physiol*. 2002;283:R174–R180. doi:10.1152/AJPREGU.00619.2001.

[255] Sudheer PS, Logan SW, Ateleanu B, Hall JE. Haemodynamic effects of the prone position: a comparison of propofol total intravenous and inhalation anaesthesia. *Anaesthesia*. 2006;

61:138–141. doi:10.1111/J.1365-2044.2005.04464.X.

[256] Schaefer WM, Lipke CSA, Kühl HP, Koch KC, Kaiser HJ, Reinartz P, Nowak B, Buell U. Prone Versus Supine Patient Positioning During Gated 99m Tc-Sestamibi SPECT: Effect on Left Ventricular Volumes, Ejection Fraction, and Heart Rate. *J Nucl Med*. 2004;45:2016–2020.

[257] Yap K, Campbell P, Cherk M, McGrath C, Kalff V. Effect of prone versus supine positioning on left ventricular ejection fraction (LVEF) and heart rate using ECG gated Tl-201 myocardial perfusion scans and gated cardiac blood pool scans. *J Med Imaging Radiat Oncol*. 2012; 56:525–531. doi:10.1111/J.1754-9485.2012.02438.X.

[258] Relton J, Conn A. Anaesthesia for the surgical correction of scoliosis by the Harrington method in children. *Can Anaesth Soc J*. 1963;10:603–615. doi:10.1007/BF03002093.

[259] Malehorn K, Hiniker J, Mackey T, Heumann K, Murray S, Pettitt R. Kinesio Tape® Applied to the Thorax Augments Ventilatory Efficiency during Heavy Exercise. *Int J Exerc Sci*. 2013;6:157–163.

[260] West JB, Luks AM. *Respiratory Physiology: The Essentials*. Wolters Kluwer; 2016.

[261] Critchley LAH, Conway F, Anderson PJ, Tomlinson B, Critchley JAJH. Non-invasive continuous arterial pressure, heart rate and stroke volume measure-ments during graded head-up tilt in normal man. *Clin Auton Res*. 1997;7:97–101. doi:10.1007/bf02267754.

[262] Khurana RK, Nicholas Ba EM, Khurana RK. Head-up tilt table test: how far and how long? *Clin Auton Res*. 1996;6:335–341. doi:10.1007/BF02556304.

[263] Smith JJ, Hughes CV, Ptacin MJ, Barney JA, Tristani FE, Ebert TJ. The Effect of Age on Hemodynamic Response to Graded Postural Stress in Normal Men. *J Gerontol*. 1987; 42:406–411. doi:10.1093/GERONJ/42.4.406.

[264] Asar S, Acicbe O, Sabaz MS, Tontu F, Canan E, Cukurova Z, Cakar N. Comparison of Respiratory and Hemodynamic Parameters of COVID-19 and Non-COVID-19 ARDS Patients. *Indian J Crit Care Med*. 2021;25:704. doi:10.5005/JP-JOURNALS-10071-23856.

[265] Scheel P, Ruge C, Schöning M. Flow velocity and flow volume measurements in the ex-

tracranial carotid and vertebral arteries in healthy adults: reference data and the effects of age. *Ultrasound Med Biol*. 2000;26:1261–1266. doi:10.1016/S0301-5629(00)00293-3.

[266] Krejza J, Arkuszewski M, Kasner SE, Weigele J, Ustymowicz A, Hurst RW, Cucchiara BL, Messe SR. Carotid artery diameter in men and women and the relation to body and neck size. *Stroke*. 2006;37:1103–1105. doi:10.1161/01.STR.0000206440.48756.f7.

[267] Choudhry FA, Grantham JT, Rai AT, Hogg JP. Vascular geometry of the extracranial carotid arteries: an analysis of length, diameter, and tortuosity. *J Neurointerv Surg*. 2016;8:536–540. doi:10.1136/NEURINTSURG-2015-011671.

[268] van Campen CLM, Verheugt FW, Visser FC. Cerebral blood flow changes during tilt table testing in healthy volunteers, as assessed by Doppler imaging of the carotid and vertebral arteries. *Clin Neurophysiol Pract*. 2018;3:91–95. doi:10.1016/J.CNP.2018.02.004.

[269] Palombo C, Morizzo C, Baluci M, Lucini D, Ricci S, Biolo G, Tortoli P, Kozakova M. Large artery remodeling and dynamics following simulated microgravity by prolonged head-down tilt bed rest in humans. *Biomed Res Int*. 2015;2015:342565. doi:10.1155/2015/342565.

[270] Sato K, Fisher JP, Seifert T, Overgaard M, Secher NH, Ogoh S. Blood flow in internal carotid and vertebral arteries during orthostatic stress. *Exp Physiol*. 2012;97:1272–1280. doi:10.1113/EXPPHYSIOL.2012.064774.

[271] Marshall I, Papathanasopoulou P, Wartolowska K. Carotid flow rates and flow division at the bifurcation in healthy volunteers. *Physiol Meas*. 2004;25:691. doi:10.1088/0967-3334/25/3/009.

[272] Hannerz J, Jogestrand T. Relationship Between Chronic Tension-type Headache, Cranial Hemodynamics, and Cerebrospinal Pressure: Study Involving Provocation With Sumatriptan. *Headache*. 2004;44:154–159. doi:10.1111/J.1526-4610.2004.04032.X.

[273] Ogoh S, Sato K, de Abreu S, Denise P, Normand H. Arterial and venous cerebral blood flow responses to long-term head-down bed rest in male volunteers. *Exp Physiol*. 2020;105:44–52. doi:10.1113/EP088057.

[274] Saiki K, Tsurumoto T, Okamoto K, Wakebe T. Relation between bilateral differences in

internal jugular vein caliber and flow patterns of dural venous sinuses. *Anat Sci Int*. 2013; 88:141. doi:10.1007/S12565-013-0176-Z.

[275] Padget DH. The development of the cranial venous system in man, from the viewpoint of comparative anatomy. *Contrib Embryol*. 1957;247:81–138.

[276] Okudera T, Huang YP, Ohta T, Yokota A, Nakamura Y, Maehara F, Utsunomiya H, Uemura K, Fukasawa H. Development of Posterior Fossa Dural Sinuses, Emissary Veins, and Jugular Bulb: Morphological and Radiologic Study. *Am J Neuroradiol*. 1994;15:1871–1883.

[277] Tarnoki AD, Molnar AA, Tarnoki DL, Littvay L, Medda E, Fagnani C, Arnolfi A, Farina F, Baracchini C, Meneghetti G, Pucci G, Schillaci G, Stazi MA, Nadasy GL. Heritability of the dimensions, compliance and distensibility of the human internal jugular vein wall. *PLOS ONE*. 2018;13:e0192948. doi:10.1371/JOURNAL.PONE.0192948.

[278] Doepp F, Schreiber SJ, von Münster T, Rademacher J, Klingebiel R, Valdueza JM. How does the blood leave the brain? A systematic ultrasound analysis of cerebral venous drainage patterns. *Neuroradiol*. 2004;46:565–570. doi:10.1007/S00234-004-1213-3.

[279] Culver JC, Dickinson ME. The effects of hemodynamic force on embryonic development. *Microcirculation*. 2010;17:164. doi:10.1111/J.1549-8719.2010.00025.X.

[280] Bateman AR, Bateman GA, Barber T. The relationship between cerebral blood flow and venous sinus pressure: can hyperemia induce idiopathic intracranial hypertension? *Fluids Barriers CNS*. 2021;18:5. doi:10.1186/S12987-021-00239-2.

[281] Caiazzo A, Montecinos G, Müller LO, Haacke EM, Toro EF. Computational haemodynamics in stenotic internal jugular veins. *J Math Biol*. 2015;70:745–772. doi:10.1007/S00285-014-0778-7.

[282] Siva B, Hunt A, Boudville N. The sensitivity and specificity of ultrasound estimation of central venous pressure using the internal jugular vein. *J Crit Care*. 2012;27:315.e7–315.e11. doi:10.1016/J.JCRC.2011.09.008.

[283] Dos Santos MG, Makk S, Berghold A, Eckhardt M, Haas A. Intraocular pressure difference in Goldmann applanation tonometry versus Perkins hand-held applanation tonom-

etry in overweight patients. *Ophthalmol*. 1998;105:2260–2263. doi:10.1016/S0161-6420(98)91226-X.

[284] Guyton AC, Jones CE. Central venous pressure: physiological significance and clinical implications. *Am Heart J*. 1973;86:431–437. doi:10.1016/0002-8703(73)90132-4.

[285] Wendling W, Sadel S, Jimenez D, Rosenwasser R, Buchheit W. Cardiovascular and cerebrovascular effects of the applied Valsalva manoeuvre in anaesthetized neurosurgical patients. *Eur J Anaesthesiol*. 1994;11:81–87. doi:10.1097/00132586-199410000-00001.

[286] Wysoki MG, Covey A, Pollak J, Rosenblatt M, Aruny J, Denbow N. Evaluation of various maneuvers for prevention of air embolism during central venous catheter placement. *J Vasc Interv Radiol*. 2001;12:764–766. doi:10.1016/S1051-0443(07)61451-1.

[287] Diaz-Artiles A, Wang Y, Davis MM, Abbott R, Keller N, Kennedy DM. The Influence of Altered-Gravity on Bimanual Coordination: Retention and Transfer. *Front Physiol*. 2022; 12:2378. doi:10.3389/FPHYS.2021.794705/BIBTEX.

[288] Grigoriev AI, Egorov AD. Physiological Aspects of Adaptation of Main Human Body Systems During and After Spaceflights. *Adv Space Biol Med*. 1992;2:43–82. doi:10.1016/S1569-2574(08)60017-9.

[289] Hargens AR. Fluid shifts in vascular and extravascular spaces during and after simulated weightlessness. *Med Sci Sports Exerc*. 1983;15:421–427. doi:10.1249/00005768-198315050-00014.

[290] Parazynski SE, Hargens AR, Tucker B, Aratow M, Styf J, Crenshaw A. Transcapillary fluid shifts in tissues of the head and neck during and after simulated microgravity. *J Appl Physiol*. 1991;71:2469–2475. doi:10.1152/JAPPL.1991.71.6.2469.

[291] Kirsch KA, Baartz FJ, Gunga HC, Röcker L, Wicke HJ, Bünsch B. Fluid shifts into and out of superficial tissues under microgravity and terrestrial conditions. *Clin Investig*. 1993; 71:687–689. doi:10.1007/BF00209721.

[292] Martin DS, Lee SM, Matz TP, Westby CM, Scott JM, Stenger MB, Platts SH. Internal jugular pressure increases during parabolic flight. *Physiol Rep*. 2016;4.

doi:10.14814/phy2.13068.

[293] Haas S, Haese A, Goetz AE, Kubitz JC. Haemodynamics and cardiac function during robotic-assisted laparoscopic prostatectomy in steep Trendelenburg position. *Int J Med Robot Comput Assist Surg*. 2011;7:408–413. doi:10.1002/RCS.410.

[294] Arbeille P, Fomina G, Roumy J, Alferova I, Tobal N, Herault S. Adaptation of the left heart, cerebral and femoral arteries, and jugular and femoral veins during short- and long-term head-down tilt and spaceflights. *Eur J Appl Physiol*. 2001;86:157–168. doi:10.1007/S004210100473.

[295] Patterson CA, Amelard R, Saarikoski E, Heigold H, Hughson RL, Robertson AD. Sex-dependent jugular vein optical attenuation and distension during head-down tilt and lower body negative pressure. *Physiol Rep*. 2022;10. doi:10.14814/PHY2.15179.

[296] Eckberg DL, Diedrich A, Cooke WH, Biaggioni I, Buckey JC, Pawelczyk JA, Ertl AC, Cox JF, Kuusela TA, Tahvanainen KUO, Mano T, Iwase S, Baisch FJ, Levine BD, Adams-Huet B, Robertson D, Blomqvist CG, Blomqvist CG. Respiratory modulation of human autonomic function: long-term neuroplasticity in space. *J Physiol*. 2016;594:5629–46. doi:10.1113/JP271656.

[297] Wesly RLR, Vaishnav RN, Fuchs JCA, Patel DJ, Greenfield JC. Static Linear and Nonlinear Elastic Properties of Normal and Arterialized Venous Tissue in Dog and Man. *Circulation Res*. 1975;37:509–520. doi:10.1161/01.RES.37.4.509.

[298] Journo HJ, Chanudet XA, Pannier BM, Laroque PL, London GM, Safar ME. Hysteresis of the venous pressure-volume relationship in the forearm of borderline hypertensive subjects. *Clin Sci*. 1992;82:329–334. doi:10.1042/CS0820329.

[299] Geerts BF, Aarts LP, Jansen JR. Methods in pharmacology: Measurement of cardiac output. *Br J Clin Pharmacol*. 2011;71:316–330. doi:10.1111/j.1365-2125.2010.03798.x.

[300] Takase B, Akima T, Satomura K, Fumitaka, Ohsuzu, Mastui T, Ishihara M, Kurita A. Effects of chronic sleep deprivation on autonomic activity by examining heart rate variability, plasma catecholamine, and intracellular magnesium levels. *Biomed Pharmacother*. 2004;

58:S35–S39. doi:10.1016/S0753-3322(04)80007-6.

[301] Benditt DG, van Dijk JG, Krishnappa D, Adkisson WO, Sakaguchi S. Neurohormones in the Pathophysiology of Vasovagal Syncope in Adults. *Front Cardiovasc Med*. 2020;7:76. doi:10.3389/FCVM.2020.00076.

[302] Su L, Pan P, Li D, Zhang Q, Zhou X, Long Y, Wang X, Liu D. Central Venous Pressure (CVP) Reduction Associated With Higher Cardiac Output (CO) Favors Good Prognosis of Circulatory Shock: A Single-Center, Retrospective Cohort Study. *Front Med*. 2019;6:216. doi:10.3389/FMED.2019.00216/BIBTEX.

[303] Gaffney FA, Nixon JV, Karlsson ES, Campbell W, Dowdey AB, Blomqvist CG. Cardiovascular deconditioning produced by 20 hours of bedrest with head-down tilt (-5°) in middle-aged healthy men. *Am J Cardiol*. 1985;56:634–638. doi:10.1016/0002-9149(85)91025-2.

[304] Aronen HJ, Svedström E, Yrjänä J, Bondestam S, Aronen' HJ, Svedstrom2 E, Yrjana' J, Bondestam' S. Compression Sonography in the Diagnosis of Deep Venous Thrombosis of the Leg. *Ann Med*. 1994;26:377–380. doi:10.3109/07853899409148354.

[305] Uthoff H, Thalhammer C, Potocki M, Reichlin T, Noveanu M, Aschwanden M, Staub D, Arenja N, Socrates T, Twerenbold R, Mutschmann-Sanchez S, Heinisch C, Jaeger KA, Mebazaa A, Mueller C. Central venous pressure at emergency room presentation predicts cardiac rehospitalization in patients with decompensated heart failure. *Eur J Heart Fail*. 2010;12:469–476. doi:10.1093/EURJHF/HFQ024.

[306] Uthoff H, Breidthardt T, Klima T, Aschwanden M, Arenja N, Socrates T, Heinisch C, Noveanu M, Frischknecht B, Baumann U, Jaeger KA, Mueller C. Central venous pressure and impaired renal function in patients with acute heart failure. *Eur J Heart Fail*. 2011; 13:432–439. doi:10.1093/EURJHF/HFQ195.

[307] Baer RM, Hill DW. Retinal vessel responses to passive tilting. *Eye*. 1990;4:751–756. doi:10.1038/eye.1990.107.

[308] Blomqvist CG, Nixon JV, Johnson RL, Mitchell JH. Early cardiovascular adaptation to zero gravity simulated by head-down tilt. *Acta Astronaut*. 1980;7:543–53. doi:10.1016/0094-

5765(80)90043-0.

[309] Blomqvist CG, Stone HL. Cardiovascular Adjustments to Gravitational Stress. In: *Handbook of Physiology, The Cardiovascular System, Peripheral Circulation and Organ Blood Flow*. John Wiley & Sons, Inc.; 2011. doi:10.1002/cphy.cp020328.

[310] Petersen LG, Carlsen JF, Nielsen MB, Damgaard M, Secher NH. The hydrostatic pressure indifference point underestimates orthostatic redistribution of blood in humans. *J Appl Physiol*. 2014;116:730–735. doi:10.1152/japplphysiol.01175.2013.

[311] Petersen LG, Petersen JC, Andresen M, Secher NH, Juhler M. Postural influence on intracranial and cerebral perfusion pressure in ambulatory neurosurgical patients. *Am J Physiol Regul Integr Comp Physiol*. 2016;310:R100–4. doi:10.1152/ajpregu.00302.2015.

[312] Draeger J, Schwartz R, Groenhoff S, Stern C. Self-tonometry under microgravity conditions. *Aviat Space Environ Med*. 1995;66:568–570.

[313] Mader TH, Gibson CR, Caputo M, Hunter N, Taylor G, Charles J, Meehan RT. Intraocular pressure and retinal vascular changes during transient exposure to microgravity. *Am J Ophthalmol*. 1993;115:347–350. doi:10.1016/S0002-9394(14)73586-X.

[314] Arora N, McLaren JW, Hodge DO, Sit AJ. Effect of Body Position on Episcleral Venous Pressure in Healthy Subjects. *Investig Ophthalmol Vis Sci*. 2017;58:5151–5156. doi:10.1167/IOVS.17-22154.

[315] Blecha S, Harth M, Schlachetzki F, Zeman F, Blecha C, Flora P, Burger M, Denzinger S, Graf BM, Helbig H, Pawlik MT. Changes in intraocular pressure and optic nerve sheath diameter in patients undergoing robotic-assisted laparoscopic prostatectomy in steep 45° Trendelenburg position. *BMC Anesthesiol*. 2017;17:40. doi:10.1186/s12871-017-0333-3.

[316] Chiquet C, Custaud MA, Le Traon AP, Millet C, Gharib C, Denis P. Changes in intraocular pressure during prolonged (7-day) head-down tilt bedrest. *J Glaucoma*. 2003;12:204–208. doi:10.1097/00061198-200306000-00004.

[317] Laurie SS, Vizzeri G, Taibbi G, Ferguson CR, Hu X, Lee SM, Ploutz-Snyder R, Smith SM, Zwart SR, Stenger MB. Effects of short-term mild hypercapnia during head-down tilt on

intracranial pressure and ocular structures in healthy human subjects. *Physiol Rep*. 2017; 5:e13302. doi:10.14814/phy2.13302.

[318] Mayalı H, Tekin B, Kayıkçıoğlu \R, Kurt E, İlker SS. Evaluation of the effect of body position on intraocular pressure measured with rebound tonometer. *Turk J Ophthalmol*. 2019;49:6–9. doi:10.4274/tjo.galenos.2018.90359.

[319] Cheng M, Todorov A, Tempelhoff R, McHugh T, Crowder C, Lauryssen C. The Effect of Prone Positioning on Intraocular Pressure in Anesthetized Patients. *Anesthesiol*. 2001; 95:1351–1355. doi:10.1097/00000542-200112000-00012.

[320] He Z, Vingrys AJ, Armitage JA, Bui BV. The role of blood pressure in glaucoma. *Clin Exp Optom*. 2011;94:133–149. doi:10.1111/J.1444-0938.2010.00564.X.

[321] Schmidl D, Garhofer G, Schmetterer L. The complex interaction between ocular perfusion pressure and ocular blood flow – Relevance for glaucoma. *Exp Eye Res*. 2011;93:141–155. doi:10.1016/J.EXER.2010.09.002.

[322] Sultan MB, Mansberger SL, Lee PP. Understanding the Importance of IOP Variables in Glaucoma: A Systematic Review. *Surv Ophthalmol*. 2009;54:643–662. doi:10.1016/J.SURVOPHTHAL.2009.05.001.

[323] Yun C, Ahn J, Kim M, Hwang SY, Kim SW, Oh J. Ocular Perfusion Pressure and Choroidal Thickness in Early Age-Related Macular Degeneration Patients With Reticular Pseudodrusen. *Investig Ophthalmol Vis Sci*. 2016;57:6604–6609. doi:10.1167/IOVS.16-19989.

[324] Basaran B, Yilbas AA, Gultekin Z. Effect of interscalene block on intraocular pressure and ocular perfusion pressure. *BMC Anesthesiol*. 2017;17:1–7. doi:10.1186/S12871-017-0436-X.

[325] Kalmar AF, Foubert L, Hendrickx JF, Mottrie A, Absalom A, Mortier EP, Struys MM. Influence of steep Trendelenburg position and CO2 pneumoperitoneum on cardiovascular, cerebrovascular, and respiratory homeostasis during robotic prostatectomy. *Br J Anaesthesia*. 2010;104:433–439. doi:10.1093/BJA/AEQ018.

[326] Lawley J, Babu G, Janssen S, Petersen L, Hearon Jr C, Dias K, Sarma S, Williams M,

Whitworth L, Levine B. Daily generation of a footward fluid shift attenuates ocular changes associated with head-down tilt bed rest. *J Appl Physiol*. 2020;129:1220–1231. doi:10.1152/JAPPLPHYSIOL.00250.2020.

[327] Petersen L, Hargens A, Bird E, Ashari N, Saalfeld J, Petersen J. Mobile Lower Body Negative Pressure Suit as an Integrative Countermeasure for Spaceflight. *Aerosp Med Hum Perform*. 2019;90:993–999. doi:10.3357/AMHP.5408.2019.

[328] Berdahl J, Yu D, Morgan W. The translaminar pressure gradient in sustained zero gravity, idiopathic intracranial hypertension, and glaucoma. *Med Hypotheses*. 2012;79:719–724. doi:10.1016/J.MEHY.2012.08.009.

[329] Morgan WH, Yu DY, Cooper RL, Alder VA, Cringle SJ, Constable IJ. The influence of cerebrospinal fluid pressure on the lamina cribrosa tissue pressure gradient. *Investig Ophthalmol Vis Sci*. 1995;36:1163–1172.

[330] Chua J, Chin CWL, Hong J, Chee ML, Le TT, Ting DSW, Wong TY, Schmetterer L. Impact of hypertension on retinal capillary microvasculature using optical coherence tomographic angiography. *J Hypertension*. 2019;37:572. doi:10.1097/HJH.0000000000001916.

[331] Chua J, Chin CWL, Tan B, Wong SH, Devarajan K, Le TT, Ang M, Wong TY, Schmetterer L. Impact of systemic vascular risk factors on the choriocapillaris using optical coherence tomography angiography in patients with systemic hypertension. *Sci Rep*. 2019;9:1–11. doi:10.1038/s41598-019-41917-4.

[332] Bhatt A, Nguyen C, Mosaed S, Minckler D. Clinical and pathological correlation of cotton wool spots in secondary angle closure glaucoma. *Am J Ophthalmol Case Rep*. 2018;10:192. doi:10.1016/J.AJOC.2018.02.028.

[333] Jonas JB, Wang N, Nangia V. Ocular Perfusion Pressure vs Estimated Trans–Lamina Cribrosa Pressure Difference in Glaucoma: The Central India Eye and Medical Study (An American Ophthalmological Society Thesis). *Trans Am Ophthalmol Soc*. 2015;113:6–7.

[334] Zhai G, Lin Z, Wang FH, Wang Y, Li D, Wen L, Ding XX, Jiang J, Feng KM, Liang YB, Xie C. Association between Mean Ocular Perfusion Pressure and Diabetic

Retinopathy in a Northeastern Chinese Population. *Biomed Environ Sci*. 2020;33:701–707. doi:10.3967/BES2020.091.

[335] Leske M. Ocular perfusion pressure and glaucoma: clinical trial and epidemiologic findings. *Curr Opin Ophthalmol*. 2009;20:73–78. doi:10.1097/ICU.0B013E32831EEF82.

[336] Wen T, Deibert CM, Siringo FS, Spencer BA. Positioning-Related Complications of Minimally Invasive Radical Prostatectomies. *J Endourol*. 2014;28:660–667. doi:10.1089/END.2013.0623.

[337] Weber ED, Colyer MH, Lesser RL, Subramanian PS. Posterior ischemic optic neuropathy after minimally invasive prostatectomy. *J Neuroophthalmol*. 2007;27:285–287. doi:10.1097/WNO.0B013E31815B9F67.

[338] Ristin L, Dougherty Wood S, Sullivan-Mee M, Rixon A, Bence B, Ballinger R. Change in Intraocular Pressure and Ocular Perfusion Pressure Due to Trendelenburg Positioning. *Optom Vis Sci*. 2020;97:857–864. doi:10.1097/OPX.0000000000001584.

[339] Lee LA. Perioperative visual loss and anesthetic management. *Curr Opin Anaesthesiol*. 2013;26:375–381. doi:10.1097/ACO.0B013E328360DCD9.

[340] R Core Team. R: A Language and Environment for Statistical Computing, version 4.2.2. 2023.

URL `https://www.r-project.org/`

[341] Diaz-Canestro C, Pentz B, Sehgal A, Montero D. Sex Differences in Orthostatic Tolerance Are Mainly Explained by Blood Volume and Oxygen Carrying Capacity. *Crit Care Explor*. 2022;4:e0608. doi:10.1097/CCE.0000000000000608.

[342] Sarafian D, Miles-Chan JL. The Influence of Gender and Anthropometry on Haemodynamic Status at Rest and in Response to Graded Incremental Head-Up Tilt in Young, Healthy Adults. *Front Physiol*. 2017;7. doi:10.3389/fphys.2016.00656.

[343] Badrov MB, Okada Y, Yoo JK, Vongpatanasin W, Shoemaker JK, Levine BD, Fu Q. Sex Differences in the Sympathetic Neural Recruitment and Hemodynamic Response to Head-Up Tilt in Older Hypertensives. *Hypertension*. 2020;75:458–467.

doi:10.1161/HYPERTENSIONAHA.119.14009.

[344] Afrin Rimi S, Rezwana I, Sultana S, Ferdousi S. Gender differences in circulatory adjustment to head-up tilt test in health. *Med Sci Pulse*. 2020;14:1–17. doi:10.5604/01.3001.0014.2323.

[345] Robertson AD, Papadhima I, Edgell H. Sex differences in the autonomic and cerebrovascular responses to upright tilt. *Auton Neurosci Basic Clin*. 2020;229:102742. doi:10.1016/j.autneu.2020.102742.

[346] Schäfer Olstad D, Frey MT, Herzig D, Trachsel LD, Wilhelm M. Sex-specific reaction of the cardiac autonomic nervous system to different training phases in Swiss elite runners. *Swiss Sports Exerc Med*. 2017;65. doi:10.34045/SSEM/2017/5.

[347] Dart AM, Du XJ, Kingwell BA. Gender, sex hormones and autonomic nervous control of the cardiovascular system. *Cardiovasc Res*. 2002;53:678–687. doi:10.1016/S0008-6363(01)00508-9.

[348] Joyner MJ, Barnes JN, Hart EC, Wallin BG, Charkoudian N. Neural Control of the Circulation: How Sex and Age Differences Interact in Humans. In: *Comprehensive Physiology*. John Wiley & Sons, Ltd; 2014. doi:10.1002/cphy.c140005.

[349] Baker PJ, Ramey ER, Ramwell PW. Androgen-mediated sex differences of cardiovascular responses in rats. *Am J Physiol*. 1978;235:H242–246. doi:10.1152/ajpheart.1978.235.2.H242.

[350] Zukowska-Grojec Z, Shen GH, Capraro PA, Vaz CA. Cardiovascular, neuropeptide Y, and adrenergic responses in stress are sexually differentiated. *Physiol Behav*. 1991;49:771–777. doi:10.1016/0031-9384(91)90317-h.

[351] Zukowska-Grojec Z. Neuropeptide Y. A novel sympathetic stress hormone and more. *Ann N Y Acad Sci*. 1995;771:219–233. doi:10.1111/j.1749-6632.1995.tb44683.x.

[352] Joshi H, Hynes LM, Edgell H. Influence of a neck compression collar on cerebrovascular and autonomic function in men and women. *PLOS ONE*. 2019;14:e0225868. doi:10.1371/journal.pone.0225868.

[353] Convertino VA. Gender differences in autonomic functions associated with blood pressure regulation. *Am J Physiol Regul Integr Comp Physiol*. 1998;275. doi:10.1152/AJPREGU.1998.275.6.R1909.

[354] Hinojosa-Laborde C, Shade RE, Muniz GW, Bauer C, Goei KA, Pidcoke HF, Chung KK, Cap AP, Convertino VA. Validation of lower body negative pressure as an experimental model of hemorrhage. *J Appl Physiol*. 2014;116:406. doi:10.1152/JAPPLPHYSIOL.00640.2013.

[355] Greenwald SH, Macias BR, Lee SM, Marshall-Goebel K, Ebert DJ, Liu JH, Ploutz-Snyder RJ, Alferova IV, Dulchavsky SA, Hargens AR, Stenger MB, Laurie SS. Intraocular pressure and choroidal thickness respond differently to lower body negative pressure during spaceflight. *J Appl Physiol*. 2021;131:613–620. doi:10.1152/JAPPLPHYSIOL.01040.2020.

[356] Lightfoot JT, Hilton F, Fortney SM. Repeatability and protocol comparability of presyncopal symptom limited lower body negative pressure exposures. *Aviat Space Environ Med*. 1991; 62:19–25.

[357] Convertino VA, Ludwig DA, Cooke WH. Stroke volume and sympathetic responses to lower-body negative pressure reveal new insight into circulatory shock in humans. *Auton Neurosci Basic Clin*. 2004;111:127–134. doi:10.1016/J.AUTNEU.2004.02.007.

[358] Franke WD, Johnson CP, Steinkamp JA, Wang R, Halliwill JR. Cardiovascular and autonomic responses to lower body negative pressure: Do not explain gender differences in orthostatic tolerance. *Clin Auton Res*. 2003;13:36–44. doi:10.1007/s10286-003-0066-x.

[359] Goswami N, Loeppky JA, Hinghofer-Szalkay H. LBNP: past protocols and technical considerations for experimental design. *Aviat Space Environ Med*. 2008;79:459–471. doi:10.3357/asem.2161.2008.

[360] Goswami N, Lackner HK, Grasser EK, Hinghofer-Szalkay HG. Individual stability of orthostatic tolerance response. *Acta Physiol Hung*. 2009;96:157–166. doi:10.1556/APhysiol.96.2009.2.2.

[361] Johnson PC. Fluid volumes changes induced by spaceflight. *Acta Astronaut*. 1979;6:1335–

1341. doi:10.1016/0094-5765(79)90125-5.

[362] Kelly DE, Scroop GC, Tonkin AL, Thornton AT. Cardiovascular responses to orthostatic and other stressors in men and women are independent of sex. *Clin Exp Pharmacol Physiol*. 2004;31:50–56. doi:10.1111/J.1440-1681.2004.03949.X.

[363] Khan MH, Sinoway LI, MacLean DA. Effects of graded LBNP on MSNA and interstitial norepinephrine. *Am J Physiol Heart Circ Physiol*. 2002;283:2038–2044. doi:10.1152/AJPHEART.00412.2001.

[364] Scherrer U, Vissing SF, Victor RG. Effects of lower-body negative pressure on sympathetic nerve responses to static exercise in humans. Microneurographic evidence against cardiac baroreflex modulation of the exercise pressor reflex. *Circulation*. 1988;78:49–59. doi:10.1161/01.CIR.78.1.49.

[365] Frey MA, Hoffler GW. Association of sex and age with responses to lower-body negative pressure. *J Appl Physiol*. 1988;65:1752–1756. doi:10.1152/JAPPL.1988.65.4.1752.

[366] White DD, Gotshall RW, Tucker A. Women have lower tolerance to lower body negative pressure than men. *J Appl Physiol*. 1996;80:1138–1143. doi:10.1152/JAPPL.1996.80.4.1138.

[367] Carter R, Hinojosa-Laborde C, Convertino VA. Sex comparisons in muscle sympathetic nerve activity and arterial pressure oscillations during progressive central hypovolemia. *Physiol Rep*. 2015;3. doi:10.14814/PHY2.12420.

[368] Ogoh S, Hirasawa A, Shibata S. Influence of head-up tile and lower body negative pressure on the internal jugular vein. *Physiol Rep*. 2022;10. doi:10.14814/PHY2.15248.

[369] Macias BR, Liu JH, Grande-Gutierrez N, Hargens AR. Intraocular and intracranial pressures during head-down tilt with lower body negative pressure. *Aerosp Med Hum Perform*. 2015; 86:3–7. doi:10.3357/AMHP.4044.2015.

[370] Kruschke JK. Rejecting or Accepting Parameter Values in Bayesian Estimation. *Adv Meth Pract Psychol Sci*. 2018;1:270–280. doi:10.1177/2515245918771304.

[371] Cohen J. *Statistical Power Analysis for the Behavioral Sciences*. Routledge Academic;

1988.

[372] Hoffman JI, Buckberg GD. The Myocardial Oxygen Supply:Demand Index Revisited. *J Am Heart Assoc*. 2014;3. doi:10.1161/JAHA.113.000285.

[373] Wadehn F, Heldt T. Adaptive Maximal Blood Flow Velocity Estimation From Transcranial Doppler Echos. *IEEE J Transl Eng Health Med*. 2020;8:1800511. doi:10.1109/JTEHM.2020.3011562.

[374] Reynolds RJ. Using Bayesian Estimation to Quantify the Risks of Spaceflight. In: *NASA Human Research Program Investigators Workshop*. 2020; 1–17.

[375] McElreath R. *Statistical Rethinking: A Bayesian Course with Examples in R and Stan*. CRC Press; 2020.

[376] Hong H, Carlin BP, Shamliyan TA, Wyman JF, Ramakrishnan R, Sainfort F, Kane RL. Comparing Bayesian and Frequentist Approaches for Multiple Outcome Mixed Treatment Comparisons. *Med Decis Mak*. 2013;33:702–714. doi:10.1177/0272989X13481110.

[377] Rupp AA, Dey DK, Zumbo BD. To Bayes or Not to Bayes, From Whether to When: Applications of Bayesian Methodology to Modeling. *Struct Equ Model*. 2004;11:424–451. doi:10.1207/s15328007sem1103_7.

[378] Kruschke JK. Bayesian Analysis Reporting Guidelines. *Nat Hum Behav*. 2021;5:1282–1291. doi:10.1038/s41562-021-01177-7.

[379] Jeffreys H. *The Theory of Probability*. Clarendon Press; 1961.

[380] Gelman A. Prior distributions for variance parameters in hierarchical models (comment on article by Browne and Draper). *Bayesian Anal*. 2006;1:515–534. doi:10.1214/06-BA117A.

[381] Lewandowski D, Kurowicka D, Joe H. Generating random correlation matrices based on vines and extended onion method. *J Multivar Anal*. 2009;100:1989–2001. doi:10.1016/J.JMVA.2009.04.008.

[382] van Zundert C, Somer E, Miočević M. Prior Predictive Checks for the Method of Covariances in Bayesian Mediation Analysis. *Struct Equ Model*. 2022;29:428–437. doi:10.1080/10705511.2021.1977648.

[383] Stan Development Team. Stan Modeling Language Users Guide and Reference Manual, Version 2.26.1. 2022.
URL https://mc-stan.org

[384] Bürkner PC. brms: An R Package for Bayesian Multilevel Models Using Stan. *J Stat Softw*. 2017;80:1–28. doi:10.18637/jss.v080.i01.

[385] Bürkner PC. Advanced Bayesian Multilevel Modeling with the R Package brms. *R J*. 2018; 10:395–411. doi:10.32614/RJ-2018-017.

[386] Bürkner PC. Bayesian Item Response Modeling in R with brms and Stan. *J Stat Softw*. 2021;100:1–54. doi:10.18637/jss.v100.i05.

[387] Gelman A, Rubin DB. Inference from Iterative Simulation Using Multiple Sequences. *Stat Sci*. 1992;7:457–472. doi:10.1214/SS/1177011136.

[388] Vehtari A, Simpson D, Gelman A, Yao Y, Gabry J. Pareto Smoothed Importance Sampling. *arXiv*. 2015;doi:10.48550/arxiv.1507.02646.

[389] Makowski D, Ben-Shachar MS, Chen SHA, Lüdecke D. Indices of Effect Existence and Significance in the Bayesian Framework. *Front Psychol*. 2019;10. doi:10.3389/fpsyg.2019.02767.

[390] Kruschke JK, Liddell TM. The Bayesian New Statistics: Hypothesis testing, estimation, meta-analysis, and power analysis from a Bayesian perspective. *Psychon Bull Rev*. 2018; 25:178–206. doi:10.3758/S13423-016-1221-4.

[391] Schwaferts P, Augustin T. Bayesian Decisions using Regions of Practical Equivalence (ROPE): Foundations. *Tech. Rep. 235*, Department of Statistics, University of Munich, Munich, Germany. 2020.
URL http://www.statistik.uni-muenchen.de

[392] DeMaris A. A Tutorial in Logistic Regression. *J Marriage Fam*. 1995;57:956–968. doi:10.2307/353415.

[393] Khan S, Kirubarajan A, Lee M, Pitha I, Buckey JC. The Correlation Between Body Weight and Intraocular Pressure. *Aerosp Med Hum Perform*. 2021;92:886–897.

doi:10.3357/AMHP.5769.2021.

[394] Murray RH, Thompson LJ, Bowers JA, Albright CD. Hemodynamic effects of graded hypovolemia and vasodepressor syncope induced by lower body negative pressure. *Am Heart J*. 1968;76:799–811. doi:10.1016/0002-8703(68)90266-4.

[395] Levine BD, Giller CA, Lane LD, Buckey JC, Blomqvist CG. Cerebral versus systemic hemodynamics during graded orthostatic stress in humans. *Circulation*. 1994;90:298–306. doi:10.1161/01.CIR.90.1.298.

[396] Roddie IC, Shepherd JT. Receptors in the high-pressure and low-pressure vascular systems; their role in the reflex control of the human circulation. *Lancet*. 1958;1:493–496. doi:10.1016/S0140-6736(58)90808-0.

[397] Victor RG, Mark AL. Interaction of cardiopulmonary and carotid baroreflex control of vascular resistance in humans. *J Clin Investig*. 1985;76:1592–1598. doi:10.1172/JCI112142.

[398] Convertino VA, Rickards CA, Ryan KL. Autonomic mechanisms associated with heart rate and vasoconstrictor reserves. *Clin Auton Res*. 2012;22:123–130. doi:10.1007/S10286-011-0151-5.

[399] Cooke WH, Convertino VA. Heart rate variability and spontaneous baroreflex sequences: implications for autonomic monitoring during hemorrhage. *J Trauma*. 2005;58:798–805. doi:10.1097/01.TA.0000151345.16338.FD.

[400] Cooke WH, Rickards CA, Ryan KL, Convertino VA. Autonomic compensation to simulated hemorrhage monitored with heart period variability. *Crit Care Med*. 2008;36:1892–1899. doi:10.1097/CCM.0B013E3181760D0C.

[401] Pomeranz B, B Macaulay RJ, Caudill MA, Kutz I, Adam D, Gordon D, Kilborn KM, Clifford Barger A, Shannon DC, Cohen RJ, Benson H, Kilborn KnM, Shannon DC, BENSON Assessment H. Assessment of autonomic function in humans by heart rate spectral analysis. *Am J Physiol Heart Circ Physiol*. 1985;248:H151–H153. doi:10.1152/AJPHEART.1985.248.1.H151.

[402] Joyner MJ, Shepherd JT, Seals DR. Sustained increases in sympathetic outflow during

prolonged lower body negative pressure in humans. *J Appl Physiol*. 1990;68:1004–1009. doi:10.1152/JAPPL.1990.68.3.1004.

[403] Rea RF, Wallin BG. Sympathetic nerve activity in arm and leg muscles during lower body negative pressure in humans. *J Appl Physiol*. 1989;66:2778–2781. doi:10.1152/JAPPL.1989.66.6.2778.

[404] Ryan KL, Rickards CA, Hinojosa-Laborde C, Cooke WH, Convertino VA. Sympathetic responses to central hypovolemia: New insights from microneurographic recordings. *Front Physiol*. 2012;3 APR. doi:10.3389/FPHYS.2012.00110/PDF.

[405] Convertino VA. Neurohumoral mechanisms associated with orthostasis: Reaffirmation of the significant contribution of the heart rate response. *Front Physiol*. 2014;5 JUN. doi:10.3389/FPHYS.2014.00236/PDF.

[406] Convertino VA, Sather TM. Effects of cholinergic and beta-adrenergic blockade on orthostatic tolerance in healthy subjects. *Clin Auton Res*. 2000;10:327–336. doi:10.1007/BF02322256.

[407] Goswami N, Evans J, Schneider S, Wiesche Mvd, Mulder E, Rössler A, Hinghofer-Szalkay H, Blaber AP. Effects of Individualized Centrifugation Training on Orthostatic Tolerance in Men and Women. *PLOS ONE*. 2015;10:e0125780. doi:10.1371/JOURNAL.PONE.0125780.

[408] Hinojosa-Laborde C, Aden JK, Goei KA, Convertino VA. Evidence for a higher risk of hypovolemia-induced hemodynamic instability in females: implications for decision support during prehospital triage. *Mil Med*. 2015;180:19–23. doi:10.7205/MILMED-D-14-00394.

[409] Frey MA, Mathes KL, Hoffler GW. Cardiovascular responses of women to lower body negative pressure. *Aviat Space Environ Med*. 1986;57:531–538.

[410] Jeon JC, Ik Choi W, Lee JH, Lee SH. Anatomical Morphology Analysis of Internal Jugular Veins and Factors Affecting Internal Jugular Vein Size. *Medicina*. 2020;56. doi:10.3390/MEDICINA56030135.

[411] Magnano C, Belov P, Krawiecki J, Hagemeier J, Beggs C, Zivadinov R. Internal Jugular Vein Cross-Sectional Area Enlargement Is Associated with Aging in Healthy Individuals. *PLOS ONE*. 2016;11. doi:10.1371/JOURNAL.PONE.0149532.

[412] Robb AO, Mills NL, Newby DE, Denison FC. Endothelial progenitor cells in pregnancy. *Reproduction*. 2007;133:1–9. doi:10.1530/REP-06-0219.

[413] Yang JX, Pan YY, Wang XX, Qiu YG, Mao W. Endothelial progenitor cells in age-related vascular remodeling. *Cell Transplant*. 2018;27:786. doi:10.1177/0963689718779345.

[414] Katori R. Normal cardiac output in relation to age and body size. *Tohoku J Exp Med*. 1979; 128:377–387. doi:10.1620/TJEM.128.377.

[415] Cioccari L, Luethi N, Glassford NJ, Bellomo R. The normal cardiac index in older healthy individuals: A scoping review. *Crit Care Resusc*. 2019;21:9–17.

[416] Fındıkoğlu G, Cetin E, Sarsan A, Senol H, Yildirim C, Ardic F. Arterial and intraocular pressure changes after a single-session hot-water immersion. *Undersea Hyperb Med*. 2015; 42:65–73.

[417] Samsudin A, Isaacs N, Tai MLS, Ramli N, Mimiwati Z, Choo MM. Ocular perfusion pressure and ophthalmic artery flow in patients with normal tension glaucoma. *BMC Ophthalmol*. 2016;16. doi:10.1186/S12886-016-0215-3.

[418] Kristiansson H, Nissborg E, Bartek JJ, Andresen M, Reinstrup P, Romner B. Measuring Elevated Intracranial Pressure through Noninvasive Methods: A Review of the Literature. *J Neurosurg Anesthesiol*. 2013;25:372. doi:10.1097/ANA.0b013e31829795ce.

[419] Lightfoot JT, Febles S, Fortney SM. Adaptation to repeated presyncopal lower body negative pressure exposures. *Aviat Space Environ Med*. 1989;60:17–22.

[420] Howden R, Tranfield PA, Lightfoot JT, Brown SJ, Swaine IL. The reproducibility of tolerance to lower-body negative pressure and its quantification. *Eur J Appl Physiol*. 2001; 84:462–468. doi:10.1007/s004210100398.

[421] Heldt T, Mukkamala R, Moody GB, Mark RG. CVSim: An Open-Source Cardiovascular Simulator for Teaching and Research. *Open Pacing, Electrophysiol Ther J*. 2010;3:45–54.

[422] Defares J, Osborn J, Hara H. Theoretical synthesis of the cardiovascular system. Study I: The controlled system. *Acta Physiol et Pharmacol Neerlandica*. 1963;12:189–265.

[423] de Boer R, Karemaker JM, Stracke J. Description of the Heart Rate Variability Data in Accordance With a Physiological Model for the Genesis of Heartbeats. *Psychophysiology*. 1985;22:147–155. doi:10.1111/j.1469-8986.1985.tb01577.x.

[424] Mead J, Gaensler EA. Esophageal and pleural pressures in man, upright and supine. *J Appl Physiol*. 1959;14:81–83. doi:10.1152/jappl.1959.14.1.81.

[425] Ferris BG, Mead J, Frank NR. Effect of body position on esophageal pressure and measurement of pulmonary compliance. *J Appl Physiol*. 1959;14:521–524. doi:10.1152/jappl.1959.14.4.521.

[426] Smit AA, Halliwill JR, Low PA, Wieling W. Pathophysiological basis of orthostatic hypotension in autonomic failure. *J Physiol*. 1999;519:1–10. doi:10.1111/j.1469-7793.1999.0001o.x.

[427] Bie P, Secher NH, Astrup A, Warberg J. Cardiovascular and endocrine response to head-up tilt and vasopressin infusion in humans. *Am J Physiol Regul Integr Comp Physiol*. 1986; 251:R735–41. doi:10.1152/ajpregu.1986.251.4.r735.

[428] Minson CT, Wladkowski SL, Pawelczyk JA, Kenney WL. Age, splanchnic vasoconstriction, and heat stress during tilting. *Am J Physiol Regul Integr Comp Physiol*. 1999;276. doi:10.1152/ajpregu.1999.276.1.r203.

[429] Foldager N, Andersen TA, Jessen FB, Ellegaard P, Stadeager C, Videbæk R, Norsk P. Central venous pressure in humans during microgravity. *J Appl Physiol*. 1996;81:408–412. doi:10.1152/jappl.1996.81.1.408.

[430] Buckey JC, Anderson A, Archambault-Leger V, Phillips SD, Anderson AP, Chepko AB, Masterova KS, Fellows AM, Cowan DR. The Importance of Tissue Weight and Tissue Compressive Forces in Human Spaceflight. In: *68 th International Astronautical Congress (IAC)*. 2017; 25–29.

[431] Niederer SA, Smith NP. At the heart of computational modelling. *J Physiol*. 2012;

590:1331–1338. doi:10.1113/jphysiol.2011.225045.

[432] Marino S, Hogue IB, Ray CJ, Kirschner DE. A methodology for performing global uncertainty and sensitivity analysis in systems biology. *J Theor Biol*. 2008;254:178–196. doi:10.1016/j.jtbi.2008.04.011.

[433] Kleiber M. Body size and metabolism. *Hilgardia*. 1932;6:315–353. doi:10.3733/hilg.v06n11p315.

[434] McMahon TA. Size and shape in biology. *Sci*. 1973;179:1201–1204. doi:10.1126/science.179.4079.1201.

[435] McMahon TA. Scaling physiological time. *Lect Math Life Sci*. 1980;13:131–163.

[436] Leggett RW, Williams LR. A proposed blood circulation model for reference man. *Health Phys*. 1995;69:187–201. doi:10.1097/00004032-199508000-00003.

[437] Gibson BYJG, Evans WA. Clinical studies of the blood volume. II. The relation of plasma and total blood volume to venous pressure, blood velocity rate, physical measurements, age and sex in ninety normal humans. *J Clin Investig*. 1937;16:317–328. doi:10.1172/JCI100860.

[438] Sjöstrand T. Volume and Distribution of Blood and Their Significance in Regulating the Circulation. *Physiol Rev*. 1953;33:202–228. doi:10.1152/physrev.1953.33.2.202.

[439] Khan AA, Lye L, Husain T. Latin hypercube sampling for uncertainty analysis in multiphase modelling. *J Environ Eng Sci*. 2008;7:617–626. doi:10.1139/S08-031.

[440] Feola AJ, Myers JG, Raykin J, Mulugeta L, Nelson ES, Samuels BC, Ethier CR. Finite Element Modeling of Factors Influencing Optic Nerve Head Deformation Due to Intracranial Pressure. *Investig Ophthalmol Vis Sci*. 2016;57:1901–1911. doi:10.1167/iovs.15-17573.

[441] Helton JC, Davis FJ. Latin hypercube sampling and the propagation of uncertainty in analyses of complex systems. *Reliab Eng Syst Saf*. 2003;81:23–69. doi:10.1016/S0951-8320(03)00058-9.

[442] Gomero B. Latin Hypercube Sampling and Partial Rank Correlation Coefficient analysis applied to an optimal control problem. 2012.

[443] Yu H, Chung CY, Wong KP, Lee HW, Zhang JH. Probabilistic load flow evaluation with hybrid latin hypercube sampling and cholesky decomposition. *IEEE Trans Power Syst*. 2009;24:661–667. doi:10.1109/TPWRS.2009.2016589.

[444] McKay MD, Beckman RJ, Conover WJ. Comparison of three methods for selecting values of input variables in the analysis of output from a computer code. *Technometrics*. 1979; 21:239–245. doi:10.2307/1268522.

[445] Iman RL. Latin Hypercube Sampling. In: *Encyclopedia of Quantitative Risk Analysis and Assessment*, edited by Melnick EL, Everitt BS. John Wiley & Sons, Ltd; 2008. doi:https://doi:10.1002/9781118445112.stat03803.

[446] Stein M. Large Sample Properties of Simulations Using Latin Hypercube Sampling. *Technometrics*. 1987;29:143–151. doi:10.1080/00401706.1987.10488205.

[447] Viana FAC, Venter G, Balabanov V. An algorithm for fast optimal Latin hypercube design of experiments. *Int J Numer Meth Eng*. 2010;82:135–156. doi:10.1002/nme.2750.

[448] Minasny B, McBratney AB. A conditioned Latin hypercube method for sampling in the presence of ancillary information. *Comput Geosci*. 2006;32:1378–1388. doi:10.1016/j.cageo.2005.12.009.

[449] Taylor R. Interpretation of the correlation coefficient: a basic review. *J Diagn Med Sonogr*. 1990;6:35–39. doi:10.1177/875647939000600106.

[450] Hauke J, Kossowski T. Comparison of Valuess of Pearson's and Spearman's Correlation Coefficients of the Same Sets of Data. *Quaest Geogr*. 2011;30:87–93. doi:10.2478/v10117-011-0021-1.

[451] Kendall MG. *Rank Correlation Methods*. Oxford University Press; 1990.

[452] Nelder JA, Baker RJ. Generalized linear models. In: *Encyclopedia of Statistical Sciences*, edited by Kotz S, Read C, Balakrishnan N, Vidakovic B, Johnson N. John Wiley & Sons, Ltd; 2006.

[453] Gallego G, Moon I. The Distribution Free Newsboy Problem: Review and Extensions. *J Oper Res Soc*. 1993;44:825–834. doi:10.2307/2583894.

[454] Recek C. Calf pump activity influencing venous hemodynamics in the lower extremity. *Int J Angiol*. 2013;22:23–30. doi:10.1055/s-0033-1334092.

[455] Greenway CV, Lautt WW. Blood volume, the venous system, preload, and cardiac output. *Can J Physiol Pharmacol*. 1986;64:383–387. doi:10.1139/y86-062.

[456] Joyner MJ, Wilkins BW. Exercise hyperaemia: is anything obligatory but the hyperaemia? *J Physiol*. 2007;583:855–860. doi:10.1113/jphysiol.2007.135889.

[457] Skoog J, Lindenberger M, Ekman M, Holmberg B, Zachrisson H, Länne T. Reduced venous compliance: An important determinant for orthostatic intolerance in women with vasovagal syncope. *Am J Physiol Regul Integr Comp Physiol*. 2016;310:R253–R261. doi:10.1152/ajpregu.00362.2015.

[458] Coats BW, Sharp KM. Simulated stand tests and centrifuge training to prevent orthostatic intolerance on earth, moon, and mars. *Ann Biomed Eng*. 2010;38:1119–1131. doi:10.1007/s10439-010-9943-3.

[459] Blanco PJ, Trenhago PR, Fernandes LG, Feijóo RA. On the integration of the baroreflex control mechanism in a heterogeneous model of the cardiovascular system. *Int J Numer Meth Biomed Eng*. 2012;28:412–433. doi:10.1002/cnm.1474.

[460] Bulpitt CJ, Cameron JD, Rajkumar C, Armstrong S, Connor M, Joshi J, Lyons D, Moioli O, Nihoyannopoulos P. The effect of age on vascular compliance in man: Which are the appropriate measures? *J Hum Hypertension*. 1999;13:753–758. doi:10.1038/sj.jhh.1000879.

[461] van Duijnhoven NT, Bleeker MW, Groot PC, Thijssen DH, Felsenberg D, Rittweger J, Hopman MT. The effect of bed rest and an exercise countermeasure on leg venous function. *Eur J Appl Physiol*. 2008;104:991–998. doi:10.1007/s00421-008-0854-z.

[462] Maron BJ, Pelliccia A, Spirito P. Cardiac disease in young trained athletes: Insights into methods for distinguishing athlete's heart from structural heart disease, with particular emphasis on hypertrophic cardiomyopathy. *Circulation*. 1995;91:1596–1601. doi:10.1161/01.CIR.91.5.1596.

[463] MacDonald JR. Potential causes, mechanisms, and implications of post exercise hypoten-

sion. *J Hum Hypertension*. 2002;16:225–236. doi:10.1038/sj.jhh.1001377.

[464] Bull RK, Davies CT, Lind AR, White MJ. The human pressor response during and following voluntary and evoked isometric contraction with occluded local blood supply. *J Physiol*. 1989;411:63–70. doi:10.1113/jphysiol.1989.sp017560.

[465] Aubert AE, Beckers F, Verheyden B, Pletser V. What Happens to the Human Heart in Space?-Parabolic Flights Provide Some Answers Parabolic Flights. *esa Bull*. 2004;119:31–38.

[466] Norsk P, Damgaard M, Petersen L, Gybel M, Pump B, Gabrielsen A, Christensen NJ. Vasorelaxation in space. *Hypertension*. 2006;47:69–73. doi:10.1161/01.HYP.0000194332.98674.57.

[467] Mukai CN, Lathers CM, Charles JB, Bennett BS, Igarashi M, Patel S. Acute Hemodynamic Responses to Weightlessness During Parabolic Flight. *J Clin Pharmacol*. 1991;31:993–1000. doi:10.1002/j.1552-4604.1991.tb03662.x.

[468] Cooper VL, Hainsworth R. Effects of head-up tilting on baroreceptor control in subjects with different tolerances to orthostatic stress. *Clin Sci*. 2002;103:221–226. doi:10.1042/cs1030221.

[469] Iwasaki KI, Zhang R, Zuckerman JH, Pawelczyk JA, Levine BD. Effect of head-down-tilt bed rest and hypovolemia on dynamic regulation of heart rate and blood pressure. *Am J Physiol Regul Integr Comp Physiol*. 2000;279:R2189–R2199. doi:10.1152/ajpregu.2000.279.6.R2189.

[470] Dell'Italia LJ, Walsh RA. Application of a time varying elastance model to right ventricular performance in man. *Cardiovasc Res*. 1988;22:864–874. doi:10.1093/cvr/22.12.864.

[471] Henry JP. The significance of the loss of blood volume into the limbs during pressure breathing. *J Aviat Med*. 1951;22:31–8.

[472] Gotshall RW, Tsai PF, Frey MA. Gender-based differences in the cardiovascular response to standing. *Aviat Space Environ Med*. 1991;62:855–9.

[473] Siamwala JH, Macias BR, Lee PC, Hargens AR. Gender differences in tibial microvascular

flow responses to head down tilt and lower body negative pressure. *Physiol Rep*. 2017; 5:e13143. doi:10.14814/phy2.13143.

[474] Evans JM, Knapp CF, Goswami N. Artificial Gravity as a Countermeasure to the Cardiovascular Deconditioning of Spaceflight: Gender Perspectives. *Front Physiol*. 2018;9:716. doi:10.3389/fphys.2018.00716.

[475] Fong KJ, Arya M, Paloski WH. Gender differences in cardiovascular tolerance to short radius centrifugation. *J Gravit Physiol*. 2007;14:P15–9.

[476] Berkes P, Wood F, Pillow J. Characterizing neural dependencies with copula models. *Adv Neural Inf Process Syst*. 2008;21:1–8. doi:10.5555/2981780.2981797.

[477] Gisolf J, Van Lieshout JJ, Van Heusden K, Pott F, Stok WJ, Karemaker JM. Human cerebral venous outflow pathway depends on posture and central venous pressure. *J Physiol*. 2004; 560:317–327. doi:10.1113/jphysiol.2004.070409.

[478] Zhang LF. Invited Review: Vascular adaptation to microgravity: what have we learned? *J Appl Physiol*. 2001;91:2415–2430. doi:10.1152/jappl.2001.91.6.2415.

[479] Cirovic S, Walsh C, Fraser WD, Gulino A. The effect of posture and positive pressure breathing on the hemodynamics of the internal jugular vein. *Aviat Space Environ Med*. 2003;74:125–131.

[480] Gray H. *Anatomy of the Human Body*. Lea & Febiger; 1878.

[481] Singh M, Jaiswal S, Sharma PK, Vaidya VK. A cadaveric study of the length of the brachial artery and its clinical correlation. *Era's J Med Res*. 2020;7:72–74. doi:10.24041/ejmr2020.12.

[482] Vriz O, Magne J, Driussi C, Brosolo G, Ferrara F, Palatini P, Aboyans V, Bossone E. Comparison of arterial stiffness/compliance in the ascending aorta and common carotid artery in healthy subjects and its impact on left ventricular structure and function. *Int J Cardiovasc Imaging*. 2017;33:521–531. doi:10.1007/s10554-016-1032-8.

[483] Gamble G, Zorn J, Sanders G, MacMahon S, Sharpe N. Estimation of arterial stiffness, compliance, and distensibility from M-mode ultrasound measurements of the common carotid

artery. *Stroke*. 1994;25:11–16. doi:10.1161/01.STR.25.1.11.

[484] Amelard R, Flannigan N, Patterson CA, Heigold H, Hughson RL, Robertson AD. Assessing jugular venous compliance with optical hemodynamic imaging by modulating intrathoracic pressure. *J Biomed Opt*. 2022;27:116005. doi:10.1117/1.JBO.27.11.116005.

[485] Barratt-Boyes BG, Wood EH. Cardiac output and related measurements and pressure values in the right heart and associated vessels, together with an analysis of the hemodynamic response to the inhalation of hight oxygen mixtures in healthy subjects. *J Lab Clin Med*. 1958;51:72–90.

[486] Sejersen C, Christiansen T, Secher NH. To identify normovolemia in humans: The stroke volume response to passive leg raising vs. head-down tilt. *Physiol Rep*. 2022;10:e15216. doi:10.14814/phy2.15216.

[487] Wang Z, Heshka S, Wang J, Wielopolski L, Heymsfield SB. Magnitude and variation of fat-free mass density: a cellular-level body composition modeling study. *Am J Physiol Endocrinol Metab*. 2003;284:E267–273. doi:10.1152/ajpendo.00151.2002.

[488] Nelson ES, Myers JG, Lewandowski BE, Ross Ethier C, Samuels BC. Acute effects of posture on intraocular pressure. *PLOS ONE*. 2020;15:e0226915. doi:10.1371/journal.pone.0226915.

[489] Gambino S, Mirochnik M, Schechter S. Center of Mass of a Human. In: *The Physics Factbook*, edited by Elert G. Hypertextbook; 2006.

[490] Ogden CL. *Mean Body Weight, Height, and Body Mass Index: United States 1960-2002*. Department of Health and Human Services, Centers for Disease Control and Prevention, National Center for Health Statistics; 2004.

[491] Jain RB. Geometric Means, Reference Ranges, and Selected Percentile Points for Blood Volume Measurements by Age, Race/Ethnicity, and Gender. *J Adv Nutr Hum Metab*. 2016; doi:10.14800/janhm.1288.

[492] Thrall SF, Tymko MM, Green CLM, Wynnyk KI, Brandt RA, Day TA. The effect of hypercapnia on regional cerebral blood flow regulation during progressive lower-body negative

pressure. *Eur J Appl Physiol*. 2021;121:339–349. doi:10.1007/s00421-020-04506-2.

[493] Tymko MM, Rickards CA, Skow RJ, Ingram-Cotton NC, Howatt MK, Day TA. The effects of superimposed tilt and lower body negative pressure on anterior and posterior cerebral circulations. *Physiol Rep*. 2016;4:e12957. doi:10.14814/phy2.12957.

[494] Neumann S, Burchell AE, Rodrigues JC, Lawton CB, Burden D, Underhill M, Kobetić MD, Adams ZH, Brooks JC, Nightingale AK, Paton JFR, Hamilton MC, Hart EC. Cerebral Blood Flow Response to Simulated Hypovolemia in Essential Hypertension: A Magnetic Resonance Imaging Study. *Hypertension*. 2019;74:1391–1398. doi:10.1161/HYPERTENSIONAHA.119.13229.

[495] White RJ, Blomqvist CG. Central venous pressure and cardiac function during spaceflight. *J Appl Physiol*. 1998;85:738–746. doi:10.1152/jappl.1998.85.2.738.

[496] Silverman A, Petersen NH. Physiology, Cerebral Autoregulation. In: *StatPearls*. StatPearls Publishing; 2023.

[497] Paulson OB, Strandgaard S, Edvinsson L. Cerebral autoregulation. *Cerebrovasc Brain Metab Rev*. 1990;2:161–192.

[498] Whittle RS, Dunbar BJ, Diaz-Artiles A. Acute dose-response of the internal jugular vein to graded head up and head down tilt. *Aerosp Med Hum Perform*. 2023;94:327.

[499] Hall EA, Whittle RS, Diaz-Artiles A. Effect of lower body negative pressure on ocular perfusion pressure. *Aerosp Med Hum Perform*. 2023;94:311.

[500] Whittle RS. Quantifying and modeling the acute cardiovascular response to altered-gravity and spaceflight countermeasures. In: *2022 Rising Stars in Aerospace Symposium*. Boulder, CO. 2022; 1–14.

[501] Whittle RS, Keller N, Hall EA, Vellore HS, Stapleton LM, Findlay KH, Dunbar BJ, Diaz-Artiles A. Hemodynamic and autonomic response of the cardiovascular system to tilt: gravitational dose-response curves. In: *NASA Human Research Program Investigators Workshop*. Virtual. 2022; 1–32.

[502] Whittle RS, Petersen LG, Lee JH, Sieker J, Petersen JCG, Diaz-Artiles A. Modeling changes

in intraocular pressure associated with the physiological response to changes in the gravitational vector. *Aerosp Med Hum Perform*. 2021;92:512.

[503] Whittle RS, Keller N, Stapleton LM, Hall EA, Dunbar BJ, Diaz-Artiles A. Acute gravitational dose-response curves in hemodynamic and ocular variables induced by tilt. In: *Proceedings of the 2021 International Society of Gravitational Physiology (ISGP) Meeting*, edited by Bagher P, Bloomfield S, Diaz-Artiles A, Custaud MA. 2021; 234–239. doi:10.3389/978-2-88971-011-9.

[504] Whittle RS, Keller N, Dunbar BJ, Diaz-Artiles A. Sex differences in cardiovascular response to lower body negative pressure. In: *poster session presented at the NASA Human Research Program Investigators Workshop*. Galveston, TX. 2023; 1.

[505] Diaz-Artiles A, Whittle RS, Keller N, Hall EA, Dunbar BJ. Predicting acute cardiovascular and ocular changes due to tilt, LBNP, and centrifugation: Status report and next steps. In: *poster session presented at the NASA Human Research Program Investigators Workshop*. Galveston, TX. 2023; 1.

[506] Whittle RS, Real Fraxedas F, Keller N, Dunbar BJ, Diaz-Artiles A. Quantifying the cardiovascular response to fluid shifts induced by graded lower body negative pressure (LBNP). In: *poster session presented at the American Society for Gravitational and Space Research (ASGSR) 2022 Meeting*. Houston, TX. 2022; 1.

[507] Diaz-Artiles A, Whittle RS, Real Fraxedas F, Hall EA, Vellore HS, Dunbar BJ. Gravitational dose-response curves during tilt, LBNP, and centrifugation. In: *poster session presented at the NASA Human Research Program Investigators Workshop*. Virtual. 2022; 1.

[508] Real Fraxedas F, Whittle RS, Diaz-Artiles A. Modeling gravitational dose-response curves during tilt, LBNP, and centrifugation. In: *poster session presented at the NASA Human Research Program Investigators Workshop*. Virtual. 2022; 1.

[509] Diaz-Artiles A, Whittle RS, Stapleton L, Keller N, Dunbar BJ. Predicting acute CV and ocular changes due to changes in the gravitational vector. In: *poster session presented at the NASA Human Research Program Investigators Workshop*. Virtual. 2021; 1.

[510] Whittle RS, Diaz-Artiles A. A multidisciplinary approach to characterizing the long duration impact of hypogravity exposure on the cardiovascular system. In: *poster session presented at the NASA Human Research Program Investigators Workshop*. Galveston, TX. 2020; 1.

[511] Lee J, Whittle RS, Diaz-Artiles A, Sieker J, Petersen JCG, Petersen LG. Gravitational effects on ocular perfusion pressure. In: *poster session presented at the NASA Human Research Program Investigators Workshop*. Galveston, TX. 2020; 1.

[512] Whittle RS, Diaz-Artiles A. Understanding Cardiovascular Changes on Long Duration Spaceflight. In: *poster session presented at Paving the Road to Living in Space: Asgardia's First Science and Investment Congress*. Darmstadt, Germany. 2019; 1.

[513] Whittle RS, Alonso DA, Diaz-Artiles A. Individual Differences in Cardiovascular Responses to Orthostatic Stress. In: *poster session presented at the NASA Human Research Program Investigators Workshop*. Galveston, TX. 2019; 1.

[514] Ahlgrim C, Birkner P, Seiler F, Grundmann S, Baumstark MW, Bode C, Pottgiesser T. Applying the Optimized CO Rebreathing Method for Measuring Blood Volumes and Hemoglobin Mass in Heart Failure Patients. *Front Physiol*. 2018;9. doi:10.3389/fphys.2018.01603.

[515] Ahlgrim C, Seiler F, Birkner P, Staudacher DL, Grundmann S, Bode C, Pottgiesser T. Time course of red cell volume and plasma volume over six months in compensated chronic heart failure. *ESC Heart Fail*. 2021;8:1696–1699. doi:10.1002/ehf2.13179.

[516] Lundgren KM, Aspvik NP, Langlo KAR, Braaten T, Wisløff U, Stensvold D, Karlsen T. Blood Volume, Hemoglobin Mass, and Peak Oxygen Uptake in Older Adults: The Generation 100 Study. *Front Sports Act Living*. 2021;3:638139. doi:10.3389/fspor.2021.638139.

[517] Khan MN, Shallwani H, Khan MU, Shamim MS. Noninvasive monitoring intracranial pressure – A review of available modalities. *Surg Neurol Int*. 2017;8:51. doi:10.4103/sni.sni_403_16.

[518] Fois M, Maule SV, Giudici M, Valente M, Ridolfi L, Scarsoglio S. Cardiovascular Response

to Posture Changes: Multiscale Modeling and in vivo Validation During Head-Up Tilt. *Front Physiol*. 2022;13. doi:10.3389/fphys.2022.826989.

[519] Ursino M, Giannessi M. A Model of Cerebrovascular Reactivity Including the Circle of Willis and Cortical Anastomoses. *Ann Biomed Eng*. 2010;38:955–974. doi:10.1007/s10439-010-9923-7.

[520] Huo B, Fu RR. Recent advances in theoretical models of respiratory mechanics. *Acta Mech Sin*. 2012;28:1–7. doi:10.1007/s10409-012-0024-8.

APPENDIX A

CARDIOVASCULAR MODEL PARAMETERS

Figure A.1 shows a complete schematic of the model developed in Section 6.4. Tables A.1 to A.13 detail the model parameters used as a baseline.

In Figure A.1, the model is composed of four sections: head and arms, thorax, abdomen, and legs. The 19 systemic compartments are numbered as followed: 1, proximal aorta; 2, brachiocephalic arteries; 3, brachial arteries and 4, veins; 5, superior vena cava; 6, thoracic aorta; 7, abdominal aorta; 8, renal arteries and 9, veins; 10, splanchnic arteries and 11, veins; 12, leg arteries and 13, veins; 14, abdominal veins; 15, inferior vena cava; H1, carotid arteries; H2, head arteries and H3, veins; H4, jugular veins. Capillary beds are represented by five microvascular resistances: head r_{ceph}, arms r_{arm}, kidneys r_{rc}, splanchnic r_{sc}, and legs r_{lc}. Pulmonary circulation is represented by r_{pc} and the vertebral plexus by r_{vp}. Upper and lower body interstitial compartments, arterial baroreflex, and cardiopulmonary reflex are not shown.

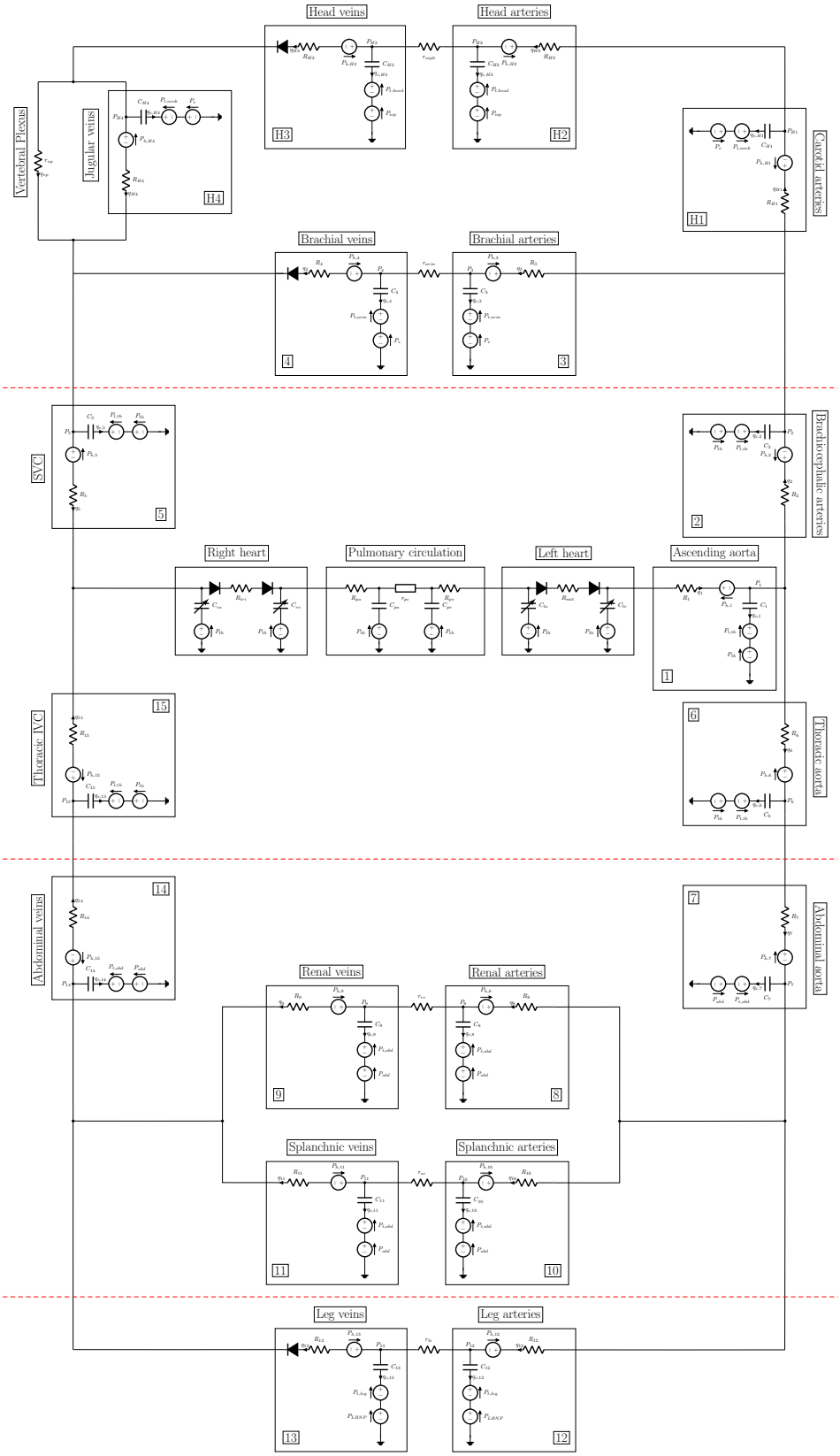

Figure A.1: Circuit representation of the 25-compartment model, see text for details.

Table A.1: Compartment definitions for the 25-compartment lumped-parameter cardiovascular model.

Compartment Definitions	
Compartment	**Definition**
1	Ascending Aorta
2	Brachiocephalic Arteries
3	Brachial Arteries
4	Brachial Veins
5	Superior Vena Cava
6	Descending Aorta
7	Abdominal Aorta
8	Renal Arteries
9	Renal Veins
10	Splanchnic Arteries
11	Splanchnic Veins
12	Leg Arteries
13	Leg Veins
14	Abdominal Veins
15	Inferior Vena Cava
H1	Carotid Arteries
H2	Head Arteries
H3	Head Veins
H4	Jugular Veins
pa	Pulmonary Arteries
pv	Pulmonary Veins
ra	Right Atrium
rv	Right Ventricle
la	Left Atrium
lv	Left Ventricle

Table A.2: Compartment inner ($r_{i,n}$) and outer ($r_{o,n}$) radii and vertical length ($l_{v,n}$).

Vascular Length				
Compartment, n		$r_{i,n}$	$r_{o,n}$	$l_{v,n}$
1	*cm*	39.5	49.5	10.0
2	*cm*	35.0	39.5	4.5
3	*cm*	35.0	101.0	66.0*
4	*cm*	35.0	101.0	66.0*
5	*cm*	35.0	49.5	14.5
6	*cm*	39.5	55.5	16.0
7	*cm*	55.5	70.0	14.5
8	*cm*	65.0	65.0	0.0
9	*cm*	65.0	65.0	0.0
10	*cm*	70.0	80.0	10.0
11	*cm*	70.0	80.0	10.0
12	*cm*	70.0	175.0	105.0*
13	*cm*	70.0	175.0	105.0*
14	*cm*	55.5	70.0	14.5
15	*cm*	49.5	55.5	6.0
H1	*cm*	15.0	35.0	20.0
H2	*cm*	5.0	25.0	20.0
H3	*cm*	5.0	25.0	20.0
H4	*cm*	15.0	35.0	20.0

Notes:
*Effective vertical length is 1/3 of l_v for compartments 3, 4, 12, and 13.

Table A.3: Compartment resistances, R_n, in PRU (mmHg.s/ml). R_{tri} is the resistance of the tricuspid valve, R_{mit} is the resistance of the mitral valve.

Resistance		
R_1	*PRU*	0.007
R_2	*PRU*	0.003
R_3	*PRU*	0.014
R_4	*PRU*	0.11
R_5	*PRU*	0.028
R_6	*PRU*	0.011
R_7	*PRU*	0.01
R_8	*PRU*	0.1
R_9	*PRU*	0.11
R_{10}	*PRU*	0.07
R_{11}	*PRU*	0.07
R_{12}	*PRU*	0.09
R_{13}	*PRU*	0.1
R_{14}	*PRU*	0.019
R_{15}	*PRU*	0.008
R_{H1}	*PRU*	0.014
R_{H2}	*PRU*	0.014
R_{H3}	*PRU*	0.05
R_{H4}	*PRU*	0.05
R_{pa}	*PRU*	0.006
R_{pv}	*PRU*	0.006
R_{tri}	*PRU*	0.006
R_{mit}	*PRU*	0.01

Table A.4: Microvascular resistances, r. Abbreviations: $ceph$, head; arm, arms; rc, renal circulation; sc, splanchnic circulation; lc, leg circulation; vp, vertebral plexus; pc, pulmonary circulation.

Microvascular Resistance		
r_{ceph}	*PRU*	9.0
r_{arm}	*PRU*	10.8
r_{rc}	*PRU*	5.2
r_{sc}	*PRU*	3.3
r_{lc}	*PRU*	4.5
r_{vp}	*PRU*	0.068
r_{pc}	*PRU*	0.07

Table A.5: Compartment compliances, C_n. $C_{es,n}$ and $C_{d,n}$ represent the end-systolic and diastolic compliances, respectively, for the variable capacitors in the heart compartments.

Compliance		
C_1	*ml/mmHg*	0.28
C_2	*ml/mmHg*	0.13
C_3	*ml/mmHg*	0.26
C_4	*ml/mmHg*	1.2
C_5	*ml/mmHg*	1.3
C_6	*ml/mmHg*	0.21
C_7	*ml/mmHg*	0.1
C_8	*ml/mmHg*	0.21
C_9	*ml/mmHg*	5
C_{10}	*ml/mmHg*	0.42
C_{11}	*ml/mmHg*	50
C_{12}	*ml/mmHg*	0.42
C_{13}	*ml/mmHg*	27
C_{14}	*ml/mmHg*	1.3
C_{15}	*ml/mmHg*	0.5
C_{H1}	*ml/mmHg*	0.07
C_{H2}	*ml/mmHg*	0.08
C_{H3}	*ml/mmHg*	3.35
C_{H4}	*ml/mmHg*	2.45
C_{pa}	*ml/mmHg*	3.4
C_{pv}	*ml/mmHg*	9.0
$C_{es,ra}$	*ml/mmHg*	1.35
$C_{d,ra}$	*ml/mmHg*	3.33
$C_{es,rv}$	*ml/mmHg*	0.77
$C_{d,rv}$	*ml/mmHg*	19
$C_{es,la}$	*ml/mmHg*	1.64
$C_{d,la}$	*ml/mmHg*	2.0
$C_{es,lv}$	*ml/mmHg*	0.40
$C_{d,lv}$	*ml/mmHg*	9

Table A.6: Compartment zero-pressure filling volumes, ZV_n.

Zero-Pressure Filling Volume		
ZV_1	*ml*	21
ZV_2	*ml*	5
ZV_3	*ml*	72
ZV_4	*ml*	360
ZV_5	*ml*	16
ZV_6	*ml*	16
ZV_7	*ml*	10
ZV_8	*ml*	20
ZV_9	*ml*	30
ZV_{10}	*ml*	300
ZV_{11}	*ml*	1146
ZV_{12}	*ml*	200
ZV_{13}	*ml*	716
ZV_{14}	*ml*	79
ZV_{15}	*ml*	33
ZV_{H1}	*ml*	20
ZV_{H2}	*ml*	108
ZV_{H3}	*ml*	250
ZV_{H4}	*ml*	35
ZV_{pa}	*ml*	160
ZV_{pv}	*ml*	430
ZV_{ra}	*ml*	14
ZV_{rv}	*ml*	46
ZV_{la}	*ml*	24
ZV_{lv}	*ml*	55

Table A.7: Nonlinear compartment maximum volumes. Refer to $V_{max,n}$ in Equation 6.6 for details.

Nonlinear Volumes		
$Vmax_{sp}$	*ml*	1500
$Vmax_{ll}$	*ml*	1000
$Vmax_{ab}$	*ml*	650

Table A.8: Compartment external pressures. Abbreviations: icp, intracranial pressure; th, thorax; abd, abdomen; e, external (atmospheric).

External Pressure			
P_{icp}	*mmHg*	H2, H3	10
P_{th}	*mmHg*	1, 2, 5, 6, 15	–4
P_{abd}	*mmHg*	7, 8, 9, 10, 11, 14	0
P_e	*mmHg*	3, 4, 12, 13, H1, H4	0

Table A.9: Body Radii, $h_{t,n}$. Abbreviations: th, thorax; abd, abdomen.

Body Radii			
$h_{t,head}$	*cm*	H2, H3	10
$h_{t,neck}$	*cm*	H1, H4	7
$h_{t,arm}$	*cm*	3, 4	7
$h_{t,th}$	*cm*	1, 2, 5, 6, 15	14
$h_{t,abd}$	*cm*	7, 8, 9, 10, 11, 14	12
$h_{t,leg}$	*cm*	12, 13	10

Table A.10: Global parameters. HR_{nom} represents the nominal heart rate; V_{tot} represents the total blood volume; $Vmax_{tilt}$, $Vmax_{lbnp}$, $Vmax_{src}$, and $Vmax_{ub}$ are the maximum blood volumes lost to the interstitium in the reference condition for tilt, LBNP, SRC, and the upper body, respectively. See Tables 6.1, 6.2, 6.3, and Section 6.4.2 for details.

Global Parameters		
HR_{nom}	*bpm*	67
V_{tot}	*ml*	5150
$Vmax_{tilt}$	*ml*	700
$Vmax_{lbnp}$	*ml*	982
$Vmax_{src}$	*ml*	700
$Vmax_{ub}$	*ml*	200
τ	*s*	276

Table A.11: Arterial baroreflex (ABR) parameters.

Arterial Baroreflex (ABR)			
P_{aspa}	*mmHg*	ABR Pressure Set Point	93
h_{CS}	*cm*	Height of the Carotid Sinus Above the Heart	25
$G^{A,S}_{R-R}$	—	ABR RR Interval Sympathetic Gain	9
$G^{A,S}_{Clv}$	—	ABR Left Ventricular Compliance Sympathetic Gain	0.007
$G^{A,S}_{Crv}$	—	ABR Right Ventricular Compliance Sympathetic Gain	0.022
$G^{A,S}_{Rh}$	—	ABR Head Resistance Gain	–0.05
$G^{A,S}_{Rub}$	—	ABR Arm Resistance Gain	–0.05
$G^{A,S}_{Rrc}$	—	ABR Renal Resistance Gain	–0.05
$G^{A,S}_{Rsc}$	—	ABR Splanchnic Resistance Gain	–0.05
$G^{A,S}_{Rlc}$	—	ABR Leg Resistance Gain	–0.05
$G^{A,S}_{Vh}$	—	ABR Head Volume Gain	2
$G^{A,S}_{Vub}$	—	ABR Arm Volume Gain	4
$G^{A,S}_{Vrc}$	—	ABR Renal Volume Gain	2
$G^{A,S}_{Vsc}$	—	ABR Splanchnic Volume Gain	15
$G^{A,S}_{Vlc}$	—	ABR Leg Volume Gain	8
$G^{A,P}_{R-R}$	—	ABR RR Interval Parasympathetic Gain	9

Table A.12: Cardiopulmonary reflex (CPR) parameters.

Cardiopulmonary Reflex (CPR)			
P_{aspc}	*mmHg*	CPR Pressure Set Point	6
$G_{Rh}^{CP,S}$	—	CPR Head Resistance Gain	–0.05
$G_{Rub}^{CP,S}$	—	CPR Arm Resistance Gain	–0.05
$G_{Rrc}^{CP,S}$	—	CPR Renal Resistance Gain	–0.05
$G_{Rsc}^{CP,S}$	—	CPR Splanchnic Resistance Gain	–0.05
$G_{Rlc}^{CP,S}$	—	CPR Leg Resistance Gain	–0.05
$G_{Vh}^{CP,S}$	—	CPR Head Volume Gain	3.5
$G_{Vub}^{CP,S}$	—	CPR Arm Volume Gain	9.5
$G_{Vrc}^{CP,S}$	—	CPR Renal Volume Gain	3
$G_{Vsc}^{CP,S}$	—	CPR Splanchnic Volume Gain	64
$G_{Vlc}^{CP,S}$	—	CPR Leg Volume Gain	30

Table A.13: Constants.

Constants			
g_E	Earth gravity	*m/s²*	9.81
ρ_{fft}	Density of fat-free tissue	*g/cm³*	1.10
ρ_b	Density of blood	*g/cm³*	1.06
d	Distance from top of head to center of rotation	cm	0